CHONDROITIN SULFATE PROTEOGLYCAN SULFATION PATTERNS PREVENT SYMPATHETIC NERVE REGENERATION AFTER MYOCARDIAL INFARCTION

By

Matthew R. Blake

A DISSERTATION

Presented to the Physiology and Pharmacology Program
and Oregon Health and Science University
School of Medicine
In Partial fulfillment of
the requirements for the degree of

Doctor of Philosophy

April 2022

Table of Contents

List of Figures

Chapter 1: Introduction

Chapter 2: Manuscript 1 – Chondroitin Sulfate Proteoglycan 4,6 sulfation regulates sympathetic nerve regeneration after myocardial infarction

Chapter 3: Loss of CSPG inhibition allows delayed sympathetic reinnervation after myocardial infarction

Chapter 4: Manuscript 2 – Small molecules targeting PTPσ—Trk interactions promote sympathetic nerve regeneration

Chapter 5: Using FRET biosensors to monitor Chondroitin Sulfate Proteoglycan signaling in sympathetic neurons

Chapter 6: Summary of Results and Discussion

Chapter 8: Appendix

List of Abbreviations

123-MIBG	123-metaiodobenzylguanadine
AAV9	adeno-associated virus 9
Ach	acetylcholine
AKT	protein kinase B
AngII	angiotensin II
APD	action potential duration
AR	adrenergic receptor
ARSB	arylsulfatase-B
ATP	adenosine triphosphate
AV	atrioventricular
BDNF	brain derived neurotrophic factor
BIM	Bisindolylmaleimide I
cAMP	cyclic adenosine monophosphate
CFP	cyan fluorescent protein
chABC	chondroitinase ABC
CHST3	chondroitin-6-sulfotransferase
CHST11	chondroitin-4-sulfotransferase
CHST15	4S-dependent chondroitin-6-sulfotransferase
CHX	cyclohexamide
CNS	central nervous system
CNTF	ciliary neurotrophic factor
ColI	collagen

CREB	cAMP response element-binding protein
CS	chondroitin sulfate
CS-GAG	chondroitin sulfate glycosaminoglycan
CSPGs	chondroitin sulfate proteoglycans
DAD	delayed afterdepolarization
DAG	diacylglycerol
DHBA	dihydroxybenzylamine
DMSO	dimethyl sulfoxide
ECC	excitation-contraction coupling
ECG	electrocardiogram
ECM	extracellular matrix
EGFR	epidermal growth factor receptor
ERK	extracellular signal-related kinase
FAK	focal adhesion kinase
Fib	fibrinogen
FRET	Forster resonance energy transfer
GAGs	glycosaminoglycans
Gal-N-Ac	N-acetyl-galactosamine
GFP	green fluorescent protein
GRK2	G-protein coupled receptor kinase 2
HA	hyaluronan
HMW	high molecular weight
HPLC	high performance liquid chromatography
HR	heart rate

HRP	horseradish peroxidase
HSPG	heparin sulfate proteoglycans
IHC	immunohistochemistry
IP	intraperitoneal
IP3	inositol-3-phosphate
I-R	ischemia-reperfusion
ISO	isoproterenol
ISP	intracellular sigma peptide
JNK	c-Jun N-terminus kinase
KO	knock out
LAD	left anterior descending artery
Lam	laminin
LAR	leukocyte antigen-related tyrosine phosphatase
LIF	leukemia inhibitory factor
LMW	low molecular weight
LV	left ventricle
MAPK	mitogen activated protein kinase proteins
MI	myocardial infarction
MMP	matrix metalloprotease
MS	multiple sclerosis
NCX	sodium-calcium exchanger
NE	norepinephrine
NG2	neuron-glial antigen 2
NGF	nerve growth factor

NgR1	nogo receptor 1
NgR3	nogo receptor 3
NT-3	neurotrophin 3
NT-4/5	neurotrophin 4/5
OPC	oligodendrocyte precursor cell
$p75^{NTR}$	p75 neurotrophin receptor
PBS	phosphate buffered saline
PCA	perchloric acid
PE	phenylephrine
PI3K	phosphoinositide-3-kinase
PKA	protein kinase A
PKC	protein kinase C
PLB	phospholamban
PLC	phospholipase C
PLL	poly-l lysine
PMA	phorbol 12-myristate 12- acetate
PNN	peri-neuronal net
PNS	peripheral nervous system
PTPσ	protein tyrosine phosphatase sigma
PVC	premature ventricular complex
Rac1	Rac family small GTPase 1
RFP	red fluorescent protein
RhoA	Ras homolog family member A
ROCK	Rho-associated kinase

ROI	region of interest
RyR	ryanodine receptor
SA	sinoatrial
SCD	sudden cardiac death
SCI	spinal cord injury
SCG	superior cervical ganglion
Sem3a	semaphorin 3a
Sem5a	semaphorin 5a
siRNA	silencing-RNA
SR	sarcoplasmic reticulum
Src	proto-oncogene tyrosine-protein kinase sarcoma
STAT3	signal transducer and activator of transcription
TBI	traumatic brain injury
TBTA	tris[(1-benzyl-1*H*-1,2,3-triazol-4-yl)methyl]amine
TCEP	tris(2-carboxyethyl)phosphine
TH	tyrosine hydroxylase
Trk	tropomyosin-related kinase
WB	western blot
WT	wild type
YFP	yellow fluorescent protein

Acknowledgments

First and foremost, I want to thank my mentor, Dr. Beth Habecker for her guidance throughout graduate school. I have benefited significantly from her approach to mentorship. She has given me the freedom to explore my interests both in terms of time and resources. Most importantly, she gave me space to develop as an independent scientist. Beth is an excellent scientist with an incredible gift for writing. She has helped me design better experiments and provided an immense amount of writing support. In my next phase I hope to emulate her scientific acumen.

I would like to thank my committee: Dr. Michael Cohen, Dr. Kevin Wright, Dr. Stephen Back, and Dr. Philip Copenhaver. Throughout this training period my committee has helped to direct my research focus and provided valuable feedback. I am grateful to have had such a supportive group that takes mentorship seriously. I would also like to thank Dr. Doris Kretzschmar for serving on my exam committee. A collaboration with Dr. Kretzschmar during my undergraduate research introduced me to OHSU and her recommendation letters helped me get here, it is an honor to have her on my committee.

The Habecker lab has been an incredible place to do research and I have benefitted from all the people who have passed through the lab. Foremost among this group are Dr. Ryan Gardner and Dr. Joseph Sepe who provided countless hours of mentorship and who have become dear friends. I would also like to thank Dr. Bill Woodward for being a great mentor in the lab, I feel lucky to have had the support of someone with so much expertise. Bill is the kind of person I hope to be when I grow up. Melanie Staffenson, Dr. Courtney Clyburn, and Diana Parrish have been wonderful partners in the lab; generating experimental animals, providing technical expertise or writing feedback and also being all-around great colleagues.

In the Chemical Physiology and Biochemistry Department at OHSU I have benefitted from several departmental collaborations that I am grateful for. Work with Dr. Carsten Schultz's Lab, specifically with Alix Thomas helped teach me all about FRET and basketball. Dr. Michael Cohen and his lab were crucial partners on the small molecule development project described in Chapter 4. Dr. Cohen provided a huge amount of

experimental advice for this project and many other members of the Cohen lab were amazing technical resources including: Dr. Ian Carter-O'Connell, Dr. Ilsa Kirby, Dr. Kelsie Rodriguez, Dr. Justina Sileikyte, Daniel Sanderson, and Daniel Bejan. Through these collaborations I have learned so much about chemical biology from so many talented scientists. Outside of the department, I would like to thank the Advanced light microscopy core, specifically Dr. Stefanie Kaech Petrie and Dr. Brian Jenkins, whose technical assistance made nearly every project described in this dissertation possible. OHSU is lucky to have these two immensely talented imaging specialists.

Before arriving at OHSU, I benefited from so many scientific mentors including Dr. Helen Blau and Dr. David Burns at Stanford University. My journey here would not be possible without my first research job at Oregon State University in Dr. Jaga Giebultowicz's Lab. Why Jaga responded to an email from a 19-year-old kid with construction experience, I will never know. Jaga is the person who made me fall in love with research, she has a passion for science unparalleled. In Jaga's lab, Dr. Joanna Kotwica-Rolinska was the first to tell me I could achieve this goal and pushed me to pursue a career in science. Thank you Aska. Of course, I would not have been interested in science at all if not for the wonderful teachers I had in my K-12 education. One in particular, Jeffery Crapper, was my middle and high school sports medicine teacher who piqued my interest in science. Thank you for inspiring me, Jeff.

Last but not least, I want to thank the friends and family whose support has enabled me to be here today. Thank you to my best friends, Tim and Galen, who have always been my intellectual and personal role models. My parent in-laws, Dan and Kathie Bridges, have been in my corner for the last 10 years and I am so grateful for them putting up with me. My parents, Nancy and Russell Blake, have been my greatest benefactors, their unending love and support made this possible. My parents are my heroes without question, they have inspired me to work hard and to always grow and learn. Ultimately, I want to thank my wife, Allie, for her unfailing love and support through this journey. Believe me when I say that if not for Allie, I would not be here today.

Abstract

Sympathetic nerves are lost in the damaged myocardium (infarct) after myocardial infarction (MI), and the relative area of denervation predicts risk of sudden cardiac arrest due to arrhythmias (Boogers et al., 2010; Fallavollita et al., 2014; Nishisato et al., 2010; Stanton et al., 1989; Vaseghi et al., 2014; Zipes & Rubart, 2006) leading to the hypothesis that sympathetic reinnervation of the infarct could reduce arrhythmias. Sympathetic nerves have the capacity to regenerate after MI but do not because of Chondroitin Sulfate Proteoglycans (CSPGs) in the cardiac scar (infarct) (Gardner & Habecker, 2013). In many contexts, CSPGs elicit effects via Chondroitin Sulfate Glycosaminoglycan (CS-GAGs) sugar side chains attached to the core protein (E. J. Bradbury et al., 2002; Massey et al., 2008). CS-GAGs can be post-translationally modified by sulfation at the 4^{th} and 6^{th} position carbons of sugars that form the GAG (Miller & Hsieh-Wilson, 2015). Sulfated CS-GAGs bind Receptor Protein Tyrosine Phosphatase Sigma (PTPσ), which suppresses axon outgrowth signaling (C. H. Coles et al., 2011; Faux et al., 2007). Here we demonstrate that 4,6-sulfated CS-GAGs are enriched in the infarct. We found that CSPG tandem-sulfation enzyme (CHST15) is increased after MI and that CSPG 4-sulfatase (ARSB) is decreased after MI, suggesting a mechanism of CS-GAG sulfation production and maintenance after MI. Reducing 4,6-sulfation of CS-GAGs by knockdown of *Chst15* restored sympathetic nerves to the infarct and reduced arrhythmia susceptibility after MI. Despite data in support of sympathetic reinnervation after MI, we asked whether regeneration of the infarct immediately after MI had long-term negative consequences, given evidence that excess norepinephrine (NE) after MI can lead to heart failure (Florea

& Cohn, 2014). We wondered if reinnervation of the infarct would amplify the effects of excess NE after MI and reduce cardiac pump function at later time points post-injury. For this experiment, we compared the cardiac outcomes of mice at 40 days after MI that were treated with Intracellular Sigma Peptide (ISP; promotes reinnervation) or with vehicle. When we examined reinnervation 40 days after MI to verify that ISP was effective, we found that vehicle-treated mice had infarcts with restored sympathetic nerves, similar to animals treated with ISP. This complicated our interpretation of the results, but broadly speaking, we found that 40 days after MI, animals had restored cardiac performance, similar to sham-surgery animals from previous studies (Gardner et al., 2015). These data provide evidence that reinnervation of the infarct is not deleterious for cardiac performance at later time points. In looking for a possible explanation for spontaneous regeneration in 40-day post-MI vehicle-treated animals we examined 4,6-sulfation of CS-GAGs. We found that 40-day post-MI vehicle-treated animals had reduced 4,6-sulfation of CSPGs and reduced core proteoglycan Neuron-glial Antigen 2 (NG2) levels, similar to healthy unoperated left ventricle. These results suggest that, in mice, cardiac remodeling after MI leads to a permissive environment for sympathetic axon outgrowth. With the evidence that CSPGs suppress sympathetic nerve regeneration in the heart after MI, we sought to develop new therapeutics to promote reinnervation. Two novel small molecules, HJ-01 and HJ-02, disrupted PTPσ interactions with Tropomyosin-related Kinase A (TrkA), which promoted axon outgrowth signaling and enhanced sympathetic axon outgrowth across CSPGs (Blake et al., 2022). This dissertation also describes an attempt to use genetically encoded FRET-biosensors to understand signaling pathways downstream of

TrkA altered by CSPGs. Due to a number of technological challenges, we limited our assessment to Protein Kinase A (PKA) and Protein Kinase C (PKC) sensors in primary sympathetic neurons but we did not observe any significant responses to CSPGs.

Chapter 1

Introduction

I. The Big Picture

Cardiovascular disease (CVD) is the leading cause of pre-mature mortality globally. A recent 2019 analysis from over 271 countries estimated the prevalence of CVD at over 500 million cases (Roth et al., 2020). A critical contributor to this disease burden is the approximately 1.2 million people in the U.S. who suffer a myocardial infarction (MI; heart attack) each year (Roger et al., 2012). Improved treatment via reperfusion of coronary artery blockage has saved many lives, but this presents a paradoxical relationship, since following reperfusion patients have increased risk of arrhythmias and sudden cardiac arrest (Pouleur et al., 2010; Solomon et al., 2005). These secondary adverse cardiac events claim the lives of more than 300,000 people each year, illustrating the need for effective interventions aimed at reducing arrhythmia risk (Solomon et al., 2005). Research in both animals and humans suggests that arrhythmias following MI are the result of the inconsistent nerve distribution and activity in the damaged myocardium known as the infarct. Specifically, loss of sympathetic nerves in the infarct predicts the risk of ventricular arrhythmias after MI (Barber, Mueller, Henry, Felten, & Zipes, 1983; Boogers et al., 2010; Fallavollita et al., 2014; La Rovere, Bigger, Marcus, Mortara, & Schwartz, 1998; Rubart & Zipes, 2005; Stanton et al., 1989; Vaseghi et al., 2014). Given the evidence that arrhythmias following MI are driven by heterogeneous patterns of sympathetic innervation, reinnervation of the damaged myocardium represents a feasible

strategy to reduce arrhythmias (Gardner, Ripplinger, Myles, & Habecker, 2016). The objective of this dissertation is to better understand the molecular details underlying sympathetic denervation in the heart after MI. The ultimate goal of this work is to inspire better therapeutic strategies to promote sympathetic nerve regeneration after MI, reduce cardiac arrhythmias, and diminish risk of sudden cardiac arrest.

II. Interplay of Nervous and Cardiovascular Systems

A. Composition of the nervous system

The mammalian nervous system can be divided into two branches: the central nervous system (CNS), composed of the brain and spinal cord, and the peripheral nervous system (PNS), composed of both somatic and autonomic nerves. Distinguishing the CNS and PNS can in part be done by the anatomical distribution of each respective branch: CNS nerves are confined to brain and spinal cord, while PNS nerves are distributed across the body, where they affect physiology locally. In the PNS, somatic nerves include those involved in recognizing and transmitting sensory input, in addition to controlling voluntary motor activity. The autonomic branch of the PNS controls involuntary physiological responses to external stimuli including; breathing rate, perspiration, digestion, and heart function (Martin, 2021).

B. Autonomic branch of the peripheral nervous system

The autonomic nervous system is made up of two distinct branches, one composed of sympathetic nerves and the other parasympathetic nerves. Both branches consist of CNS-originating preganglionic fibers that synapse with post-ganglionic nerves

in PNS-residing ganglia. Post-ganglionic nerves proceed to innervate a variety of target tissues where they control physiological homeostasis (Figure 1.1,1.2). For example, post-ganglionic sympathetic nerves that innervate the heart largely emanate from the stellate ganglia.

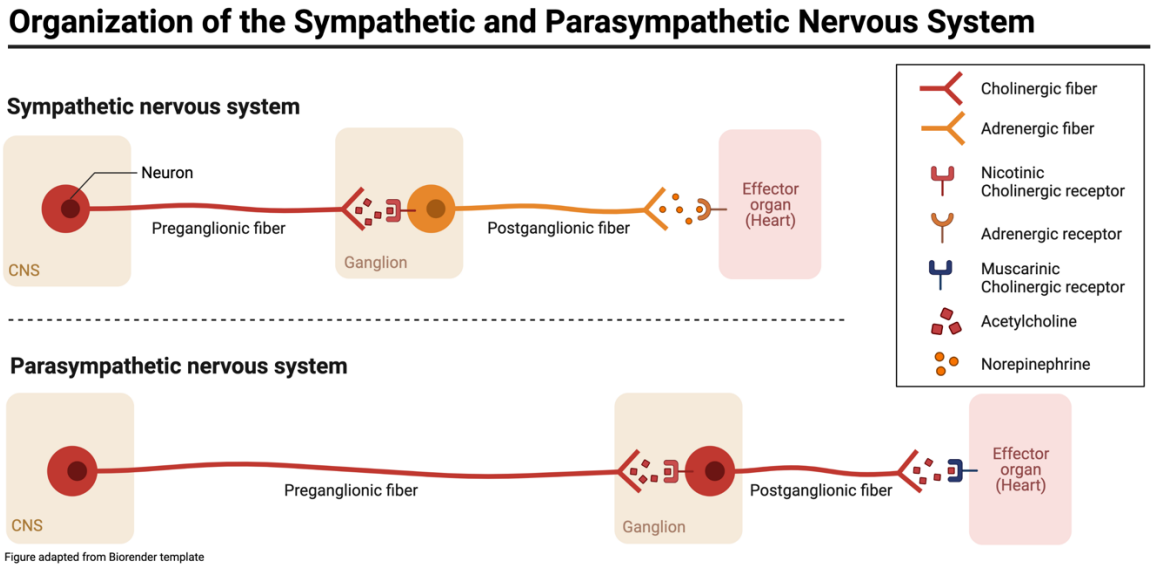

Figure 1.1: Autonomic neural input from the CNS is translated to tissue targets (effector organs) by secretion of neurotransmitters which facilitate rapid propagation of action potentials across nerves. Preganglionic sympathetic nerves, originating in the CNS, transmit signals across the synapse via secreted acetylcholine (ACh) which interacts with Nicotinic Cholinergic receptors on postganglionic sympathetic nerves in paravertebral ganglia. These signals induce an action potential across the axon where secretion of Norepinephrine (NE) stimulates adrenergic receptors on effector organs (e.g., heart). Preganglionic parasympathetic nerves, originating in the CNS, at the synapse transmit signals via secretion of acetylcholine (ACh) which interacts with Nicotinic Cholinergic receptors on postganglionic parasympathetic neurons in the ganglia near the effector organ. These signals induce an action potential across the axon where secretion of ACh stimulates Muscarinic Cholinergic receptors on effector organs (e.g., heart).

Aside from the spatial distinction, the two branches of the autonomic nervous system can be distinguished biochemically. The pre-ganglionic nerves of both autonomic branches accomplish neurotransmission via release of the neurotransmitter Acetylcholine (ACh), which then activates nicotinic ACh receptors of the post-ganglionic neurons. Post-ganglionic nerves of the parasympathetic nervous system also release Ach, activating

muscarinic ACh receptors on target cells (Figure 1.1). By contrast, the majority of post-ganglionic sympathetic nerves synthesize and release norepinephrine (NE), activating β-adrenergic receptors (β-AR) on target cells (Figure 1.1). It is worth noting that a small subset of sympathetic nerves release ACh as well in select circumstances. The heart provides an excellent example of the functional distinction between these two branches of the autonomic nervous system. Parasympathetic stimulation of the heart slows the rate of depolarization in cardiac myocytes, thereby reducing heart rate; sympathetic stimulation of the heart increases the rate and magnitude of depolarization in cardiac myocytes, thus raising heart rate (Figure 1.2). This functionality is colloquially referred to as the “rest and digest” response for parasympathetic activation and the “fight or flight” response for sympathetic activation” (Kandel, 2013).

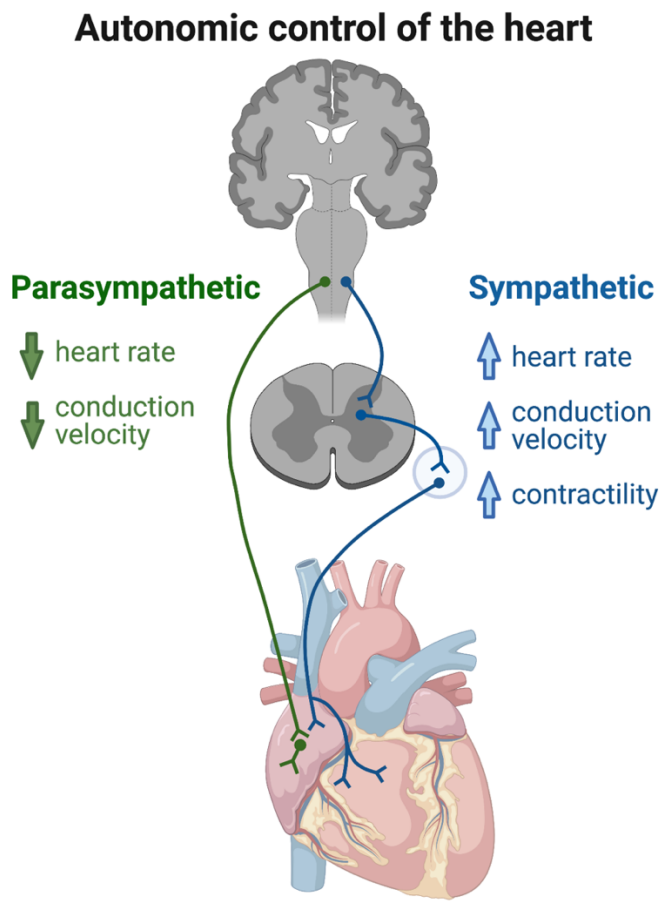

Figure 1.2: Autonomic control of the cardiac function is accomplished by the sympathetic and parasympathetic nerves that innervate the heart. Sympathetic nerves stimulate increased heart rate, conduction velocity, and contractility which enables adaptation to increased cardiac demands. Parasympathetic nerves on the contrary reduce heart rate and conduction velocity which enables the heart function to slow as needed. Proper autonomic neural control of the heart is critical for overall physiological adaptability, since this system effects perfusion of tissues across the body.

C. Excitation-Contraction Coupling

Understanding the ways that sympathetic stimulation of the heart augments cardiac contractility requires a brief overview of cardiac excitation-contraction coupling (ECC). The cardiac electrical conduction system translates electrical input into physical changes in myocyte structure. Electrical activity in the heart (Figure 1.3) begins with pacemaker cells of the Sino-Atrial (SA) node. From the SA node, a wave of electrical activity propagates through the atrium to the Atrial-Ventricular (AV) node. From the AV

node, action potentials propagate rapidly to the apex of the heart via Purkinje fibers. From the apex, activity conducts back towards the base through the walls of the myocardium, triggering the cardiomyocytes to contract. Cardiomyocytes are physically connected in fiber arrangements via structural proteins and electrically conductive gap junctions (connexin proteins), enabling action potentials to rapidly fire from one myocyte to the next. The conduction system travels fast, particularly in Purkinje cells, leading to rhythmic depolarization first in the Atria and then in the Ventricles. Autonomic nerves in the heart act, in part, by modulating this endogenous conduction system which functions to move blood into circulation.

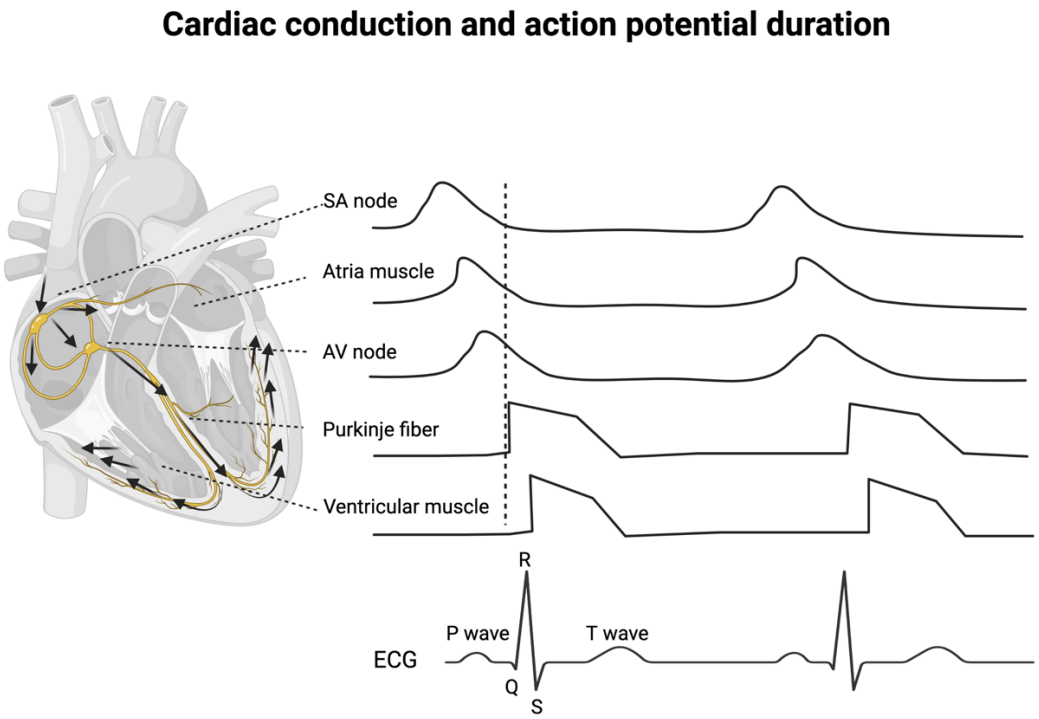

Figure 1.3: A sequence of depolarization events in the heart lead to synchronous contraction of cardiac chambers. Depolarization of cells at the Sinoatrial (SA) node propagates an action potential and subsequent depolarization in the atria. Shortly after, the Atrioventricular (AV) node depolarizes which propagates rapid depolarization of Purkinje fibers. These events culminate with a rapid depolarization of the ventricles. A summation of depolarization events is modeled

by the electrocardiogram (ECG) where the P-wave indicates atria depolarization and simultaneous contraction. QRS wave complex indicates the rapid ventricular depolarization and contraction while the T-wave represents repolarization of the ventricles. Repolarization of the atria is not appreciable by the ECG.

At the cellular level, ECC is the coordinated movement of ions, notably K^+, Na^+, Ca^{2+}, which rapidly alter the resting membrane potentials in myocytes. In ECC, depolarization of a cardiac myocyte is the result of rapid elevation in cytosolic intracellular calcium concentrations (from 0.1μM to 100μM), which spreads to adjacent myocytes. The initial release of this calcium occurs when Ca^{2+} ions flow into the cytoplasm via L-Type calcium channels, across the membrane, and into a specialized structure called the t-tubule, which brings the sarcoplasmic reticulum (SR) into close contact with the membrane. Ca^{2+} in the cytosol binds to the SR which releases Ca^{2+} into the cytosol, leading to high intracellular concentrations of the ion (Figure 1.4). High intracellular Ca^{2+} induces transient linkages between actin proteins on thin filaments and myosin proteins on thick filaments. An assembly of filaments is known as a sarcomere, and multiple sarcomeres form a myofibril leading to a bundle of contractile fibers. This bridged unit physically contracts when actin-bound myosin undergoes ATP-dependent movement, leading to shortened sarcomere structure. This cycle repeats iteratively at new actin sites to sufficiently contract a myofibril. The myosin-actin interaction is blocked in the relaxation phase by two proteins; Troponin and Tropomyosin. Ca^{2+} interactions with Troponin-C allows actin accessibility, enabling myosin interactions and subsequent contractile motor activity. Following the contraction phase, repolarization of myocytes enables relaxation via redistribution of intracellular Ca^{2+}. To accomplish this, Phospholamban-activated Ca^{2+} pumps rapidly sequester ~80% of the calcium back into the SR while Na^+-Ca^{2+} exchange

(NCX) pumps on the cell membrane extrude much of the rest back into the extracellular space (Figure 1.4). One key way that ECC in cardiac myocytes differs from skeletal muscle is that the amount of Ca^{2+} reaching the myofilament can alter the level of contractility, making the contraction highly adaptable, which is critical for autonomic modulation of cardiac contractility (Mohrman & Heller, 1997).

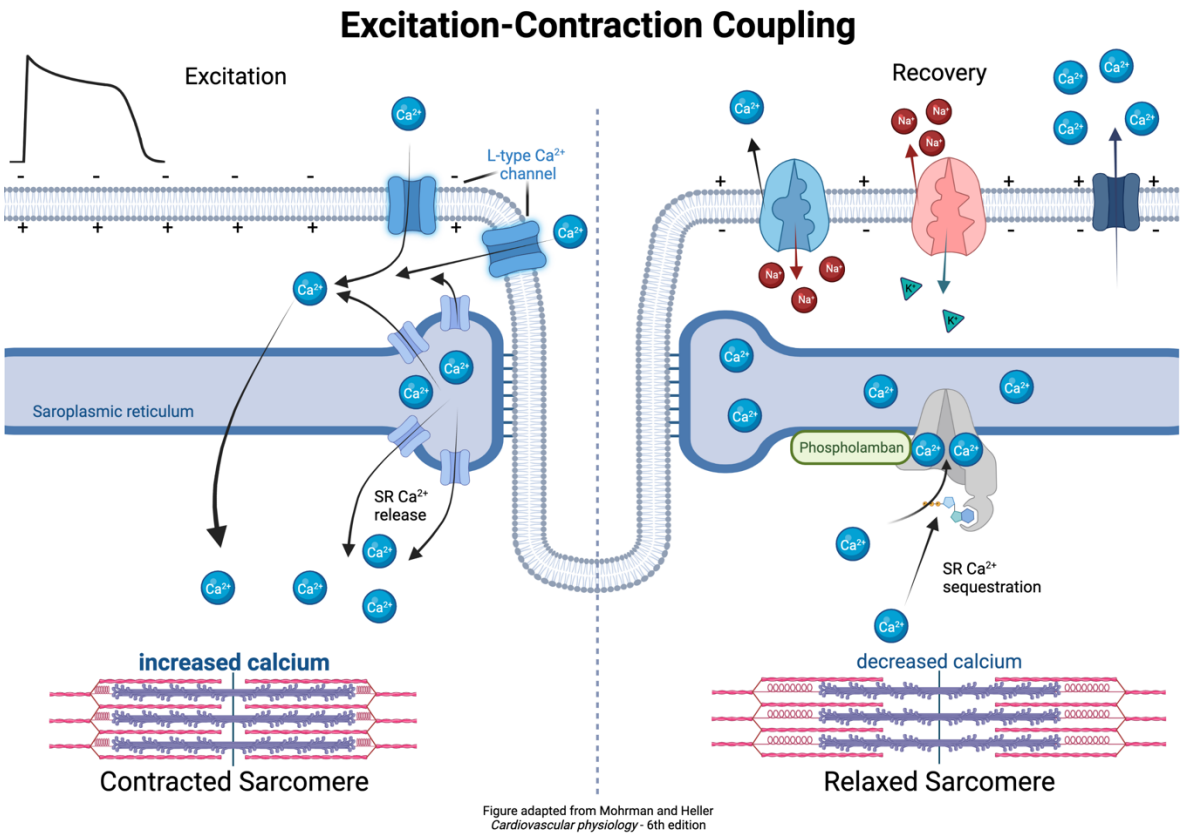

Figure 1.4: Excitation-Contraction Coupling is the process by which chemical excitation in the form of cellular membrane depolarization is translated into mechanical contraction of cardiac nerve fibers. Cardiac myocyte excitation is exemplified in the wave form on the top left corner. Excitation occurs by inward flow of Ca^{2+} ions into the cellular cytoplasm via L-type Ca^{2+} channels. Elevated cytoplasmic Ca^{2+} causes the sarcoplasmic reticulum (SR) to release a flood of Ca^{2+} increasing intracellular concentrations of the ion from 0.1μM to 100μM. Increased Ca^{2+} at the sarcomere changes molecular interactions which enable repeated ATP-facilitated actin-myosin interactions that contract sarcomere units. Sarcomere relaxation is initiated by a reversal of this process. Activation of the protein Phospholamban promotes Ca^{2+} reuptake by the SR while Na^{+}-Ca^{2+} exchange (NCX) pumps, Na^{+}-K^{+} exchange pumps,

and other Ca^{2+} pumps at the membrane extrude Ca^{2+} out of the cytoplasm to repolarize the membrane for the next round of depolarization and also prevent contractile actin-myosin interactions.

D. Sympathetic activation of cardiac myocytes

The biochemical basis of sympathetic activation of cardiac myocytes hinges on synaptic release of NE, activating β-adrenergic receptors (β-AR) on cardiomyocytes (Figure 1.5) (Wilson-Pauwels, Stewart, & Akesson, 1997). The β-AR family of proteins are G-protein-coupled receptors (GPCR) that achieve intracellular signaling via a collection of heterotrimeric G-proteins (Vassilatis et al., 2003). The effect of NE on cardiac contractility is primarily the result of β_1-AR signaling (Figure 1.5). β_1-AR activation releases the G_s subunit protein of this signaling complex, activating the $G\alpha_s$ protein which in turn activates Adenylate Cyclase (AC). AC produces cyclic Adenosine Mono-Phosphate (cAMP), which acts as second messenger to stimulate cAMP-dependent Protein Kinase A (PKA). PKA phosphorylates Troponin I, the L-type Ca^{2+} channel, Ryanodine receptor (RyR), and Phospholamban (PLB) (Freedman & Lefkowitz, 2004; Mohrman & Heller, 1997). This cascade results in an increased amplitude of intracellular Ca^{2+} and reuptake by the SR, enhancing the magnitude of the next depolarization and quickening the rate of relaxation(Mohrman & Heller, 1997).

β_2-AR signaling is coupled to the G_s and G_i subunit proteins, activating AC via G_s but also inhibiting AC via G_i, which in turn downregulates cAMP and PKA (Figure 1.5). The inhibitory effect of β_2-AR is a critical difference in the divergent physiological outcomes of each respective β-receptor. Signaling by these receptors leads to efficient changes in intracellular Ca^{2+}, which promotes increased cardiac contractility (Pavoine & Defer, 2005). Suppression of β-AR is accomplished by the G-protein Receptor Kinase 2

(GRK2). Desensitization of β-AR is initiated by free G$\beta\gamma$ subunit of the G-protein released into cytoplasm following β-AR activation; this subunit binds to GRK2 and brings it to the plasma membrane. At the plasma membrane, GRK2 is able to phosphorylate specific sites of the β-AR c-terminal tail, recruiting the β-Arrestin protein to the signaling complex, which promotes endocytosis and desensitization of the signaling complex (Claing, Laporte, Caron, & Lefkowitz, 2002).

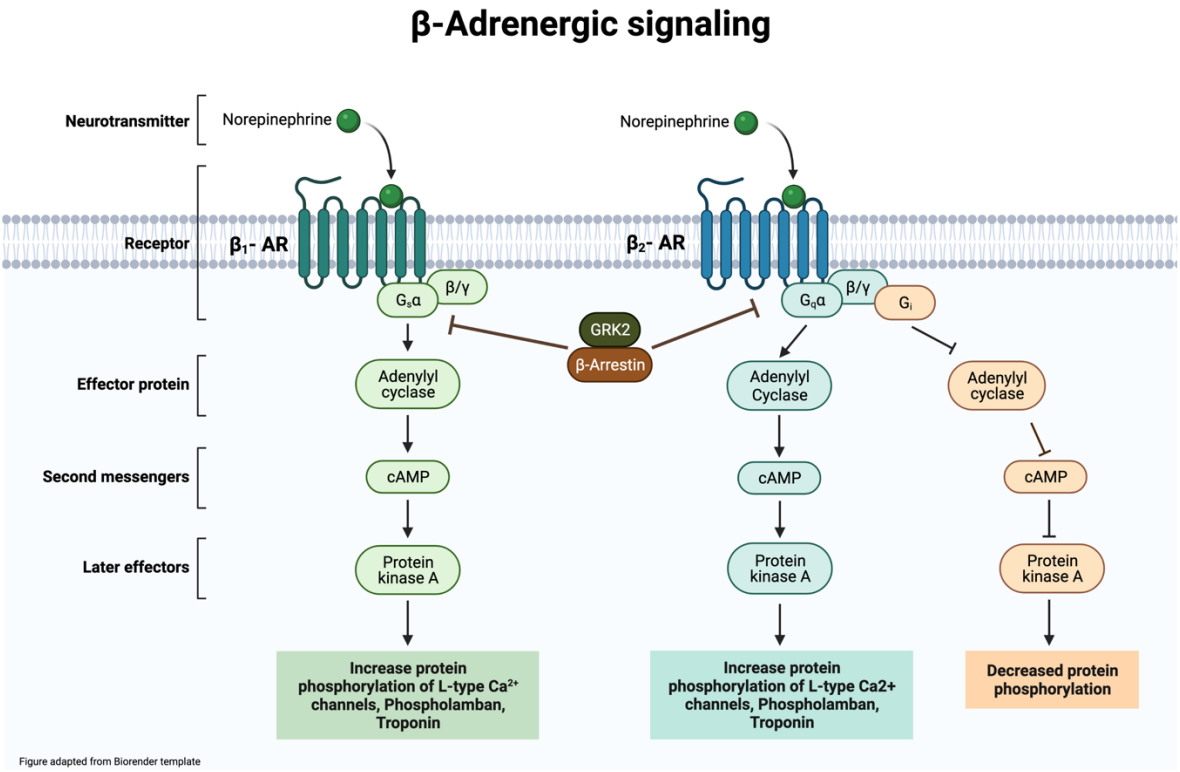

Figure 1.5: β-Adrenergic receptor (β-AR) signaling is the molecular mechanism by which sympathetic neurons, via norepinephrine (NE) secretion, stimulate changes in target organs like the heart. NE stimulation of β-AR on cardiac myocytes accelerates the magnitude and duration of the Excitation-Contraction coupling complex in Figure 1.4. Neurotransmitter activated G-protein Coupled Receptor, β-AR, activates G-protein subunits, notably G_s which activates Adenylyl Cyclase (AC) to produce cyclic-AMP which acts as a second messenger to activate Protein Kinase A (PKA). PKA phosphorylates critical ECC proteins including; L-type Ca^{2+} channels, Phospholamban, and Troponin which enables these proteins to have downstream effects on ECC. β_2-AR has an additional negative feedback pathway via the G_i subunit protein which downregulates AC and AC-stimulated pathways. β-ARs are desensitized by GRK2 which phosphorylates the β-AR c-terminal tail, recruiting β-Arrestin, which promotes internalization of the receptor and subsequently degradation.

E. Sympathetic nerves in the heart after myocardial infarction

Sympathetic nerves are thought to be the most significant regulator of cardiac contractility (Mohrman & Heller, 1997). Following MI, consensus has emerged that arrhythmogenicity is caused by a pathological distribution of sympathetic nerves in the heart. Early observations of large denervated regions in the infarcted myocardium suggested a role for improper distribution of nerves (Dae, O'Connell, Botvinick, & Chin, 1995). This discovery was facilitated by PET-imaging techniques utilizing iodine-123-metaiodobenzylguanidine (123-MIBG) to label sympathetic nerves and examine post-MI patients (Stanton et al., 1989). The relative area of denervated myocardium, assessed by 123-MIBG labeling of nerves, correlated with increased risk of sudden cardiac arrest in humans (Fallavollita et al., 2014; Simula et al., 2000; Stanton et al., 1989). This led to a hypothesis that promoting sympathetic reinnervation of the denervated infarct might reduce arrhythmias and risk of sudden cardiac arrest after MI. This idea is somewhat counterintuitive, given that sympathetic input by norepinephrine (NE) promotes post-MI arrhythmias, while blocking sympathetic nerve activity (either pharmacologically with beta-blockers or physically by severing the sympathetic ganglia) represent effective treatments to reduce post-MI arrhythmias (Barwad et al., 2021; Dae et al., 1995; Freemantle, Cleland, Young, Mason, & Harrison, 1999; Meredith, Broughton, Jennings, & Esler, 1991; Ziegler et al., 2018). Despite the efficacy of these interventions, they have the downside of reduced sympathetic activity overall and decreased ability of the heart to adapt to changing demands. Taken together, these observations suggest that the heterogeneity of sympathetic input is the culprit for arrhythmia generation, not the

denervation itself, as such, therapeutics which reduce heterogeneity of sympathetic neurotransmission and do not reduce cardiac adaptability are highly desirable.

1. Generation of ventricular arrhythmias by sympathetic stimulation

Arrhythmias generated by improper activation of β-AR are the result of pathological remodeling of sympathetic nerves in the post-MI heart (Zipes & Rubart, 2006). As previously mentioned, sympathetic nerves in the heart enable adaptation to increased cardiac demands via stimulation of β-AR by the sympathetic neurotransmitter NE, a change which increases heart rate, conduction velocity, and contractility (Mohrman & Heller, 1997). Changes to the distribution of sympathetic nerves after MI alter this adaptive response, such that some regions of the heart respond to NE while other regions cannot (Lorentz et al., 2010). Arrhythmogenic sympathetic remodeling can be divided into four categories: hyperinnervation (too many nerves), denervation (too few nerves), altered neurotransmitter or neuropeptide secretion, and improper neuronal excitability (Zipes & Rubart, 2006).

Exactly how sympathetic nerve remodeling causes ventricular arrhythmias is unknown, but the heterogeneity in neurotransmitter release between hyperinnervated and denervated regions clearly plays a role (Lorentz et al., 2010). One result of this heterogeneous innervation density is the remodeling of viable cardiac myocytes that remain after MI. Electrical remodeling in the cardiomyocytes of hyperinnervated regions can produce increased L-type Ca^{2+} channel current density and decreased K^{+} current density, which would prolong action potential duration (Cutler, Jeyaraj, & Rosenbaum,

2011). Cardiac remodeling can also result in increased NCX expression or decreased cell-cell gap junction coupling, due to cell composition changes which can alter action potential duration (Poelzing & Rosenbaum, 2004; Pogwizd, Qi, Yuan, Samarel, & Bers, 1999). Excess release of NE can occur following increased physical demand, inducing heterogeneous depolarization responses in various regions of the myocardium and thus triggering an arrhythmia. This is primarily thought to be propagated at the cellular level via delayed after depolarizations (DAD), which are spontaneous depolarizations that occur during the repolarization phase of cardiac action potentials (Figure 1.6) (Pogwizd & Bers, 2004). The direct cause of these events is increased calcium load in both the cytosol and SR, which can cause spontaneous opening of Ryanodine receptors (RyR), and activation of the NCX exchanger. If stimulated sufficiently, this chain of events can lead to spontaneous propagation of an action potential (Pogwizd, Schlotthauer, Li, Yuan, & Bers, 2001). If enough cells experience this spontaneous DAD at the same time, a focal arrhythmia can occur. Regional cardiomyocyte remodeling due to hyperinnervation is often able initiate DAD, causing reentrant arrhythmias in response to sympathetic neurotransmitter surges (Figure 1.6) (Xie, Sato, Garfinkel, Qu, & Weiss, 2010). Denervated

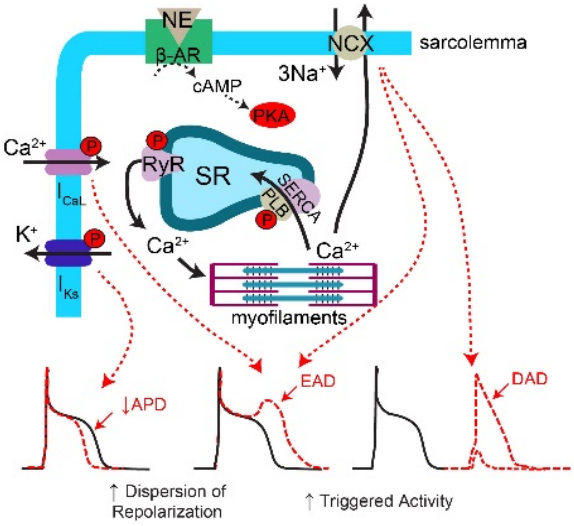

Figure 1.6: Acute effects of sympathetic stimulation on arrhythmia generation. NE stimulation decreases action potential duration (APD). In pathological settings, excess NE stimulates inappropriate levels of cytosolic Ca^{2+} which can trigger early after depolarizations (EAD) or delayed after depolarizations (DAD) which can trigger arrhythmias. (Ripplinger, Noujaim, & Linz, 2016)

regions are also critical in generation of post-MI arrhythmias. Regions of viable myocardium that exist next to scar tissue can be denervated, and display hypersensitive responses to β-AR stimulation which can occur following a surge in NE release. This super-sensitivity is likely the result of reduced GRK2, which leads to reduced SR Ca^{2+} and increased cytosolic Ca^{2+}, which can initiate DAD (Raake et al., 2012). At the tissue level, this hypersensitivity to β-AR makes propagating arrhythmias increasingly likely. Calcium handling studies in animal models have demonstrated this effect, where heterogeneous regions of innervation cause non-uniform distribution of calcium transients, which is highly arrhythmogenic (Myles, Wang, Kang, Bers, & Ripplinger, 2012; Vaseghi, Lux, Mahajan, & Shivkumar, 2012).

2. Current standard of care to treat ventricular arrhythmias

Given this background information, it is easy to understand why β-AR blockade remains one of the most effective treatments to reduce arrhythmia risk after MI. All these arrhythmia-generating pathways essentially converge on heterogenous β-AR stimulation, such that broad disruption of the pathway reduces arrhythmias. Decades of using β-Blockers has significantly reduced mortality from sudden cardiac death across almost all types of coronary artery disease (Herring, Kalla, & Paterson, 2019). Sympathectomy, or physical removal of sympathetic nerves, has also emerged as a treatment to reduce the risk of reentrant arrhythmias and has shown promise clinically in reducing mortality (Barwad et al., 2021). Despite the clinical benefit of β-AR blockade (Lopez-Sendon et al., 2004), it is also obvious why these treatments have downsides for patient quality of life,

as they reduce the ability of the heart to react to increased demand. Since β-AR blockade reduces β-AR-induced heterogeneous electrical activity, therapies restoring uniform distribution of nerves after MI might normalize electrical activity and preserve cardiac responses to increasing demand (Figure 1.7). Animal studies support this hypothesis with genetic and pharmacological interventions that restore nerves in the damaged myocardium, normalizing Ca^{2+} transients in the heart and reducing arrhythmia susceptibility in response to the β-AR agonist isoproterenol (Gardner et al., 2015). Given these results, it is of great clinical interest to find novel strategies that promote reinnervation of the damaged myocardium.

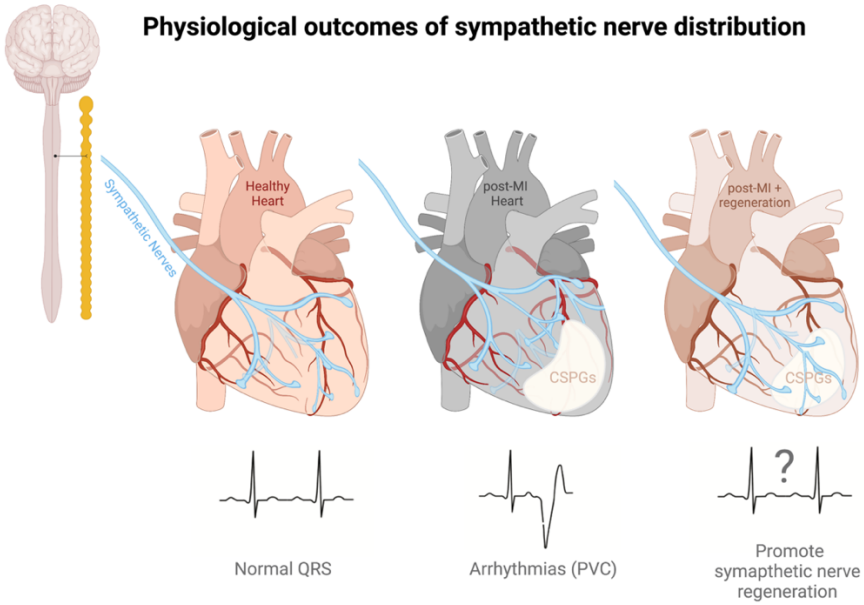

Figure 1.7: Sympathetic nerve regeneration in the heart after MI hypothesis graphic. Healthy hearts generate cyclical depolarization and contraction of the Atria and Ventricle which is exemplified by the normal ECG trace. After a myocardial infarction (MI), nerves are pathologically redistributed such that damaged myocardium is denervated of sympathetic nerves while regions of hyperinnervation exist in adjacent viable myocardium. This atypical distribution of sympathetic nerves leads to arrhythmogenic depolarizations of the heart in response to β-AR stimulation exemplified by the premature ventricular complex shown in the ECG trace below the MI heart. We hypothesize that reinnervation of the damaged myocardium reduces arrhythmia risk, an idea that has been demonstrated in our animal model of MI. The goal of this dissertation is to outline novel strategies to promote sympathetic nerve regeneration in the infarcted myocardium.

III. Nerve Regeneration

A. History of nerve growth research

Peripheral nerve outgrowth is a well-studied phenomenon, owing to the fact that these neurons were used in many of the earliest studies dissecting the mechanisms of nerve growth. Early developmental studies examined the distance that peripheral axons traveled to innervate target tissues and concluded that a precise mechanism of attractive cues must govern such consistent patterning. This led to the hypothesis that a secreted factor in target tissues was responsible for nerve route finding (V. Hamburger, 1934; V. Hamburger, 1939). This work came to a forefront when Rita Levi-Montalcini and Viktor Hamburger discovered this secreted factor from mouse salivary gland and dubbed it Nerve Growth Factor (NGF) (V Hamburger & Levi-Montalcini, 1949; Levi-Montalcini & Hamburger, 1953). The seeds to this discovery were sewn just over a decade earlier by Viktor Hamburger, who had shown that removal of wing buds in developing chick embryos reduced both the number of neurons that developed in the lateral motor column within the spinal cord and the number of sensory neurons of the dorsal root ganglion (DRG), while adding additional wing buds to the developing embryo produced more motor and sensory neurons (V. Hamburger, 1934; V. Hamburger, 1939). This observation led to the formation of the “Neurotrophic Factor Hypothesis”, and subsequently the development of an entire field of neurobiology. The discovery of a secreted factor in the mouse salivary gland and cobra venom led to the purification and identification of NGF by Stanley Cohen (Cohen, 1960; Cohen & Levi-Montalcini, 1956). This work demonstrated the significance of the secreted factor *in vivo*: treating developing rodents with the anti-serum against NGF

caused massive neuronal die off. This led to the idea that NGF promoted neuronal differentiation and survival instead of causing neurogenesis. Work demonstrating that NGF only effected some neurons and not others led to discovery of other neurotrophic factors. Today we now know these as Brain Derived Neurotrophic Factor (BDNF) (Barde, Edgar, & Thoenen, 1982), Neurotrophin-3 (NT3) (Hohn, Leibrock, Bailey, & Barde, 1990; K. R. Jones & Reichardt, 1990; Maisonpierre et al., 1990; Rosenthal et al., 1990), and Neurotrophin-4/5 (NT4) (Berkemeier et al., 1991; Ip et al., 1992).

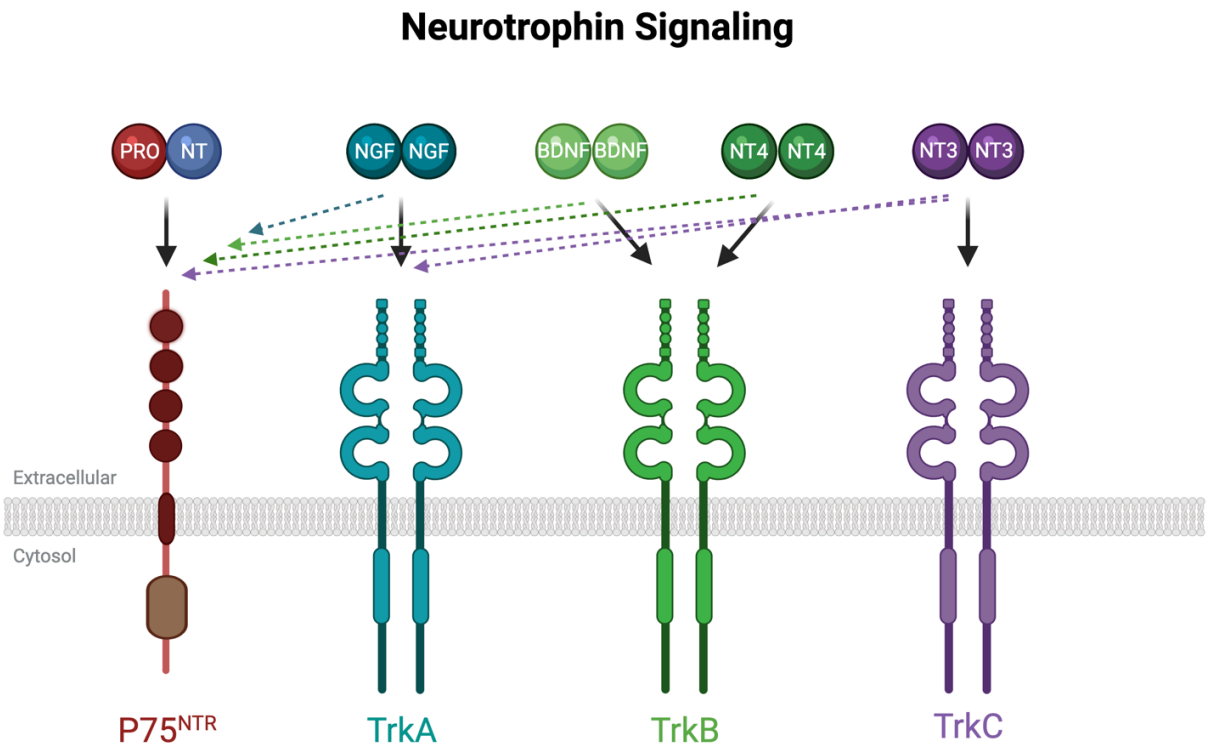

Figure 1.8: Neurotrophins and their cognate receptors. $P75^{NTR}$ binds all neurotrophins and all unprocessed proneurotrophins (PRO-NT). TrkA binds NGF and NT3. TrkB binds BDNF and NT4. TrkC binds NT3.

B. Extracellular activation of neurotrophin signaling

Neurotrophins are synthesized as dimeric propeptides in the endoplasmic reticulum, where they are packaged into secretory vesicles. Cleavage of the prodomain by several different proteases produces an active c-terminus of the protein, which remains in dimeric form throughout signaling (Seidah, Benjannet, Pareek, Chretien, & Murphy, 1996). Active neurotrophins exist as dimers that approximate 13.5 kDa and have picomolar affinities for their respective receptors (M. A. Bothwell & Shooter, 1977). The discovery of each neurotrophin led to a parallel search for their receptors, which we know now to be $P75^{NTR}$ and the Tropomyosin-receptor kinase (Trk) family; TrkA, TrkB, and TrkC. TrkA binds to NGF; TrkB binds BDNF and NT4; TrkC binds NT3 (Figure 1.8). In some cases, NT3 also binds and activates TrkA or TrkB, but is not the signaling equivalent of NGF or BDNF respectively (Clary & Reichardt, 1994; Harrington et al., 2011). $P75^{NTR}$ binds to all pro and mature neurotrophins. In neurons expressing the Trk receptor and $P75^{NTR}$, both receptors can interact to form functional signaling complexes (Figure 1.9) (M. Bothwell, 1991; Hempstead, Martin-Zanca, Kaplan, Parada, & Chao, 1991). These receptors are responsible for the relay of extracellular neurotrophic signaling to intracellular targets. In response to neurotrophin binding, neurotrophin receptors dimerize and autophosphorylate intracellular domains, enabling signaling activity (Figure 1.10). Despite the fact that these are all considered neurotrophin receptors, their functions within the neuron can be quite divergent (Figure 1.9). Trk receptor promotion of axon growth and survival remains the most often discussed signaling outcome (Huang & Reichardt, 2003); NGF expressed in the developing heart promotes innervation of TrkA expressing

sympathetic neurons, and this signaling pathway sustains sympathetic innervation throughout life. Diverging outcomes occur when proneurotrophins bind $P75^{NTR}$, an interaction that has been shown to induce apoptosis and cell death (Figure 1.9) (F. S. Lee, Rajagopal, & Chao, 2002; R. Lee, Kermani, Teng, & Hempstead, 2001). For this apoptotic pathway to initiate, the interaction of the c-terminal domain of the proneurotrophin interacts with $P75^{NTR}$, while the pro-domain interacts with the protein Sortilin, forming a signaling complex (Figure 1.9) (Teng et al., 2005). This pathway plays a critical role in neuronal development, where apoptosis is critical for proper target innervation (Naumann et al., 2002) and in neuronal cell death after CNS injury (Harrington et al., 2004). Proneurotrophin-$P75^{NTR}$ signaling has also been proposed as a contributing factor during aging, since proneurotrophin expression increases and is thought to induce neuronal cell loss (Al-Shawi et al., 2008). Put simply, $P75^{NTR}$ signaling has a complicated role in neuronal survival. One well-supported model suggests that actively growing neurons secrete the opposing neurotrophin to stimulate death of adjacent neurons (Deppmann et al., 2008). The mechanistic basis for such interactions suggested that trans-neurotrophin (e.g., BDNF binding $P75^{NTR}$ on a TrkA expressing neuron) binding leads to $P75^{NTR}$ induction of neuronal cell death (Bamji et al., 1998). For the purposes of this dissertation. However, the most critical role of proneurotrophins is the interaction between $P75^{NTR}$ and proNGF following myocardial infarction, where proNGF is produced by damaged cardiomyocytes and contributes to sympathetic denervation of the ischemic zone (Lorentz et al., 2010).

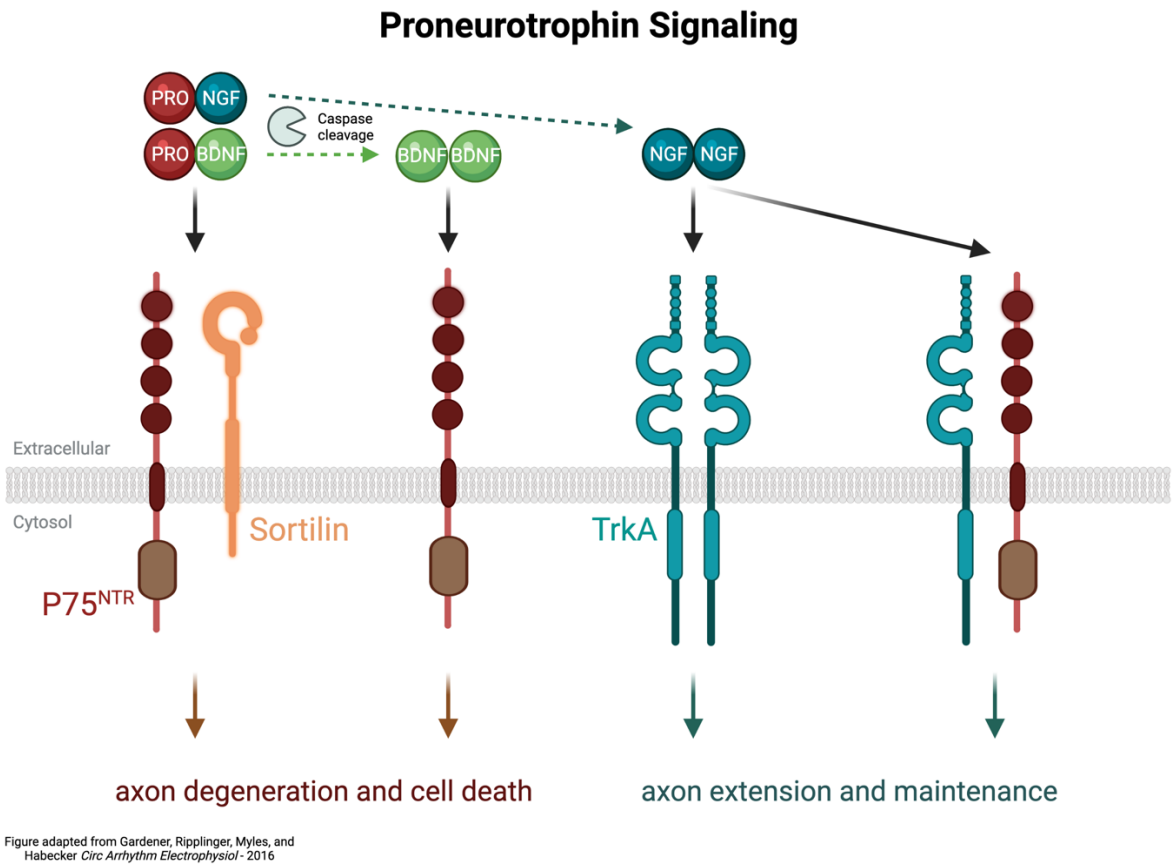

Figure 1.9: Proneurotrophins and P75^{NTR} in axon degeneration and extension. Proneurotrophins are processed into mature dimeric proteins by caspases. Dimeric neurotrophins bind and stimulate their cognate receptors as described in Figure 1.8. Proneurotrophins stimulate axon degeneration via P75^{NTR} binding in complex with the receptor Sortilin. P75^{NTR} can also induce cell death if a neurotrophin from a non-cognate receptor binds P75^{NTR} (e.g. BDNF binding P75^{NTR} in neurons that express TrkA). P75^{NTR} can also complex with Trk forming active neurotrophin signaling complexes which promote axon extension (e.g. TrkA- P75^{NTR} binding NGF).

C. Neurotrophin-induced intracellular signaling

The divergent pathways of neurotrophin signaling and subsequent dramatic effects on physiology have made them the focus of decades of research. Recently, technological advances have led to an exponential increase in our understanding of the intracellular signaling cascades stimulated by neurotrophins. Trk receptors share many of the same downstream signaling partners, owing to their significant homology and intracellular scaffolding nature (Grimes et al., 1996). The phosphorylated intracellular domains of

neurotrophin-bound dimerized Trk receptors serve as signaling scaffolds for a diverse array of molecules that dock and propagate signaling in several canonical pathways (Huang & Reichardt, 2003). These pathways are often subdivided into 3 branches (Figure 1.10); the Map kinase associated pathway, the PI3-kinase/AKT pathway, and the PLCγ/PKC pathway. In response to neurotrophin signaling, Map kinase pathway activation propagates a phosphorylation cascade activating Ras-Raf-MEK-ERK1/2, ultimately enabling CREB translocation to the nucleus, where it promotes axon differentiation and extension via induction of transcriptional networks (Finkbeiner et al., 1997; Howe, Valletta, Rusnak, & Mobley, 2001). PI3-kinase pathway activation suppresses the cell death-associated protein BAD and induces phosphorylation of AKT, enhancing pro-survival cell signaling at the transcriptional level (York et al., 2000). Activation of PLCγ induces signaling by producing diacylglycerol (DAG) and inositol-3-phosphate (IP3) to alter cellular Ca^{2+}, activate CAM kinases as well as PKC-ERK signaling to augment synaptic plasticity and differentiation (Chuang et al., 2001). Activation of all these pathways relies upon assembly of highly coordinated active signaling complexes, the details of which remain to be fully understood.

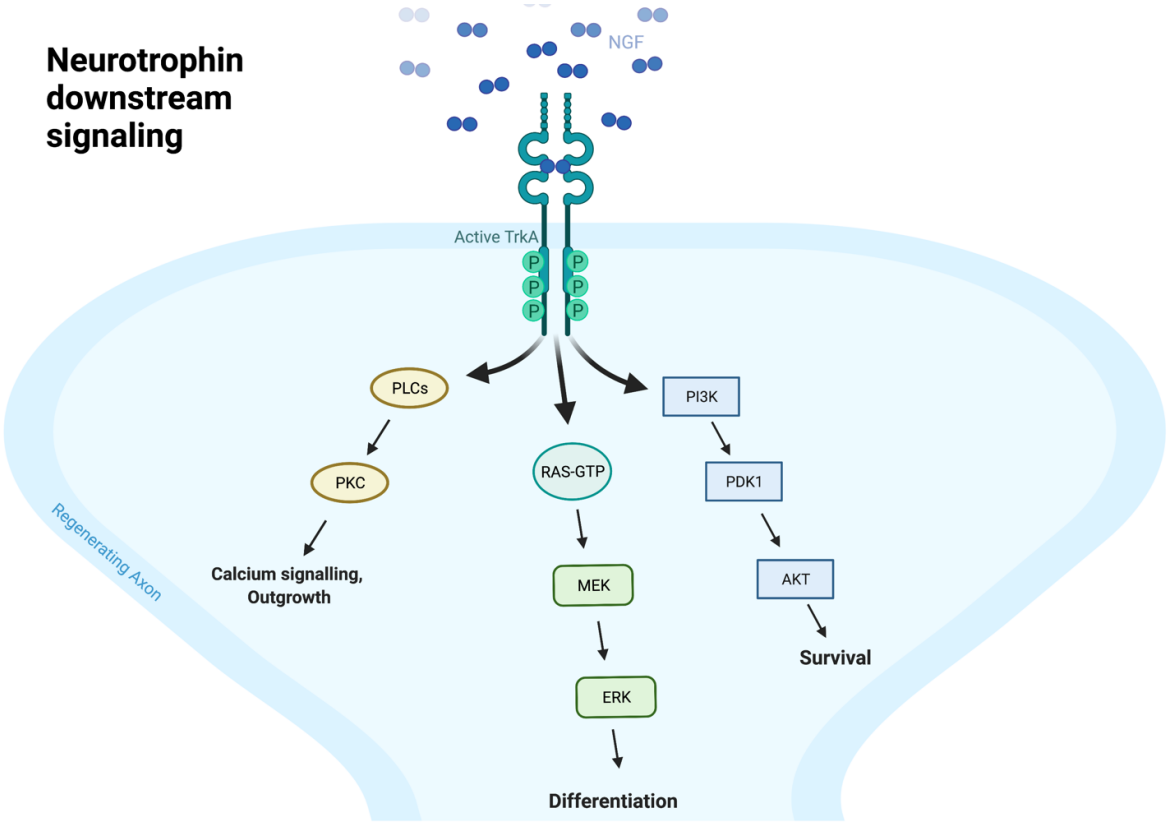

Figure 1.10: Simplified Trk-Neurotrophin signaling cascade. NGF bound TrkA dimers autophosphorylate tyrosines on cytoplasmic tails, enabling formation of an active Trk signaling complex which includes many effector proteins. These effector proteins lead to a cascade that activates three canonical downstream signaling pathways. The First is stimulation of phospholipase C (PLC), which alters calcium handling and promotes axon outgrowth by activating Protein Kinase C (PKC). Second is the Ras-MEK-ERK pathway, where a cascade of kinase activation and phosphorylation leads to transcriptional changes that promote neurite differentiation and outgrowth. The third pathway is the PI3-kinase – AKT pathway, which promotes survival by suppressing cell death signaling.

Dissecting the nuances of neurotrophin signaling has been facilitated by the development of the compartmentalized cell-culture chamber; originally the Campenot chamber, and more recently various microfluidic designs, that isolate cell body (soma) and axonal compartments. These chambers enable the addition of stimuli to distinct cellular compartments, which has been particularly insightful to understand how axonal stimulation imparts cell soma effects. A traditional view of neurotrophin signaling is that neurotrophin, secreted from cellular targets of the nerve, binds to neurotrophin receptor

on the tip of axonal growth cones to elicit a cellular effect; notably axon growth and survival (Huang & Reichardt, 2003; Levi-Montalcini & Angeletti, 1968). This effect relies upon the efficient transmission of signaling across huge distances relative to the size of a cell, due to the highly polarized nature of the neuron (Horton & Ehlers, 2003). For example, lumbar motor neuron axons can extend up to 10,000 times the length of the cell soma (Ibanez, 2007). Thus, mechanisms must be in place to transmit signals rapidly across such distance. This system relies on trafficking of neurotrophin-bound active signaling receptors from the distal axon back towards the cell body, and efficient mechanisms to replenish neurotrophin receptors in the distal axon depending upon the needs of the cell (Figure 1.11) (Hendry, Stockel, Thoenen, & Iversen, 1974; Horton & Ehlers, 2003). A complex system of trafficking proteins exists within the polarized neuron to facilitate such movement. Kinesins are a family of motor proteins that traffic cargo from the cell soma out towards the distal axon in a movement known as anterograde transport (Hirokawa, Noda, Tanaka, & Niwa, 2009). In contrast, dynein family motor proteins traffic proteins from the distal axon towards the cell soma in what is called retrograde transport (Heerssen, Pazyra, & Segal, 2004; Kardon & Vale, 2009). Trk receptors utilize these pathways to transport active signaling receptor complexes from the distal axon to the soma, to recycle and degrade inactivated receptors, and to replenish Trk receptors in the distal axon (Ibanez, 2007).

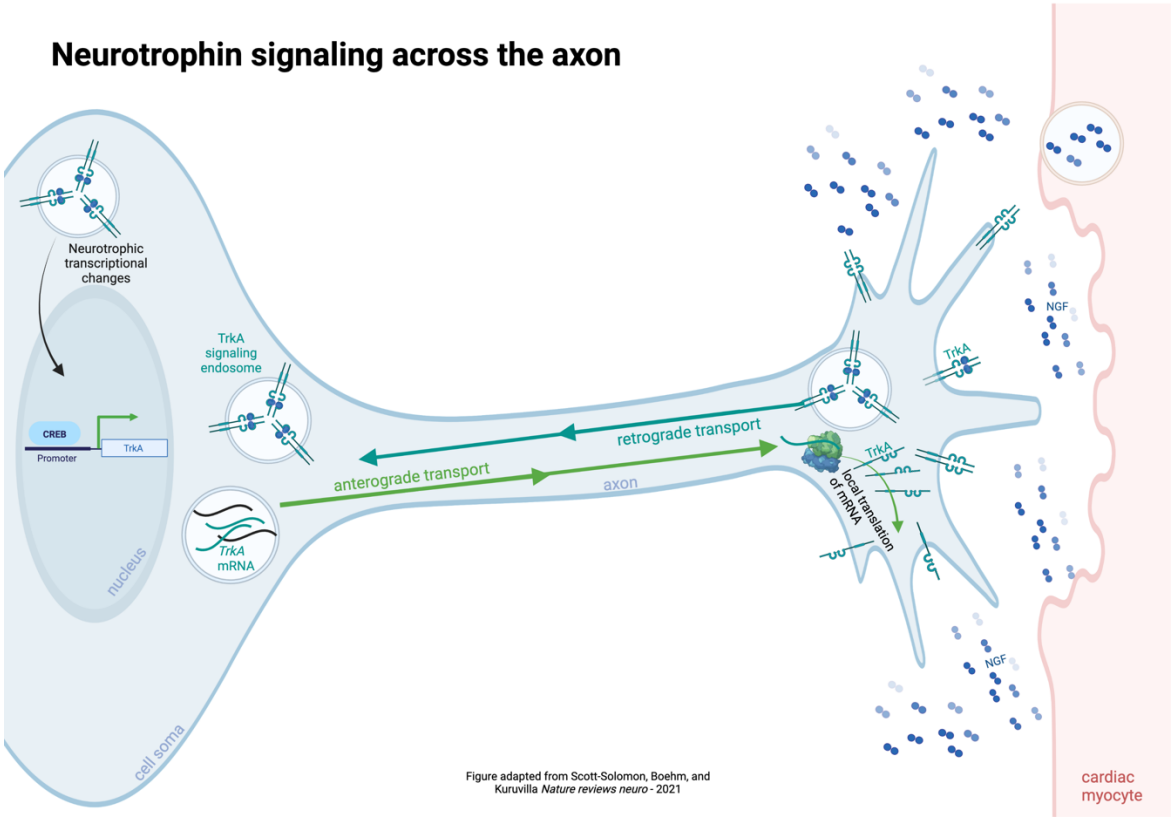

Figure 1.11: Neurotrophin signaling across the polarized neuron requires efficient translation of signaling over a distance. This is catalyzed by an assembly of motor proteins that transport cargo from the distal axon to the cell soma (retrograde) or from the soma out to the distal axon (anterograde). Retrograde transport is accomplished by Dynein motor proteins whose cargo includes active Trk signaling endosomes that are taken back to the cell soma where they can affect dendrite formation and transcriptional changes like increased expression of the *TrkA* gene. Anterograde transport is catalyzed by Kinesin motor proteins whose cargo can include *TrkA* mRNA which is taken out to the distal axon for local translation. This transport example enables efficient replenishment of TrkA at the membrane and enables neurotrophic signaling continuity. This cartoon exemplifies a TrkA expressing peripheral neuron that is attempting to innervate a cardiac myocyte thanks to release of NGF.

Active neurotrophin-bound Trk receptor complexes are internalized into endocytic vesicles and trafficked through the axon (Figure 1.11). After internalization, these active Trk complexes continue to propagate positive signaling in endosomes (Howe & Mobley, 2004). Signaling endosomes undergo retrograde transport via dynein motor proteins through the axon back to the cell soma, where they propagate neurotrophic signaling (Kuruvilla et al., 2004). Increasing evidence suggests that this retrograde Trk signaling is

also important for proper dendrite function (B. Zhou, Cai, Xie, & Sheng, 2012). Many tyrosine kinase receptors are internalized in active signaling endosomes and most, like Epidermal Growth Factor Receptor (EGFR), are targeted to the proteasome for rapid degradation, in turn ending the active signaling complex (Haglund, Shimokawa, Szymkiewicz, & Dikic, 2002). Trk receptors avoid this fate (to some extent) by employing a more complicated mechanism of proteasomal degradation involving multi-step ubiquitination, in essence requiring more steps to degrade an active signaling complex (Georgieva, de Pablo, Sanchis, Comella, & Llovera, 2011; Marmor & Yarden, 2004). A complex series of steps and interacting proteins enable efficient anterograde and retrograde signaling of neurotrophin-bound Trk receptor complexes, the extent of which is only starting to be understood, thanks to new molecular tools and imaging techniques. Increasing evidence suggests a critical role for the local translation of axon-targeted mRNAs, including a recent paper describing locally translated and modified prenylated-Rac1 in promoting NGF-dependent axon outgrowth and proper trafficking of TrkA signaling endosomes (Kuruvilla et al., 2004). Additional evidence has shown that the Trk receptors can recycle back to the membrane and again form active signaling complexes (Chen, Ieraci, Tanowitz, & Lee, 2005; Saxena et al., 2005). Anterograde trafficking is equally important as retrograde to manage Trk receptor signaling. In response to retrograde neurotrophin signaling, anterograde transport of nerve growth-associated mRNAs is increased and targeted to the axonal growth cone via kinesin motors for local translation (Figure 1.11) (Willis et al., 2007). Impairment of anterograde mRNA transport in response to neurotrophin stimulus can cause neuronal cell loss (Andreassi et al., 2010).

D. Neurotrophins in the heart

In addition to effecting nervous system development, neurotrophins play important roles in development and maintenance of various organ systems, including the gastrointestinal tract, kidney, lungs, and most importantly for this dissertation, the heart (Huang & Reichardt, 2001). Neurotrophic signaling has broad reaching effects on both angiogenesis and cardiac myocytes across developmental stages and in various pathologies. In heart development BDNF, NT3, and Trk receptors B and C have been shown to play critical roles using knockout animals (Donovan, Hahn, Tessarollo, & Hempstead, 1996; Hiltunen, Arumae, Moshnyakov, & Saarma, 1996; Tessarollo et al., 1997; Wagner et al., 2005). Lack of BDNF-TrkB signaling reduces endothelial cell-cell adhesion, subsequently reducing the number of blood vessels in the heart (Donovan et al., 2000; Wagner et al., 2005). NT3-TrkC signaling is required for proper atria and cardiac outflow tract development, and absence of this signal impairs cardiac morphology (Donovan et al., 1996). The role of $P75^{NTR}$ in cardiac development is complicated, but its critical role in proper development of cardiac vasculature is clear (von Schack et al., 2001). Much of the work focusing on TrkA centers on its significance in proper development of the sympathetic nerves that innervate the heart. The post-ganglionic nerves that innervate the heart initially require NT3 signaling via TrkA to reach the heart, where the shift to NGF is required for proper target innervation and survival (Glebova & Ginty, 2005; Kuruvilla et al., 2004). NGF signaling via TrkA in sympathetic neurons of the heart ensures proper synapse formation, homogenous innervation density in atria and ventricle, and regulates levels of the sympathetic neurotransmitter Norepinephrine (NE)

(Glebova & Ginty, 2004; Habecker et al., 2008; Lorentz et al., 2010). Beyond their role in proper development, neurotrophin signaling has been shown to be a critical player in cardiac pathologies. Ischemic insult to the heart is perhaps the most well studied of these pathologies and also the most important for this dissertation. Following cardiac ischemia, NGF is upregulated both at the transcriptional level (Hiltunen, Laurikainen, Vakeva, Meri, & Saarma, 2001) and protein level, in addition to increased TrkA expression (Meloni et al., 2010). The production and secretion of mature NGF via infiltrating and resident macrophages and myofibroblasts during the post-ischemia inflammatory phase enables NGF activity on a host of cell types (Hasan et al., 2006). NGF activation of TrkA and VEGF in endothelial cells after injury enables proliferation and survival by promoting angiogenesis following hind limb ischemia (Emanueli et al., 2002), and likely following MI (Meloni et al., 2010). Increased angiogenesis is known to promote healing of the infarcted myocardium. In other ischemic muscle injuries, BDNF-TrkB and NT3-TrkC promote recovery in the vasculature by acting on endothelial cells that express each respective Trk receptor (Cristofaro et al., 2010; Kermani et al., 2005). $P75^{NTR}$ plays an important role after MI in pericytes, binding to proNGF (upregulated after MI) and reducing pericyte function, increasing vascular permeability, and increasing size of the cardiac infarct (Siao et al., 2012).

Given these observations, promoting mature neurotrophin signaling in the heart after ischemia-reperfusion injury is a compelling therapeutic target. In theory, enhanced neurotrophin signaling could promote angiogenesis to damaged tissue, reduce deleterious inflammation, and also promote nerve regeneration after MI. Work in the

Habecker group has contributed to our understanding of the mechanism of NGF-induced sympathetic axon signaling after MI, demonstrating that NGF-TrkA signaling is vital for proper regeneration of the sympathetic nerves. TrkA activation in sympathetic nerves leads to phosphorylation of the Signal Transducer and Activator of Transcription 3 (STAT3), which is important for its downstream signaling activation. STAT3 signaling is also affected by cytokine release converging on the gp130 receptor; cytokines like Leukemia Inducible Factor (LIF) and Ciliary neurotrophic factor (CNTF) activate gp130 and stimulate tyrosine phosphorylation of STAT3. This work demonstrated that STAT3 phosphorylation at critical serine and tyrosine residues are required for induction of NGF-TrkA stimulated sympathetic axon extension (Pellegrino & Habecker, 2013). As mentioned previously, NGF is increased in the heart after MI, and it is worth noting that increased NGF signaling via TrkA in sympathetic nerves attempting to regrow in the cardiac scar leads to hyperinnervation of the border zone region outside the infarct but does not restore nerves to the infarct (Meloni et al., 2010; S. Zhou et al., 2004). This local hyperinnervation coupled with denervation of the infarct promotes focal arrhythmias and likely increases risk for sudden cardiac arrest after MI (Zipes & Rubart, 2006), emphasizing the need to promote *proper* innervation of sympathetic nerves in the heart after MI (Gardner et al., 2016).

E. Clinical modulation of Trk signaling

Since their discovery and classification as neurotrophic factors, neurotrophins have been thought of as molecules with therapeutic potential, given their dysregulation or disfunction in many pathologies. However, decades of work have shown that their therapeutic use is complicated. One of the more interesting applications of neurotrophins in the clinic has been in modulating pain sensitivity. Early studies showed that infusion of NGF to regenerate peripheral nerves promoted severe mechanical and thermal allodynia (hyper sensitive pain response) (Lewin & Mendell, 1993; Petty et al., 1994). Interestingly, this observation might explain why NGF is enriched in both rodent salivary glands and viper venom, since NGF enrichment may be an evolutionary adaptation to rapidly induce pain (Jackson, 2007). In response to these observations, however, NGF blocking strategies have been used to reduce hyperalgesia in peripheral neuropathic pain and various other pain-related pathologies without affecting normal pain sensation. Unfortunately, due to some adverse events in clinical trials, a monoclonal antibody (Tanezumab) developed for this purpose was not approved by the FDA this past year (B. Zhang, Tian, Qu, Liu, & Yang, 2021). Other clinical applications of neurotrophin signaling are TrkB and TrkC agonist antibodies, which have been proposed to treat nerve degeneration and neuropathy. However, no candidate has successfully reached clinical trials. A host of clinically approved small molecules are known Trk receptor modulators, including selective serotonin reuptake inhibitors and tricyclic anti-depressants, which all serve to increase neurotrophin expression (Price, Milne, Sharkey, & Matsuoka, 2007). One small molecule, xaliproden, enhances NGF action and also serves to stimulate 5-

HT_{1a} receptors. It has been shown to improve outcomes in chemotherapy-induced sensory neuropathy but has had limited success in treating Alzheimer's disease-related cognitive decline (Andoh, Sakamoto, & Kuraishi, 2013; Douillet & Orgogozo, 2009). Generally speaking, promoting neurotrophin signaling has not served as a feasible strategy to promote nerve regeneration, which may be the result of other factors that potently suppress neurotrophic signaling. Ultimately, nerve regeneration is a balance of intrinsic and extrinsic cues, where the relative abundance of one cue can dominate the other. This is typified after MI, where an abundance of NGF is present in the heart but nerves do not regenerate into the scar. We now understand that negative growth cues in the extracellular matrix that forms the scar prevents nerve regeneration, much like the scar that forms after spinal cord injury. Therapies to promote nerve regeneration may be best achieved by targeting inhibitory factors of neurotrophin signaling.

IV. Chondroitin Sulfate Proteoglycan roles in axon outgrowth

A. Inhibitory scar tissues

In past decades, examining the factors preventing nerve regeneration following injury has been the focus of many research groups. Much of this work has focused on spinal cord injury, where physical trauma causes complete or partial severance of nerves, resulting in significant physical impairment. The resulting site of injury undergoes a wave of inflammation, which repairs the tissue until homeostasis is reached. The ultimate physical result of this is stable scar tissue, known as the glial scar, that forms and persists long after inflammation is resolved. The glial scar plays a critical role in the healing process, acting as a scaffold for infiltrating astrocytes, monocytes, and other leukocytes

in an effort to resolve the injury (Anderson et al., 2016). This scaffold is composed of a myriad of extracellular matrix proteins including chondroitin sulfate proteoglycans (CSPGs). CSPGs have been appreciated for inhibitory effects on nerve growth for over 30 years, making them a key research focus and therapeutic target to promote axon regeneration (E. J. Bradbury et al., 2002; Busch & Silver, 2007; L. L. Jones, Margolis, & Tuszynski, 2003; McKeon, Schreiber, Rudge, & Silver, 1991; Snow, Lemmon, Carrino, Caplan, & Silver, 1990).

B. CSPG family proteins

CSPGs are a family of proteins characterized by post-translational attachment of glycosaminoglycan (GAGs) side chains to a core protein. The most widely studied proteoglycans in the CNS include; the Letican family (Versican, Brevican, Neurocan, and Aggrecan), Phosphocan, and the structurally distinct protein NG2, also known as CSPG4 (Bandtlow & Zimmermann, 2000). These proteoglycans each have distinct GAG attachment sites, leading to varying degrees of glycosylation, and the non-templated nature of GAGs makes for an incredibly diverse set of proteins.

Adding to this complexity is the further modification of the sugar n-acetyl-galactosamine (Gal-N-Ac) which, along with glucuronic-acid, makes up the sugar backbone of GAGs (Miller & Hsieh-Wilson, 2015). Gal-N-Ac can be modified by covalent addition of a sulfate to the 4^{th} (4S, CS-A) or 6^{th} (6S, CS-C) position hydroxyls of the sugar via sulfotransferase enzymes (Figure 1.12). Specifically, chondroitin-4-sulfotransferase (CHST11) adds 4S to GAGs, while chondroitin-6-sulfotransferase (CHST3) adds 6S to GAGs. GAGs can be tandem sulfated at the 4 and 6 positions of Gal-N-Ac by the 4-

sulfation-dependent 6-sulfotransferase (CHST15), which adds 6S to previous 4-sulfated GAGs (4S,6S, CS-E). Sulfation can also be added to the 2nd position of glucuronic-acid (2S,6S CS-D) (Mencio, Hussein, Yu, & Geller, 2021; Miller & Hsieh-Wilson, 2015). Collectively, these side chains are referred to as CS-GAGs. While some core proteins, including Aggrecan and NG2, have been shown in certain contexts to suppress axon outgrowth; the primary inhibitory effect is thought to come from CS-GAGs (Dou & Levine, 1994; L. S. Sherman & S. A. Back, 2008; Ughrin, Chen, & Levine, 2003).

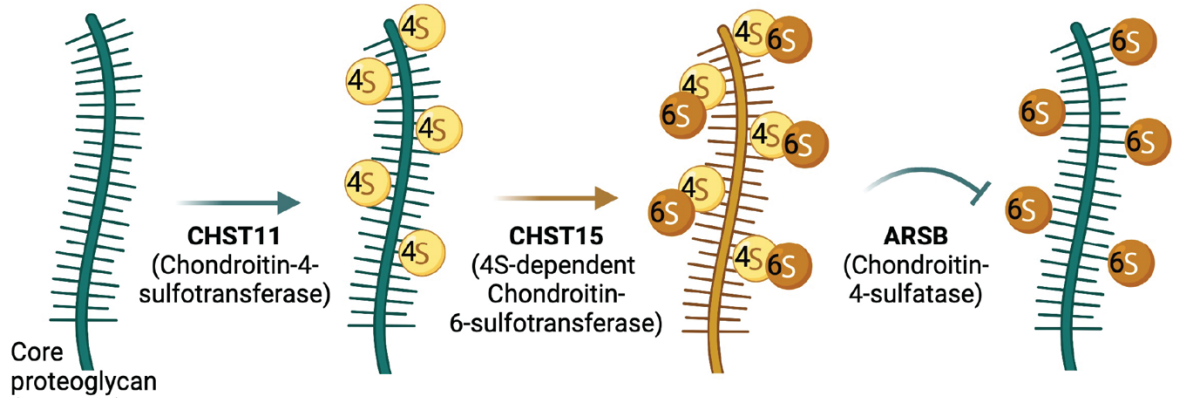

Figure 1.12: Simplified diagram of Chondroitin Sulfate Proteoglycan (CSPG) sulfation patterning by select enzymes. As example, CSPG glycosaminoglycans (CS-GAGs) can be post-translationally modified by sulfation on the sugar N-Acetyl-Galactosamine (Gal-N-Ac) at the 4th position carbon (4S, CS-A) by the chondroitin-4-sulfotransferase (CHST11) or at the 4th and 6th position carbons (4S,6S, CS-E) by 4S-dependent 6-sulfotransferase (CHST15). An endogenously expressed 4-sulfatase, ARSB, can remove 4S in the cytosol, extracellularly, or at the membrane. CS-A and CS-E have been shown to inhibit axon outgrowth in specific disease contexts and neuronal subtypes. ARSB has been shown to promote axon outgrowth in certain contexts as well. We hypothesized that CS-E is the predominant inhibitor of sympathetic axon outgrowth in the infarcted myocardium after an MI.

C. CSPG interacting molecules

CS-GAGs bind many cell surface receptors implicated in axon outgrowth inhibition, including Protein-Tyrosine Phosphatase Receptor Sigma (PTPσ) and Leukocyte Common Antigen Related (LAR) Protein-Tyrosine Phosphatase (Fisher et al., 2011; Shen

et al., 2009b). Additionally, CS-GAGs bind many other molecules including Nogo receptors (NgR1 and NgR3), Semaphorin 5a (Sem5a), Semaphorin 3a (Sem3a), Integrins, EGFR, Trk receptors, as well as NGF (Bhattacharyya, Feferman, & Tobacman, 2014; Dick et al., 2013; Dickendesher et al., 2012; Kantor et al., 2004; Miller & Hsieh-Wilson, 2015). The diverse nature of these interactions is thought to be driven by ionic interactions between negatively charged sulfates on CS-GAGs and positively charged receptor binding domains (Gama et al., 2006).

D. CSPG signaling in axon regeneration

Given the critical role of CSPGs in various pathologies, many groups have examined signaling pathways activated by their stimulation. PTPσ and LAR represent two prominent CSPG-stimulated receptors that affect axon outgrowth via similar downstream signaling pathways (Ohtake, Wong, Abdul-Muneer, Selzer, & Li, 2016). CSPG stimulation of PTPσ/LAR activates the Rho/ROCK kinase pathway, inducing cytoskeletal rearrangements that cause growth cone collapse and inhibit AKT activation to suppress axon outgrowth. Active PTPσ can bind to all Trk receptors, suppressing Trk phosphorylation and downstream neurotrophin signaling, resulting in suppression of axon outgrowth(Faux et al., 2007). This phosphatase activity leads to reduced ERK phosphorylation and subsequently diminishes axon outgrowth (Ohtake et al., 2016). Chemorepulsive stimulation of other CSPG receptors (NgR1, NgR3, Sem3a, Sema5a) suppresses axon outgrowth by similar pathways as PTPσ/LAR, whereas Integrin binding of growth promoting molecules is blocked by CSPGs (Dick et al., 2013; Dickendesher et al., 2012; Kantor et al., 2004; Ohtake & Li, 2015).

E. Prominent roles for Chondroitin Sulfate GAGs

Much debate has surfaced about how specific CS-GAG patterns inhibit axon outgrowth. This debate is primarily due to methodological differences, antibodies used, and subsequent interpretation of results. One thing certain from all reports, is that the injury context and neuronal subtype involved seem to dictate the effect of the CS-GAG. For example, CS-A (4S) is thought to be the primary inhibitor of axon outgrowth after cortical impact and optic nerve crush injury (Pearson, Mencio, Barber, Martin, & Geller, 2018; H. Wang et al., 2008; Yi et al., 2012), while CS-E (4S,6S) has been shown to inhibit axon extension in spinal cord injury and in DRG neurons (Brown et al., 2012; Gilbert et al., 2005). CS-C (6S) has even been shown to *promote* axon outgrowth in the context of spinal cord injury (Lin, Rosahl, Whiting, Fawcett, & Kwok, 2011). It is worth noting that much of our understanding of CS-GAGs comes from the field of neurodevelopment. In development, CSPG sulfation has been shown to regulate neurogenesis(Gates et al., 1995), proper patterning of the retina (Brittis, Canning, & Silver, 1992), axon midline crossing(Pires-Neto, Braga-De-Souza, & Lent, 1998), and assist in proper pathfinding during assembly of the corticospinal tract (Hsu, Stein, & Xu, 2005). In the adult brain, CS-GAGs are enriched the peri-neuronal nets (PNNs) (Deepa et al., 2006), where they augment circuit stability and play a role in suppression of neuronal plasticity (Smith et al., 2015). In addition to the effect of CSPGs on nerves, they have also been shown to play a role in cancer-cell motility, fibrosis and inflammation during colitis, and even in the heart during heart failure (Bhattacharyya, Feferman, Terai, Dudek, & Tobacman, 2017; Suzuki et al., 2016; Suzuki et al., 2017; Watanabe et al., 2015).

F. CSPGs in the heart after Myocardial Infarction

Given the significant body of literature demonstrating the critical role of CSPGs in preventing axon extension, it seemed logical that a similar cue from the extracellular matrix might play a role in the denervation that exists in the cardiac scar after myocardial ischemia-reperfusion injury. Unlike the glial scar, which primarily helps to contain the inflammatory response (Anderson et al., 2016), the cardiac scar plays an additional role in maintaining the rigidity of the heart after MI and ensures adequate left-ventricular function (Fomovsky & Holmes, 2010; Fomovsky, Thomopoulos, & Holmes, 2010). This rigidity is largely accomplished by deposition of collagen, a molecule also known to promote axon extension. The abundance of a growth promoting molecule only suggested the presence of a more potent inhibitor of axon outgrowth, perhaps similar to the glial scar. This led members of our lab to hypothesize and determine that CSPGs were enriched in the cardiac scar, and played a key role in preventing sympathetic axon extension back into the scar (Gardner & Habecker, 2013). This work demonstrated that CSPG interaction with PTPσ was necessary and sufficient to prevent sympathetic nerve growth back into the scar after MI (Gardner et al., 2015). This was an interesting observation on several points. First, the data showed that CSPGs were the key reason for axon outgrowth inhibition, ruling out other ECM molecules enriched in the scar (e.g., low and high molecular weight hyaluronic acid). Second, the data showed that a single CSPG receptor was responsible for mediating this inhibitory response (Gardner & Habecker, 2013). In other nerve injury paradigms, multiple CSPG receptors, including PTPσ and LAR, likely need to be suppressed to achieve complete regeneration (Fisher

et al., 2011; Ohtake et al., 2016; Shen et al., 2009b; Y. Zhang et al., 2005). Finally, the data showed that it was the CS-GAGs specifically that played an inhibitory role in CSPG suppression of sympathetic axon outgrowth. CSPGs treated with chondroitinase ABC (chABC) to remove CS-GAGs from the core protein did not inhibit sympathetic axon outgrowth (Gardner & Habecker, 2013).

The observation that CS-GAGs were the primary inhibitors of growth was not entirely surprising, given the previously mentioned observations that some sulfation patterns of CS-GAGs possess inhibitory activity (Brown et al., 2012; Gilbert et al., 2005; Pearson et al., 2018; H. Wang et al., 2008). In hindsight, what was surprising is that the main core proteoglycan enriched in the scar after MI is NG2 (Tian et al.). NG2 has been shown to mediate much of its inhibitory effect via the core proteoglycan despite possessing CS-GAGs (Dou & Levine, 1994; Ughrin et al., 2003). The data to follow in Chapter 2 of this dissertation suggest that in the case of the cardiac scar, NG2 elicits its effect primarily through attached CS-GAGs. The fact that CS-GAGs play such a critical role in the scar is in line with our previous observations that inhibiting PTPσ in an animal model of MI restored axon outgrowth (Gardner & Habecker, 2013; Gardner et al., 2015). The extracellular domain of PTPσ binds with high affinity to heavily sulfated CS-GAGs, specifically CS-E (Brown et al., 2012). CS-GAGs bind PTPσ and physically prevent its ability to form homodimers, resulting in active PTPσ monomers. Dimeric PTPσ intracellular phosphatase domain is inhibited by homotypic interactions between wedge domains of other PTPσ molecules (Majeti, Bilwes, Noel, Hunter, & Weiss, 1998; Shen et al., 2009b; Wu et al., 2017). Interestingly, this strategy was used when designing the

therapeutic Intracellular Sigma Peptide (ISP), which disrupts PTPσ interactions but does not inhibit phosphatase activity (Lang et al., 2015). By contrast, Heparin sulfate proteoglycans (HSPGs) are thought to bind and cluster PTPσ molecules together, preventing phosphatase activity on its targets (Aricescu, McKinnell, Halfter, & Stoker, 2002). In the absence of intervention, sulfated CSPGs deposited in the ECM interact in-trans with PTPσ receptors on the surface of extending axons (Lang et al., 2015). This enables monomeric PTPσ activity in the membrane with target receptors like TrkA, TrkB, and TrkC (Faux et al., 2007). PTPσ phosphatase activity on Trk receptors ultimately reduces Trk phosphorylation, blocking neurotrophin signaling, suppressing axon outgrowth(Faux et al., 2007) via augmentation of the cytoskeleton, and ultimately leading to growth cone collapse. While playing a crucial role in disease states like SCI, TBI, and MI, this interaction also enables appropriate axon guidance during development and in maintaining PNN structure in the brain (Deepa et al., 2006; Smith et al., 2015). However, for the purposes of this document we will focus on the more deleterious side of these interactions following MI (Figure 1.13).

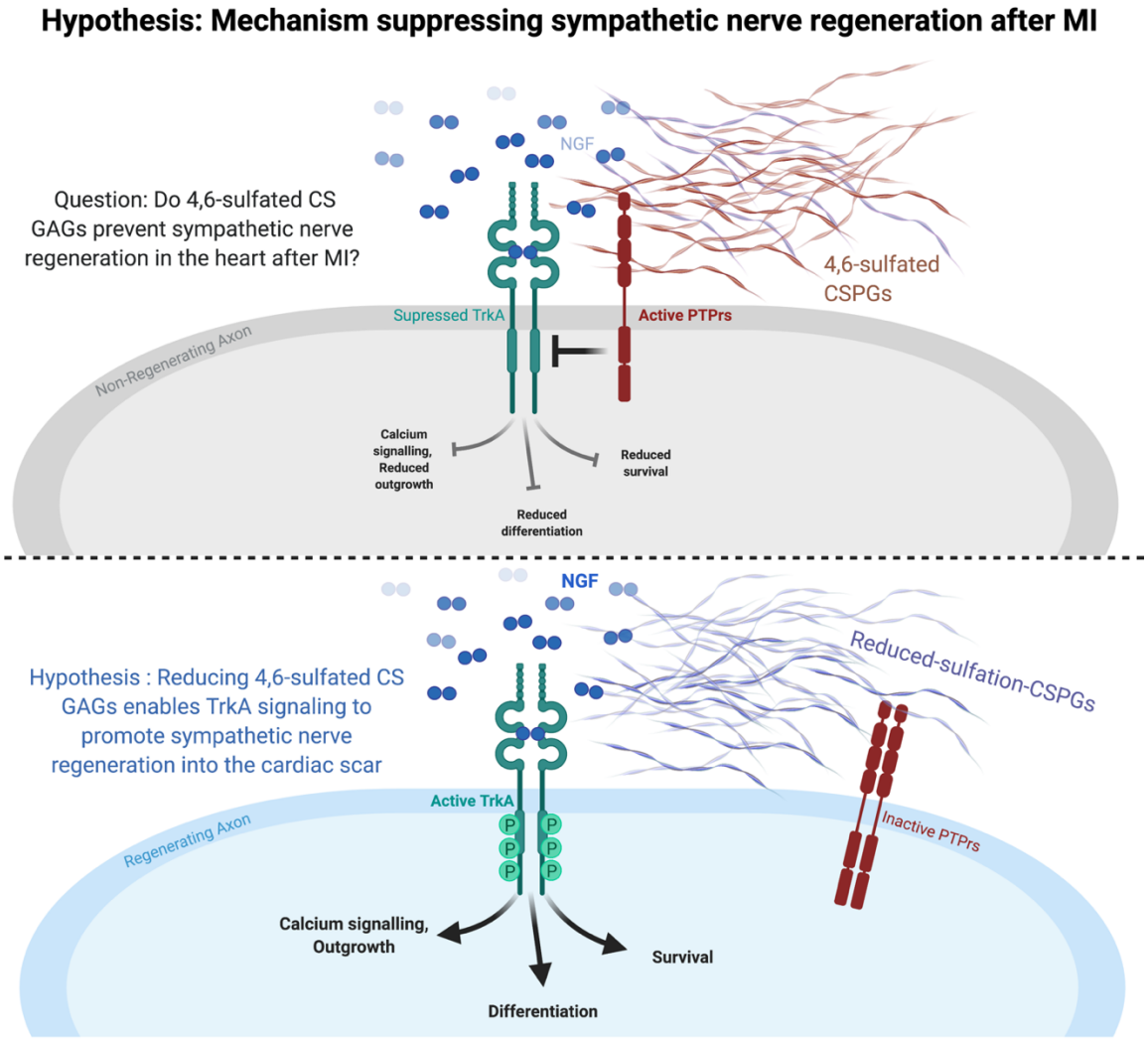

Figure 1.13: CSPG sulfation hypothesis overview in the context of regenerating sympathetic nerves in the presence of highly 4,6-sulfated CSPGs in the infarcted myocardium. Top panel, 4,6-sulfated CSPGs in the infarcted myocardium interact with PTPσ on the tip of regenerating sympathetic axons leading to PTPσ phosphatase activity. PTPσ activity downregulates active NGF-bound TrkA signaling complexes, blocking sympathetic axon extension into the infarcted myocardium. Lower Panel, reducing 4,6-sulfated CSPGs in the infarcted myocardium prevents activation of PTPσ which enables continued NGF-TrkA signaling, subsequently promoting sympathetic axon extension in the infarcted myocardium.

Perhaps the most critical finding from previous work in the Habecker Lab is the discovery that inhibiting CSPG signaling restored sympathetic nerves to the infarct and normalized cardiac electrophysiology after MI (Gardner et al., 2015). As mentioned earlier, reinnervation of the infarct has been hypothesized as a strategy to reduce post-

MI arrhythmias. Data from our animal model of myocardial infarction suggests that restoration of sympathetic nerves reduces arrhythmias in the heart, as measured by generation of premature ventricular complexes (PVCs) and normalizes calcium handling in the post-MI heart (Gardner et al., 2015). The process by which restored nerves in the infarct normalize electrophysiology is not well understood, but it is likely that differentiated myofibroblasts that replace much of the necrotic cardiomyocytes are able to passively propagate action potentials and reduce the electrically insulating properties of the scar tissue (Rog-Zielinska, Norris, Kohl, & Markwald, 2016). Much remains to be understood on this topic but the results clearly demonstrate sympathetic nerve restoration as a viable strategy to normalize cardiac electrophysiology after MI.

V. Dissertation overview

The overarching goal surrounding the work summarized in this dissertation is aimed at improving our understanding of the molecular basis for CSPG suppression of sympathetic nerve regeneration after MI. While previous work showed that ISP might be a therapeutic strategy to promote nerve regeneration in the heart, peptide-based therapeutics have downsides in terms of cost, administration, and persistence of therapeutic effects. This led us to attempt developing a small-molecule therapeutic that could replicate these results. What follows in Chapter 4 is the description of the *in vitro* work to characterize novel small molecules HJ-01 and HJ-02, which promote sympathetic axon outgrowth across CSPGs. These novel small molecules elicit effects through disruption of PTPσ-Trk interactions, thereby promoting axon outgrowth and growth signaling. Work that is documented elsewhere demonstrates how these small molecules

promote nerve regeneration after MI *in vivo (Sepe, 2022).* In Chapter 2 of this dissertation, the molecular basis of CSPG inhibition is explored in greater detail. This work demonstrates how specific sulfation patterns on CS-GAGs (most likely CS-E) inhibits sympathetic axon outgrowth. We show that this CS-GAG sulfation pattern is upregulated after MI and that reducing CS-E by transient knockdown of the CSPG 4,6-sulfation enzyme *Chst15,* sympathetic nerve regeneration in the infarct is restored. This work provides two new potential mechanisms to restore nerves in the cardiac scar. Chapter 3 describes the interesting phenomena of spontaneous nerve regeneration in our murine MI model, wherein aged animals eventually regrow axons in the infarct. This work also demonstrates that early restoration of sympathetic neurotransmission in the heart with ISP has no deleterious effects on cardiac function in aged MI animals. Chapter 5 and appendix A, describe two “misadventures” during this dissertation, which hopefully provide insight for future experiments aimed at understanding CSPG signaling and sympathetic nerve regeneration in the heart after MI.

Chapter 2

Chondroitin Sulfate Proteoglycan 4,6 sulfation regulates sympathetic nerve regeneration after myocardial infarction

Matthew R. Blake BS, Diana C. Parrish BS, Melanie A. Staffenson BS, Shanice Sueda, William R. Woodward PhD, Beth A. Habecker PhD

As of April 5, 2022 this manuscript is currently under review at *eLife*

Acknowledgements

The authors would like to thank Kevin Wright Ph.D for crucial comments on the manuscript and Ryan Gardner Ph.D for critical insight during the early stages and development of this project. We would also like to thank Tammi Howard for early technical assistance on this project. This work was supported by NIH F31HL152490 (MRB), AHA 20PRE35210768 (MRB), the Steinberg Endowment for Graduate Education (MRB), Portland State University EXITO Scholars Program funds (SS), and NIH R01 HL093056 (BAH).

Abstract

Sympathetic denervation of the heart following myocardial infarction (MI) is sustained by chondroitin sulfate proteoglycans (CSPGs) in the cardiac scar, and denervation predicts risk of sudden cardiac death. Blocking CSPG signaling restores sympathetic axon outgrowth into the cardiac scar, decreasing arrhythmia susceptibility. Axon growth inhibition by CSPGs is thought to depend on the sulfation status of the glycosaminoglycans (CS-GAGs) attached to the core protein. Tandem sulfation of CS-GAGs at the 4th (4S) and 6th (6S) positions of n-acetyl-galactosamine inhibits outgrowth in several types of neurons within the central nervous system, but it is not known if sulfation is similarly critical during peripheral nerve regeneration. We asked if CSPG sulfation prevented sympathetic axon outgrowth. Sympathetic neurite outgrowth across purified CSPGs is restored *in vitro* by reducing 4S with the 4-sulfatase enzyme Arylsulfatase-B (ARSB). Additionally, we co-cultured cardiac scar tissue with sympathetic ganglia *ex vivo* and found that reducing 4S with ARSB restored axon outgrowth to control levels. We examined levels of the enzymes responsible for adding and removing sulfation to CS-GAGs by western blot to determine if they were altered in the left ventricle after MI. We found that CHST15 (4S dependent 6-sulfotransferase) was upregulated, and ARSB was downregulated after MI. Increased CHST15 combined with decreased ARSB suggests a mechanism for production and maintenance of sulfated CSPGs in the cardiac scar. We altered tandem sulfated 4S,6S CS-GAGs *in vivo* by transient siRNA knockdown of *Chst15* and found that reducing 4S,6S restored Tyrosine Hydroxylase (TH) positive sympathetic nerve fibers in the cardiac scar after MI and reduced arrhythmias. Overall, our results suggest that modulating CSPG-sulfation after

MI may be a therapeutic target to promote sympathetic nerve regeneration in the cardiac scar and reduce post-MI cardiac arrhythmias.

I. Introduction

Sympathetic denervation following myocardial infarction (MI) is well documented in both animal models and in humans, and highly predictive of ventricular arrhythmias and sudden cardiac death (Boogers et al., 2010; Fallavollita et al., 2014; Nishisato et al., 2010). Following an early period of axon degeneration after MI, sympathetic nerves grow back through undamaged myocardium but do not enter the scar due to the presence of chondroitin sulfate proteoglycans (CSPGs) (Gardner & Habecker, 2013). This heterogeneity in sympathetic innervation increases risk for arrhythmias and sudden cardiac death, and blocking sympathetic transmission with beta receptor antagonists or surgical sympathectomy prevents arrhythmias and prolongs life (Herring et al., 2019). However, beta blockers and surgical sympathectomy have unwanted side effects and a therapeutic intervention restoring sympathetic innervation in the cardiac scar by modulating CSPGs may improve health outcomes for patients suffering post-MI arrhythmias.

CSPGs are a diverse family of extracellular matrix proteins modified by chondroitin sulfate (CS) side chains that inhibit nerve regeneration in numerous injury paradigms including MI, spinal cord injury, and traumatic brain injury (Brown et al., 2012; Gardner & Habecker, 2013; Lang et al., 2015; McKeon, Jurynec, & Buck, 1999; Miller & Hsieh-Wilson, 2015; Yi et al., 2012). CSPGs are heterogeneous but all are composed of a core

protein that is covalently linked to repeating disaccharide side chains known as glycosaminoglycans (GAGs). While some evidence suggests that the CSPG core protein itself plays a role in regulating axon outgrowth (Dou & Levine, 1994; Ughrin et al., 2003), the primary effect is thought to occur via the post-translational addition of sulfate to GAGs (Mencio et al., 2021; Miller & Hsieh-Wilson, 2015). CS-GAGs in scar tissues bind CSPG receptors like PTPσ (protein tyrosine phosphatase receptor sigma) on regenerating axons (C. H. Coles et al., 2011; Shen et al., 2009b). CSPG sulfation is attached to specific locations of the CS-GAG by sulfotransferase enzymes, yielding unique structures that differentially affect axon outgrowth. Specifically, 4-sulfation (4S) and 6-sulfation (6S) of n-acetyl-galactosamine are critical regulators of axon outgrowth (Brown et al., 2012; Gilbert et al., 2005; H. Wang et al., 2008). 4S CS-GAGs are produced by the chondroitin-4-sulfotransferase, CHST11, while 4,6 tandem sulfated GAGs (4S,6S) are produced by a 4S dependent chondroitin-6-sulfotransferase, CHST15 (Miller & Hsieh-Wilson, 2015). 4S CS-GAGs can also be removed by an endogenously expressed 4-sulfatase, Arylsulfatase-B (ARSB) (Figure 2.1A) (Pearson et al., 2018; H. Wang et al., 2008). Evidence from spinal cord injury (SCI) and traumatic brain injury (TBI) indicate that tandem sulfated 4S,6S CS-GAGs potently suppress axon outgrowth (Brown et al., 2012; Gilbert et al., 2005). Removal of all CS-GAGs from cardiac scar tissue by treatment with the enzyme chondroitinase ABC (chABC) restores sympathetic axon outgrowth *in vitro* (Gardner & Habecker, 2013) but it remains unknown whether CSPG sulfation is critical to inhibit regeneration of peripheral nerves.

Here we show that 4,6 tandem sulfated CSPGs are enriched in the cardiac scar after MI, and that this sulfation is important for preventing nerve regeneration in the heart. Sulfation-related enzymes are altered in the heart after MI, and reducing sulfation of CS-GAGs by transient siRNA knockdown of *Chst15* promotes reinnervation of the cardiac scar. Reinnervation decreases isoproterenol-induced arrhythmias.

II. Results

A. 4,6-sulfation of CS-GAGs increased in the heart after MI

To establish whether CSPG sulfation occurs after MI we used antibodies specific to 4S and 6S CS-GAGs (Yi et al., 2012) to compare CSPG sulfation in unoperated left ventricle to day 14 post-MI scar tissue. Day 14 represents a time point when scar tissue is relatively stable and sympathetic nerves are excluded from entering the scar. Myocardial infarction led to increased 4,6 sulfation of CSPGs in the cardiac scar (Figure 2.1B-D).

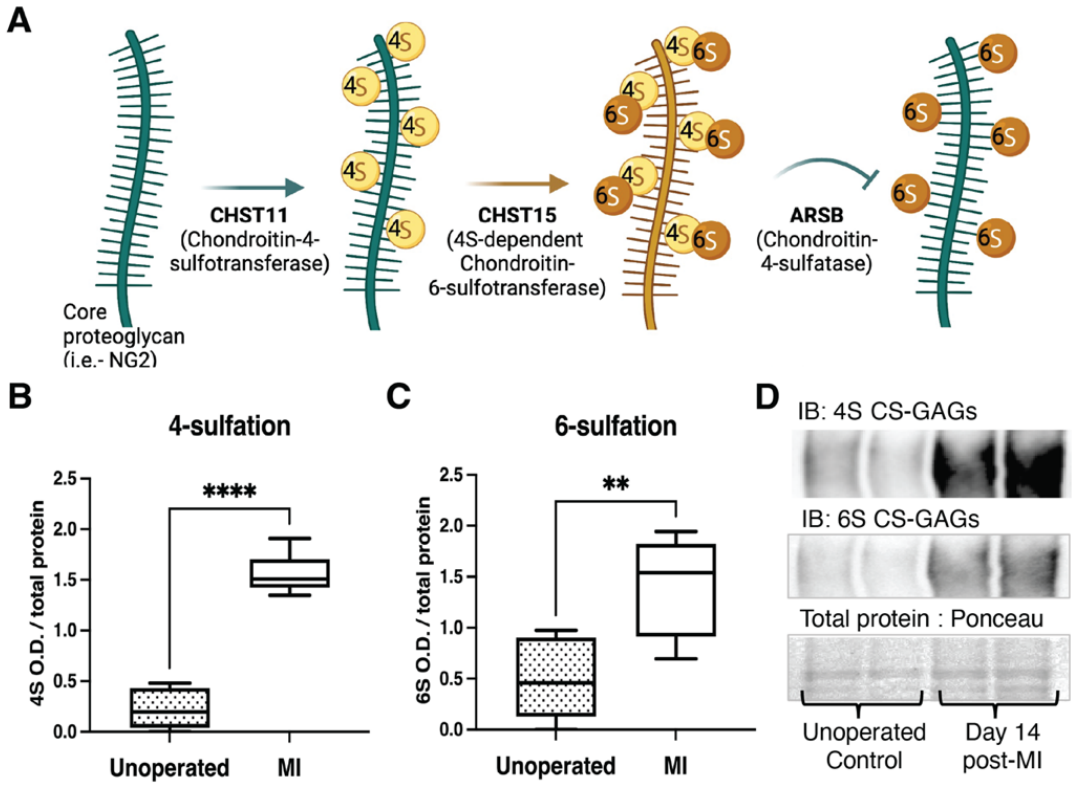

Figure 2.1: CSPG 4,6 Sulfation increases in the cardiac scar after MI. **(A)** CSPG-sulfation patterning schematic with key enzymes. **(B)** 4-sulfation (4S CS-GAGs) or **(C)** 6-sulfation (6S CS-GAGs) quantification assessed by western blot in the healthy myocardium (unoperated) or cardiac scar 14 days after MI (MI). Quantification of n=6 animals per treatment group, statistics; student t-test (Welch's test), **p-value<0.01, ****p-value<0.0001 **(D)** Example blot images for 4S CS-GAGs, 6S CS-GAGs, and total protein from two unoperated and two MI animals.

B. Reducing 4-sulfation with ARSB promotes sympathetic neurite outgrowth in vitro

To test whether 4-sulfation of CS-GAGs prevented neurite outgrowth across CSPGs we enzymatically removed 4S from purified CSPGs using the 4-sulfatase, ARSB. An effective ARSB dose was identified in pilot studies to remove 4S while leaving 6S intact (Figure 2.8). Sympathetic neurons were then grown on CSPGs treated with vehicle or ARSB. Sympathetic neurite extension across untreated CSPGs was suppressed 40 hours post-plating compared to laminin alone, while ARSB treatment restored neurite outgrowth in a dose-dependent manner (Figure 2.2A,B). These results indicate that 4-sulfation of CS-GAGs inhibits sympathetic neurite extension.

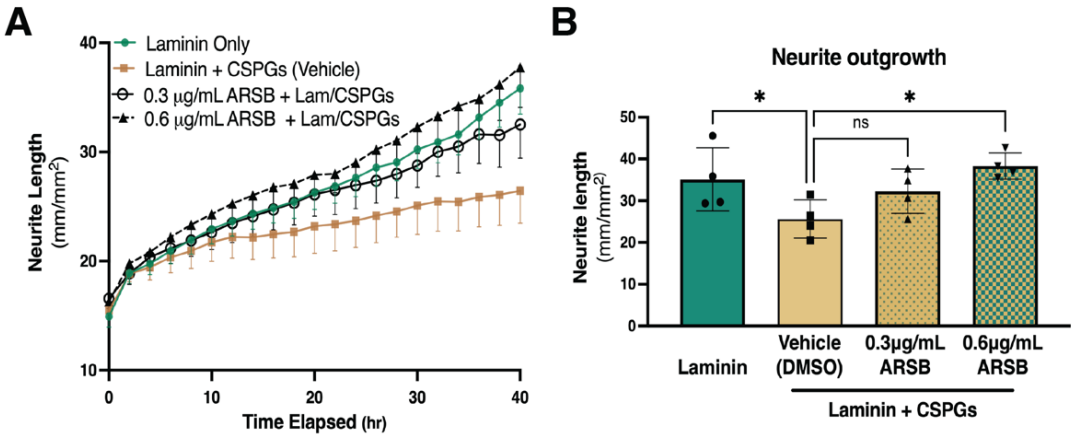

Figure 2.2: Reducing CS-GAG 4-sulfation promotes sympathetic neurite outgrowth *in vitro*. **(A)** Example of neurite outgrowth experiment with ARSB. Data are mean neurite-length ± SD at 9 locations per well and 3 wells per condition. **(B)** Removal of 4-sulfation with ARSB restores neurite outgrowth to control levels. Quantification of dissociated sympathetic neurite length at 40 hours post-plating on indicated plate coatings. Statistics; one-way ANOVA, (Dunnett's post-test). All comparisons made to neurite outgrowth on Laminin + CSPG coated wells, ns - not significant, *p<0.05, n=4 experiments.

C. Reducing 4-sulfation of cardiac scar tissue with ARSB restores sympathetic axon outgrowth ex vivo

We treated cardiac scar tissue with ARSB to test whether removing 4-sulfation from CS-GAGs in cardiac scar tissue could restore sympathetic axon outgrowth in explant co-cultures. Ganglion explants co-cultured (Figure 2.3A) with unoperated left ventricle (Figure 2.3B) displayed uniform axon outgrowth in all directions while explants cultured alongside cardiac scar tissue (10-14 days post-MI) exhibited shorter axons growing in the direction of the scar tissue (Figure 2.3C). Interestingly, ARSB treatment (0.6µg/mL) of scar tissue fully restored axon outgrowth towards the scar (Figure 2.3D), while growth away from the scar tissue was normal in all conditions (Figure 2.3E). These data suggest that reducing 4-sulfation of CS-GAGs in the cardiac scar is sufficient to enable sympathetic axon regeneration.

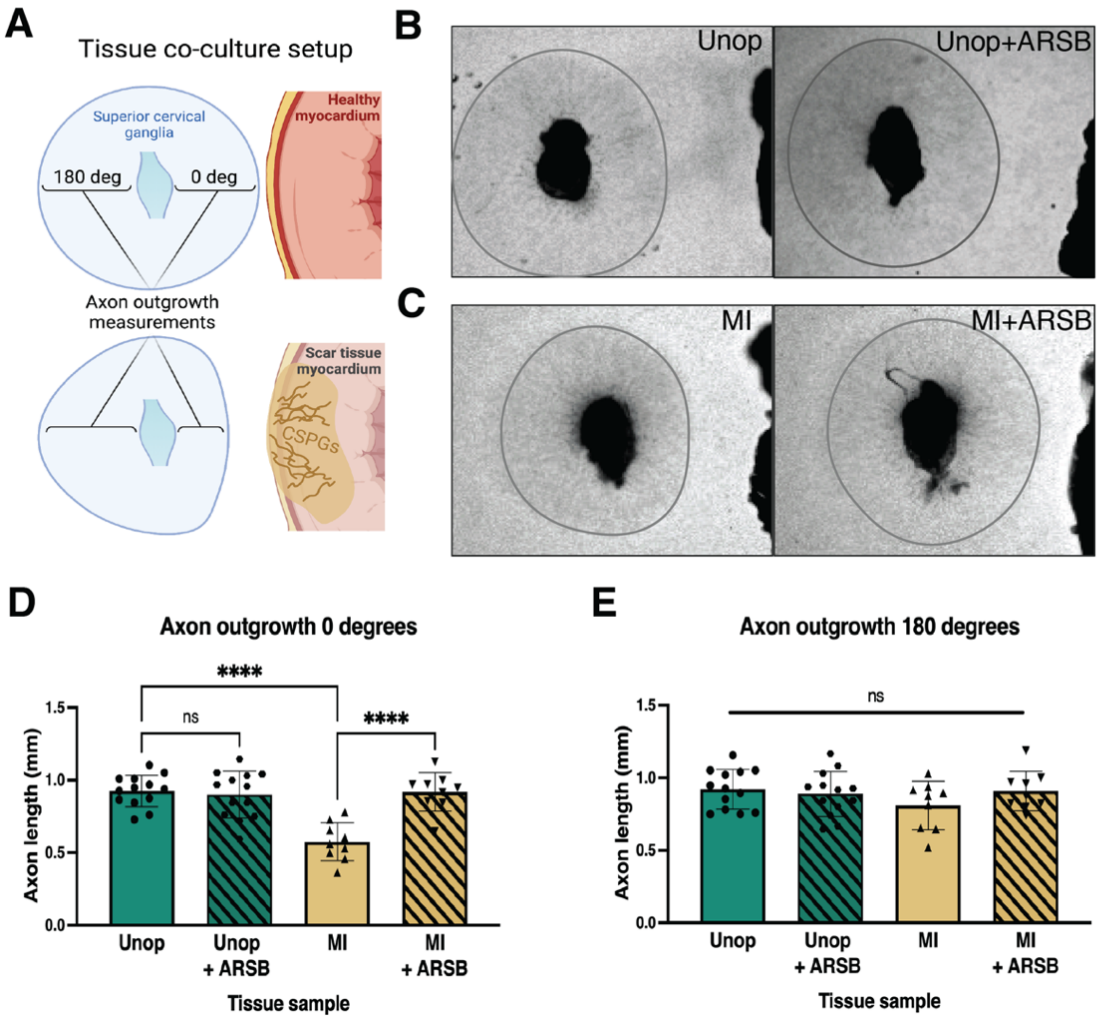

Figure 2.3: Reducing CS-GAG 4-sulfation in cardiac scar tissue *ex vivo* restores sympathetic axon outgrowth. **(A)** Explant co-culture schematic. Ganglion axon extension towards (0 degree) and away from (180 degree) myocardium was measured. **(B)** Example images of ganglia axon outgrowth in the presence of healthy LV tissue (Unop) or **(C)** cardiac scar tissue (MI) treated with or without ARSB. Gray circle approximates boundary of axon extension 48 hours after plating. **(D)** Quantification of ganglion axon outgrowth towards myocardium of either healthy tissue (Unop) or scar tissue (MI) treated with vehicle (5% DMSO) or ARSB (0.6µg/mL). **(E)** Quantification of ganglion axon outgrowth away from myocardium of either healthy tissue (Unop) or scar tissue (MI) treated with vehicle (5% DMSO) or ARSB (0.6µg/mL). Statistics for D, E; one-way ANOVA (Dunnett's post-test), comparisons made to vehicle treated MI tissue; ns - not significant, $p<0.0001$, n=13 animals control tissue and n=9 MI tissue.

D. Expression of CSPG sulfation enzymes is altered after MI

To understand the mechanisms by which CS-GAG sulfation increases after MI we examined protein levels of three critical CSPG sulfation enzymes, comparing post-MI

expression to unoperated left ventricle. We examined chondroitin-4-sulfotransferase CHST11, 4S-dependent chondroitin-6-sulfotransferase CHST15 (4,6 tandem sulfation enzyme), and 4-sulfatase ARSB (Figure 2.1A). CHST11 levels decreased significantly within 24 hours, persisting until day 7 (Figure 2.4A,D), while CHST15 was increased significantly at days 7 and 14 post-MI (Figure 2.4B,D). ARSB levels decreased significantly by day 3 and remained low through day 14 (Figure 2.4C,D).

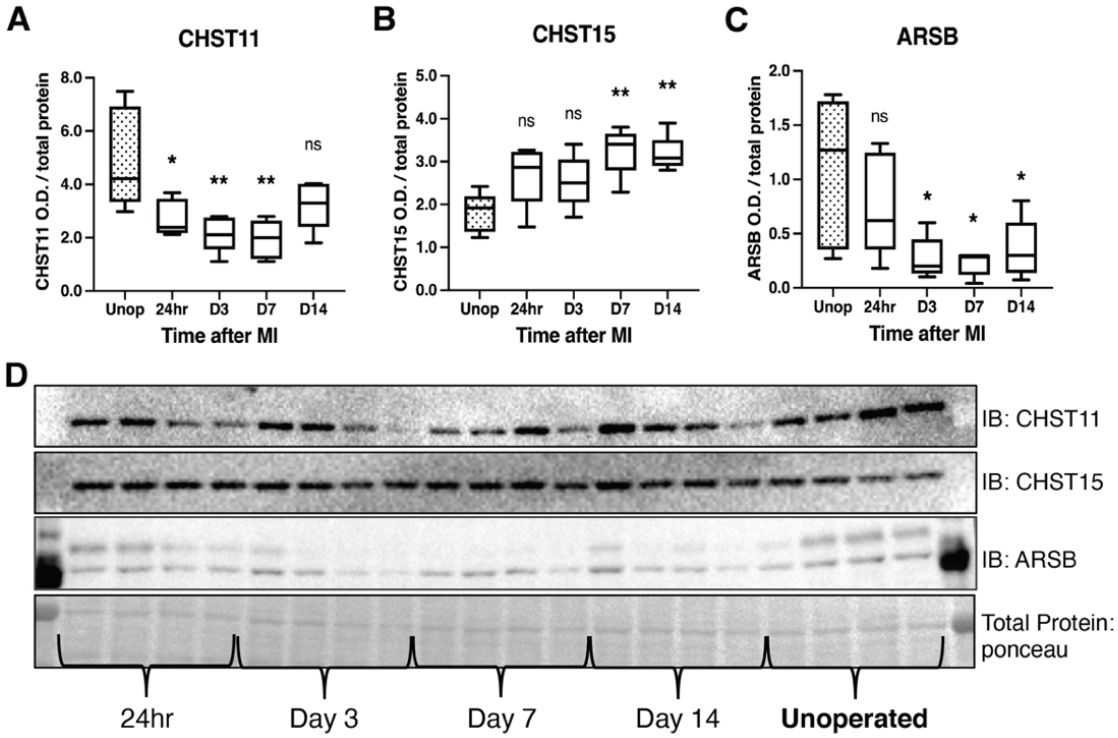

Figure 2.4: CSPG-sulfation enzyme expression is altered after MI. Western blot quantification of protein expression for **(A)** chondroitin-4-sulfotransferase (CHST11), **(B)** chondroitin-6-sulfotransferase (CHST15) and, (**C)** 4-sulfatase (ARSB) protein expression in control left-ventricle (Unop), or in the days after MI (24hr, D3, D7, or D14). Statistics; one-way ANOVA (Dunnett's post-test); ns- not significant, *p-value<0.05, **p-value<0.01, comparisons to unoperated tissue, n=5 animals per group. **(D)** Example western blot images for CSPG-sulfation enzymes.

In light of protein changes in CSPG sulfation enzymes after MI, we examined CS-GAG sulfation at these same time points. 4S and 6S CS-GAGs are significantly increased in the infarct by day 7 post-MI extending through day 14 (Figure 2.5A,B,E). We also asked

if the CSPG core protein NG2 (also called CSPG4) was altered after MI, and found that NG2 was increased in the infarct by 7 days after MI (Figure 2.5C,E). Thus, core proteins and sulfation of CS-GAG side chains are both in greater abundance. We chose to look at NG2 because it was prominently expressed in a recent glycoproteomics analysis of cardiac scar tissue whereas another commonly studied core proteoglycan, Aggrecan, was not detected (Tian et al., 2014). In an effort to better understand how this process may be coordinated, we examined the expression of a key wound healing regulator, Galectin-3, which has also been connected to CSPG sulfation and ARSB expression (Bhattacharyya et al., 2020; Bhattacharyya et al., 2017; Bhattacharyya et al., 2014; Bhattacharyya et al., 2015). Galectin-3 was increased significantly by 24 hours after MI, which may contribute to altered expression of CSPG sulfation enzymes at later time points (Figure 2.5D,E). These data suggest that increased CHST15 and decreased ARSB expression contribute to increased 4,6 sulfation of CS-GAGs observed by day 7 post-MI.

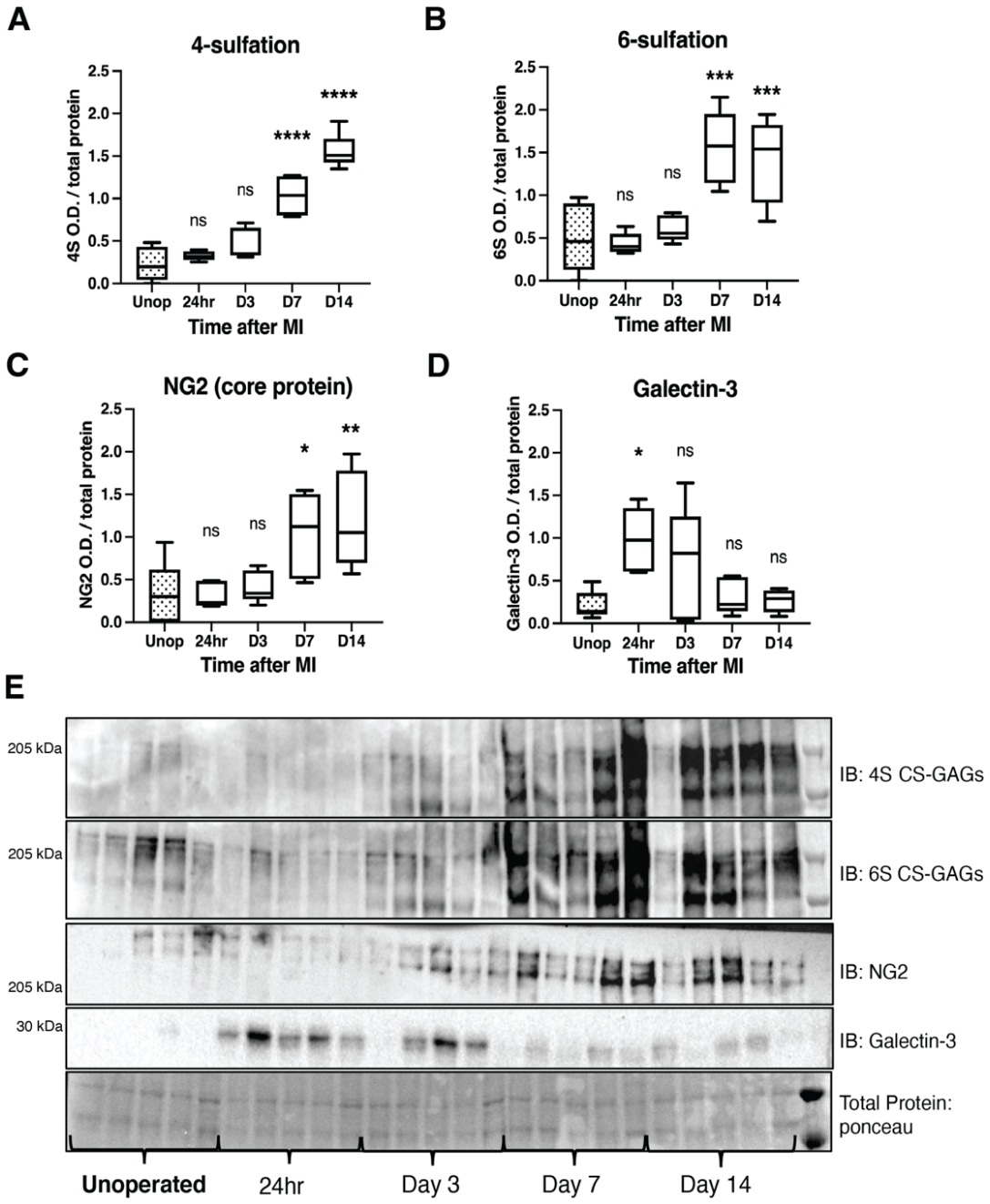

Figure 2.5: Time course of CSPG sulfation and core protein expression after MI in cardiac scar tissue. Western blot quantification of **(A)** 4-sulfation (4S CS-GAGs), **(B)** 6-sulfation **(**6S CS-GAGs), **(C)** NG2 core protein, and **(D)** Galectin-3 in the days after MI. Statistics; one-way ANOVA (Dunnett's post-test), ns- not significant, *p-value<0.05, **p-value<0.01, ***p-value<0.001, ****p-value<0.0001, comparisons to unoperated tissue, n=5 animals per group. **(E)** Example western blot images of A-D.

E. siRNA knockdown of Chst15 reduces 4,6 tandem sulfation of CSPGs and restores sympathetic axons in the cardiac scar after MI

To determine if CSPG sulfation suppresses sympathetic nerve regeneration after MI we decreased 4,6-tandem sulfated CS-GAGs *in vivo* by reducing the expression of the *Chst15* gene using silencing RNA (siRNA). After identifying siRNA that decreased *Chst15* mRNA in myoblast-like C2C12 cells (Figure 2.9A,B), we tested the efficacy of our *Chst15* siRNA *in vivo*. Intravenous delivery of 100*μ*g si*Chst15* reduced CHST15 protein compared to non-targeting control siRNA (Figure 2.9C). Mice were then treated with 100*μ*g si*Chst15* on days 3, 5, and 7 post-MI, leading to a significant reduction in 4S,6S CS-GAGs. Specifically, si*Chst15* reduced the amount of 6S present 10 days post-MI compared to non-targeting siRNA control (Figure 2.6A). By 10 days after MI, CHST15 protein levels had returned to normal suggesting that transient knockdown of CHST15 is sufficient to alter 4,6 sulfation of CS-GAGs (Figure 2.9D,E). Interestingly, si*Chst15* knockdown led to increased NG2 core protein expression compared to non-targeting siRNA control (Figure 2.6C). The sympathetic neuron marker Tyrosine Hydroxylase (TH), was increased significantly in cardiac scar tissue from si*Chst15* treated animals compared to non-targeting siRNA control animals (Figure 2.6D), suggesting successful sympathetic reinnervation of the cardiac scar. Neuronal norepinephrine (NE) content was not increased (Figure 2.9F), consistent with previous studies showing regulation of NE synthesis and reuptake by inflammatory cytokines (Parrish et al., 2010).

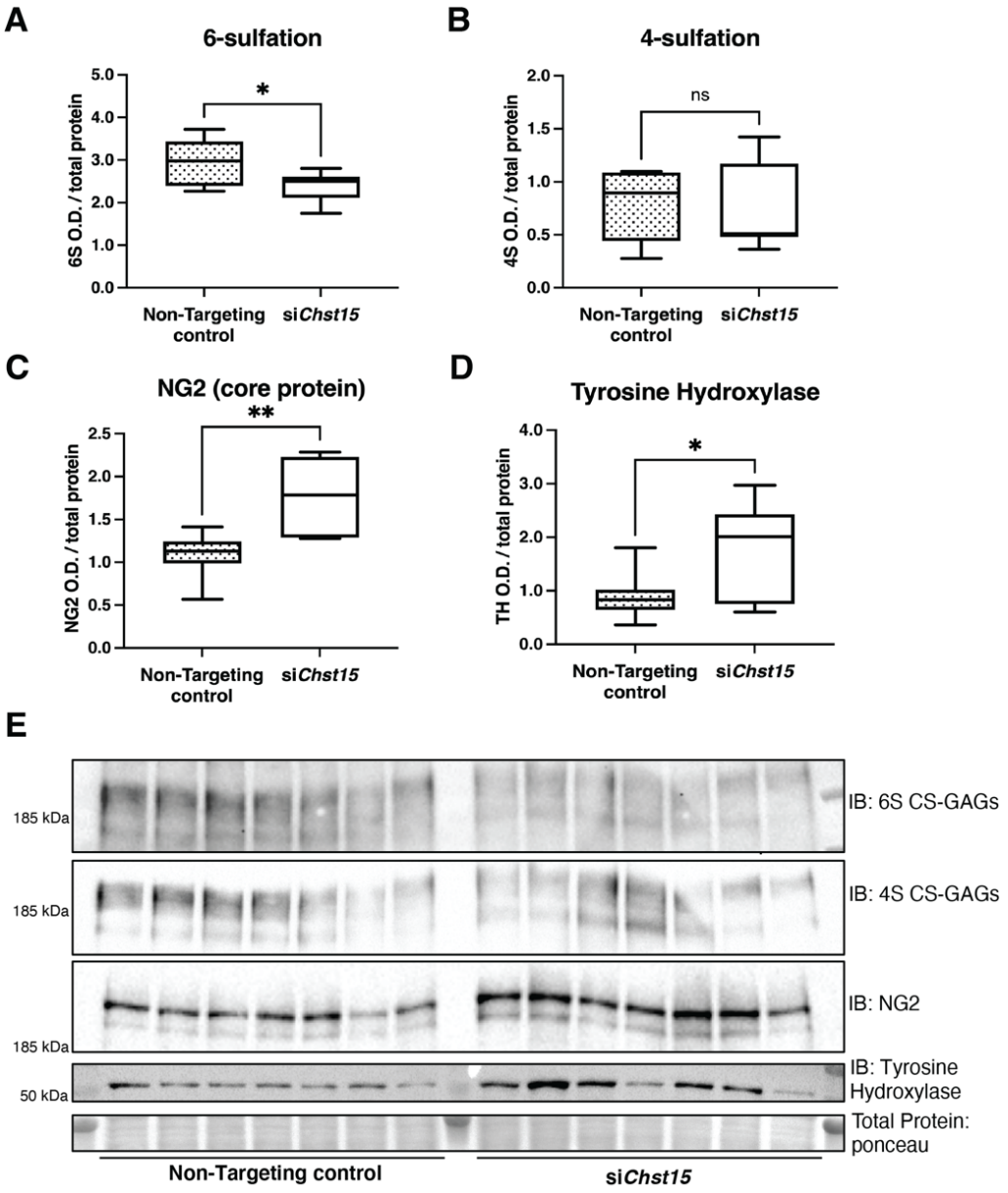

Figure 2.6: Reducing CS-GAG 4,6 tandem-sulfation *in vivo* promotes sympathetic nerve regeneration into the cardiac scar after MI. Western blot quantification of **(A)** 6-sulfation (6S CS-GAGs), **(B)** 4-sulfation (4S CS-GAGs), **(C)** NG2 core protein and, **(D)** the sympathetic neuron marker Tyrosine Hydroxylase (TH) in the cardiac scar after transient *Chst15* knockdown or treatment with a non-targeting siRNA control. Tissue was collected 10 days after MI, n=7 animals per group; student t-test (Welch's test), ns - not significant, *p-value<0.05, **p-value<0.01. **(E)** Western blot images of A-D.

To ensure that reinnervation of the cardiac scar occurred after *Chst15* knockdown we examined the cardiac scar (labeled by fibrinogen) for TH positive sympathetic nerve

fibers by immunohistochemistry (IHC). IHC analysis in animals treated with a non-targeting siRNA control showed clear denervation of the infarct (Figure 2.7A) compared to the peri-infarct region adjacent to the scar (Figure 2.7B). Animals treated with an siRNA targeting *Chst15* had restored TH positive fibers in the infarct (Figure 2.7C) at the same innervation density as the peri-infarct region (Figure 2.7D). TH innervation density was significantly higher in the infarct of *Chst15* targeted animals compared to non-targeting siRNA treated animals (Figure 2.7E). Cardiac scar size was examined between the two groups and no significant difference existed (Figure 2.7G,H). To examine whether restoration of nerves reduced arrhythmia susceptibility we examined arrhythmias by ECG after administration of the β-agonist Isoproterenol(Gardner et al., 2015). Restoration of nerves with *Chst15* siRNA treatment reduced arrhythmias when compared to non-targeting siRNA control treated animals (Figure 2.7F). These results indicate that reducing 4,6 tandem sulfated CS-GAGs in the cardiac scar after MI promotes sympathetic nerve regeneration back into the cardiac scar and reduces arrhythmia susceptibility after MI.

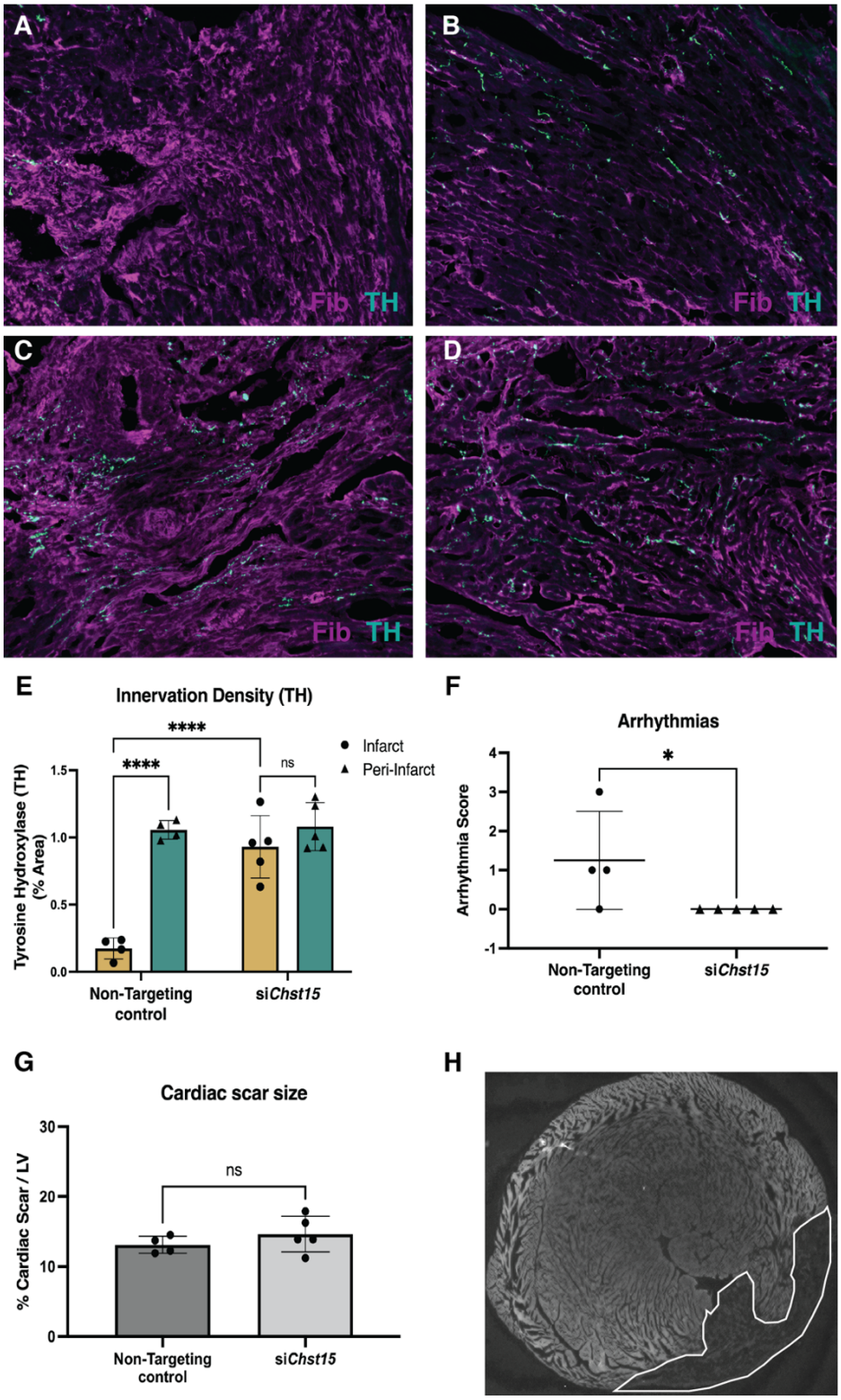

Figure 2.7: Reducing 4,6 tandem-sulfation of CS-GAGs *in vivo* promotes sympathetic nerve regeneration into the cardiac scar. Fibrinogen was used to label scar (magenta) and TH was used to label sympathetic neurons (cyan). Example image of **(A)** denervated infarct in non-targeting control treated animal versus **(B)** normal density of TH+ fibers in the peri-infarct region adjacent to the scar. Systemic delivery of siRNA against *Chst15* post-MI restored TH+ fiber

density in **(C)** the cardiac infarct similarly to **(D)** the peri-infarct region. **(E)** Quantification of TH innervation density (% area, 20x field of view) 10 days after MI. n=4 animals for non-targeting controls and n=5 for *Chst15* siRNA treated animals. Two-way ANOVA, Tukey's post-test to compare all groups, select comparisons shown, ns - not significant, ****p-value<0.0001. **(F)** Arrhythmia scores based on the most severe arrhythmia observed in each heart after injection of isoproterenol and caffeine (0=no PVCs, 1=single PVCs, 2=bigeminy or salvos, 3= non-sustained ventricular tachycardia) See methods for details. Treatment with siRNA against *Chst15* reduced arrhythmias compared to non-targeting controls. n=4 animals for non-targeting controls and n=5 animals for *Chst15 siRNA*. Statistics; student t-test (Mann-Whitney test), *p<0.05. **(G)** Cardiac scar size assessed as a % area of total left ventricle (LV) area was unaltered in *Chst15* siRNA treated animals compared to non-targeting controls. Quantification of n=4 animals for non-targeting controls and n=5 for *Chst15 siRNA* treated animals. Statistics; student t-test (Welch's test), ns - not significant. **(H)** Example 2x image of cardiac scar in *Chst15* siRNA treated heart using autofluorescence, absence of autofluorescence indicates region of the infarct, outlined in white.

III. Discussion

This study investigated the role of CS-GAG side chain sulfation in preventing sympathetic axon regeneration in the heart after MI. We found that the CSPGs present in the cardiac scar after ischemia-reperfusion were enriched with sulfation at the 4 and 6 positions of CS-GAGs, which is often referred to as chondroitin sulfate E (CS-E) (Miller & Hsieh-Wilson, 2015). CS-E inhibits the outgrowth of several types of neurons in the CNS (Brown et al., 2012; Gilbert et al., 2005), and our data indicate that it also prevents growth of sympathetic axons, since decreasing either 4 or 6 sulfation allowed axon regeneration. Nerve regeneration was confirmed by histology and by expression of the neuronal protein Tyrosine Hydroxylase in cardiac scar tissue. Reinnervation throughout the left ventricle decreased isoproterenol induced arrhythmias, consistent with previous studies targeting the CSPG receptor PTPσ (Gardner et al., 2015).

The core protein NG2 is an important source of CSPGs in the cardiac scar (Tian et al., 2014), and there is evidence that the NG2 core protein can inhibit sensory neurite extension independent of CS sulfation in certain contexts (Dou & Levine, 1994; Ughrin et

al., 2003). Modulating the cardiac scar is of interest as a strategy to improve outcomes after MI, but removing matrix proteins presents a challenge since the scar plays an important role in maintaining structural integrity. Given the critical role of CSPG sulfation in other contexts (Brown et al., 2012; Gilbert et al., 2005; Miller & Hsieh-Wilson, 2015; Pearson et al., 2018; H. Wang et al., 2008; Yi et al., 2012) we postulated that this might present an intervention point. While our data indicate that NG2 expression increases following MI, we found that removing or preventing sulfation of CS-GAG chains was sufficient to allow axon regeneration into the cardiac scar. Thus, NG2 prevents sympathetic axon regeneration in the heart exclusively through 4,6 tandem sulfation of CS side chains.

Increased 4,6 sulfation of CS-GAGs coincided with increased expression of the 4S-dependent 6-sulfotransferase CHST15, which is the final enzyme in the production of CS-E, and depletion of the sulfatase ARSB which removes 4 sulfation. These changes in enzyme expression provide a potential mechanism for the shift to highly sulfated GAG side chains after MI. Regulation of these proteins is also linked in the context of traumatic brain injury and other diseases with a downregulation of ARSB leading to increased CHST15 (Bhattacharyya et al., 2020; Bhattacharyya et al., 2017; Bhattacharyya et al., 2014; Bhattacharyya et al., 2015). Hypoxia reduces ARSB activity, increasing the abundance of 4 sulfated CS-GAGs which enables Galectin-3 mediation of transcriptional changes (Bhattacharyya et al., 2014). Therefore, we asked if galectin-3 expression was altered in the heart after ischemia-reperfusion. To our surprise, we found that Galectin-3 increased before changes were observed expression of sulfation-related enzymes. This

suggests that increased Galectin-3 may be an early driver of the accumulating highly sulfated CS-GAGs observed by day 7 post-MI.

The inhibitory effects of CS-E on axon outgrowth in certain neuronal subtypes led many to hypothesize that reducing CHST15 activity would restore nerve growth across CSPGs (Brown et al., 2012). To that end at least one group has even generated a novel small molecule to inhibit CHST15 and promote nerve growth (Cheung et al., 2017); However, since no commercially available inhibitor exists to our knowledge, we sought a different method. Targeting *Chst15* gene expression with siRNA decreased 4,6 tandem sulfation of CS-GAGs and allowed nerve regeneration into the cardiac scar. We were inspired to test *chst15* siRNA by a colitis study in mouse showing that siRNA knockdown of *chst15* reduced CS-E (Suzuki et al., 2016; Suzuki et al., 2017). More importantly, *Chst15* siRNA has been tested in a Phase 1 Clinical for Crohn's Disease patients with active mucosal lesions, and a Phase I/IIa trial for patients with pancreatic cancer(Tsuchiya et al., 2021), and has a good safety profile (Suzuki et al., 2017). Thus, siRNA knockdown of *Chst15* is potentially translatable to large animals and eventually human studies. We treated mice on days 3, 5, and 7 post-MI with siRNA as we wanted to intervene while the cardiac scar was forming. We assessed nerve regeneration into the scar and CSPG sulfation on day 10, which is 3 days after the final injection of siRNA. Three days after the last siRNA injection, CHST15 levels were similar in non-targeting siRNA and *Chst15* siRNA hearts despite a significant reduction in 6-sulfation and reinnervation of the infarct in *Chst15* siRNA treated animals. These data indicate that a transient decrease in CHST15 protein and depletion of CS-GAG sulfation is sufficient to allow nerve restoration

in the cardiac scar where NGF is abundant. We also attempted to use an adeno-associated virus 9 (AAV9) virus to elevate ARSB expression after MI, since explant studies showed that ARSB could promote axon outgrowth in the presence of scar-derived CSPGs. However, we were unable to increase ARSB expression in the heart, although the AAV9-GFP (green fluorescent protein) control generated good expression in myocardium. ARSB is an FDA approved therapeutic (Naglazyme™) to treat Mucopolysaccharidosis IV disease (P. Harmatz et al., 2005; P. Harmatz et al., 2004; Munoz-Rojas et al., 2010), which may be of use in the therapeutic context of the post-MI heart. Ultimately this work demonstrates the critical nature of 4, 6 sulfation of CS-GAGs in preventing reinnervation of the heart after MI and provides two strategies to promote reinnervation by modulating CSPG sulfation.

IV. Methods

Western blotting: Cardiac scar tissue from the left ventricle was dissected at 24 hours, 3 days, 7 days and 14 days following MI, and control left ventricle tissue from unoperated animals. Heart tissue was pulverized in a glass douncer in NP40 lysis buffer [50mM Tris (pH 8.0), 150mM NaCl, 2mM EDTA, 10mM NaF, 10% glycerol, and 1% NP-40] containing complete protease inhibitor cocktail (Roche), phosphatase inhibitor cocktails 2 and 3 (Sigma). Lysates sat on ice for 30min with intermittent vortexing. Lysates were centrifuged (13k rpm, 10min, 4°C) and resolved on 4-12% Bis-Tris gradient gel (3-8% Tris-Acetate gel for Figure 5 sulfation studies) by SDS/PAGE, transferred to nitrocellulose membrane (GE Life Sciences), blocked in 5% nonfat milk, probed with either CHST11

(1:500; Invitrogen: PA5-68129), CHST15 (1:1000; Proteintech: 14298-1-AP), ARSB (1:500; Proteintech: 13227-1AP), NG2/CSPG4 (1:1000; Millipore: AB5320), Tyrosine Hydroxylase (1:1000; Millipore: AB1542), or Galectin-3 (1:500; Abcam: AB2785) then probed with goat anti-rabbit (or mouse) HRP-conjugated secondary antibody (1:10,000; Thermo), and detected by chemiluminescence (Thermo Scientific). For chondroitin-sulfate proteoglycan detection, lysates were treated according to the detailed deglycosylation protocol from Mariano Viapiano Ph.D. lab website (Massey et al., 2008). Briefly, 50-100μg of protein lysate was treated for 6-8hrs with chABC (100 μU/mL; R&D systems) before being subjected to traditional western blotting, probed with anti-chondroitin-4-sulfate (1:1000; Millipore: MAB2030) or anti-chondroitin-6-sulfate (1:1000; Millipore: MAB2035). Protein expression was quantified with ImageJ densitometry and normalized to total protein as measured by ponceau staining.

Sympathetic outgrowth assay: Cultures of dissociated sympathetic neurons were prepared from superior cervical ganglia (SCG) of newborn rats as described (Dziennis & Habecker, 2003). Cells were pre-plated for 1 hour to remove non-neuronal cells, and then 5,000 neurons/well were plated onto a 96 well plate (TPP) coated with (poly-L-lysine PLL, 0.01%, Sigma-Aldrich) and either laminin (10 µg/mL, Trevigen), laminin and CSPGs (2µg/mL; Millipore), or laminin and CSPGs pre-treated with ARSB (0.3 or 0.6μg/mL; R&D systems) for 6-8hrs. Neurons were cultured in serum free C2 medium (Pellegrino, Parrish, Zigmond, & Habecker, 2011) supplemented with 10 ng/mL NGF (Alomone Labs), 100 U/mL penicillin G, and 100 µg/mL streptomycin sulfate (Invitrogen). Live cell imaging was carried out using an Incucyte Zoom microscope (Essen BioScience), with 20x phase

images acquired every 2hrs over a 40hr period. Neurite length was measured using Cell Player Neurotrack software (Essen BioScience) and was used to calculate the neurite growth rate.

Myocardial ischemia/reperfusion surgery: Anesthesia was induced with 4% isoflurane and maintained with 2% isoflurane. Mice were restrained supine, intubated, and mechanically ventilated. Core body temperature was monitored by a rectal probe and maintained at 37°C throughout the surgery. The left anterior descending coronary artery (LAD) was reversibly ligated for 40 minutes and then reperfused by release of the ligature. LAD occlusion was verified by a persistent S-T wave elevation, region specific cyanosis, and wall motion abnormalities. Reperfusion was confirmed by return of S-T wave to baseline level and re-coloration of ventricle region distal to occlusion(Gardner & Habecker, 2013; Parrish et al., 2010).

Explant Co-culture Assay: Explants were generated as previously described (Gardner & Habecker, 2013). Briefly, newborn mouse superior cervical ganglia were explanted and placed into culture 1mm from left ventricle tissue – either cardiac scar tissue (10-14 days post-MI) or unoperated control tissue. Cardiac tissue from a single animal was split in half and cultured with the left or right ganglia from a single animal, this enabled tissue from the same mice to be treated with either vehicle (5% DMSO) or ARSB to remove 4S-CS GAGs. The ganglia and the cardiac tissue were co-cultured inside a Matrigel bubble surrounded by C2 media supplemented with 2ng/mL NGF. ARSB was added directly to the media (0.6 μg/mL) at the time of plating and again 24hrs later. At 48hr the explants were imaged by phase microscopy with a Keyence BZ-X microscope. Neurite length from

the edge of the ganglia to the most distal tip of visible neurites was measured using ImageJ.

siRNA pool knockdown efficiency screen: A pool of 4 siRNAs targeting the *Chst15* gene were purchased from Horizon Discovery (formerly GE Dharmacon) and were tested for their efficacy in reducing gene expression in C2C12 myoblasts. C2C12 myoblasts were plated on 12-well plates coated with collagen and were transfected with the various targeting and control siRNAs using the Dharmafect transfection reagent (3μL of Dharmafect reagent per well with 120nM siRNA). The next day wells were split using Versene (Gibco), 1/3 of the cells were collected for a 24-hour time point and the other 2/3 were split into 2-wells for 48hr and 72hr knockdown timepoints. Cells were processed using an RNA Mini-kit (Qiagen) to purify RNA. 1μg of RNA was loaded into the cDNA reaction with the iScript cDNA synthesis kit. Gene expression was examined with multiplexed Taqman probes targeting *Chst15* and *Gapdh* using 2μL of cDNA template and Taqman reagents and measured with an ABI7500 Thermocycler. The delta delta ct method was used to calculate knockdown efficiency. Once an effective siRNA against *Chst15* was identified, knockdown efficiency was measured at the protein level with C2C12 myoblasts 48hr post-knockdown. CHST15 expression was assessed via western blot with a CHST15 antibody (1:1000; Proteintech: 14298-1-AP) normalized to GAPDH (1:1000; Thermo Scientific: MA1-16757); siRNA *Chst15-2* was selected for larger scale production and used for in vivo studies.

In vivo siRNA treatment: After MI surgery mice were treated with 100μg of siRNA targeting *Chst15* or a non-targeting control. siRNA was delivered systemically via tail-vein injection

on days 3, 5 and 7 following MI. Tissue was collected at day 10 post-MI for western blot analysis of CSPG sulfation and the sympathetic neuron marker TH. siRNA used for this experiment was custom synthesized by Horizon Discovery; siAccell *in vivo* formulation.

NE content by High-Performance Liquid Chromatography: NE levels in heart tissue were measured using HPLC with electrochemical detection (Li, Knowlton, Van Winkle, & Habecker, 2004). Frozen, pulverized tissue was weighed, and then homogenized in 0.2M perchloric acid and 0.5 mM dihydroxybenzylamine (DHBA). The tissue was refrigerated for 1hr and centrifuged at 14,000 rpm for 4min. Supernatant was adsorbed on alumina, followed by 15min of tumbling. The alumina was washed twice with 1.0mL of H_2O with centrifugations in between. The NE was desorbed from the alumina with 150 ml of 0.1M perchloric acid. 50μL aliquots were fractionated by reversed-phase HPLC (C18; 5 mm particle size, Rainin) using a mobile phase containing 75mM sodium phosphate (pH 3.0), 360mg l 1 of sodium octane sulfonate, 100mL l 1 triethylamine and 3.0% acetonitrile. A coulometric detector (Coulchem, ESA) was used to detect and quantify NE and DHBA. NE standards (0.5 mM) were processed in parallel with tissue samples and interspersed throughout the HPLC run. Retention time for NE was 5.0min and for DHBA was 8.5min.

Immunohistochemistry: Tyrosine hydroxylase (TH; sympathetic nerve fibers) and fibrinogen (Fib; infarct/scar) staining was carried out as described previously (Gardner et al., 2015). Tissue was collected 10 days after surgery, fixed in 4% paraformaldehyde, frozen and 12μm sections generated. To reduce autofluorescence sections were rinse 3 x 10 minutes in 10mg/mL Sodium Borohydride and rinsed for 3 x 10 minutes in PBS. Slides were placed in 2% BSA, 0.3% Triton X-100 in PBS for 1 hour and then incubated

with rabbit anti-TH (1:1000; Millipore: AB1542) and sheep anti-fibrinogen (1:300; BioRad: 4400-8004) overnight. The following day the slides were incubated with Alexa-Fluor IgG-specific antibodies (Molecular Probes, 1:1000) for 1.5 hr and rinsed 3 x 10 minutes in PBS. Background autofluorescence was reduced further with a 30min incubation in 10mM $CuSO_4$ (diluted in 50mM Ammonium Acetate). Following this, slides were rinsed 3 x 10 minutes in PBS before mounting in 1:1 glycerol:PBS and visualized by fluorescence microscopy. Threshold image analysis of TH staining has been described previously (Gardner et al., 2015) but briefly, the threshold function in ImageJ was used to generate black and white images discriminating TH+ nerves for 6 sections spanning 200μm of the infarct/scar or peri-infarct region from each heart. Percent area TH+ fiber density (20x field of view) was quantified within the infarct and the area immediately adjacent to the infarct (peri-infarct). Images were acquired with a Keyence BZ-X 800 microscope.

Quantification of Cardiac Scar (infarct) size: Infarct size was determined 10 days after myocardial ischemia-reperfusion injury and tissue was prepared for immunohistochemistry as previous mentioned omitting the steps to reduce autofluorescence. Autofluorescence in the GFP channel was used to image the infarct size. Scar tissue is notably lacking autofluorescence enabling easy identification of the infarct. Images were acquired with a Keyence BZ-X 800 microscope at 2x magnification and analyzed using Image J freehand selection tool. Left ventricle (LV) and infarct was outlined, measured and the percent area of cardiac scar was determined by (infarct area/ LV area) x 100. The scar was imaged in 6 sections across 200μm of the infarct as previously described(Gardner et al., 2015).

Arrhythmia Assessment: Anesthesia was induced with 4% isoflurane and maintained with 2% isoflurane in day 10 post-MI animals treated with siRNA. ECG leads were connected to monitor arrhythmias and animals were maintained at 37°C throughout the analysis. All parameters were monitored with Powerlab LabChart software (AD Instruments). A 30-minute baseline was used to assess spontaneous arrhythmia susceptibility prior to administration of β-agonist Isoproterenol (50μg) and caffeine (3mg) as described previously(L. Wang et al., 2014). Arrhythmias were measured for 30 minutes following drug administration and scored according to the modified Lambeth conventions (Curtis et al., 2013) on a scale of 0-4. Individual animals received a single score based on the most severe arrhythmia observed. 0 indicates no arrhythmia. 1 indicates 1-2 premature ventricular contractions (PVCs) followed by normal sinus rhythm of at least 2 beats. 2 indicates bigeminy (1 PVC followed by one normal sinus beat, repeating for 4 or more continuous cycles) or salvo (3-5 PVCs in a row). 3 indicates non-sustained ventricular tachycardia (nsVT) defined as 6 or more PVCs in a row lasting less than 30 seconds. 4 indicates sustained VT (>30 seconds) or Torsades de Pointes.

Statistics: Student's t-test was used for comparisons of just two samples. Data with more than two groups were analyzed by one-way ANOVA using the Tukey post-hoc test to compare all conditions or the Dunnet's post-test when comparing to a single control group. Data with multiple variables was analyzed by two-way ANOVA. All statistical analyses were carried out using Prism 9.

V. Supplemental Data

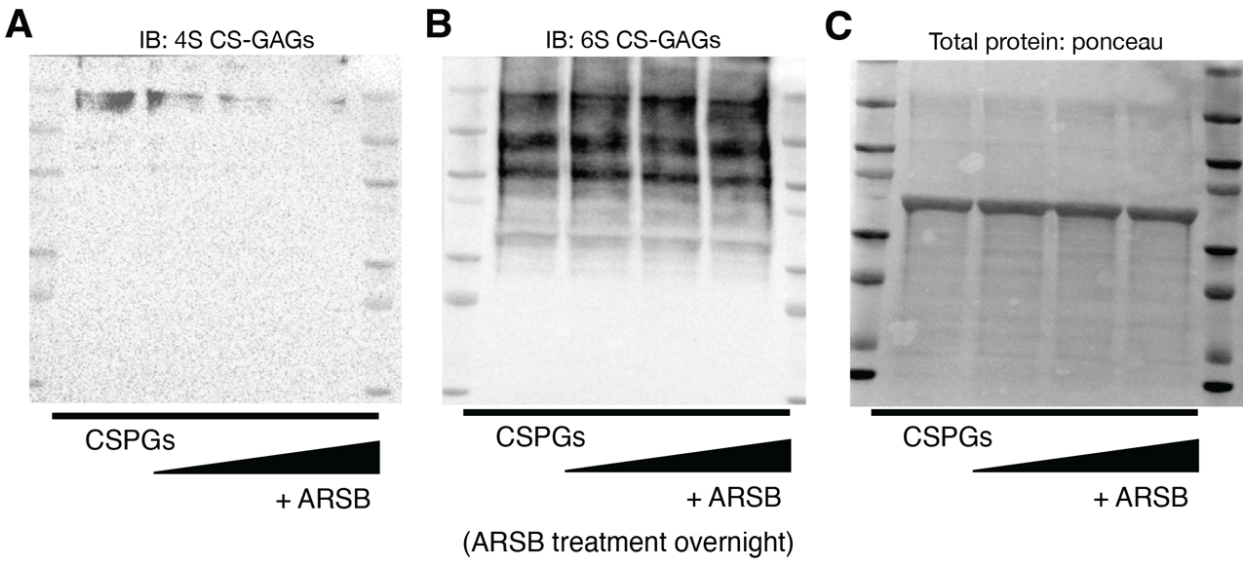

Figure 2.8: ARSB removes 4S CS-GAGs and leaves 6S CS-GAGs intact. **(A)** Western blot of 4S content using purified CSPGs upon treatment of increasing concentrations of ARSB; vehicle, 0.3µg/mL, 0.6µg/mL, and 1.2µg/mL respectively left to right. **(B)** Western blot of 6S using purified CSPGs upon treatment of increasing concentrations of ARSB; vehicle, 0.3µg/mL, 0.6µg/mL, and 1.2µg/mL respectively left to right. **(C)** Total protein loaded of purified CSPGs treated with increasing concentrations of ARSB; vehicle, 0.3µg/mL, 0.6µg/mL, and 1.2µg/mL respectively left to right.

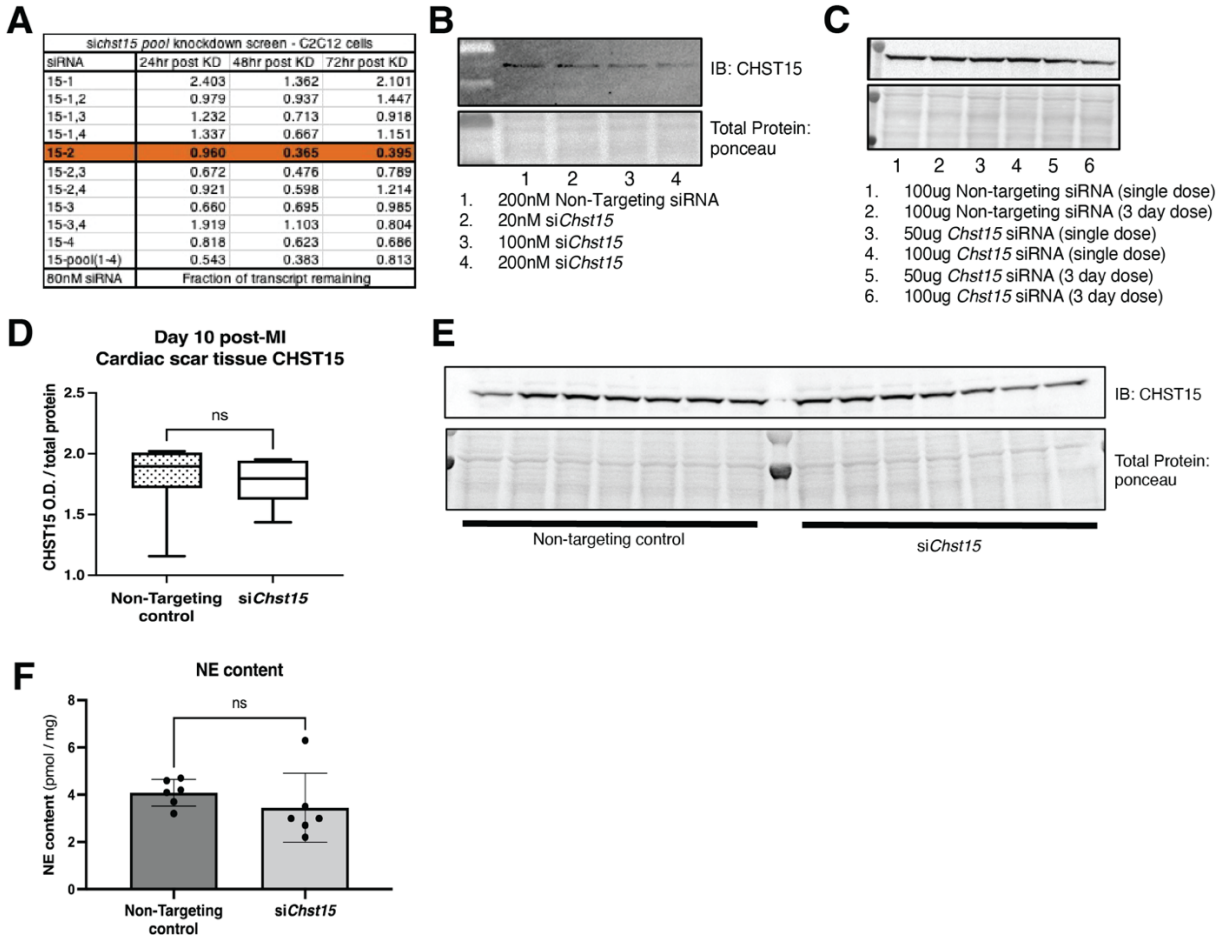

Figure 2.9: Identification of an effective siRNA against *Chst15.* **(A)** qPCR knockdown of siRNA pool in C2C12 cells in 3 days after knockdown. Data shown fraction of transcript remaining, si*Chst15-2* was most effective in knockdown of *Chst15.* This transcript was selected for *in-vivo* studies **(B)** Western blot of CHST15 protein knockdown in C2C12 cells to confirm efficacy of si*Chst15-2,* comparison to Non-Targeting controls **(C)** Tail vein injection in mouse to determine ideal dosing for *in-vivo* si*Chst15* knockdown. Western blot of tail vein injection dosing trial for si*Chst15* with either 1 day or 3 days of injections. CHST15 protein in left ventricle (LV) 48hr after final tail vein injection, comparison to Non-Targeting controls, all unoperated (non-MI) animals. **(D)** Full siRNA CHST15 experimental trial, CHST15 protein expression on D10 post MI quantified, siRNA injection D3, 5, 7 post-MI, n=7 animals per treatment group, statistics; student t-test (Welch's test), ns – not significant. **(E)** Western blot of CHST15 protein expression D10 post-MI in siRNA treated animals. **(F)** NE content in the cardiac scar following siRNA treatment. Quantification of n=6 animals for non-targeting controls and *Chst15 siRNA* treatment. Statistics; student t-test (Welch's test), n.s.- not significant.

Chapter 3

Loss of CSPG inhibition allows delayed sympathetic reinnervation after myocardial infarction

Matthew R. Blake BS, Diana C. Parrish BS, Melanie A. Staffenson BS, William R. Woodward PhD, and Beth A Habecker PhD

Planned submission to *AJP Heart* pending publication of Chapter 2 work on CSPG sulfation

I. Introduction

Coronary artery disease is a leading cause of mortality in the United States, and a critical contributor to this is the approximately 1.2 million Americans who suffer a myocardial infarction (MI) each year (Roger et al., 2012). Those who survive an MI have increased risk of sudden cardiac arrest (Pouleur et al., 2010; Rubart & Zipes, 2005; Solomon et al., 2005). The amount of sympathetic denervation in the damaged myocardium predicts the risk of ventricular arrhythmias that often follow MI (Boogers et al., 2010; Fallavollita et al., 2014; Nishisato et al., 2010; Vaseghi et al., 2014).

Sympathetic denervation after MI is sustained by chondroitin sulfate proteoglycans (CSPGs) in the cardiac scar (Gardner & Habecker, 2013). CSPGs are a component of the extra-cellular matrix (ECM) (Gilbert et al., 2005) that bind Protein Tyrosine Phosphatase Receptor Sigma (PTPσ) on sympathetic neurons, suppressing nerve regeneration (Gardner & Habecker, 2013; Gardner et al., 2015). We previously showed that blocking PTPσ interactions using Intracellular Sigma Peptide (ISP) or the compounds HJ-01 and HJ-02 restores sympathetic nerve regeneration into the cardiac scar (infarct) and prevents cardiac arrhythmias after MI (Blake et al., 2022; Gardner et al., 2015; Sepe, 2022). This demonstrates that reinnervation as a therapeutic strategy reduces arrhythmias, but raises questions about longer-term consequences of increasing sympathetic neurotransmission after MI, given the many pathological effects of excessive sympathetic stimulation of the heart (Florea & Cohn, 2014; Lopez-Sendon et al., 2004; Meredith et al., 1991; Vaseghi et al., 2014).

We asked whether reinnervation of the infarct immediately after MI had long-term negative consequences, given evidence that excess norepinephrine (NE) after MI can lead to heart failure (Florea & Cohn, 2014). We wondered if reinnervation of the infarct would amplify the effects of excess NE after MI and reduce cardiac pump function at later time points post-injury. To answer that question, we compared cardiac function 40 days after MI in mice treated with vehicle or with ISP to promote reinnervation. We also assessed nerve density to confirm that reinnervation was maintained in ISP treated animals. To our surprise, vehicle and ISP treated animals both had normal innervation density in the infarct 40 days after ischemia-reperfusion. Cardiac function and arrhythmia susceptibility in both groups of day 40 post-MI animals were similar to sham-surgery animals from previous studies (Gardner et al., 2015). In looking for a mechanism behind reinnervation of infarct in vehicle treated animals, we found that 4,6-sulfation of CSPG sugar side chains (Chondroitin Sulfate Glycosaminoglycans (CS-GAGs)) was reduced to unoperated left-ventricle levels in the infarcts of 40-day post-MI animals. Our previous work showed that 4,6-sulfation of CS-GAGs suppressed sympathetic nerve regeneration after MI. These data suggest that nerve regeneration after MI does not lead to reduced cardiac function at later time points, and that the factors preventing nerve regeneration ultimately resolve and allow for delayed reinnervation without intervention in our mouse model.

II. Results

A. Day 40 post-MI vehicle and ISP treated animals have restored sympathetic innervation of the infarct

We examined sympathetic innervation of the infarcted myocardium in animals treated with ISP 40 days (D40) after MI to see if innervation was sustained similarly to 14 days after MI (Gardner et al., 2015). To our surprise, D40 post-MI vehicle treated animals had innervation densities similar to ISP treated animals and significantly more than day 10 (D10) post-MI animals (Figure 3.1A-D). No significant difference was observed between vehicle and ISP treated groups but, sympathetic reinnervation of the infarct in D40 vehicle treated animals was more heterogeneous than animals treated with ISP (Figure 3.1D). We examined NE content in the infarct of D40 vehicle treated animals to confirm whether or not nerves in D40 vehicle treated animals were functional and found that NE content was restored to levels similar to unoperated LV tissue (Figure 3.1G). Cardiac scar (infarct) size was not significantly different between vehicle and ISP treated groups and was similar to D10 post-MI animals (Figure 3.1E-F). Innervation density in the D40 ISP treated animals was similar between the infarcted myocardium and peri-infarct (Figure 3.1D) supporting that notion that ISP promotes reinnervation of the scar and is maintained after injury.

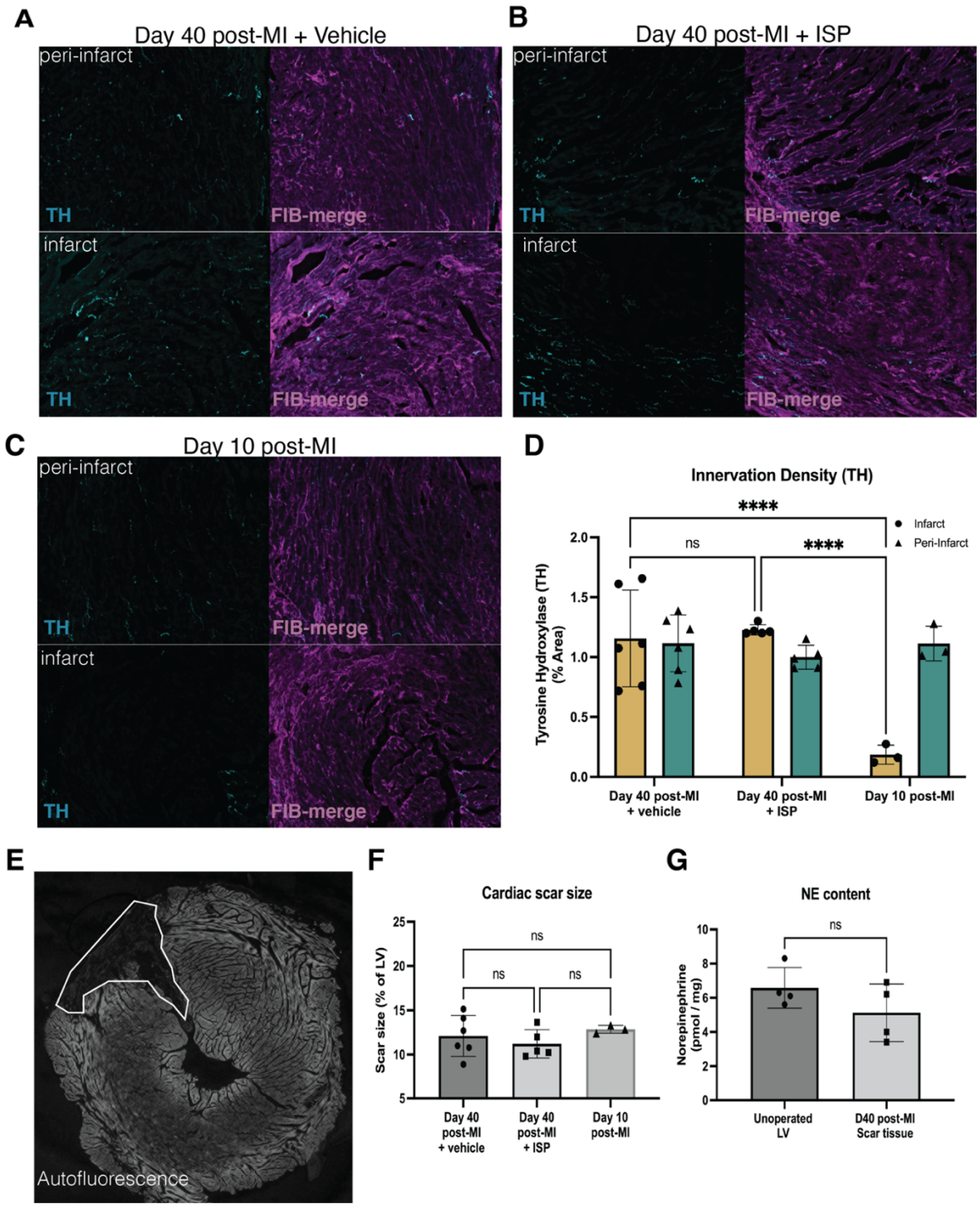

Figure 3.1: Sympathetic nerve regeneration into the infarct occurs spontaneously without interventions like ISP 40 days after MI. Fibrinogen was used to label scar (magenta) and TH was used to label sympathetic neurons (cyan). **(A)** Example image of D40 post-MI innervation density after treatment with vehicle. Innervation density of TH+ fibers in the infarct is restored to similar levels as the peri-infarct. **(B)** Example image of D40 post-MI innervation density after treatment with ISP. Innervation density of TH+ fibers in the infarct is restored to similar levels as the peri-infarct. **(C)** D10 post-MI untreated hearts have denervated infarcts as opposed to the normal distribution of TH+ nerve fibers in the

peri-infarct. **(D)** Quantification of TH+ nerve fiber density in the infarct versus peri-infarct region of D40 post-MI vehicle treated, D40 post-MI ISP treated, or D10 post-MI animals. TH innervation density expressed as % area, 20x field of view. n=6 animals D40 post-MI + vehicle, n=5 for D40 post-MI + ISP, and n=3 D10 post-MI. Two-way ANOVA, Tukey's post-test to compare all groups, select comparisons shown, ns - not significant, ****p-value<0.0001. **(E)** Example image of infarct (cardiac scar) at 2x magnification, absence of autofluorescence (outlined by white line) indicates cardiac scar/infarct. **(F)** Cardiac scar size assessed as a % area of total left ventricle (LV) area was similar in D40 post-MI vehicle treated, D40 post-MI ISP treated and D10 post-MI vehicle control animals. Quantification of n=6 animals for D40 post-MI vehicle treated animals, n=5 for D40 post-MI ISP treated animals, and n=3 for D10 post-MI animals. Statistics; one-way ANOVA with Tukey's post-test, ns - not significant. Select comparisons shown **(G)** Norepinephrine content in D40 post-MI vehicle treated animal infarct tissue is similar to unoperated left-ventricle tissue. Statistics; student t-test (Welches test), ns- not significant.

B. Cardiac function of Day 40 post-MI vehicle and ISP treated animals is the same

We assessed cardiac function by echocardiography to see if ISP treatment, which restores sympathetic neurotransmission by 14 days after MI, led to reduced cardiac function by 40 days after MI. Increased sympathetic neurotransmission after MI can reduce cardiac function towards heart failure (Florea & Cohn, 2014) and we wondering if reinnervation would accelerate this phenotype. We found that ISP animals had similar ejection fraction and cardiac output when compared to vehicle treated animals (Figure 3.2A,B). Interpreting these results is confounded by the fact that vehicle treated animals had reinnervated infarcts by D40. None of the typical metrics of cardiac function i.e. ejection fraction, stroke volume, heart rate, or LV mass were different between the two groups (Figure 3.2A-F). Previous work from our lab showed that 14 days after MI, animals had significantly reduced cardiac function compared to sham surgery animals, while ISP reinnervated day 14 post-MI animals with had restored cardiac function similar to sham surgery animals (Gardner et al., 2015). Both vehicle and ISP treated Day 40 post-MI animals had cardiac performance (cardiac output and ejection fraction) that closely resembles sham-surgery animals from previous studies (Gardner et al., 2015). Together

these data suggest that restoring sympathetic neurotransmission to the infarcted myocardium promotes normal cardiac function that is sustained after the injury and does not induce the hallmark reduction in cardiac pump function associated with heart failure 40 days post-MI.

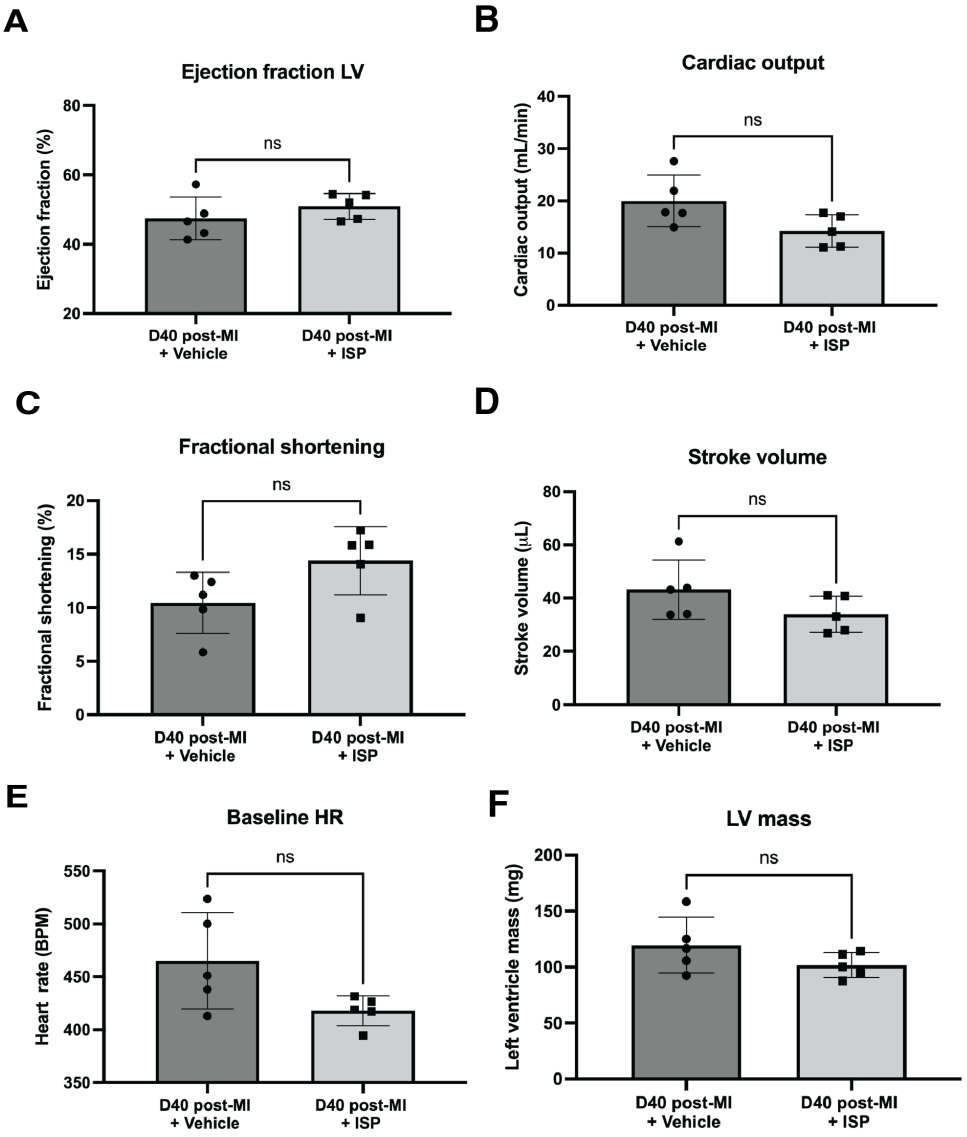

Figure 3.2: Cardiac function by echocardiography 40 days post-MI is the same regardless of innervation time. **(A)** Cardiac ejection fraction is the same in D40 post-MI animals treated with vehicle or ISP. N=5 animals assessed for D40 post-MI vehicle or ISP treatment. Statistics; student t-test (Welches test), ns- not significant. **(B)** Cardiac output is the same in D40 post-MI animals treated with vehicle or ISP. N=5 animals assessed for D40 post-MI vehicle or ISP treatment. Statistics; student t-test (Welches test), ns- not significant. **(C)** Fraction shortening is the same in D40 post-MI animals treated with vehicle or ISP. N=5 animals assessed for D40 post-MI vehicle or ISP treatment. Statistics;

student t-test (Welches test), ns- not significant. **(D)** Stroke volume is the same in D40 post-MI animals treated with vehicle or ISP. N=5 animals assessed for D40 post-MI vehicle or ISP treatment. Statistics; student t-test (Welches test), ns- not significant. **(E)** Baseline heart rate (HR) is the same in D40 post-MI animals treated with vehicle or ISP. N=5 animals assessed for D40 post-MI vehicle or ISP treatment. Statistics; student t-test (Welches test), ns- not significant. **(F)** Left ventricle (LV) mass is the same in D40 post-MI animals treated with vehicle or ISP. N=5 animals assessed for D40 post-MI vehicle or ISP treatment. Statistics; student t-test (Welches test), ns- not significant.

C. Day 40 post-MI vehicle and ISP treated animals have similar arrhythmia susceptibility

We assessed whether innervation immediately after MI with ISP effected arrhythmia susceptibility 40 days after MI. We found that both vehicle and ISP treated animals had similar susceptibility to arrhythmias induced by isoproterenol and caffeine (Table 3.1, Figure 3.3). Compared to animals 14 days post-MI these animals had reduced arrhythmia susceptibility(Gardner et al., 2015). Unexpectedly, animals reinnervated immediately after MI with ISP had a significantly lower average change in heart rate following isoproterenol administration when compared to vehicle treated animals 40 days after MI. Taken together these data suggest that reinnervation after MI with ISP or without intervention have reduced arrhythmia susceptibility, in line with previous work that suggests that reinnervation of the infarct reduces arrhythmia susceptibility.

Day 40 + vehicle					
Animal Number	Pre ISO HR	Post ISO HR	delta HR %	Score	PVC count
1	517.53	662.15	21.84	4*	133*
2	488.57	625.58	21.90	0	0
3	445.71	615.43	27.58	1	14
4	474.22	579.92	18.23	1	2
5	479.53	672.35	28.68	0	0
6	503.38	622.83	19.18	1	1

Day 40 + ISP					
Animal Number	Pre ISO HR	Post ISO HR	delta HR %	Score	PVC count
1	551.88	646.58	14.65	1	2
2	542.85	616.87	12.00	0	0
3	536.08	605.96	11.53	0	0
4	516.34	626.92	17.64	1	10
5	563.36	617.26	8.73	1	4
6	524.33	618.04	15.16	1	9

Table 3.1: Arrhythmia susceptibility is similar 40 days post-MI +/- ISP. We assessed heart rate pre and post administration of the β-agonsist Isoproterenol (ISO). Following ISO administration, we looked at the arrhythmia susceptibility of D40 post-MI animals treated with vehicle or ISP and counted Premature ventricular complex (PVC) formation. Arrhythmia scores based on the most severe arrhythmia observed in each heart after injection of isoproterenol and caffeine (0=no PVCs, 1=single PVCs, 2=bigeminy or salvos, 3= non-sustained ventricular tachycardia). *- outlier not included in analysis and graph in Figure 3.3.

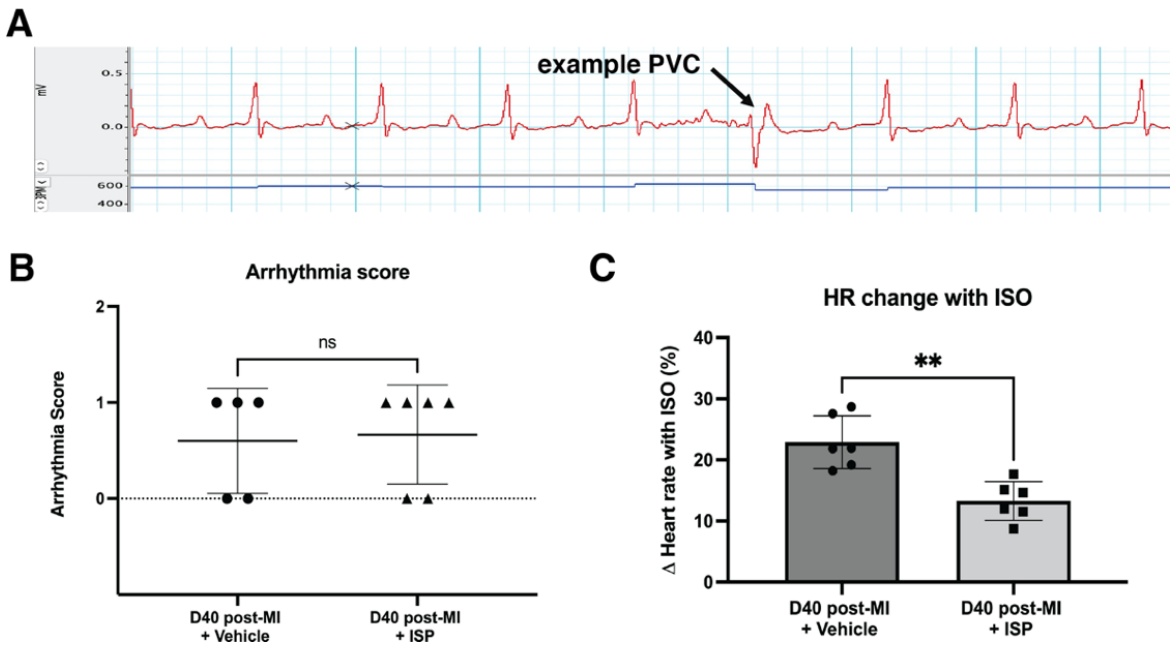

Figure 3.3: Arrhythmia susceptibility similar 40 days post-MI +/- ISP **(A)** Example PVC in ECG trace after administration of the β-agonsist Isoproterenol in a D40 post-MI vehicle treated animal **(B)** Arrhythmia scores were similar in D40 post-MI animals treated with vehicle or ISP. Arrhythmia scores based on the most severe arrhythmia observed in each heart after injection of isoproterenol and caffeine (0=no PVCs, 1=single PVCs, 2=bigeminy or salvos, 3= non-sustained ventricular tachycardia) See methods for details. Vehicle treated animals compared to ISP treated animals. n=5 animals

for vehicle controls and n=6 animals for ISP treatment. Statistics; student t-test (Welch's test), ns- not significant. **(C)** Heart rate change (% change of baseline) after administration of β-agonsist Isoproterenol was significantly reduced in D40 post-MI ISP treated animals when compared to vehicle treated animals. n=6 animals for vehicle controls and for ISP treatment. Statistics; student t-test (Welch's test), ** - p-value<0.01.

D. Day 40 post-MI animals have reduced levels of Chondroitin Sulfation in the infarct

Our previous work demonstrated that 4,6-sulfation of CS-GAGs is a critical inhibitor of sympathetic axon regeneration in the infarct after MI (Chapter 2). In light of the spontaneous sympathetic nerve regeneration that occurred 40 days after MI in mice, we wondered if CS-GAG sulfation levels were altered. Using antibodies specific to chondroitin 4 and 6-sulfation we found that sulfation was reduced in the infarct (scar tissue) 40 days post-MI and similar to unoperated LV tissue. Interestingly levels of the core proteoglycan NG2 in the infarct 40 days post-MI were reduced to levels significantly lower than unoperated LV (Figure 3.4). Taken together, these data provide a plausible explanation about how sympathetic nerves regenerate into the infarct 40 days after MI without ISP treatment in mice.

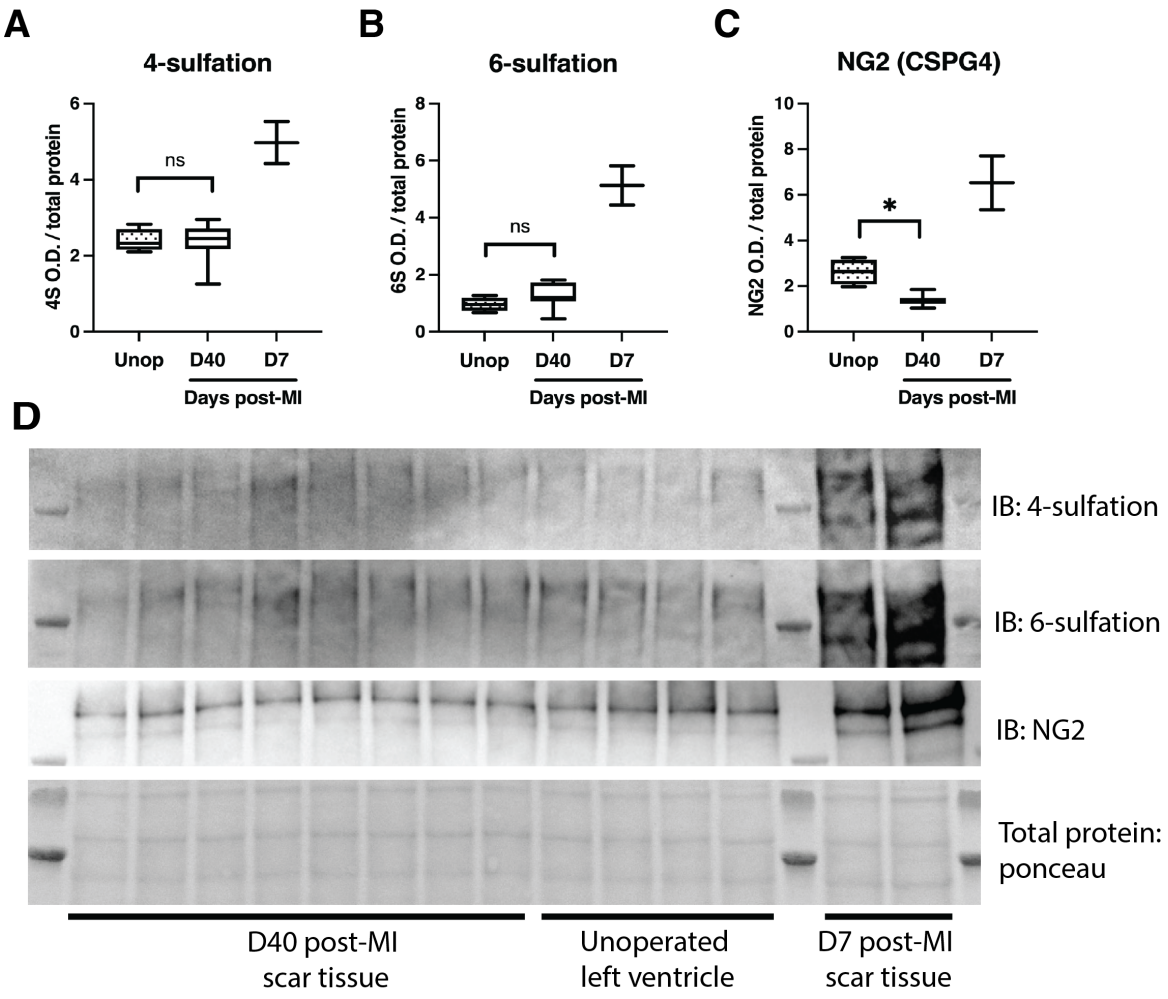

Figure 3.4: Chondroitin 4,6-sulfation reduced to unoperated levels 40 days after MI. Western blot quantification of **(A)** 4-sulfation (4S CS-GAGs), **(B)** 6-sulfation (6S CS-GAGs), and **(C)** NG2 core protein and in the infarct 40 days after MI compared to unoperated left-ventricle tissue. For visual comparison, two samples in the blots are from D7 post-MI when sulfation levels are high in the infarct, these were quantified but not used for statistical comparison due to sample size. n=8 animals for D40 post-MI vehicle treated and n=4 animals for unoperated left-ventricle group; student t-test (Welch's test), ns - not significant, *p-value<0.05, **p-value<0.01. **(E)** Western blot images of A-C.

III. Discussion

Promoting sympathetic nerve regeneration in the heart after MI has proven to be a feasible strategy to reduce arrhythmias in animal models of MI (Gardner et al., 2015), a result that may one day translate into humans where denervation of the infarct promotes arrhythmia susceptibility and increases risk of sudden cardiac arrest (Boogers et al.,

2010; Fallavollita et al., 2014; Vaseghi et al., 2014). Despite this promising result we wondered if increased sympathetic neurotransmission via excess NE in reinnervated hearts has long term deleterious effects. This question is pertinent given that excess NE after MI promotes arrhythmias (Meredith et al., 1991) and often leads to reduced cardiac function and heart failure (Florea & Cohn, 2014). Thus, we examined post-MI hearts treated with vehicle or with ISP to promote reinnervation 40 days after injury. Much to our surprise, both vehicle and ISP treated animals had reinnervated infarcts at 40 days post-MI compared to denervated infarcts 10 days post-MI. This was an interesting observation pointing to the regenerative capacity of peripheral nerves and potentially to remodeling of the infarct following MI. We examined cardiac function 40 days after MI in vehicle and ISP treated animals, and compared those data to our previously reported values 14 days post-MI (Gardner et al., 2015). Day 40 post-MI animals had similar cardiac function (ejection fraction and cardiac output) compared to sham-surgery animals from previous echocardiography studies (Sepe, 2022). Furthermore, we examined arrhythmia susceptibility in Day 40 post-MI vehicle and ISP treated animals and found that animals had similar arrhythmia susceptibilities to ISP reinnervated animals 14 days post-MI and sham-surgery animals (Gardner et al., 2015). This data provides functional evidence that similar reinnervation occurred in both vehicle and ISP treated animals 40 days after MI. More importantly, day 40 post-MI data suggests that reinnervation after MI, and thus increased NE in the infarct, does not reduce cardiac function and progress the heart towards heart failure at later time points post-injury.

We previously showed that 4,6-sulfation of CS-GAGs prevented nerve regeneration in the heart after MI (Chapter 2), so we asked if sulfation was altered 40 days after MI. We found that CS-GAG 4,6-sulfation was reduced in day 40 post-MI hearts treated with either vehicle or ISP. Interestingly, the core proteoglycan NG2 onto which the majority of CS-GAGs are attached in the heart was also reduced in all day 40 post-MI animals. This data suggests that significant remodeling occurs in the infarct ECM after MI, this result is likely driven by matrix metalloproteinase secretion from innate immune cells like Mast cells in the scar (Gentek & Hoeffel, 2017). In previous studies we examined the heart 14 days post-injury (Gardner et al., 2015). At day 14 post-MI the infarct is considered more stable than at earlier time points but this data from 40 days post-MI suggests that significant remodeling occurs long after the injury. The data provides some mechanistic explanation about why 40-day post-MI vehicle treated animals have reinnervated infarcts. The obvious question raised by this observation is; to what extent does similar remodeling occur in the human infarct? It is well established that minimal reinnervation occurs in human infarcts even after one year (Hartikainen, Kuikka, Mantysaari, Lansimies, & Pyorala, 1996), unlike the 40-day post-MI vehicle treated hearts described here. It would be interesting to examine the sulfation status of CS-GAGs in post-mortem human MI hearts to see if changes to CS-GAGs occur. If levels of CS-GAG sulfation remain high it could explain why reinnervation does not occur in humans and may support the idea that modulating sulfation of CS-GAGs after MI could promote sympathetic nerve regeneration in the infarct.

IV. Methods

Animals: C57BL/6J mice obtained from Jackson Laboratories West (Sacramento, CA) were used for all experiments. All mice were kept on a 12h:12h light-dark cycle with *ad libitum* access to food and water. Age and gender-matched male and female mice 12-18 weeks old were used for surgeries. Animals were treated daily for 7 days with vehicle (5% DMSO/saline) or ISP (10μM) via IP injection beginning 3 days post-MI. All procedures were approved by the OHSU Institutional Animal Care and Use Committee and comply with the Guide for the Care and Use of Laboratory Animals published by the National Academies Press (8^{th} edition).

Myocardial Ischemia Reperfusion procedure: Anesthesia was induced with 4% isoflurane and maintained with 2% isoflurane. The left anterior descending coronary artery (LAD) was reversibly ligated for 40 min and then reperfused by release of the ligature. Occlusion was confirmed by sustained S-T wave elevation and regional cyanosis. Reperfusion was confirmed by the return of color to the ventricle distal to the ligation and reperfusion arrhythmia. Core body temperature was monitored by a rectal probe and maintained at 37°C, and a two-lead electrocardiogram was monitored.

Left ventricle tissue collection/processing: At the indicated time point, left ventricle tissue was collected and processed for downstream analysis. Either MI animals or unoperated WT control animals were euthanized and the heart was excised and rinsed in saline solution to remove as much blood as possible. With the heart tissue cleaned, the heart was placed into a brain slicer and sectioned into 1mM sections. Infarct tissue was dissected from left ventricle (LV) of post-MI hearts and tissue from a similar region was

dissected from unoperated control heart. Tissue was processed for immunohistochemistry, western blot, or norepinephrine content. For western blot and NE content, tissue was snap frozen in LN2 and stored at -80C for batch processing. For immunohistochemistry, hearts were excised and fixed for 1hr in 4% paraformaldehyde, rinsed in PBS, cryoprotected in 30% sucrose overnight and frozen in mounting media for sectioning.

NE content by High-Performance Liquid Chromatography: NE levels in heart tissue were measured by HPLC with electrochemical detection (Li et al., 2004). Frozen, pulverized tissue was weighed and homogenized in 300 μL of 0.1 M perchloric acid (PCA) containing 0.5 μM dihydroxxybenzylamine (DHBA, internal standard). The homogenate was centrifuged and NE in 100 μL of the supernatant was adsorbed onto 15 mg alumina. The alumina was washed twice with ddH_2O and the catechols desorbed with 150 μL of 0.1 M PCA. The catechols were separated by reversed-phase HPLC on a C18 column (Agilent Microsorb, 150x4.6 mm, 5 µm) and measured by an electrochemical detector (Coulochem III; ESA, Bedford, MA) with the electrode potential set at +180 mV as described previously (Parish et al. 2010). The mobile phase used consisted of 75 mM sodium phosphate (pH 3.0), 1.7 mM sodium octane sulfonate, 3.0% acetonitrile. NE standards (0.5 μM were processed in parallel with the tissue samples.

Cardiac tissue Immunoblotting: Infarct tissue was collected at several time points following MI or left ventricle tissue from unoperated animals. Heart tissue was pulverized in a glass douncer in an NP40 lysis buffer [50mM Tris (pH 8.0), 150mM NaCl, 2mM EDTA, 10mM NaF, 10% glycerol, and 1% NP-40] containing complete protease inhibitor cocktail

(Roche), phosphatase inhibitor cocktails 2 and 3 (Sigma). Lysates were centrifuged (13k rpm, 10min, 4°C) and resolved by SDS/PAGE, transferred to nitrocellulose membrane (GE Life Sciences), blocked in 5% nonfat milk, probed with primary antibody, then probed with goat anti-mouse HRP (1:10,000; Thermo) and detected by chemiluminescence (Thermo). For chondroitin-sulfate proteoglycan detection, lysates were first treated for 6-8hrs with chABC before being subjected to traditional western blotting, probed with mouse anti-chondroitin-4-sulfate (1:1000; Millipore), mouse anti-chondroitin-6-sulfate (1:1000; Millipore) or rabbit anti- NG2/CSPG4 (1:1000; Millipore) and developed with chemiluminescence. Protein expression was quantified with ImageJ densitometry and normalized to total protein in each well as measured by ponceau staining.

Immunohistochemistry: Tyrosine hydroxylase (TH; sympathetic nerve fibers) and Fibrinogen (Fib; infarct/cardiac scar) was carried out as described previously (Lorentz et al., 2010). Hearts were collected 40 days after surgery, and processed as described above. 10μm transverse sections were thaw-mounted onto charged slides. To reduce fixative-induced fluorescence, sections were treated with a 10mg/mL solution of sodium borohydride in 1X PBS, 3 times for 10 minutes. The slides were then rinsed in PBS and blocked in 2% B.S.A, 0.3% Triton X-100 in PBS at room temperature for 1 hour. Sections were then incubated with either rabbit anti-Tyrosine Hydroxylase (Chemicon, 1:1000) or sheep anti-fibrinogen (1:300) overnight. The following day the slides were incubated with Alexa-Fluor IgG-specific antibodies (Molecular Probes, 1:1000) and visualized by fluorescence microscopy. Staining was quantified using ImageJ in a least 6 sections

across 200μm from each infarct. Percent area of TH+ fiber density was quantified within the infarct and the area adjacent to the infarct (peri-infarct).

Quantification of Cardiac Scar (infarct) size: Sections analyzed for innervation density were stored at -20°C for two weeks to allow recovery of autofluorescence. Scar tissue is notably lacking autofluorescence enabling easy identification of the infarct (Gardner et al., 2015). Images were acquired with a Keyence BZ-X 800 microscope at 2x magnification and analyzed using Image J freehand selection tool. Left ventricle (LV) and cardiac scar (infarct) were outlined and measured. The percent area of the infarct was determined by calculating (infarct area/ LV area) x 100. 6 sections across 200μm of the LV-infarct were imaged, which was established in previous studies as sufficient to measure infarct size.

Echocardiography: Cardiac function was assessed using echocardiography. High-frequency fundamental imaging (Vevo 2100) was performed between 25 and 40 MHz. Mice were sedated with inhaled isoflurane (1.0%–1.5%). Cardiac function was analyzed under basal conditions and in response to the β-adrenergic agonist isoproterenol (10 µg or ~0.5 mg/kg). Images were obtained in the parasternal long-axis plane and parasternal short-axis planes at the midpapillary level. LV function was assessed by measurement of LV end-diastolic, end-systolic area (short axis) and end-diastolic, end-systolic length (long axis). Stroke volume was determined using the left ventricular outflow tract area and time-velocity integral on pulsed-wave Doppler.

Arrhythmia Assessment: Anesthesia was induced with 4% isoflurane and maintained with 2% isoflurane in day 40 post-MI animals treated with vehicle or ISP. ECG leads were connected to monitor arrhythmias and animals were maintained at 37°C throughout the analysis. All parameters were monitored with Powerlab LabChart software (AD Instruments). A 30-minute baseline was used to assess spontaneous arrhythmia susceptibility prior to administration of β-agonist Isoproterenol (50μg) and caffeine (100μg) as described previously (L. Wang et al., 2014). Arrhythmias were measured for 30 minutes following drug administration and scored according to the modified Lambeth conventions(Curtis et al., 2013) on a scale of 0-4. Individual animals received a single score based on the most severe arrhythmia observed. 0 indicates no arrhythmia. 1 indicates 1-2 premature ventricular contractions (PVCs) followed by normal sinus rhythm of at least 2 beats. 2 indicates bigeminy (1 PVC followed by one normal sinus beat, repeating for 4 or more continuous cycles) or salvo (3-5 PVCs in a row). 3 indicates non-sustained ventricular tachycardia (nsVT) defined as 6 or more PVCs in a row lasting less than 30 seconds. 4 indicates sustained VT (>30 seconds) or Torsades de Pointes.

Statistics: Student's t-test was used for comparisons of just two samples. Data with more than two groups were analyzed by one-way ANOVA using the Tukey's post-hoc test to compare all conditions. For experiments comparing different surgical groups and a second variable (drug treatment, surgical group) two-way ANOVA was carried out using the Tukey's post-hoc test. All statistical analyses were carried out using Prism 9.

Chapter 4

Small molecules targeting PTPσ—Trk interactions promote sympathetic nerve regeneration

Matthew R. Blake[1,2#], Ryan T. Gardner[1,5#], Haihong Jin[1,6], Melanie A. Staffenson[1], Nicole J. Rueb[3], Amy M. Barrios [3], Gregory B. Dudley[4], Michael S. Cohen[1*], Beth A. Habecker[1*]

Published in *ACS Chemical Neuroscience* February 14, 2022

[1]Department of Chemical Physiology and Biochemistry, [2]Graduate Program in Biomedical Sciences, Oregon Health and Science University, Portland, OR 97239, USA. [3]Department of Medicinal Chemistry, University of Utah College of Pharmacy, Salt Lake City, UT 84112, USA. [4]C. Eugene Bennett Department of Chemistry, West Virginia University, Morgantown, WV 26506, USA.

#Authors contributed equally

Abstract

Chondroitin Sulfate Proteoglycans (CSPGs) prevent sympathetic nerve regeneration in the heart after myocardial infarction, and prevent central nerve regrowth after traumatic brain injury and spinal cord injury. Currently there are no small molecule therapeutics to promote nerve regeneration through CSPG-containing scars. CSPGs bind to monomers of receptor protein tyrosine phosphatase sigma (PTPσ) on the surface of neurons, enhancing the ability of PTPσ to bind and dephosphorylate Trk tyrosine kinases, inhibiting their activity and preventing axon outgrowth. Targeting PTPσ—Trk interactions is thus a potential therapeutic target. Here we describe the development and synthesis of small molecules (HJ-01, HJ-02) that disrupt PTPσ interactions with tropomyosin receptor kinases (Trks), enhance Trk signaling, and promote sympathetic nerve regeneration over CSPGs.

I. Introduction

The lack of nerve regeneration after spinal cord injury, traumatic brain injury, extremity injury, and even myocardial infarction is due, in part, to inhibitory extracellular matrix components including chondroitin sulfate proteoglycans (CSPGs). A current approach to overcoming CSPG inhibition of axon outgrowth focuses on enzymatic degradation of chondroitin sulfate side chains using chondroitinase ABC (ChABC). Intrathecal treatment with ChABC (E.J. Bradbury et al., 2002), local injection of the enzyme near nerve grafts (Tom, Kadakia, Santi, & Houle, 2009; Tom et al., 2013), or viral expression of modified ChABC (Zhao et al., 2011) has proven successful in restoring nerve regeneration after spinal cord injury. However, the need to express or inject a functional enzyme *in vivo*, and maintain levels for an extended period of time, raises concerns about safety and applicability to humans. Recent studies identified protein tyrosine phosphatase receptor sigma (PTPσ) as a receptor for CSPGs (Shen et al., 2009a), and showed that knockout of PTPσ in mice enhanced nerve regeneration after spinal cord injury (Fry, Chagnon, Lopez-Vales, Tremblay, & David, 2010) or myocardial infarction (Gardner & Habecker, 2013). Likewise, modulating PTPσ activity with intracellular sigma peptide (ISP), a cell permeable peptide that disrupts PTPσ-substrate binding (Lang et al., 2015) enhanced nerve regeneration after spinal cord injury in rats (Lang et al., 2015) and restored nerve regeneration after myocardial infarction in mice (Gardner et al., 2015). Development of the therapeutic peptide was a significant milestone but no small molecule therapeutics exist to overcome CSPG inhibition of nerve regeneration.

The mechanisms by which PTPσ and homologues such as LAR (Leukocyte common antigen-related receptor) inhibit axon outgrowth are not fully understood, but interactions with Trk neurotrophin receptors (TrkA, TrkB, and TrkC) are thought to play a key role (Faux et al., 2007; Xie et al., 2006). PTPσ and LAR both bind to and dephosphorylate Trk receptors, inhibiting their kinase activity and decreasing axon outgrowth (Faux et al., 2007). Removing PTPσ or disrupting phosphatase binding to Trk receptors enhances Trk signaling (Xie et al., 2006) and axon outgrowth (Gardner et al., 2015; Lang et al., 2015). These studies suggest that inhibiting PTPσ or disrupting the interaction between PTPσ and TrkA should enhance sympathetic axon outgrowth across CSPGs.

Here, we describe small molecules (HJ-01 and HJ-02) inspired by illudalic acid, a natural product shown to inhibit PTPσ catalytic activity (Fulo et al., 2021; Ling et al., 2008; McCullough, Batsomboon, Hutchinson, Dudley, & Barrios, 2019). Surprisingly, HJ-01 and HJ-02 do not inhibit PTPσ activity, but instead disrupt the interaction between PTPσ and TrkA. HJ-01 and HJ-02 enhance Trk signaling and restore sympathetic axon outgrowth across CSPGs.

II. Results

A. Design and Synthesis of a PTPσ inhibitor

We sought to identify an inhibitor of PTPσ catalytic activity and were inspired by the natural product Illudalic acid (Figure 4.1) which inhibits PTPσ and the related phosphatase LAR. Illudalic acid exhibits an IC50 of <<250 nM against PTPσ catalytic

activity *in vitro* (Fulo et al., 2021). Illudalic acid contains an aldehyde as well as a hemi-acetal lactone that opens up to an aldehyde at physiological pH; the bis-aldehyde is required for activity, presumably because it is required to form a stable covalent bond with the active site cysteine of LAR/PTPσ. Because of (i) potential cellular instability of the bis-aldehyde and (ii) the complex, multi-step synthesis of illudalic acid we envisaged a simpler analog with better physiochemical properties for in cell and *in vivo* studies. Inspired by illudalic acid and closely related analogs, we rationally designed two small molecules, HJ-01 and HJ-02 (Figure 4.1). Similar to illudalic acid analogs, HJ-01 and HJ-02 are based on *p*-hydroxy benzoic acid scaffold, however, the bis-aldehyde was replaced with an acrylamide group designed to react with the catalytic cysteine in PTPσ. HJ-01 and HJ-02 could be synthesized in four steps from commercially available starting material (Scheme S1, Supporting Information).

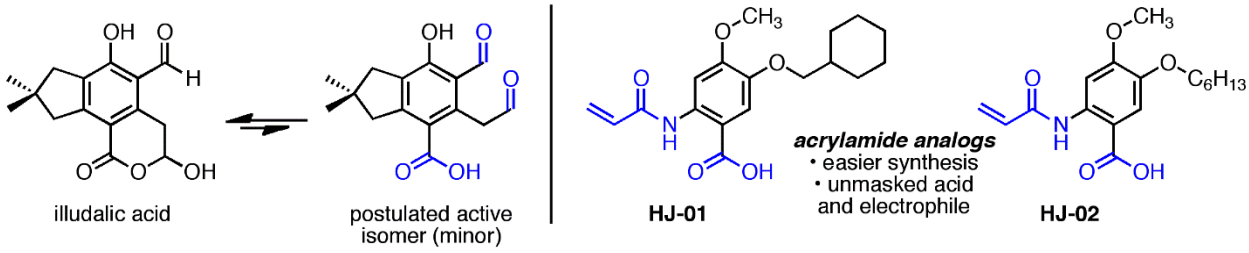

Figure 4.1. Structures of HJ-01 and HJ-02 and the natural product that inspired their design, Illudalic acid. For full synthesis scheme and chemical products, refer to Supplemental Scheme 1. The unmasked acid and electrophiles (bis-aldehyde for illudalic acid and acrylamide for HJ-01/2) are in blue.

B. HJ-01 and HJ-02 rescue neurite and axon outgrowth over CSPGs

CSPGs are potent inhibitors of central and peripheral neuron outgrowth. The primary CSPG receptor in sympathetic neurons is PTPσ, and deleting PTPσ or disrupting PTPσ-substrate interactions with ISP enhances sympathetic axon growth across CSPGs

(Gardner & Habecker, 2013; Gardner et al., 2015). We asked if our small molecules could restore sympathetic axon outgrowth over inhibitory CSPGs, performing live cell imaging of neurons grown on plates coated with laminin or a combination of laminin and CSPGs. Additional cells were treated with HJ-03, a structural analog of HJ-01 and HJ-02 in which the acrylamide was replaced with a non-reactive ethylamide isostere (Scheme S1, Supporting Information), illudalic acid, or ISP. CSPGs significantly limited axon outgrowth as expected, and HJ-01 and HJ-02 restored axon outgrowth in a dose dependent manner (Figure 4.2). HJ-01 and HJ-02 fully restored growth at 100 nM. ISP also restored axon growth over CSPGs at 1 μM, but HJ-03 and illudalic acid did not (Figure 4.2). These results show that HJ-01 and HJ-02 promote sympathetic axon outgrowth across CSPGs, and their activity is dependent on the acrylamide electrophile, consistent with covalent inhibition.

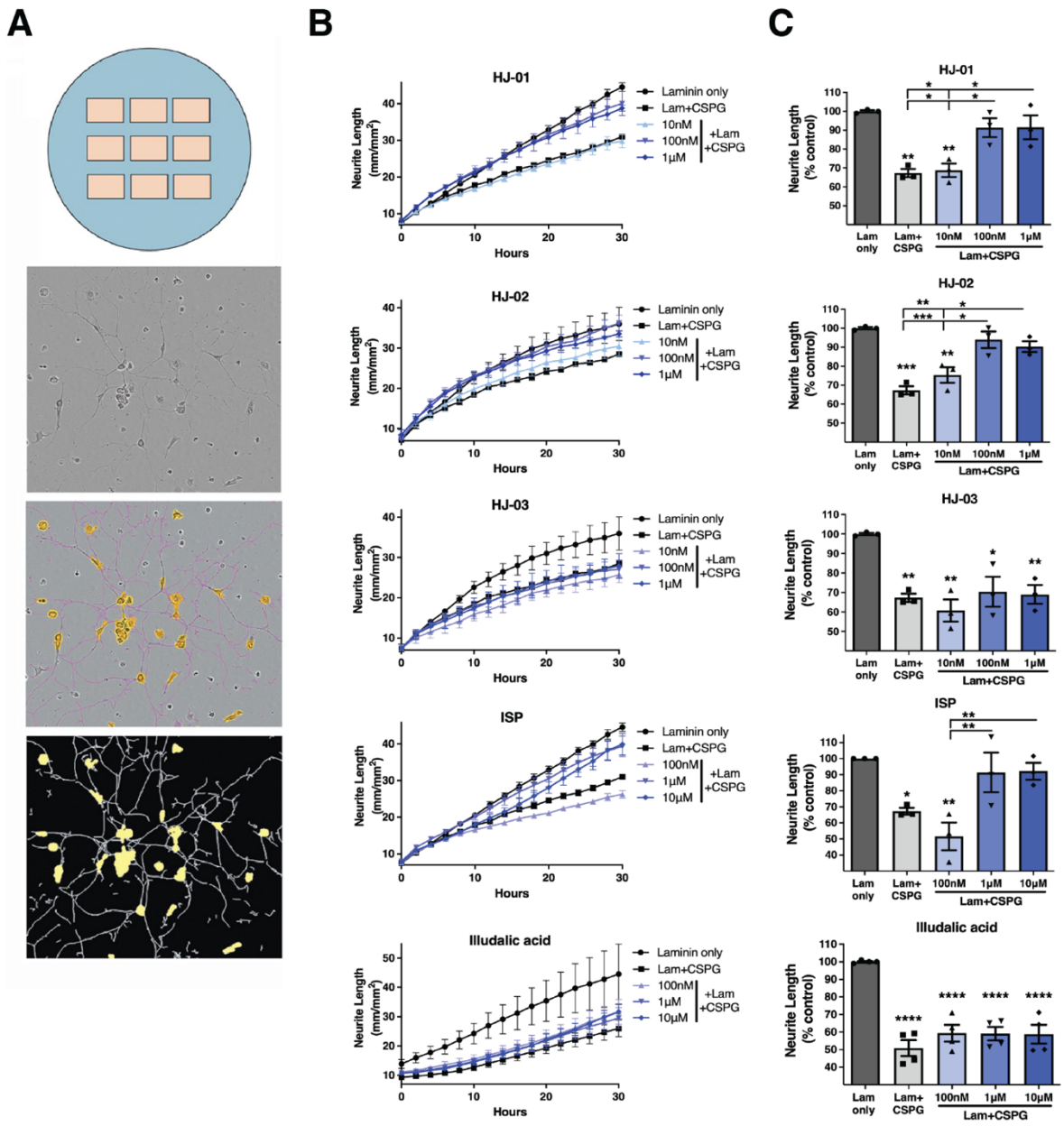

Figure 4.2. Compounds restore sympathetic neurite outgrowth over CSPGs *in vitro.* (A) Illustration of a single well, the 9 fields of view/well that were photographed repeatedly, and a representative phase image of dissociated sympathetic neurons. Neurons are "masked" by the NeuroTrack software, cell bodies (yellow) and neurites (purple) are identified, and neurite length normalized to cell body area is calculated by the software. **(B, C)** Quantification of sympathetic neurite growth on Laminin only or Laminin and CSPGs in the presence of vehicle (5% DMSO), HJ-01, HJ-02, HJ-03, ISP, or Illudalic acid. **(B)** Representative growth curves from individual experiments are mean neurite length ± SEM of 9 locations/well and 3 wells per condition. Similar results were obtained in at least 3 independent experiments. **(C)** Data shown are the average of at least 3 experiments expressed as a percent of laminin-only vehicle (5% DMSO) treated controls; mean neurite length ± SD. Statistics: one-way ANOVA (Tukey's post-test), comparisons are to Laminin only control unless indicated by brackets *p<.05, **p<.01, ***p<0.001, ****p<0.0001.

CSPGs inhibit axon outgrowth *in vivo* through interaction with the distal axon. To confirm that these compounds acted on axons, we cultured sympathetic neurons in microfluidic chambers to separate the cell bodies from the axons, with treatments confined to the axon compartment. The distal axon compartment was coated with either collagen or collagen and CSPGs prior to adding neurons. After axons had extended into the distal compartment, the axon compartment was treated for 3 hours with vehicle (5% DMSO), 100 nM HJ-01, 100 nM HJ-02, or 4 μU/mL chondroitinase ABC as a positive control to disrupt CSPGs. Acute treatment with the small molecules (Figure 4.3) or the positive control chondroitinase ABC (data not shown) stimulated the defasiculation of axon bundles growing over CSPGs and enhanced the rate of axon outgrowth. These results suggest HJ-01 and HJ-02 target axons to promote outgrowth across CSPGs.

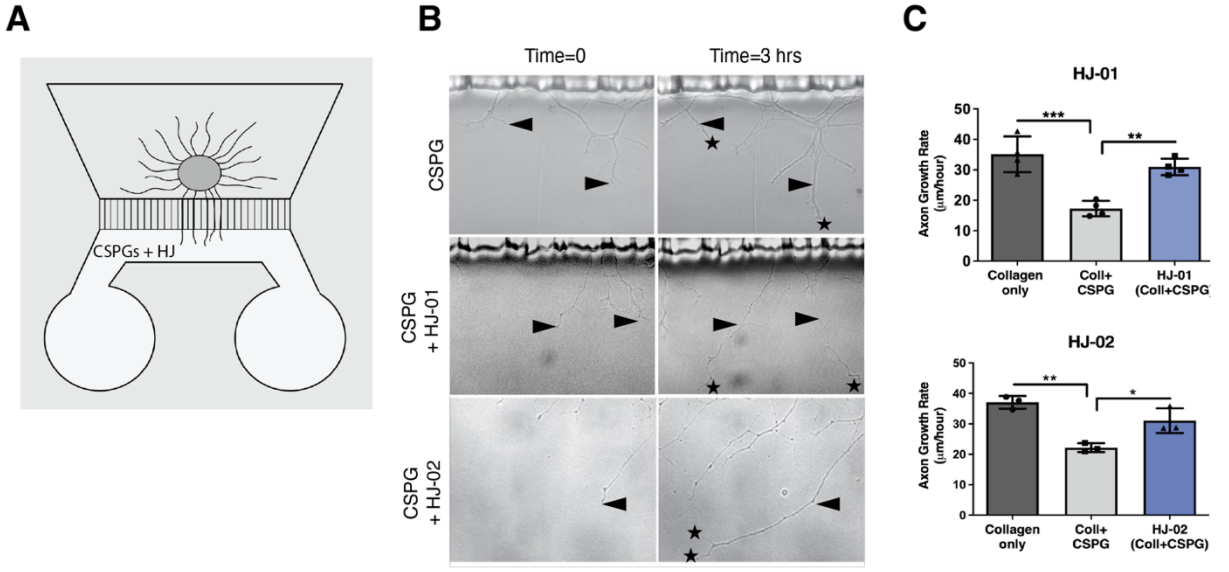

Figure 4.3. Axonal application of HJ-01 and HJ-02 is sufficient to promote sympathetic axon growth over CSPGs (A) Illustration of microfluidic chambers, where whole ganglia are cultured in the cell body compartment and axons extend into the coated compartment where treatments are added to the media. **(B)** Representative images of axons in microfluidic chambers coated with CSPGs, taken at t=0 and t=3 hrs. Axons were treated with vehicle (5% DMSO), 100nM compound HJ-01, or HJ-02. Triangles identify the leading edge of the axon at t=0, and the asterisks identify the final position of the axon at t=3 hrs. **(C)** Quantification of axon growth rate in microfluidic chambers across

collagen-only treated with vehicle, collagen and CSPGs treated with vehicle or, collagen and CSPGs treated with HJ-01 or HJ-02. Data are mean ± SEM of at least 8 axons per conditions across 3 separate experiments. Statistics; one-way ANOVA, (Tukey's post-test), Comparisons directly to collagen + CSPG treated samples, *p<.05, **p<.01, ***p<0.001.

C. HJ-01 and HJ-02 do not inhibit phosphatase activity

Based on the mechanism of action of illudalic acid, we hypothesized that HJ-01 and HJ-02 would irreversibly inhibit the catalytic activity of PTPσ by reacting with the active site cysteine in the D1 catalytic domain via a Michael addition with their acrylamide. To test the hypothesis that these compounds inhibit PTPσ D1 catalytic activity, we expressed and purified a peptide including the D1 domain and the inactive D2 pseudocatalytic domain. We used the compound p-nitrophenol phosphate (p-NPP) to monitor phosphatase activity through a colorimetric reaction. We incubated D1D2 peptide with either vehicle (5% DMSO), 1 μM HJ-02, or the phosphatase inhibitor orthovanadate (10 mM) as a negative control in the presence of either 2 mM or 10 mM p-NPP. HJ-02 did not inhibit D1 phosphatase activity at 1 μM concentration, even though lower doses restored axon outgrowth *in vitro*. Samples treated with orthovanadate had negligible phosphatase activity as expected (Figure 4.4A,B). We also tested higher doses of HJ-01 and HJ-02 against a panel of protein phosphatases and found minimal inhibition of phosphatase activity with 100 μM HJ-01 or HJ-02 (Figure 4.4C,D), which is three orders of magnitude higher than the dose needed to restore axon outgrowth. These results show that HJ-01 and HJ-02 do not inhibit the catalytic activity of PTPσ at biologically relevant concentrations and conditions and suggest that they affect PTPσ function via a different

mechanism. In contrast, illudalic acid fully inhibited PTPσ activity at 1 μM (Figure 4.4E) but had no effect on axon outgrowth at concentrations up to 10 μM.

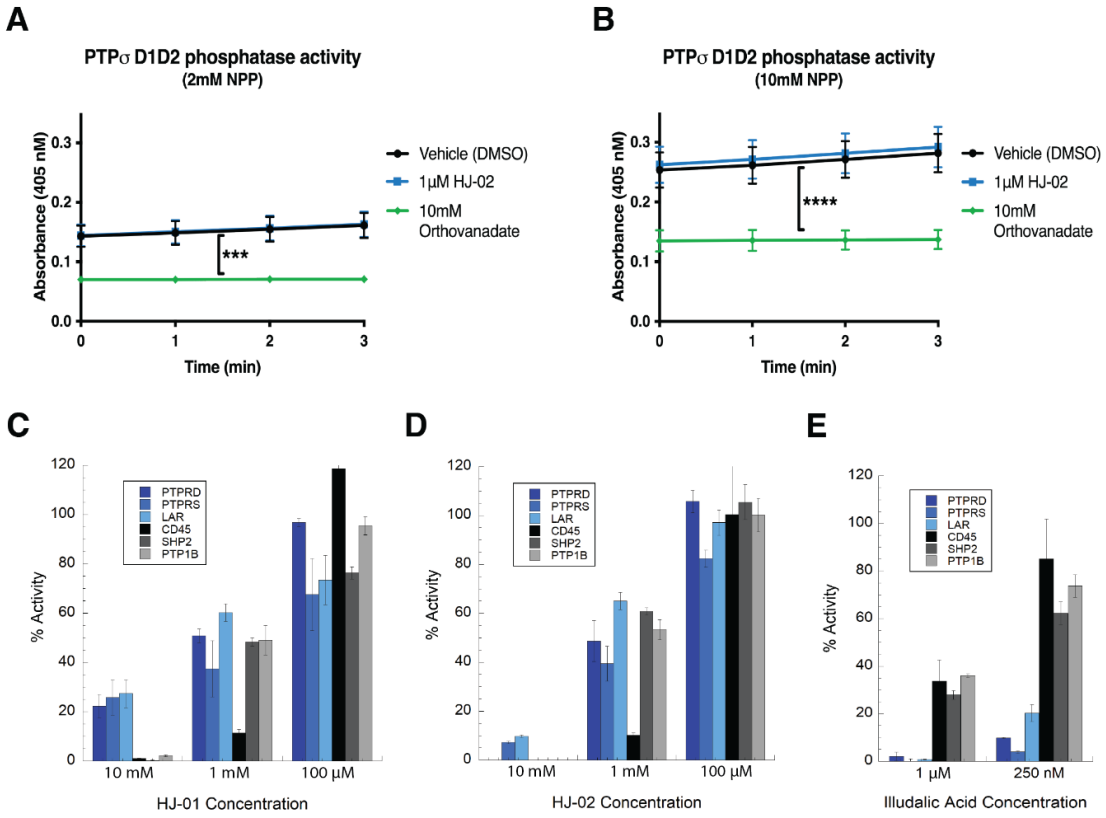

Figure 4.4. HJ-01 and HJ-02 do not inhibit PTPσ phosphatase activity at biologically relevant concentrations. **(A,B)** PTPσ phosphatase activity was quantified in the presence of 1μM HJ-02 using purified PTPσ D1D2 phosphatase domain. HJ-02 did not inhibit D1D2 phosphatase activity at any time point or substrate concentration, while the phosphatase inhibitor orthovanadate significantly reduced phosphatase activity at all times and substrate concentrations. Data are absorbance at 405nm mean ± SD, n=3 experiments, ***p<0.001, ****p<0.0001, two-way ANOVA (Dunnett multiple comparisons test). **(C-E)** PTP protein family members were screened to examine the ability of HJ-01 (C), HJ-02 (D), or Illudalic Acid (E) to inhibit enzymatic activity; PTPRδ (PTPRD, dark blue), PTPσ (PTPRS, blue), LAR (light blue), CD45 (black), SHP2 (dark grey), and PTP1B (light grey). Data are mean ± SEM of three independent experiments.

D. HJ-01 and HJ-02 disrupt TrkA—PTPσ interactions

Interaction of PTPσ with its protein substrates is required for efficient dephosphorylation. Trk tyrosine kinase receptors are critical substrates of PTPσ in

neurons, and disrupting PTPσ binding to Trk receptors enhances Trk signaling (Xie et al., 2006) and axon outgrowth (Gardner et al., 2015; Lang et al., 2015). Thus, we asked if HJ-01 and HJ-02 altered the interaction between PTPσ and TrkA, the Trk receptor present in sympathetic neurons.

We transfected HEK 293T cells with PTPσ and TrkA tagged with red fluorescent protein (TrkA-RFP), and examined the ability of HJ-01 and HJ-02 to disrupt TrkA—PTPσ binding. Cells were treated with vehicle (DMSO), HJ-01, HJ-02, or the biologically inactive compound HJ-03 and were stimulated simultaneously with NGF and CSPGs. These conditions were used to mimic the environmental conditions present during sympathetic nerve regeneration in our experimental model. We immunoprecipitated TrkA-RFP using an RFP-nanobody and compared the PTPσ pulled down following HJ-01 or HJ-02 treatment (100 nM and 1 μM) with the amount pulled down in vehicle treated cells. The small molecules HJ-01 and HJ-02 disrupted TrkA—PTPσ interactions as measured by pulldown efficiency, while the biologically inactive structural analog, HJ-03, did not disrupt TrkA—PTPσ binding (Figure 4.5A-C). To further test the specificity of these compounds, we asked if HJ-02 disrupted TrkA interactions with the p75 neurotrophin receptor (p75NTR), which together form the high-affinity binding site for NGF. Addition of HJ-02 did not alter the ability of TrkA-RFP to pull down p75NTR (Figure 4.5D), suggesting selectivity for disrupting TrkA—PTPσ interactions. These data support the model that HJ-01 and HJ-02 promote axon outgrowth by disrupting the interaction between PTPσ and TrkA, but the concentration required to break Trk—PTP complexes was higher than the concentration that restored axon outgrowth. This suggests that HJ-01 and HJ-02

modulate Trk—PTPσ interactions and subsequent Trk signaling at lower concentrations than are necessary to significantly disrupt Trk—PTPσ complexes.

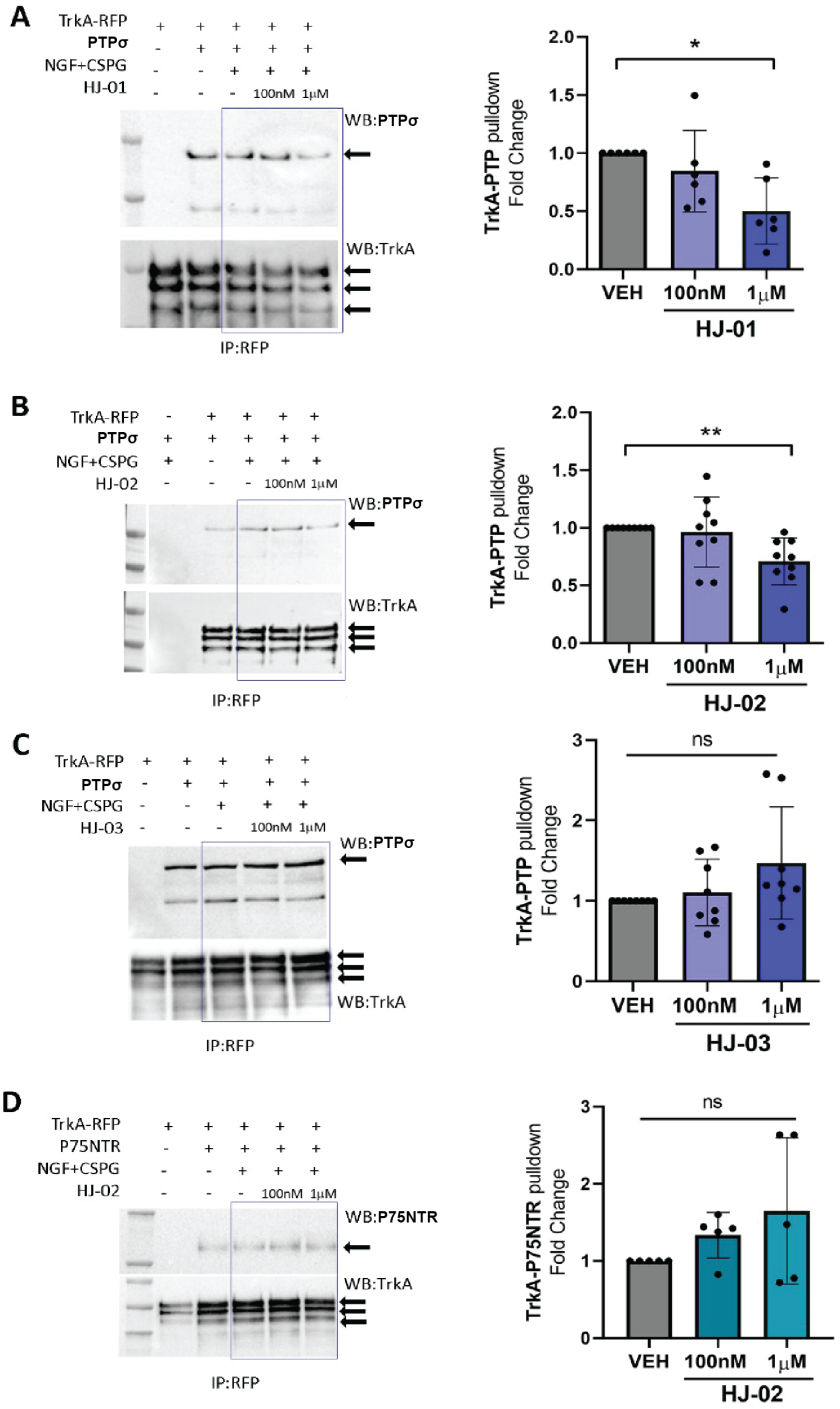

Figure 4.5. HJ-01and HJ-02 reduce the interaction between PTPσ and TrkA. Representative western blots **(left)** probing for PTPσ and TrkA following TrkA-RFP immunoprecipitation. HEK-293t cells were transfected with TrkA-RFP and PTPσ, treated with either vehicle (DMSO), **(A)** HJ-01, **(B)** HJ-02, or **(C)** HJ-03 then stimulated with CSPGs and

NGF. Quantification **(right)** of PTPσ that co-immunoprecipitated with TrkA-RFP normalized to vehicle treated cells. HJ-01 and HJ-02 reduced the amount of PTPσ that bound to TrkA-RFP at 1μM, but HJ-03 had no effect. **(D)** HEK-293t cells were transfected with TrkA-RFP and p75NTR, treated with vehicle (DMSO) and HJ-02, then stimulated with CSPGs and NGF. Quantification **(right)** of p75NTR that co-immunoprecipitated with TrkA-RFP normalized to vehicle treated cells. Data are mean ± SD, n=5-9 experiments; n.s.- not significant, *p<.05, **p<.01 vs. vehicle treated control, one-way ANOVA (Dunnett multiple comparisons post-test).

E. HJ-01 and HJ-02 reverse PTPσ-inhibition of Trk signaling

PTPσ dephosphorylates Trk receptors (Faux et al., 2007) and the absence of PTPσ enhances Trk signaling, noted by increased phosphorylation of downstream signaling proteins including ERK1/2 and Akt (Sapieha et al., 2005). To determine if disruption of Trk—PTPσ complexes by HJ-01 and HJ-02 prevented PTPσ inhibition of Trk signaling, we used HEK 293T cells stably expressing TrkB (HEK-TrkB). Co-expression of full-length PTPσ in HEK-TrkB cells decreased BDNF-induced ERK1/2 phosphorylation, and addition of HJ-01 or HJ-02 restored ERK1/2 phosphorylation to normal BDNF-stimulated levels (Figure 4.6A,B). Similar to the neurite outgrowth data in TrkA-expressing sympathetic neurons, HJ-02 was slightly more potent than HJ-01 in rescuing PTPσ-suppressed ERK1/2 phosphorylation. Likewise, both compounds restored ERK phosphorylation at 100 nM, consistent with the dosing that restored axon outgrowth in neurons, but lower than the dose needed to significantly disrupt TrkA—PTPσ binding in pull-down experiments. Taken together these results support the notion that HJ-01 and HJ-02 prevent PTPσ-mediated dephosphorylation of Trk receptors by modulating the interaction between PTPσ and Trks. Since HJ compounds did not inhibit PTPσ activity, but did inhibit downstream signaling, we asked if HJ-01 or HJ-02 disrupted signaling downstream from tyrosine phosphatase PTP1B and its substrate the insulin receptor (IR-

β) (Boutselis, Yu, Zhang, & Borch, 2007). Both receptors are present in the human hepatic cell line HepG2. Insulin stimulation of IR-β in HepG2 cells increased phosphorylation of ERK1/2, and inhibiting PTP1B with CinnGel 2ME further enhanced ERK signaling. Conversely, HJ-01 and HJ-02 had no effect on ERK1/2 phosphorylation in insulin-stimulated HepG2 cells, indicating they do not disrupt PTP1B dephosphorylation of IR-β (Figure 4.6C,D).

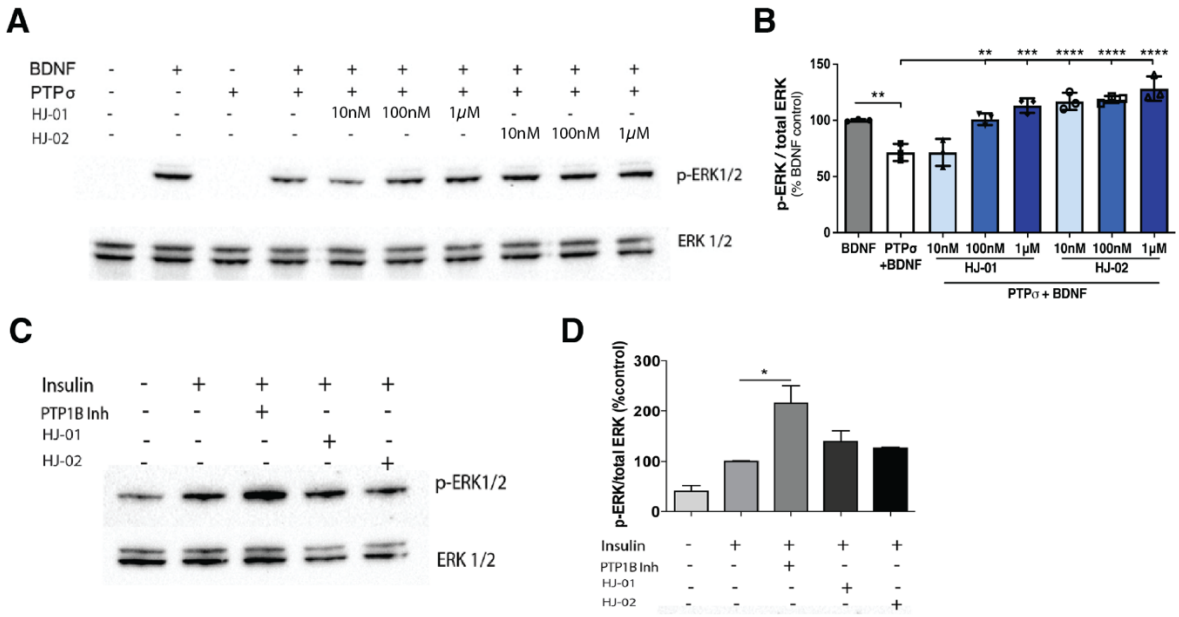

Figure 4.6. **HJ-01 and HJ-02 block PTPσ reduction in TrkB signaling (A)** Representative Western blot of TrkB downstream signaling in the presence of PTPσ. Addition of PTPσ decreased BDNF-stimulated ERK1/2 phosphorylation. Both HJ-01 and HJ-02 restored ERK1/2 phosphorylation in response to BDNF. **(B)** Quantification of Phospho-ERK1/2 relative to Total-ERK1/2. Data are graphed as percent of vehicle control (BDNF stimulated cells); mean ± SD, n=3 experiments, ***p<0.001, ****p<0.0001 as noted by lines, one-way ANOVA (Tukey multiple comparisons test). **(C,D)** Western blot analysis examining potential effect of HJ-01 or HJ-02 on PTP1B/IR- β signaling in response to insulin. Mean ± SD, n=3 experiments, *p<0.05 vs. insulin control, one-way ANOVA, (Tukey multiple comparisons test).

III. Discussion

There is a great need for therapeutics that can facilitate axon regeneration and cell migration through CSPG-laden scar tissue. Small molecules that promote axon outgrowth

through inhibitory environments are promising therapeutics for spinal cord injury, traumatic brain injury, or myocardial infarction (Gardner et al., 2015; Lang et al., 2015; Shen et al., 2009a; L.S. Sherman & S.A. Back, 2008). In this study, we synthesized two natural product-inspired, acrylamide-based compounds, HJ-01 and HJ-02, which were designed to covalently inactivate PTPσ activity. HJ-01 and HJ-02, restored axon outgrowth across inhibitory CSPGs *in vitro*. A compound (HJ-03) lacking an acrylamide had no biological activity, suggesting that covalent binding was important for function. Our experiments with primary neurons found no evidence of non-specific binding or toxicity. Importantly, there are several examples of FDA approved drugs (e.g., BTK inhibitor, Ibrutinib) that contain acrylamides, demonstrating that compounds with this type of electrophile are effective *in vivo*.

PTPσ regulation of axon dynamics depends on its ability to bind to and dephosphorylate substrate proteins including Trk tyrosine kinases (Faux et al., 2007). Modulation of substrate binding can occur through two distinct mechanisms, one extracellular and one intracellular. Extracellular CSPGs bind to PTPσ monomers, which can then bind to and dephosphorylate substrate proteins like Trk receptors, decreasing axon outgrowth. In contrast, extracellular heparin sulfate proteoglycans (HSPGs) stimulate oligomerization of PTPσ into aggregates sequestered from Trk receptors, promoting axon outgrowth (Charlotte H. Coles et al., 2011). Intracellular binding of peptides like ISP or small molecules to the D2 pseudocatalytic domain of PTPσ can also disrupt substrate binding and enhance axon outgrowth (Xie et al., 2006). Unexpectedly, we found that HJ-01 and HJ-02 did not block PTPσ phosphatase activity, but rather

modulated PTPσ—Trk receptor signaling, and at higher doses disrupted the PTPσ—Trk complex. Interestingly, the PTPσ inhibitor illudalic acid did not rescue axon outgrowth, in distinct contrast to ISP, HJ-01, and HJ-02 which do not inhibit the phosphatase but modulate PTPσ—Trk interactions. The disruption of the interaction between PTPσ—TrkA by HJ-01 and HJ-02 in a cysteine-dependent manner may be similar to the disruption of IRAK4—MyD88 interactions by the multiple sclerosis drug dimethyl fumarate (DMF) (Zaro et al., 2019). These results suggest that HJ-01 and HJ-02 elicit their effects via altering PTPσ—Trk interactions by covalently binding to either PTPσ or Trk; however, due to the lack of direct binding data, we cannot rule out that HJ-01 and HJ-02 bind to an unidentified protein involved in PTPσ—Trk complex formation.

We generated novel small molecules designed to target PTPσ in order to promote nerve regeneration through CSPG-containing scars. Two compounds that we generated restore nerve growth *in vitro* at nanomolar concentrations. Although our focus was on sympathetic neurons, CSPGs in the glial scar inhibit nerve regeneration after traumatic brain injury and spinal cord injury, preventing cognitive or motor recovery (L.S. Sherman & S.A. Back, 2008). CSPG-PTPσ interactions also disrupt myelin repair in multiple sclerosis by inhibiting oligodendrocyte precursor cell (OPC) migration into demyelinated regions and preventing differentiation of OPCs into oligodendrocytes (Luo et al., 2018; Ohtake, Saito, & Li, 2018; Pu, Stephenson, & Yong, 2018). HJ-01 and HJ-02 may prove useful for ameliorating disease progression in these situations. Small molecules are simpler to produce and easier to administer than the peptide (ISP) and enzyme (chondroitinase ABC)-based strategies that are the primary current focus of therapeutic

development. Thus, HJ-01 and HJ-02 are an important advance in the development of therapies designed to overcome CSPG actions.

IV. Methods

General Chemistry methods: Found in published paper

Animals: Pregnant Sprague Dawley rats were obtained from Jackson Laboratories West (Sacramento, CA). Rats were kept on a 12h:12h light-dark cycle with *ad libitum* access to food and water. Superior cervical ganglia from male and female neonatal rats were used for microfluidic explants and dissociated cultures. All procedures were approved by the OHSU Institutional Animal Care and Use Committee and comply with the Guide for the Care and Use of Laboratory Animals published by the National Academies Press (8th edition).

Sympathetic outgrowth assay: Cultures of dissociated sympathetic neurons were prepared from superior cervical ganglia (SCG) of newborn rats as described (Dziennis & Habecker, 2003). Cells were pre-plated for 1 hour to remove non-neuronal cells, and then 5,000 neurons/well were plated onto a 96 well plate (TPP) coated with poly-L-lysine (PLL, 0.01%, Sigma-Aldrich) and either laminin (2 µg/mL, Trevigen) or laminin and CSPGs (1-2 µg/mL, Millipore; concentration was calibrated to inhibit outgrowth by 40-50% and differed between batches). Neurons were cultured in serum free C2 medium (Lein, Johnson, Guo, Rueger, & Higgins, 1995; Pellegrino et al., 2011) supplemented with 10 ng/mL NGF (Alomone Labs), 100 U/mL penicillin G, 100 µg/mL streptomycin sulfate (Invitrogen), and 2µM 5-Fluoro-2'-Deoxyuridine (Sigma). Neurons were treated with

either vehicle (DMSO) or the compounds HJ-01, HJ-02, HJ-03, ISP or Illudalic acid at various concentrations as described in figure legends. Live-cell imaging was carried out using an Incucyte Zoom microscope (Essen BioScience), with 20x phase images acquired every 2 hrs over a 30 hr period. Neurite length was measured using Cell Player Neurotrack software (Essen BioScience) and used to calculate the neurite growth.

Compartmentalized cultures: Micro-fluidic chambers were generated by adding SYLGARD 184 silicone elastomer (Dow Corning) into a pre-cast mold, and heating at 50-60° C for 2 hours. Cleaned chambers were placed in 10 cm culture dishes (Corning) pre-coated with 0.01% PLL. The axonal compartment was then coated with 10 µg/mL collagen or collagen + 1 µg/mL CSPGs. SCG were placed in reduced growth factor Matrigel (BD Bioscience) within the cell body compartment. C2 media supplemented with 10 ng/mL NGF was added to both compartments and cultures were maintained at 37° C in a humidified 5% CO_2 incubator. After 24 hours, or when axons were first visible in the axonal compartment, images were acquired (t=0) and vehicle (5% DMSO), 100nM HJ-01, 100nM HJ-02, or 4μU/mL chondroitinase ABC were added to the axonal compartment. Additional images were obtained 3 hours later (t=3), and a growth rate was calculated based on the distance extended during that 3 hour period.

Western blotting: Immunoblotting protein samples were prepared using 4x XT sample buffer and 20x XT reducing reagent (Biorad). Samples were boiled for 10 minutes at 95°C before being spun down and added to protein gels. To separate proteins by SDS-PAGE, Criterion pre-cast 4-12% gradient Bis-tris gels were used and run for 2 hours at 120V. Proteins were transferred to PVDF membranes by semi-dry transfer at 25V for 45

minutes. Protein laden PVDF membranes were blocked for 1 hour in 5% milk dissolved in TBST. Membranes were briefly rinsed with TBST and incubated with primary antibodies diluted in 5% BSA TBST for either 1 hour at room temperature or overnight at 4°C depending on the antibody. Following primary incubation blots were rinsed with TBST 3 times for 10 minutes each and placed in HRP-conjugated Igg secondary diluted in 5% milk TBST for 1 hour at room temperature. Blots were rinsed 3 times for 10 minutes each and imaged using SuperSignal HRP chemiluminescent substrate (ThermoFisher Scientific).

PTPσ D1 D2 protein purification: D1D2 plasmid was a gift from (Brad Lang and Jerry Silver, Case Western Reserve University). Rosetta 2(DE3) competent cells (Novagen) were transformed with 1μL of D1D2 DNA and grown overnight at 37°C on LB agar plates supplemented with kanamycin and chloramphenicol. A ¼ swath of the bacteria from the LB agar plate was spiked into 50mL of LB media (with 50μg/mL kanamycin and 34μg/mL chloramphenicol) and grown at 37°C overnight with 225rpm shaking. The next day the 50mL starter culture was pitched into 1L of terrific broth (TB) media (12 g bacto tryptone, 24 g yeast extract, 0.4% glycerol, 17mM KH2PO4, 72mM K2HPO4, 1% glucose, 50 µg/ml Kanamycin, 34 µg/ml chloramphenicol) and grown at 37°C, 225rpm until reaching an OD600 reading of 0.6. At this point the TB media was placed on ice and the protein expression of D1D2 was induced with 0.4mM Isopropyl-β-thiogalactoside (IPTG, Sigma-Aldrich) and grown at 37°C overnight, 225rpm. Cells were harvested by centrifugation at 4000rpm 4°C for 15 min. The cell pellet was resuspended in 50mL of lysis buffer (20 mM HEPES, pH 7.5, 1 mM β-mercaptoethanol, 1 mM benzamidine, 0.2% NP-40, 0.2%

Tween-20, 500 mM NaCl, 1 mM phenylmethylsulfonyl fluoride, 8.3 mg/L DNAse I) with a glass douncer and sonicated, on ice, 6 times for 30 seconds each time with 2 minutes rest between each cycle (Branson sonifier 450). The resulting lysate was cleared by centrifugation at 12,000 x G, 4°C, for 30 minutes. Purification of the D1D2 protein was achieved using the attached his-tag by Ni-NTA affinity chromatography (Ni-NTA resin, Qiagen). The resulting purified protein was verified by size using 10% SDS-PAGE before use in enzymatic activity assays.

PTPσ D1 D2 catalytic activity assessment: The catalytic activity of purified PTPσ D1D2 catalytic domain was assessed using p-nitrophenyl phosphate (p-NPP, Sigma-aldrich), a commonly used indicator of phosphatase activity. D1D2 is capable of using p-NPP as a substrate and catalysis of the phosphate group results in a colorimetric reaction that can be monitored by 405nm absorbance. The assay was conducted in ice cold 50mM MES buffer with either 2mM or 10mM p-NPP. To this reaction mixture 30nM of D1D2 protein were added with either vehicle, 1μM HJ-02, or 12.5mM of sodium-orthovanadate (Sigma-Aldrich) as a control tyrosine phosphatase inhibitor. The reaction mixture was added to clear flat-bottom 96-well plates and kept on ice until the plate reading. A Spectra Max i3 (Molecular Devices) multi-well plate reader was used to measure 405nm absorbance. The reaction was induced by incubation at 30°C and measured continuously for 3 minutes.

Phosphatase Inhibition Assays: The ability of compounds HJ-01, HJ-02, and Illudalic acid to inhibit a small panel of tyrosine phosphatase enzymes was investigated. The enzymes PTPσ, PTPRδ (protein tyrosine phosphatase receptor delta), LAR (leukocyte antigen-

related tyrosine phosphatase), CD45 (cluster of differentiation antigen 45; also known as protein tyrosine phosphatase receptor C), SHP2 (Src homology 2 domain–containing phosphatase 2), and PTP1B (protein tyrosine phosphatase 1B) were incubated with 10 mM DTT for 30 min on ice in a buffer containing 50 mM HEPES pH 7.5, 100 mM NaCl, 1 mM EDTA, and 0.02% tween. The activity assays were performed in black 96-well plates in a total volume of 50 μL and 10% DMSO. The final concentration of enzyme in each reaction was180 pM for PTPσ, 9.7 nM for PTPRδ, 4.2 nM for LAR, 5 nM for CD45, 5 nM for SHP2, and 5 nM for PTP1B. Each enzyme was incubated with HJ-01 or HJ-02 for 30 min at 37°C, after which time the reaction was initiated by addition of the fluorogenic substrate DiFMUP to a final concentration of 30 μM. Enzyme activity was measured relative to an inhibitor-free control by monitoring the increase in fluorescence as DiFMUP was hydrolyzed to DiFMU. The fluorescence (λex = 350 nm, λem= 455 nm) was measured every 30 s for 30 min at 37°C. Each concentration was tested in triplicate.

Cell signaling: TrkB-HEK-293t cells (a kind gift from Dr. Moses Chao, NYU) were used to examine the effects of HJ-01 and HJ-02 on TrkB stimulated ERK phosphorylation. Cells were plated on 6-well plates in HG-DMEM (Gibco) with 10%FBS (Hyclone), 1% Penicillin/streptomycin (Gibco) and Geniticin (400 µg/mL; Life Technologies). At the appropriate density cells with rinsed twice with 1x PBS and media was replaced with Opti-MEM (Gibco) containing 2%FBS. Cells were transfected with Lipofectamine 2000 (7μL per well) and with either 2.5μg full-length PTPσ plasmid or 1μg GFP control plasmid per well. After 6 hours cells were rinsed once with 1x PBS and replaced with regular growth media and grown for 12 hours. Cells were then serum starved for 2 hours in HG-DMEM

+ B27. Following serum starving cells were incubated with either HJ-01 or HJ-02 at 10nM, 100nM, or 1μM for 1 hour and then stimulated with 5ng/mL human BDNF (Alomone Labs) for 5 minutes. Cells were then rinsed with ice-cold PBS and lysed on ice with intermittent agitation for 30 minutes with Erk lysis buffer [50mM Tris (pH 8.0), 150mM NaCl, 2mM EDTA, 10mM NaF, 10% glycerol, and 1% NP-40] containing protease inhibitor cocktail (Roche), phosphatase inhibitor cocktails (Sigma), and 5mM iodoacetamide. Lysates sat on ice for 30min and were then treated with 10mM dithiothreitol to inactive any remaining iodoacetamide. Protein lysate was cleared by centrifugation at 13,000 x G for 10 minutes. The soluble fraction was removed and diluted with 4x XT sample buffer and 20x XT reducing reagent (Biorad) for western blot analysis as described above. Blots were probed with phospho-Erk1/2 (1:1000 Phospho-p44/42MAPK, Cell Signaling #9101) and Total-Erk1/2 (1:1000 p44/42MAPK, Cell Signaling #9102) antibodies.

Immunoprecipitation assay: *To* test the hypothesis that small molecules HJ-01 and HJ-02 disrupt the binding of TrkA and PTPσ, HEK-293t cells were transfected with full length PTPσ or p75NTR (Addgene plasmid # 24091) and TrkA-RFP plasmid (Addgene plasmid #24093), and pulled down using RFP-trap nanobody conjugated to magnetic agarose (Chromotek). HEK-293t cells were plated onto 6-well plates coated with 0.01% poly-l-lysine (Sigma) in high-glucose DMEM (Gibco) supplemented with 10%FBS (Hyclone) and 1%Anti-Anti (Gibco). 12 hours later cells were rinsed with 1x PBS and media was replaced with Opti-MEM (Gibco) containing 2%FBS. Cells were transfected using Lipofectamine 3000 (Thermofisher Scientific). For transfection, 1μg of TrkA-RFP and 1μg of PTPσ plasmid, 6μL of P3000 reagent, and 5μL of lipofectamine reagent were added to each

well of the 6-well plate. 12-16 hours later cells were rinsed twice with 1xPBS and media was replaced with DMEM and B27 supplement (Gibco) and serum starved for 4 hours. Cells were then treated with small molecules or vehicle (DMSO) for 1 hour and stimulated for an additional hour with 50ng/mL NGF (Alomone Labs #N-100) + 2μg/mL Chondroitin Sulfate Proteoglycans (EMD-Millipore CC117). Cells were rinsed twice with ice-cold 1x PBS and lysed with IP lysis buffer (150mM NaCl, 50mM Hepes, 1.5mM $MgCl_2$, 1mM EGTA, 1% Triton-X, 10% glycerol, 1x Roche complete protease inhibitor cocktail, and 1x Sigma phosphatase inhibitor cocktails 2 and 3). Two wells of each 6-well plate were pooled per condition, and cells were lysed for 30 minutes on ice with intermittent vortexing. Lysate was centrifuged at 13,000 x G for 10 minutes leaving the soluble fraction. 10% of this lysate was set aside as the input fraction. TrkA immunoprecipitation was accomplished using 15μL of RFP-trap magnetic agarose added to the remaining lysate and incubated overnight at 4°C on a rotator. The protein bound to the RFP-trap agarose was then separated using a magnet and rinsed 3 x 10 minutes. To remove the protein from the beads, 4x XT-sample buffer (Biorad) was diluted to 2x using the IP lysis buffer and XT reducing reagent was added the sample was then incubated at 95°C for 10 minutes and separated from the beads using a magnet. Samples were subjected to the standard western blotting protocol and probed for TrkA (1:1000; Millipore Sigma #06-574) and PTPσ (1:500; Proteintech #13008-1-AP) or, p75NTR (1:1000; Cell Signaling, D4B3 XP #8238S). To quantify pulldown of PTPσ (or p75NTR) by TrkA-RFP the levels of each protein in the pulldown were quantified by pixel density, normalized to the respective input

levels and then the ratio of PTPσ (or p75NTR) to TrkA was calculated and compared across samples.

Statistics: Data with multiple groups and one variable were analyzed by one-way ANOVA using either Dunnett or Tukey post-tests to control for multiple comparisons. Experiments with two variables were analyzed with two-way ANOVA using a Dunnett post-test. Statistical analyses were carried out using Prism version 8 or 9.

Data Availability: The datasets generated during and/or analyzed during the current study are available from the corresponding author on reasonable request.

Funding Sources: This work was supported by the Morton Cure Paralysis Fund, the OCTRI Biomedical Innovation Program, the OHSU Bioscience Innovation Program, and the M.J. Murdock Charitable Trust (MSC & BAH); NIH R01 HL093056 (BAH); NIH GM135295 (AMB); NIH P20GM103434 via the West Virginia IDeA Network for Biomedical Research Excellence (GBD); NIH T32HL094294 and AHA 19POST34460031 (RTG); NIH F31HL152490, AHA 20PRE35210768 and the Steinberg Endowment for Graduate Education (MRB).

Author Contributions: MRB, RTG, BAH designed and conducted experiments, collected and analyzed data, and wrote the manuscript. MSC developed the small molecules, designed and conducted experiments and wrote the manuscript. HJ helped design and synthesize the small molecules. MS conducted experiments and analyzed data. NJR, AMB, GBD designed, conducted, analyzed phosphatase screening experiments, produced Illudalic acid and provided input on the manuscript.

Conflicts of Interest: The authors of this study have no conflicts of interest to report.

Acknowledgments: The authors would like to thank Dr. Michael Pellegrino, Dr. Amber Bannon, **Kimberly Vreugdenhil, Seongkyung Seo,** and Antoinette Olivas for technical assistance with early studies of these compounds. We would like to thank Dr. Moses Chao (Skirball Institute, NYU) for the HEK-TrkB cells and for the TrkA-RFP and p75NTR plasmids (Addgene plasmid # 24093, 24091). The supporting table of contents figure was made with Biorender.com.

Supporting Information:

The Supporting Information includes the full synthesis scheme and chemical products and can be found in the published paper.

Chapter 5

Using FRET biosensors to monitor Chondroitin Sulfate Proteoglycan signaling in sympathetic neurons

Matthew R. Blake BS, Alix Thomas MS, Shanice Sueda, Carsten Schultz PhD, Beth A. Habecker PhD

To be uploaded to BioRxiv…

Abstract

The mechanistic details of chondroitin sulfate proteoglycan (CSPG) signaling in sympathetic neurons are not well established. Understanding how CSPGs elicit repulsive cues in neurons would help develop new therapeutic approaches aimed at nerve regeneration. We attempted to use live cell analysis with multiplexed Forster resonance energy transfer (FRET) probe imaging to examine downstream CSPG signaling in neurons, emphasizing pathways downstream of Tropomyosin-related kinase A (TrkA) due to the critical role of TrkA signaling during sympathetic axon regeneration. We used the sympathetic neuronal model cell line PC12 to examine a group of biosensors and found PKA and PKC signaling was altered by CSPGs and the TrkA ligand Nerve Growth Factor (NGF). Based on results from PC12 cells, we examined PKA and PKC biosensor responses to NGF and CSPGs in dissociated primary neurons from the superior cervical ganglia (SCG). Signaling events observed in PC12 cells did not replicate in sympathetic neurons, and PKA or PKC modulation did not promote neurite outgrowth across inhibitory CSPGs.

I. Introduction

CSPG gradients are thought to facilitate neuronal axon guidance by stimulating several cell-surface receptors including receptor protein tyrosine phosphatase sigma (PTPσ) (Lang et al., 2015; Shen et al., 2009b). In general, CSPGs prevent dimerization of PTPσ, which enables activity of its catalytic phosphatase domain. When PTPσ monomers dimerize, the wedge domain of one receptor monomer physically blocks the enzyme active site of another monomer and prevents catalytic phosphatase activity (C. H. Coles et al., 2011; Majeti et al., 1998; Wu et al., 2017). PTPσ phosphatase activity is critical for its ability to inhibit nerve outgrowth by targeting a number of signaling pathways (Ohtake et al., 2016). For example, PTPσ dephosphorylates the activated family of Tropomyosin receptor kinases (Trk), antagonizing neurotrophin signaling, a key pathway in axon outgrowth and survival (Faux et al., 2007). In sympathetic neurons Nerve Growth Factor (NGF) signaling via TrkA receptor is the key regulator of axon outgrowth(Glebova & Ginty, 2004) and is suppressed by PTPσ (Faux et al., 2007). Generally, PTPσ suppression of axon outgrowth is thought to suppress canonical growth promoting pathways downstream of TrkA including ERK and AKT activation mediated by PKA, PKC and Src (Lewin & Carter, 2014; Obara, Labudda, Dillon, & Stork, 2004; Sivasankaran et al., 2004). In addition to suppressing axon growth promoting pathways, PTPσ is thought to cause growth cone collapse by altering the cytoskeleton in a RhoA mediated mechanism (Ohtake & Li, 2015; Ohtake et al., 2016). While the Trk-PTPσ signaling axis has been studied in other neuronal sub-types, mostly of the central nervous system (Ohtake & Li, 2015), relatively little is known about this signaling pathway in peripheral

sympathetic nerves. One key limitation to understanding the large number of signaling effectors downstream of TrkA in sympathetic nerves is a lack of effective methods to study signaling in real-time. Traditional methods like western blotting are restricted to few targets at predetermined time points. Real-time signaling analysis at the single cell level has long been considered preferential to traditional bulk cell methods and to this end, many have used genetically encoded Forster-resonance energy transfer (FRET) biosensors to study specific elements of a signaling cascade (Kuchenov et al., 2016; Regot, Hughey, Bajar, Carrasco, & Covert, 2014). One particularly innovative method that inspired this work, utilized DNA printing technology to "spot" multiple DNA-encoded FRET-biosensors in tandem with reverse transfection reagents on Labtek cell-culture dishes. This setup enables transfection of cells grown on the culture dish and multiplexed analysis of signaling pathways. FRET-biosensors have been used in numerous cell types including sympathetic neurons, but technical limitations have prevented widespread use (Greenwald, Mehta, & Zhang, 2018; Nunes et al., 2012; Saucerman et al., 2006).

FRET biosensors used in this study are engineered to indicate target protein activity and usually consist of a substrate domain and substrate-recognition domain. These domains are flanked by one protein of a fluorescent protein pair that can undergo FRET (e.g., CFP and YFP). One common sensor design utilizes a portion of the target protein that can be phosphorylated (similarly to the target protein and tied to protein activity). In this case the recognition domain changes proximity to the phosphorylated protein which alters FRET by changing the proximity of CFP and YFP. An alternative design used on modern FRET sensors utilizes a substrate domain that is altered by the

active target protein, this changes proximity of a recognition domain that “senses” the alteration, ultimately altering FRET by changing the proximity of CFP and YFP. For example, the PKA biosensor used in this study has a PKA pseudo-substrate domain that is phosphorylated by PKA. Phosphorylation of the substrate brings the sensing domain into closer proximity and subsequent flanking CFP and YFP proteins into closer proximity, increasing FRET. When phosphorylation of the PKA pseudo-substrate is reversed by phosphatase activity, the sensing domain stops interacting with the substrate domain and the CFP and YFP flanking proteins are further apart which reduces FRET (Figure 5.1B). These sensors enable live-cell monitoring of PKA activity in response to a stimulus. Examination of the FRET (YFP) to CFP ratio gives a glimpse at PKA activity across time. To quantify FRET, we utilized a FRET analysis platform developed previously which automates the entire process of segmentation and ratio analysis, enabling examination of large cell numbers relative to that typically examined manually.

Here we utilized transiently transfected genetically encoded FRET-biosensors to better understand CSPG and NGF signaling. We used PC12 cells to screen a number of FRET-biosensor responses to CSPG and NGF stimulation. Our screen in PC12 cells identified PKA and PKC which we then tested in dissociated sympathetic neurons. In neurons we found that CSPG and NGF stimulus had little effect on PKA or PKC activity as detected by our FRET sensors. Furthermore, we established that modulation of these pathways *in vitro* did not restore neurite outgrowth across inhibitory CSPGs. We hope that this work improves experimental design for future use of FRET-biosensors in primary neurons and other difficult to transfect or highly polarized cell-types.

II. Results

A. FRET biosensors screened to assess impact of NGF and CSPG stimulation

In order to better understand how NGF driven TrkA signaling is affected by CSPGs acting via PTPσ, we used a number of FRET biosensors to monitor downstream signaling pathways including: ERK, RhoA, FAK, Src, PKA, and PKC (Figure 5.1A). PC12 cells express TrkA, respond to NGF by extending neurites, and retract neurites in response to CSPGs (Gopalakrishnan et al., 2008; Greene, 1978), so we started by testing the response of multiple FRET sensors to NGF and CSPGs in differentiated PC12 cells. The inspiration for this work utilized DNA-spotting to print DNA encoded FRET biosensors onto a culture dish such that cells seeded across the plate surface underwent reverse transfection and expressed the biosensor. Spotting plates with multiple biosensors allowed multiplexing of biosensor analysis. We attempted to do this with PC12 cells and found that they are difficult to transfect using chemical methodologies like lipofectamine and thus were not amenable to reverse transfection on DNA-spotted plates. To overcome this, we utilized the Neon™ transfection system from Invitrogen which electroporates cells, enabling DNA-based FRET-biosensors to enter the cell and undergo gene expression. Using manufacturer recommended electroporation settings we achieved substantial improvement of transfection efficiency compared to lipofectamine with an eGFP control plasmid (Figure 5.1C). With an efficient transfection method, we were able to express genetically-encoded FRET biosensors in PC12 cells. This method limited us to analyzing a much smaller number of sensors than we had planned.

When we examined these sensors (Figure 5.1A), we found fewer consistent changes than we expected (Figure 5.1D). This may be because we intended to examine later time points following stimulus with NGF/CSPGs and our sampling rate (every 5 minutes) may have missed early signaling changes. Despite this shortcoming, we observed consistent changes in PKA and PKC FRET biosensors in response to NGF. NGF stimulated a significant reduction in PKA biosensor FRET. When cells were stimulated with NGF and CSPGs at the same time the decrease did not occur, suggesting alteration of NGF signaling by CSPGs (Figure 5.1E). A larger response occurred with the PKC biosensor. NGF reduced PKC biosensor FRET which was blocked when NGF and CSPGs stimulation occurred concurrently (Figure 5.1F). These data were consistent enough to warrant follow up validation in primary sympathetic neurons.

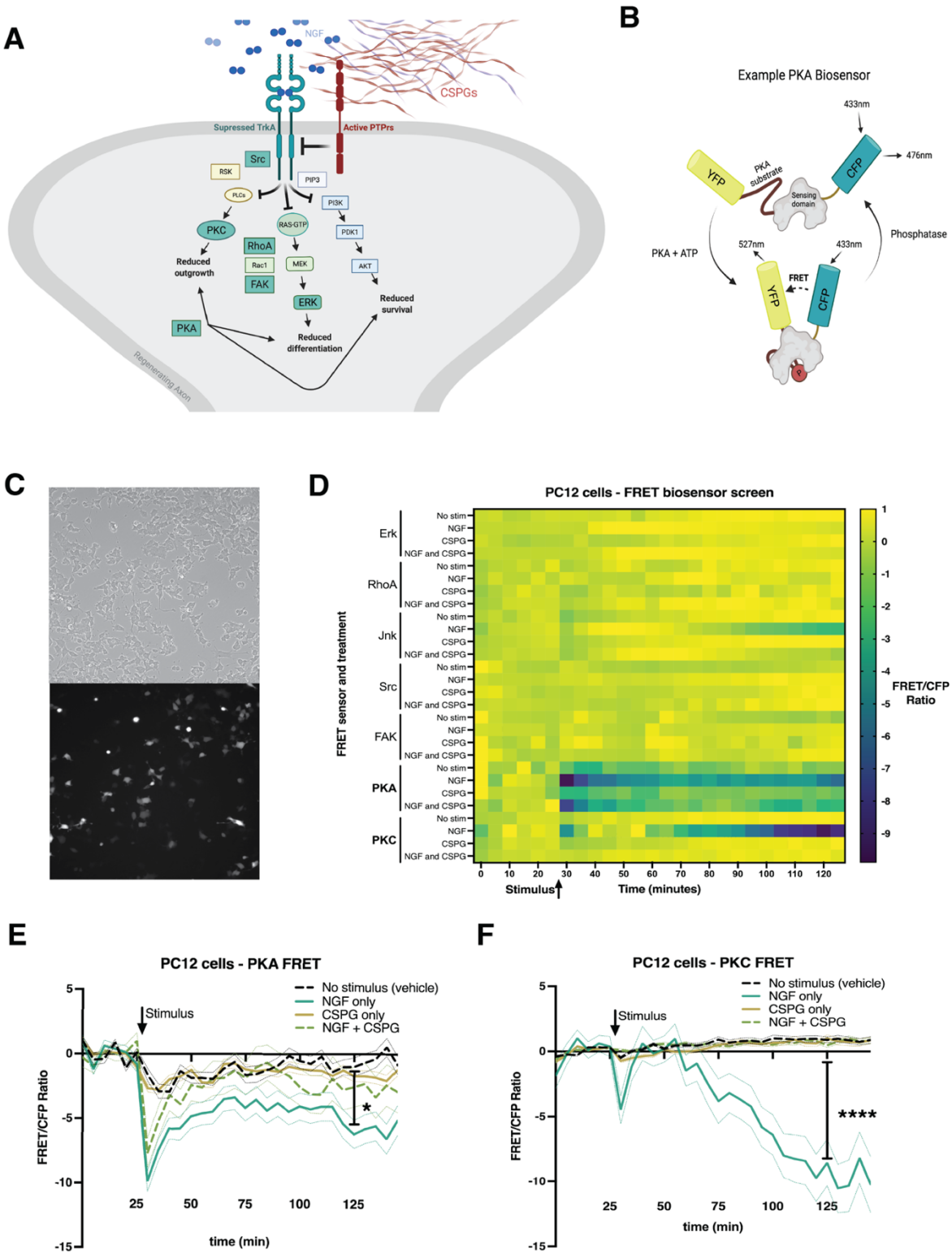

Figure 5.1: PC12 cells have varied FRET biosensor responses to NGF and CSPGs. **(A)** Cartoon outlining the pathways downstream of TrkA examined using FRET biosensors which are colored turquoise. **(B)** Example of PKA FRET biosensor, illustrating when PKA phosphorylates a PKA pseudo-substrate, changing the conformation of the sensor and leading to increased FRET between CFP and YFP protein subunits on the sensor. **(C)** Example of transfection

efficiency of an eGFP control plasmid in differentiated PC12 cells with the Neon transfection system, top image is brightfield image, bottom image is of eGFP. **(D)** Heatmap of FRET biosensors tested in screen of PC12 cell responses to NGF and CSPGs. Color change corresponds to FRET ratio across time left to right. Stimulus added at 30 minutes of imaging. **(E)** PKA FRET biosensor response, NGF induces a significant difference in FRET response as compared to no stimulus control at 125 minutes. All other responses are not significantly different from no stimulus control. Plotted are mean FRET ratios at a given time point, statistics one-way ANOVA Dunnett's post-test, comparison to no stimulus control, select comparisons shown. n>150 cells per conditions for each sensor. **(F)** PKC FRET biosensor response, NGF induces a significant difference in FRET response as compared to no stimulus control at 125 minutes. All other responses are not significantly different from no stimulus control. Plotted are mean FRET ratios at a given time point, statistics one-way ANOVA Dunnett's post-test, comparison to no stimulus control, select comparisons shown, n>150 cells per conditions.

B. PKA biosensor FRET and PKA modulation in primary SCG neurons

Given the robust response of PC12 cells to NGF and CSPGs we asked whether the same response occurred in sympathetic neurons. Neurons were transfected by electroporation, generating suitable expression of the PKA biosensor (Figure 5.2A). We intended to utilize the automated FRET analysis platform to quantify FRET in the neurons, but were unable to do so. We found that the highly polarized structure of the neuron, and the significant motility of neuronal processes across the approximately 2 hours of imaging, made it impossible to use the segmentation algorithms built in to the analysis platform. Therefore, we analyzed FRET(YFP) to CFP ratios manually using ImageJ. We visualized the change in FRET/CFP ratio normalizing to no stimulus control neurons (Figure 5.2B). There was a high degree of variability in the FRET ratio despite normalization, which can be seen in the fact that only the positive control, cAMP, significantly upregulated PKA biosensor FRET (Figure 5.2B). While these data indicate that the assay is working, they also indicate that NGF and CSPGs do not stimulate robust changes in PKA on the timescale that we examined. Additionally, we asked whether modulating PKA affected sympathetic neurite outgrowth across CSPGs in the presence of a small amount of NGF.

Sympathetic neurite outgrowth across Laminin and CSPGs was reduced roughly 50% compared to the laminin only control (Figure 5.2C). Addition of a PKA activator, cell permeable cAMP analog, or a PKA inhibitor, KT5720, had no positive or negative effect on neurite outgrowth in neurons grown on Laminin alone or Laminin and CSPGs (Figure 5.2C). This suggests that PKA does not play a dominant role in CSPG suppression of neurite outgrowth in sympathetic neurons.

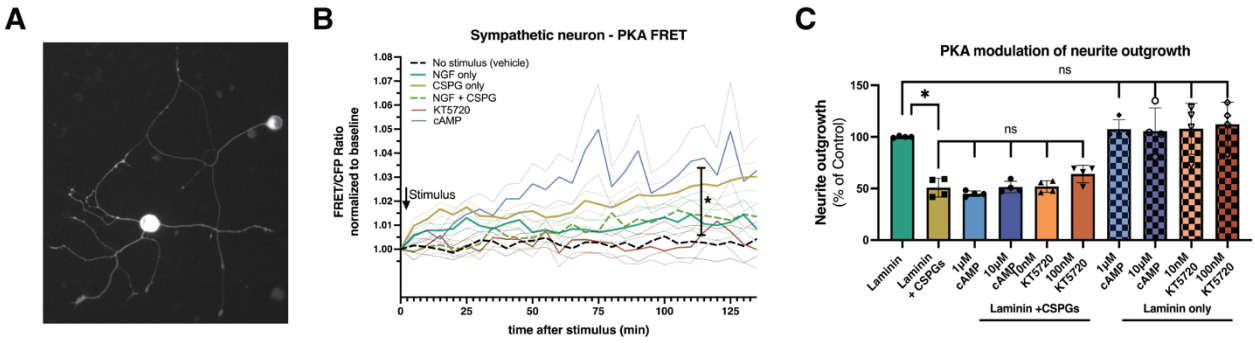

Figure 5.2: PKA FRET biosensor response in primary sympathetic neurons. **(A)** Example image of YFP fluorescence (FRET) in primary sympathetic neurons. Cell bodies were manually analyzed in response to stimuli. **(B)** PKA FRET/CFP ratio normalized to baseline no-stimulus control measurements (acquired for 30 minutes before stimulus). The only significant response when compared to no stimulus controls was cAMP (10μM) positive control cells. Mean FRET/CFP ratio fold-change over no stimulus control plotted at a given time point, statistics one-way ANOVA Dunnett's post-test, comparisons to no stimulus control cells at 115 minutes post stimulus, select comparison shown, n=70, 65, 67, 67, 68, 66 cells analyzed for no stim, NGF, CSPG, NGF+CSPG, KT5720, cAMP respectively. **(C)** Modulation of PKA does not restore primary sympathetic neurite outgrowth across CSPGs nor does it modulate neurite growth on Laminin alone. Soluble cAMP used to promote PKA activity at 1μM and 10μM. PKA inhibitor KT5720 used to reduce PKA activity at 10nM and 100nM. Plotted is the mean neurite length as a percent of Laminin-only controls across 4 independent experiments. Statistics one-way ANOVA Tukey's post-test, select comparisons shown.

C. PKC biosensor FRET and PKC modulation in primary SCG neurons

Given the significant PKC biosensor response to NGF in PC12 cells and the blockage of this response by CSPGs, we examined if this pathway was also affected in sympathetic neurons. We transfected sympathetic neurons with a PKC biosensor and examined the response to NGF and CSPGs (Figure 5.3A). We utilized the PKC agonist

PMA as a positive control and BIM as a negative control. Data were analyzed manually and normalized to no stimulus control neurons. Results were highly variable resulting in no significant difference between all groups with the exception of PMA which significantly increased PKC FRET as predicted (Figure 5.3B). These data suggest that the assay is working but that NGF and CSPGs do not stimulate significant PKC response on the timescale examined. We concurrently examined the ability of PKC modulation to alter sympathetic neurite extension across CSPGs. Data were normalized to Laminin only control neurons. Neurons grown on Laminin and CSPGs had an approximately 50% reduction in neurite outgrowth compared to Laminin alone (Figure 5.3C). Modulation of PKC with PMA or BIM did not lead to a positive or negative effect on neurite outgrowth in neurons grown on Laminin or Laminin and CSPGs. These data suggest that PKC modulation does not play a dominant role in mediating sympathetic neuronal response to CSPGs.

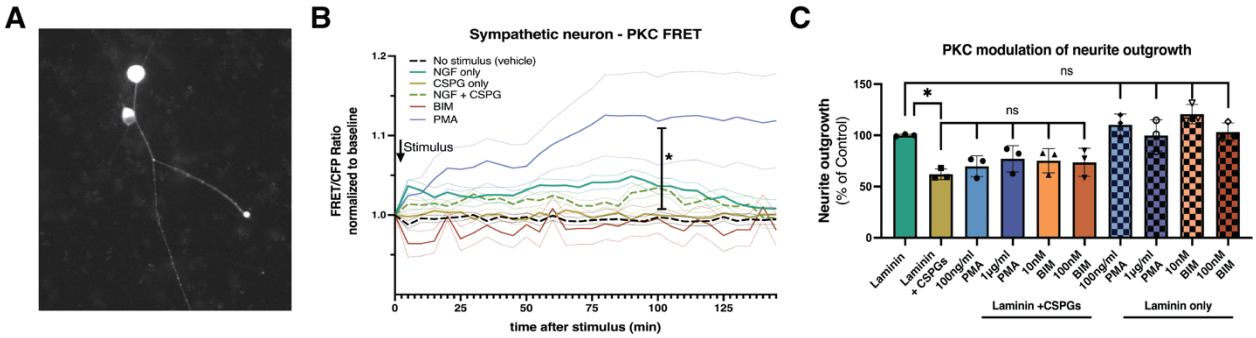

Figure 5.3: PKC FRET biosensor response in primary sympathetic neurons. **(A)** Example image of YFP fluorescence (FRET) in primary sympathetic neurons, cell bodies were manually analyzed in response to stimuli. **(B)** PKC FRET/CFP ratio normalized to baseline no-stimulus control measurements acquired for 30 minutes before stimulus. The only significant response when compared to no stimulus controls was PMA (1μg/mL) positive control cells. Mean FRET/CFP ratios fold-change over no stimulus control plotted at a given time point, statistics one-way ANOVA Dunnett's post-test, comparisons to no stimulus control cells at 100 minutes post stimulus, select comparison shown, n=32 cells per condition. **(C)** Modulation of PKC does not restore primary sympathetic neurite outgrowth across CSPGs nor does it modulate neurite growth on Laminin alone. PMA was used to promote PKC activity at 100ng/mL and 1μg/mL. PKC inhibitor BIM used to reduce PKC activity at 10nM and 100nM. Plotted is the mean neurite length as a percent of

Laminin-only controls across 4 independent experiments. Statistics one-way ANOVA Tukey's post-test, select comparisons shown.

III. Discussion

The impetus for this project was the high-throughput FRET imaging platform used to study Epidermal Growth Factor Signaling developed by our Colleagues in the Carsten Schultz Lab (Kuchenov et al., 2016). This setup utilized DNA-based FRET biosensors that could be printed onto a surface which, when cells were seeded onto the culture dish, underwent reverse transfection so that multiplexed sensor analysis could be done in the same dish. In addition to the physical experimental setup, the platform also utilized a high-throughput set of imaging analysis algorithms which could rapidly analyze large numbers of cells. Historically, use of FRET-biosensors required painstaking manual analysis since segmentation of cells presented a significant challenge for most cellular analysis programs. Given these characteristics, this platform seemed ideal to examine signaling response to NGF and CSPGs in a more efficient way than was previously possible with western blotting, which has significant spatiotemporal limitations. Furthermore, much of the genetically-encoded biosensors available corresponded to important signaling pathways involved in NGF and CSPG signaling. NGF is known to activate a canonical set of downstream signaling pathways that promote axon outgrowth by altering transcriptional programs or changing cytoskeletal structure. We chose to focus on a small subset of these biosensors, focusing on ERK, PKA, PKC, and Src for downstream growth promoting pathways that alter transcriptional programs (Lewin & Carter, 2014; Obara et al., 2004; Sivasankaran et al., 2004). For signaling changes to cytoskeletal structure, we

examined RhoA and FAK (Ohtake & Li, 2015; Ohtake et al., 2016). CSPGs are known to suppress TrkA signaling and therefore we hypothesized that these pre-selected pathways would be altered by CSPG antagonism of NGF signaling. We envisioned this platform as a way to examine real-time signaling changes in these important pathways but despite our best efforts we were unable to translate this theoretical promise into solid experimental data.

To start, we were unable to utilize the DNA spotting method of reverse transfection with PC12 cells or sympathetic neurons, which are difficult to transfect. As such, we needed to use electroporation to achieve sufficient transfection efficiency, forcing use of a 96-well plate format which meant that monitoring multiple pathways in tandem had to be done across multiple wells. Overall, this significantly reduced the number of sensors we could examine, forcing us to select specific ones (Figure 5.1A). When we began looking at signaling, we faced additional hurdles with our physical imaging setup. Adding multiple treatments to a 96-well plate takes time and this presented two separate issues. The first was that when pipetting a treatment, the environmental chamber that the cells were in had to be opened, leading to a significant drop in temperature which could be seen in FRET changes at the next sampling time point. This leads into the second issue, which was the amount of time it takes to add a treatment. Treatment with multiple stimuli (NGF and CSPG) across wells required a significant amount of time ~2 minutes and waiting for the temperature to recover required an additional 3-5 minutes meaning that signaling pathways were not assessed for 5-7 minutes after addition. This is problematic since some changes can occur rapidly (<1 minute).

PC12 cells and sympathetic neurons both express TrkA and respond to NGF by sending out neurites, which are reduced by CSPGs (Gopalakrishnan et al., 2008; Greene, 1978). Given these characteristics we examined if FRET responses in PC12 cells were replicated in sympathetic neurons. We did not observe the same robust response to NGF and CSPGs in primary neurons for either PKA or PKC biosensors that we saw in PC12 cells. Interpreting this result should be done with care as there are many reasons why this assay may not have measured any significant effect. First, electroporation of the FRET sensor may have led to saturating construct expression levels which could lead to lowered sensitivity in the assay. Evidence for this is that our positive controls had very slight changes in FRET. These amounts of both PMA and cAMP should have led to robust responses in FRET compared to the no stimulus control cells. NGF and CSPGs may simply have stimulated too subtle a change in too few biosensor molecules for us to observe a change. Perhaps the most likely reason for our results can be attributed to cell motility. Regenerating neurons send out neurites rapidly after injury. Our imaging took place approximately 18 hours after dissociation/transfection and by this time-point neurons are highly polarized (Figure 5.2A,5.3A). Additionally, neuronal processes moved around a great deal during the 2-hour imaging time course. Thus, we manually segmented cells and measured FRET ratios in the cell body which might be different than what is occurring at the axon or growth cone.

Given the evidence from the literature that PKA and PKC modulation promotes neurite outgrowth across inhibitory CSPGs (Sivasankaran et al., 2004; Udina et al., 2010) we examined this in primary sympathetic neurons. We found that neither positive or

negative stimulation of PKA and PKC led to altered neurite outgrowth. This result is confounding in context of the literature and we suspect that given the significant amount of CSPG inhibition, (~50%) neither pathway was able to overcome the inhibitory signaling. It is likely thar modulating PKA and PKC could promote axon outgrowth across CSPGs in the context of less CSPG or a secondary positive stimulus (Pearson et al., 2018).

Taken together we hope that this information can be utilized by other researchers to design better FRET experiments to assess downstream signaling. If we were to do this experiment again, we would devote our efforts to using viral-based FRET biosensors to achieve stable expression so that neurons could be assessed at later time points after dissociation and plating. This strategy would have produced more stable cell morphology and enabled more detailed examination of the FRET response in different cellular compartments like cell body versus axon responses which likely differ in this context and may provide greater assay sensitivity. This strategy has been used by several groups including one that examined PKA activity in primary sympathetic neurons (Nunes et al., 2012). Another thing we would invest time in is finding an imaging setup that could sample at a faster rate and did not see such a temperature swing when the stimuli are added. This could reduce some of our largest shortcomings which were temperature drops and missed early signaling time points when significant changes may occur.

IV. Methods

Cell lines and culturing: PC12 cells were used to model some aspects of sympathetic nerve signaling. PC12 cells express TrkA, respond to NGF by neurite extension, and retract neurites in response to CSPG (Gopalakrishnan et al., 2008; Greene, 1978). PC12 cells were maintained in RPMI-medium (ATCC) supplemented with 10% horse serum (HS, Hyclone), 5% FBS and 1% Anti-Anti. For experiments cells were differentiated for 5-7 days in RPMI fortified with 2%FBS and 50ng/mL NGF (Alomone Labs), prior to experimentation cells were serum starved in RPMI + 2ng/mL NGF for 4 hours.

Primary Neuron cell culture: Primary Sympathetic neurons were derived from P0-P2 Sprague Dawley Rat pups(Blake et al., 2022). Superior Cervical Ganglia (SCG) were isolated and enzymatically dissociated for 30 minutes in 1mg/mL Collagenase and 10mg/mL Dispase, this was followed by mechanical dissociation using a reduced bore size fire-polished borosilicate glass pipette. Once a homogenous solution was achieved, the enzymatic reaction was quenched using HG-DMEM fortified with 10% FBS, Cells were pelleted at 2000 RPM x 5 min, resuspended in growth medium and plated for 30 minutes on a 10cm plate at 37°C, 5%CO_2 to remove glial cells by sequential plating. The resulting growth medium was collected and the plate gently rinsed with growth medium to remove any neurons that may have settled during the plating, cells were pelleted and resuspended in C2 Media. C2 medium is a 50/50 mixture of F12 medium (Gibco) and low-glucose DMEM, fortified with 0.5mg/mL BSA, 30nM Selenium, 10 µg/mL Transferrin, and 10 µg/mL Insulin (Gibco). For long term culturing SCG neurons were plated onto poly-d-lysine and Laminin (2µg/mL, R&D Systems) coated plates in C2 medium fortified

with 10ng/mL NGF, 1%Penicllin/Streptomycin (Gibco) and 0.1% Fluorodeoxyuridine to kill dividing cells.

Incucyte sympathetic axon outgrowth assay: Sympathetic neuron cultures were prepared as described above (Blake et al., 2022) and 5,000 neurons/well were plated onto a 96 well plate (TPP) coated with poly-L-lysine (PLL, 0.01%, Sigma-Aldrich) and either laminin (2µg/mL, R&D Systems) or laminin and CSPGs (1-2 µg/mL, Millipore; concentration was calibrated to inhibit outgrowth by 50% and differed between batches). Neurons were cultured in serum free C2 medium supplemented with 10 ng/mL NGF (Alomone labs), 1%Penicllin/Streptomycin (Gibco) and 0.1% Fluorodeoxyuridine. Neurons were treated with either vehicle (5% DMSO) or the compounds cAMP, KT5720, PMA, or BIM at various concentrations as described in figure legends. Live cell imaging was carried out using an Incucyte Zoom microscope (Essen BioScience), with 20x phase images acquired every 2 hrs over a 40 hr period. Neurite length was measured using Cell Player Neurotrack software (Essen BioScience) and used to calculate the neurite length(Blake et al., 2022).

Transfections: To transfect PC12 cells, we used the Neon electroporation system (10μL kit, Invitrogen). Cells were trypsinized, resuspended, pelleted, rinsed with PBS and resuspended in the transfection buffer. The cell density used in each 10uL reaction was $1X10^7$ cells/mL combined in solution with 0.75ug of biosensor DNA per reaction. Manufacturer recommended electroporation settings were used for PC12 cells: pulse voltage (1500 V), pulse width (10ms), and pulse number (3). Using these parameters, we achieved substantial improvement of transfection efficiency compared to lipofectamine 2000 with an eGFP control plasmid (Figure 1C). Parameters used for primary sympathetic

neurons have been described previously (Pellegrino & Habecker, 2013) but briefly: voltage (1500 V), pulse width (20ms), and pulse number (1).

FRET Biosensor screening and quantification: Initial FRET biosensor screening was accomplished using PC12 cells differentiated using the aforementioned protocol. Four identical transfections were completed as described above, and cells were pooled in a single well of a 12-well plate before being split into 12-wells of a 96-well glass bottom plate (Cellvis, 1.5H-N) coated with PDL and laminin. Cells were plated in an optimized media consisting of Fluorobrite media (Gibco) supplemented with 0.5mg/mL BSA, 3mM L-glutamine and 2ng/mL NGF. Fluorobrite media was used to reduce background autofluorescence during imaging. 12-16 hours after transfection, cells were imaged using an Olympus spinning disc confocal microscope housed in an environmental chamber held at 37C 5%CO2. Cells were excited with a 440nm LED (SpectraX), spectra passed through a bandpass filter, 425-452nm for CFP excitation. CFP fluorescence was then passed through an emission cube (483/32 (483 peak, 32 range)) for CFP image capture. YFP fluorescence was passed through an emission cube (542/27 (542peak, 27range)) for YFP image capture. The ratio of YFP/CFP was calculated to determine the FRET emission ratio. Cells were scanned every 5 minutes for 30 minutes to establish a baseline measurement before addition of stimulus. Various stimuli were added; vehicle (Fluorobrite media), 50ng/mL NGF (diluted in Fluorobrite media), or 2ug/mL purified CSPGs (diluted in Fluorobrite media). These stimuli were added in various combinations as indicated in the figure legends then imaged for approximately 2hr. PC12 cell FRET ratios were calculated using several algorithms developed by the Carsten Schultz Lab. The first

ImageJ macro combined all CFP and YFP images across the time course (Schindelin et al., 2012). The second ImageJ macro, FluoQ, analyzes FRET ratios and has been described in detail previously (Kuchenov et al., 2016; Stein, Kress, Reither, Piljic, & Schultz, 2013). Briefly, combined CFP-YFP images are thresholded with the Triangle method, smoothed, and segmented with the binary mask generated using the Huang fuzzy method. Segmented-image FRET ratios are calculated and low-expressing cells and cells with erroneous FRET ratios are discarded. FRET/CFP ratios across the 30-minute baseline period are averaged and used to normalize FRET/CFP ratios after stimulus. FRET/CFP ratios for each cell measured are averaged at each time point and plotted in Figure 1. Automated FRET analysis was not possible when analyzing primary sympathetic neurons given the high motility and polarized nature of these neurons. To analyze primary neurons, we generated 16-bit tiff images of each respective channel (CFP and YFP-FRET) across the time course. The ImageJ "Math" tool was used to divide the FRET image by the CFP image generating a new image that corresponds to the FRET/CFP ratio. The ImageJ manual selection tool was then used to draw a region of interest (ROI) around a given cell body. Plotting the z-projection of this given ROI displays the FRET/CFP ratio over the time course which could be exported and used for analysis. The average FRET ratio across the 30-minute baseline was used to normalize the FRET ratios after cell stimulus. FRET ratios were averaged across each ROI (cell) for a given stimulus and plotted in Figures 2 and 3. Statistical analysis was done at the time point where the greatest difference was observed between stimuli.

FRET biosensors used:

Target	Sensor name	Domains	Name used	Reference
ERK	EKAR2G1	WW (phosphopeptide binding domain)-Substrate domain (PDVPRTPVDKAKLSFQFP)	ERK	(Komatsu et al., 2011)
RhoA	RhoA2G	RhoA-binding domain (RBD) of rhotekin– RhoA	RhoA	(Fritz et al., 2013)
FAK	FAK biosensor	SH2(c-Srk) -substrate	FAK	(Seong et al., 2011)
Src	Src biosensor	CFP-SH2 (Src)- Substrate (synthetic)	Src	(Ouyang, Sun, Chien, & Wang, 2008)
PKA	AKAR3EV	FHA1 domain – PKA substrate (LRRATLVD) – NES	PKA	(Komatsu et al., 2011)
PKC	Eevee-PKC	PKCβ C1 domain – FHA1 domain (phosphopeptide binding) – Substrate domain (KKKKKRFTFKDSFKL) NES	PKC	(Komatsu et al., 2011)

Animal welfare: Sprague-Dawley rats obtained from Jackson Laboratories West (Sacramento, CA) were used for all experiments. Rats were kept on a 12h:12h light-dark cycle with *ad libitum* access to food and water. Ganglia from male and female P0-P2 neonatal rats were used to generate dissociated primary sympathetic neurons. All procedures were approved by the OHSU Institutional Animal Care and Use Committee and comply with the Guide for the Care and Use of Laboratory Animals published by the National Academies Press (8^{th} edition).

Statistics: Statistical significance of FRET ratio data was analyzed at a given time point where the largest difference was observed (indicated in each respective figure). One-

way ANOVA and Dunnett's post-hoc test was used to compare all conditions to no stimulus control cells. The sample sizes across each FRET experiment differs and is indicated in each figure legend. For sympathetic neurite outgrowth experiments one-way ANOVA and Tukey's post-hoc test was used to examine differences in neurite outgrowth at the final time point. All statistical analyses were carried out using Prism 9.

Chapter 6

Discussion and conclusions

I. Dissertation summary

Sympathetic nerves are lost in the damaged myocardium (infarct) after myocardial infarction (MI) and the relative area of denervation predicts risk of sudden cardiac arrest due to arrhythmias (Boogers et al., 2010; Fallavollita et al., 2014; Nishisato et al., 2010; Stanton et al., 1989; Vaseghi et al., 2014; Zipes & Rubart, 2006) leading to the hypothesis that sympathetic reinnervation of the infarct could reduce arrhythmias. This dissertation has attempted to provide new insights on the molecular basis of sympathetic axon outgrowth inhibition after MI. Chapter 2 demonstrated that 4,6-sulfated CS-GAGs are enriched in the infarct 7 days after MI. We found expression differences in CS-GAG sulfation enzymes precede accumulation of sulfated CS-GAGs in the infarct. The CSPG tandem-sulfation enzyme, CHST15, is increased after MI and CSPG 4-sulfatase, ARSB, is decreased after MI; suggesting a mechanism of sulfation production and maintenance after MI. Reducing 4,6-sulfation of CS-GAGs by siRNA knockdown of *Chst15* restored sympathetic nerves to the infarct and reduced arrhythmia susceptibility after MI. This additional layer of specificity provides another therapeutic target to alter the inhibitory scar and promote axon regeneration. Despite exciting data in support of sympathetic reinnervation after MI, in chapter 3 we asked whether reinnervation of the infarct immediately after MI had long-term negative consequences, given evidence that excess

norepinephrine (NE) after MI can lead to heart failure (Florea & Cohn, 2014). We wondered if reinnervation of the infarct would amplify the effects of excess NE after MI and reduce cardiac pump function at later time points post-injury. We compared cardiac function 40 days after MI in animals treated with Intracellular Sigma Peptide (ISP; promotes reinnervation) or with vehicle. When we examined reinnervation 40 days after MI to verify that ISP had worked, we were surprised to find that vehicle treated animals had infarcts with restored sympathetic nerves similar to animals treated with ISP. This complicated interpretation of the results, but broadly speaking we found that 40 days after MI, animals had restored cardiac performance similar to sham-surgery animals from previous studies including reduced arrhythmia susceptibility (Gardner et al., 2015). These data provide evidence that reinnervation of the infarct is not deleterious for cardiac performance at later time points. In looking for a possible explanation for spontaneous regeneration in 40-day post-MI vehicle treated animals we were inspired by Chapter 2 and examined 4,6-sulfation of CS-GAGs. We found that day 40 post-MI vehicle treated animals had reduced 4,6-sulfation of CS-GAGs and reduced core proteoglycan Neuron-glial Antigen 2 (NG2) levels similar to healthy unoperated left ventricle; suggesting that in mice, cardiac remodeling after MI leads to a permissive environment for sympathetic axon outgrowth. With increasing evidence that CSPGs suppress sympathetic nerve regeneration in the heart after MI, we sought to develop new therapeutics to promote reinnervation in Chapter 4. Work with Michael S. Cohen Ph.D in Chapter 4 described novel small molecules, HJ-01 and HJ-02, that disrupt PTPσ interactions with Tropomyosin-related Kinase A (TrkA). Targeting this interaction with HJ-01 and HJ-02

promoted axon outgrowth signaling and enhanced sympathetic axon outgrowth across CSPGs(Blake et al., 2022). Chapter 5 discussed our attempt to use genetically encoded FRET-biosensors to understand signaling pathways downstream of TrkA that are altered by CSPGs. A number of technological challenges limited our assessment to Protein Kinase A (PKA) and Protein Kinase C (PKC) sensors in primary sympathetic neurons and we did not observe any significant responses to CSPGs.

II. Role of CSPG sulfation in sympathetic nerve regeneration

We knew from previous work that CS-GAGs inhibited sympathetic axon outgrowth (Gardner & Habecker, 2013) but it was unknown if CS-GAG sulfation was the key mediator of inhibition, as is the case in other nerve injury models like spinal cord injury (SCI) or traumatic brain injury (TBI) (Brown et al., 2012; Gilbert et al., 2005; Pearson et al., 2018; H. Wang et al., 2008; Yi et al., 2012). Chapter 2 demonstrated that 4,6-sulfation of CS-GAGs inhibits sympathetic axon outgrowth after MI. We showed that 4-sulfated (4S) and 6-sulfated (6S) CS-GAGs are enriched in the infarct and that enzymes involved in CSPG sulfation are altered after MI. Notably, the 4,6-tandem sulfation enzyme CHST15 is upregulated and the 4-sulfatase ARSB is downregulated after MI. These expression changes could explain increased 4 (4S) and 4,6-sulfated (4S,6S) CS-GAGs, providing a mechanism by which sulfation changes occur after MI. To test whether these sulfation patterns inhibited sympathetic axon outgrowth we used two strategies. The first used purified ARSB protein to remove 4S from CS-GAGs in an *in vitro* axon outgrowth assay. ARSB is endogenously expressed in the heart but can also be purchased as a purified

protein. Removing 4S from cardiac scar tissue with ARSB restored sympathetic axon outgrowth towards the infarct, suggesting that 4S CS-GAGs are a critical regulator of sympathetic axon outgrowth. ARSB is a clinically approved therapeutic Naglazyme™ for the treatment of mucopolysaccharidosis VI and may be of use in the heart after MI (P. Harmatz et al., 2004; P. R. Harmatz et al., 2014). The second method we used to modulate sulfation *in vivo* after MI, was transient knockdown of the tandem 4,6-sulfation enzyme, *Chst15.* Transient knockdown of *Chst15* reduced tandem 4,6-sulfated CS-GAGs, restored sympathetic nerves to the infarct, and reduced arrhythmias; suggesting that reinnervation had functional consequences. Transient knockdown of *Chst15* was inspired by pre-clinical models of colitis which utilized a similar siRNA oligo to knockdown *Chst15* known as STMN01 (Suzuki et al., 2016; Suzuki et al., 2017). STMN01 has progressed to phase II clinical trials where it has displayed a good safety profile(Tsuchiya et al., 2021). Use of these two distinct approaches suggests that 4,6-tandem sulfated CS-GAGs, also known as CS-E, are critical axon outgrowth inhibitors, since ARSB also reduces 4S on CS-E (See Introduction figure 1.12). CS-E has been shown to be a key inhibitor of axon outgrowth after spinal cord injury and reducing CS-E by targeting CHST15 promoted nerve regeneration (Brown et al., 2012).

One result that is unique to the CS-GAG sulfation in the cardiac scar when compared to other CSPG laden scars is the enrichment of NG2 core proteoglycan. We found from the literature that NG2 (CSPG4) is the most abundant core proteoglycan in the infarct (Tian et al., 2014), this was confirmed in Chapter 2. Interestingly, NG2 has been shown in other systems to inhibit axon outgrowth via its core proteoglycan despite

possessing CS-GAG attachment sites (Dou & Levine, 1994; Ughrin et al., 2003). Our data suggest that NG2 elicits inhibitory effects in the cardiac scar exclusively through 4,6-sulfation of its CS-GAGs since reducing 4,6-sulfation but leaving NG2 intact enabled sympathetic nerve regeneration in the infarct. Interestingly, transient knockdown of *Chst15* led to increased NG2 expression in the infarct despite an overall reduction in 4,6-sulfation, suggesting a feedback mechanism between CS-GAG sulfation and NG2 expression.

Perhaps the most exciting observation from chapter 2 is that promoting sympathetic reinnervation of the infarct by reducing 4,6-sulfation of CS-GAGs reduces arrhythmia susceptibility. Previous studies showed that reinnervation had the same effect (Gardner et al., 2015; Sepe, 2022), further supporting the hypothesis that sympathetic nerve regeneration in the infarct normalizes sympathetic neurotransmission; reducing arrhythmia susceptibility. In contrast to previous studies, we examined arrhythmia susceptibility at 10 days post-MI as opposed to 14 days post-MI. In studies where arrhythmias were assessed 14 days post-MI, sympathetic neurotransmitter NE content was restored in the infarct which provided a mechanism by which normalizing sympathetic neurotransmission reduced arrhythmias (Gardner et al., 2015). In chapter 2 however, NE content was not restored to control levels following *Chst15* knockdown despite reinnervation. It is known that regenerating nerves undergo a switch from regeneration to neurotransmission once target reinnervation is stable (Kimura et al., 2007). At 10 days post-MI it is likely nerves are still regenerating. Previous studies from our lab showed that tyrosine hydroxylase (TH; rate limiting enzyme in NE production) is still reduced while

nerves are regenerating towards the infarct (Parrish et al., 2010). This effect is the result of inflammatory cytokines in the damaged myocardium where Ciliary neurotrophic factor (CNTF) and Leukemia inhibitory factor (LIF) signaling via Glycoprotein 130 (gp130) receptors suppress TH activity and reduce NE production (Parrish et al., 2009; Shi & Habecker, 2012). This data explains why NE was not restored, but does not explain how these regenerating nerves reduce arrhythmia susceptibility. This is an area for follow up studies and will be discussed in the "Future directions" section to follow. Overall, data from this chapter provide evidence that 4,6-sulfation of CS-GAGs is the primary means by which CSPGs suppress sympathetic axon regeneration in the infarct after MI. Our results propose two new ways to promote reinnervation using clinically relevant therapeutics; Naglazyme™ (ARSB) or STMN01 (*Chst15* siRNA). These interventions could reduce 4,6-sulfation of CSPGs in the infarct after MI, promote sympathetic nerve regeneration, reduce arrhythmias, and reduce risk of sudden cardiac death for patients who have suffered an MI.

III. Long term effects of accelerated sympathetic nerve regeneration after MI

Despite results to suggest that sympathetic reinnervation of the infarct is an ideal strategy to reduce post-MI arrhythmias, the long-term effects of reinnervation remain untested. In humans who have suffered an MI, decades of clinically positive outcomes using β-blockers support the notion that increased sympathetic neurotransmission promotes arrhythmias after MI (Lopez-Sendon et al., 2004). Additionally, research suggests that increased NE after MI accelerates the heart towards heart failure (Florea &

Cohn, 2014) and we wondered if reinnervation immediately after MI might exacerbate this effect. To better understand the problem, we designed an experiment to reinnervate the infarct using ISP starting 3 days after MI (as done previously (Gardner et al., 2015)) and then examined cardiac outcomes 40 days later. When we examined infarcts to validate sympathetic reinnervation by ISP we were surprised that vehicle treated animals also had reinnervated infarcts. This observation made interpretation of our cardiac function data convoluted but we found that cardiac performance was equivalent in vehicle and ISP treated groups (both reinnervated) and that these data were more similar to sham-surgery animals than 14 days post-MI animals from previous studies (Gardner et al., 2015). 14 days post-MI, cardiac ejection fraction and cardiac output is reduced when compared to sham-surgery controls (Gardner et al., 2015). Importantly 40-day post-MI hearts with early reinnervation (ISP) did not possess any of the hallmarks of progression towards heart failure (e.g., reduced ejection fraction or cardiac output) which is one hypothesized outcome of increasing sympathetic neurotransmission in the infarct. Improved cardiac performance in reinnervated 40-day post-MI vehicle and ISP treated animals lends to the idea that promoting homogenous sympathetic neurotransmission after MI has long term benefits.

Sympathetic reinnervation after MI in humans is limited to the region adjacent to the infarct, even after one year post injury the infarct remains denervated (Hartikainen et al., 1996). In light of this data, we were confounded by the spontaneous sympathetic nerve regeneration observed in vehicle treated animals. In looking for a more satisfying explanation to this observation than increased regenerative capacity in mouse, we

thought of our results front chapter 2 which suggested that 4,6-sulfation of CS-GAGs are the key inhibitors of sympathetic axon regeneration. We hypothesized that cardiac remodeling after MI led to changes in the infarct extracellular matrix (ECM) that might include altered CS-GAG sulfation. To our surprise 4,6-sulfation of CS-GAGs was reduced to unoperated left ventricle levels. Core proteoglycan NG2 was also reduced to unoperated levels suggesting that significant remodeling of the ECM occurs long after the injury. This result will be discussed further in "Future directions" section to follow.

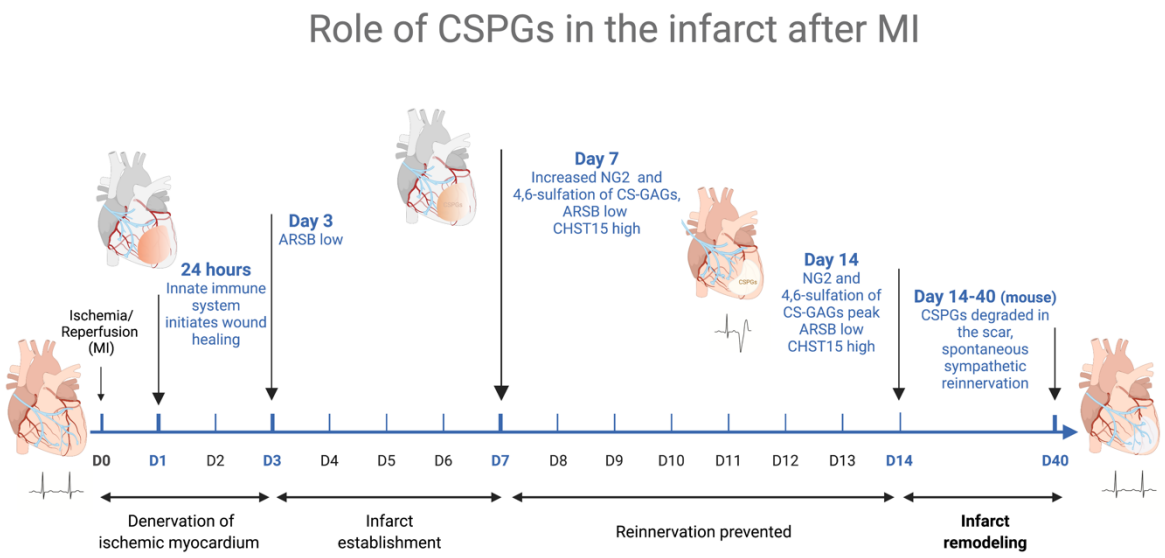

Figure 6.1 – Working model of sympathetic nerve degeneration and regeneration after MI with the timeline of CSPG deposition and CS-GAG sulfation. 14 days post-MI, an infarct highly enriched with 4,6-sulfated CS-GAGs prevents sympathetic nerve regeneration into the infarct, promoting arrhythmias. In mouse, remodeling of the infarct occurs between days 14 and 40 post-MI that reduces the CSPGs in the infarct which enables nerve regeneration back into the infarct and reduces arrhythmia susceptibility. It is likely that this remodeling does not occur in humans since human infarcts stay denervated long after MI.

IV. Novel small Molecules to promote reinnervation

After MI, CSPGs enriched in the infarcted myocardium stimulate PTPσ which suppresses axon outgrowth(Gardner & Habecker, 2013; Gardner et al., 2015). This

observation identified MI as an ideal model to test PTPσ targeting therapeutics. Early SCI experiments modulated CSPG-PTPσ signaling with the bacterial enzyme chondroitinase ABC (chABC) which removes CS-GAGs from core proteoglycans (E. J. Bradbury et al., 2002). This treatment prevents CSPG interactions with receptors including PTPσ, restoring axon outgrowth signaling (e.g., TrkA signaling (Faux et al., 2007)). chABC was thought to be a promising therapeutic to promote nerve regeneration after SCI but clinical trials failed to progress. Difficulty ensuring sufficient expression levels of the enzyme and immunogenicity of a bacterial protein presence in mammalian systems added to therapeutic challenges in regenerating CNS (Bradbury & Burnside, 2019). A search for new PTPσ targeting therapeutics led to development of the peptide ISP which blocks PTPσ association with its targets (Lang et al., 2015). ISP has successfully promoted nerve regeneration in animal models of SCI, Multiple Sclerosis (MS) and MI (Gardner et al., 2015; Lang et al., 2015; Niknam, Raoufy, Fathollahi, & Javan, 2019). ISP is currently being tested in Phase 1 clinical trials for MS and SCI under the name NVG-291. Regardless of the outcome of this trial, peptide-based therapeutics have downsides over small molecules in terms of cost of production and bioavailability and thus development of PTPσ targeting small molecules is of interest. Our small molecule development project began when Dr. Michael Cohen, approached our group about testing Illudalic acid, a natural product that has been shown to inhibit PTPσ (Ling et al., 2010). Illudalic acid did not promote neurite outgrowth across CSPGs but served to inspire two new PTPσ targeting molecules known as HJ-01 and HJ-02 described in detail in Chapter 4. To our surprise these molecules did not inhibit PTPσ enzymatic activity but rather disrupted

PTPσ interactions with Trk receptors (Figure 6.2) (Blake et al., 2022). This is a unique mechanism since it does not involve enzymatic inhibition of PTPσ but rather its association with a specific target. It remains unknown whether this is specific to TrkA and TrkB but given the fact that it did not affect other PTP family members or TrkA association with another binding partner, $P75^{NTR}$, suggests specificity.

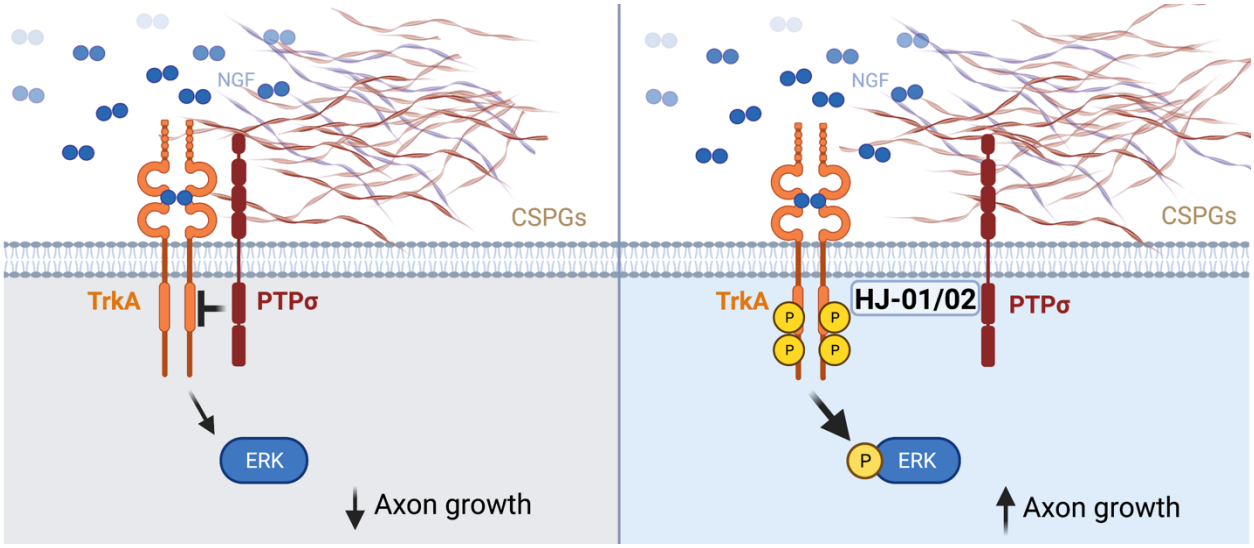

Figure 6.2- working model of how HJ-01 and HJ-02 promote axon outgrowth across CSPGs by reducing the interaction between TrkA and PTPσ, which enables axon outgrowth signaling and subsequently, axon outgrowth.

It is worth noting that these small molecules have potential clinical benefit after MI owing to their efficacy *in vivo* (Sepe, 2022). Mice treated with HJ-01and HJ-02 for one week starting 3 days after MI had restored sympathetic nerves in the infarct similarly to ISP treated animals. HJ-01 and HJ-02 had a surprising effect of improving cardiac function; restoring cardiac output to sham-surgery levels and also reducing arrhythmia susceptibility. It is possible that improvements in cardiac physiology are the result of HJ-01 and HJ-02 reducing the infarct size compared to vehicle controls. HJ-01 and HJ-02 may alter the inflammatory environment after MI which may lead to reduced infarct size. A higher number of reparative M2 macrophages were present in the MI hearts of HJ-01

and HJ-02 treated animals compared to vehicle treated animals(Sepe, 2022). This data adds to the growing body of evidence that reinnervation of the infarct reduces arrhythmia susceptibility. Overall, we are excited by the potential therapeutic benefit these compounds might have after MI or in other pathologies where CSPGs play a role in preventing nerve regeneration like SCI and TBI.

V. Limitations and Future directions

A. CSPG signaling in primary sympathetic neurons

The intracellular signaling pathways modulated by CSPGs in regenerating sympathetic nerves remains an area for further study. Our attempt at exploring signaling pathways downstream of TrkA altered by CSPGs, and failure to do so, are discussed at length in Chapter 5. A recent paper from the Kuruvilla group provided inspiration about a methodology that might help increase our understanding of CSPG signaling events. In this work the group was studying local translation and post-translational modification of Rac1 in the axon, showing that the protein was critical for retrograde TrkA signaling and axon outgrowth (Scott-Solomon & Kuruvilla, 2020). They used a culture method with sympathetic ganglia similar to the co-culturing experiment in Chapter 2. The Scott-Solomon et al. inspired experimental setup would co-culture sympathetic ganglia with or without reduced 4-sulfation of CS-GAGs (using ARSB) from infarct tissue and would examine the axonal protein environment 48 hours post plating. 48 hours is the time point we showed restoration of sympathetic axon outgrowth in the presence of Infarct treated with ARSB (Chapter 2). At 48 hours the cell soma could be excised and used for

transcriptomic analysis (TRAP-seq) to look at mRNA actively being transcribed (Reynoso et al., 2015). The remaining axons could be subjected to proteomic analysis to look at altered protein abundance in the axon (or, phospho-proteomics). This data wouldn't provide information about dynamic changes in real-time induced by CSPGs, but would provide an unbiased view of protein changes in the axon and transcriptional changes in regenerating sympathetic nerves being stimulated by CSPGs. A slight variation of this approach could be used to examine changes to local axon protein translation. To do this, sympathetic ganglion would be cultured for 48 hours and then the cell soma would be excised. The remaining axons can survive and respond to stimuli for approximately 8 hours (Andreassi et al., 2010). The axons could be treated with vehicle or soluble CSPGs and assayed approximately 6 hours later to examine changes in local protein translation (Scott-Solomon & Kuruvilla, 2020). Vehicle or CSPG stimulated axons would be additionally treated with or without cycloheximide (CHX) to block translation, enabling the comparison of CSPG stimulated changes to axon translated proteins using proteomics. This data wouldn't isolate signaling downstream of TrkA but would provide a comprehensive look at protein changes induced by CSPGs, specifically changes to local translation of axonal mRNA.

B. HJ-01 and HJ-02 Target Identification

We spent a significant amount of time trying to find the exact target and mechanism by which HJ-01 and HJ-02 promoted axon outgrowth (Appendix A). Some evidence suggests that the putative target is located in the membrane and is an approximately

60kda protein. Despite our best efforts, we were never able to identify this target by click-chemistry labeling with biotin, biotin enrichment and mass-spectrometry analysis. The fact that we were unable to do this could be the result of several factors. First, is that the protein target seems to be membrane enriched. This presents a challenge since our method for target identification has been optimized for soluble proteins. Membrane proteins are difficult to properly solubilize which presents a challenge since some detergents reduce the efficiency of our copper-catalyzed click-chemistry labeling. The second challenge is that the target appears to be of low abundance. Our experiments primarily utilized non-neuronal cells because deriving sufficient protein material for mass-spectrometry target identification is not really possible using primary sympathetic neurons. This may mean that a target abundantly expressed in neurons is not highly expressed in HEK-293t cells used for our experiments. Another possible reason for our inability to identify the target of HJ-01 and HJ-02 is that our small molecules, which are designed to interact with targets covalently, may under some conditions be reversible. The acrylamide electrophiles of HJ-01 and HJ-02 are designed to bind irreversibly to cysteines but some reports suggest it is possible that acrylamide addition to amines can be reversible under certain conditions (Zamora, Delgado, & Hidalgo, 2010). Overall, we think improvements in target identification methods and sensitivity will reveal the target of HJ-01 and HJ-02. A non-click chemistry target identification approach such as mass spectrometry-Cellular Thermal Shift Assay (MS-CETSA) may serve as an alternative approach in the future (N. Prabhu, Dai, & Nordlund, 2020).

C. CSPG origins

One exciting future direction inspired by previous work (Gardner & Habecker, 2013) and the results in Chapter 2 are the cellular origins of CSPGs enriched in the cardiac scar. It is probable that multiple CSPG origins exist, two likely candidates are resident fibroblasts in the heart and immune cells that migrate to the damaged tissue to resolve inflammation (Gentek & Hoeffel, 2017; Rog-Zielinska et al., 2016). Resident fibroblasts play many roles after MI, including deposition of ECM that maintains structural integrity of the heart after MI (Rog-Zielinska et al., 2016). Fibroblasts in the uninjured heart are activated in response to injury. Changes in mechanical stress and cytokine abundance promote fibroblast activation. These activated fibroblasts, also called myofibroblasts, possess contractile fibers and secrete ECM proteins which ultimately form an organized scar that replaces necrotic cardiomyocytes (Humeres & Frangogiannis, 2019; Ivey & Tallquist, 2016). Given the role of activated fibroblasts in ECM deposition, which *in vitro* includes secretion of sulfated CSPGs (Pearson et al., 2018), it would be interesting to alter fibroblast activation and examine CSPG deposition and CS-GAG sulfation. Infusion of Angiotensin II (AngII) and phenylephrine (PE) causes rapid activation of fibroblasts and subsequent deactivation of fibroblasts upon AngII-PE withdrawal (Kanisicak et al., 2016), this could be used to prolong fibroblast activation after MI. Myofibroblast levels typically peak 7 days post-MI and then recede after a stable scar is formed, though myofibroblasts can reside in stable scars for decades (Kanisicak et al., 2016). Interestingly, sulfation of CS-GAGs and proteoglycan NG2 expression peaked at day 7 post-MI and were maintained through day 14. By day 40 post-MI however we

observed a decrease in CS-GAGs and proteoglycan NG2 expression. It would be interesting to prolong fibroblast activation after day 14 post-MI and see if this altered CSPG deposition or sulfation of CS-GAGs. If AngII-PE infusion prolonged CSPG deposition and sulfation in the infarct, it would be fascinating to see if day 40 vehicle treated mice still had reinnervated infarcts like we observed in Chapter 3. This could be assessed by western blot with NG2 and CS-GAG sulfation antibodies. Fibroblast activation could be validated by western blot or histology using Periostin or α-Smooth Muscle Actin antibodies which are upregulated in myofibroblasts (Ivey & Tallquist, 2016). Depletion of fibroblasts after MI is a tempting strategy to assess the contribution of fibroblasts to CSPG deposition in the infarct, but given the multitude of important roles for fibroblasts after MI this strategy would lead to too many complicating factors to interpret the results (Rog-Zielinska et al., 2016).

Another CSPG source may be several different types of immune cells that migrate to the injury site after MI. The initial role of these cells in the infarct is to phagocytize debris from necrotic tissue and to coordinate the inflammatory response. Immune cells secrete a diverse array of proteins including cytokines and ECM proteins (Gentek & Hoeffel, 2017). Mast Cells are one such secretory immune cell type involved in wound healing after MI(Bot, van Berkel, & Biessen, 2008). Mast cells respond to the MI injury where they can both deposit ECM and degrade it via secretion of matrix metalloproteases(Janicki, Brower, & Levick, 2015). Interestingly, Mast cell abundance in the heart peaks at 7 days after MI, the same time when CSPGs and CS-GAG sulfation is enriched in the infarct (Ngkelo et al., 2016). It would be interesting to see if depletion of Mast cells after MI

reduced CSPG deposition or CS-GAG sulfation in the infarct. Mast cells could be reduced using “cre-master” mice that genotoxically deplete mast cells using the mast cell specific protease, carboxypeptidase A3 (Feyerabend et al., 2011). Another likely Immune cell source of CSPGs are resident or infiltrating macrophages that migrate to the infarct after MI and have been shown to secrete sulfated CSPGs (including NG2) *in vitro* and *in vivo* following spinal cord injury (Popovich et al., 1999; Uhlin-Hansen et al., 1993). Macrophages are a diverse set of cells that paradoxically have been categorized into “pro-inflammatory” M1 macrophages or “pro-healing” M2 macrophages. Much nuance exists in macrophage sub-classification but for the purposes of this discussion will remain simplified (S. D. Prabhu & Frangogiannis, 2016). After MI, an initial wave of M1 macrophages occurs early in the injury response which is followed by a wave of M2 macrophages that promote repair and wound healing. It has been shown that promoting a transition towards M2 macrophages after MI improves cardiac outcomes (S. D. Prabhu & Frangogiannis, 2016). An interesting observation from our *in vivo* novel small molecule experiments, showed that HJ-01 and HJ-02 promoted an enrichment of M2 macrophages after MI (Sepe, 2022). HJ-01 and HJ-02 treated animals had reduced scar size when compared vehicle treated controls, which may be explained by the enrichment of M2 macrophages. It would be interesting to see if promoting M2 macrophage abundance after MI with HJ-01 or HJ-02 altered CSPG deposition or CS-GAG sulfation. An alternative approach by infusing LPS to promote M1 macrophage expansion (Orecchioni, Ghosheh, Pramod, & Ley, 2019) could be an interesting way to look at M1 macrophage subtype effects on CSPG deposition and sulfation in the infarct. Macrophages could also be

depleted at different stages of the wound healing response with clodronate liposomes (Aurora et al., 2014). It would be interesting to see if depletion of macrophages before day 7 post-MI altered CSPG deposition and sulfation in the infarct.

With greater knowledge about the cellular origins of CSPGs one can envision designing cell-type specific knockout animals of either NG2 to prevent CSPG deposition or CHST15 to prevent tandem 4,6-sulfation of CS-GAGs. Modulating scar tissues has long been postulated as a possible method to reduce deleterious outcomes after spinal cord injury (McKeon et al., 1991; Sharma, Selzer, & Li, 2012). Despite our emphasis on the deleterious side effects of scars, it is important to remember they serve an important purpose for the wound healing response (Rog-Zielinska et al., 2016). Scar tissues provide structural stability and act as a scaffold for inflammatory cells to coordinate wound healing, so altering scar composition remains a complicated therapeutic strategy. This consideration makes our data regarding CS-GAG sulfation all the more interesting. Our data suggests that CS-GAG sulfation status initiates inhibition of axon outgrowth in the infarct, likely by suppressing growth signaling via PTPσ in regenerating sympathetic nerves. Reducing 4,6-sulfation of CS-GAGs in the scar might reduce the suppression of sympathetic nerve regeneration while preserving the positive attributes of the scar. In essence, this strategy could promote formation of *better* scars.

D. How do nerves reduce arrhythmias after MI?

We originally hypothesized that sympathetic reinnervation of the infarct promotes homogenous sympathetic neurotransmission by preventing heterogenous β-Adrenergic

receptor signaling across areas of denervation and normal innervation that follow MI (Gardner et al., 2016; Zipes & Rubart, 2006). Data from chapter 2 challenges this notion given that reinnervation reduced arrhythmias *before* sympathetic neurotransmission was restored in the infarct. This raises the possibility that the physical presence of nerves may alter electrical conduction in the infarct in ways other than sympathetic neurotransmission. One plausible way this might occur, is that regenerating nerves may alter the makeup of the infarct by altering the inflammatory environment after MI. Data from the *in vivo* small molecule paper showed that HJ-01, HJ-02 and ISP all promoted an M2-like macrophage shift in the heart after MI (Sepe, 2022). This shift in the inflammatory environment could alter cellular composition by maintaining myofibroblasts in the infarct (Humeres & Frangogiannis, 2019). Myofibroblasts can form passive electrical cell-cell junctions (via Connexin proteins) with other myofibroblasts or even increased gap junctional coupling with surviving cardiomyocytes in the scar and border zone. The insulating nature or absence of electrical conductivity in the infract is thought to be pro-arrhythmogenic and thus, promoting passive electrical conduction may promote action potential propagation through the infarct (Rog-Zielinska et al., 2016). Given this hypothesis, it would be interesting to examine histological changes to fibroblasts in the infarct following reinnervation, specifically looking at gap junctional coupling between cells. Increased gap junction coupling between myofibroblasts or myofibroblast and surviving cardiomyocytes could reduce arrhythmia susceptibility even before sympathetic neurotransmission has been restored. Histological examination of Connexin-40/43 staining in reinnervated

infarcts would be an ideal place to start, given that these proteins couple myofibroblasts and cardiomyocytes.

VI. Human considerations

One observation from chapter 3 seems particularly relevant when considering therapeutic strategies to promote reinnervation. The final figure from this work looked for a plausible mechanism by which vehicle treated hearts 40 days post-MI were reinnervated. We examined CS-GAG sulfation in the infarct of day 40 post-MI animals and found that 4,6-sulfation of CS-GAGs was reduced to similar levels as healthy left ventricle tissue. This fit in with Chapter 2 findings that suggested that reducing 4,6-sulfation of CS-GAGs could promote reinnervation. In humans who have suffered an MI, we know that very limited sympathetic nerve regeneration in the infarct ever occurs based on sympathetic nerve imaging studies using 123-MIBG (Hartikainen et al., 1996; Simula et al., 2000). This aligns with reduced regenerative capacity of nerves broadly in *homo sapiens* as compared to *mus musculus*. If the therapeutic interventions we propose here are to be translated to human subjects following MI, a couple things must first be verified. First, we need to validate that 4,6-sulfated CSPGs are enriched in human cardiac scars after MI. Second, we must validate that 4,6-sulfation (if enriched) persists in the scar in cases where denervation persists. In theory this could be accomplished with post-mortem tissue samples and western blotting. If these data can be replicated in humans, we think ISP, HJ-01, HJ-02, ARSB (Naglazyme^{TM}), and *Chst15* siRNA (STMN01) could have therapeutic value to reduce arrhythmias and risk of sudden cardiac arrest after MI.

VII. Conclusion

This dissertation builds upon decades of research described at length in the Introduction. Nervous system research from over 70 years ago laid the ground work for understanding peripheral sympathetic nerve regeneration (V. Hamburger, 1939; V Hamburger & Levi-Montalcini, 1949). Cardiovascular research across the past 30 years has demonstrated that post-MI arrhythmias originate from sympathetic denervation of the infarct (Boogers et al., 2010; Lopez-Sendon et al., 2004; Meredith et al., 1991; Vaseghi et al., 2014). Decades of SCI research explained how ECM inhibits nerve regeneration, highlighting the role of CSPGs (E. J. Bradbury et al., 2002; McKeon et al., 1991). This observation inspired previous work in our lab which showed that the infarct is enriched with CSPGs, which prevent nerve regeneration in the heart after MI (Gardner & Habecker, 2013; Gardner et al., 2015). Work from many other CNS nerve injury paradigms inspired us to look into CSPG sulfation in Chapter 2, which identified that 4,6-sulfation of CS-GAGs in the infarct are the primary means by which CSPGs inhibit sympathetic axon regeneration after MI (Brown et al., 2012; Gilbert et al., 2005; Pearson et al., 2018; H. Wang et al., 2008). This additional layer of understanding enabled identification of several new therapeutic targets to promote sympathetic nerve regeneration after MI by altering CSPG sulfation, including ARSB and CHST15. Other research from the nerve injury field established the role of CSPG-PTPσ signaling axis in suppression of axon outgrowth (C. H. Coles et al., 2011; Lang et al., 2015; Shen et al., 2009b) which our lab showed was the mediator of sympathetic axon outgrowth inhibition in the heart after MI (Gardner & Habecker, 2013). This work inspired the generation of two novel small molecules,

described in chapter 4, that promote sympathetic axon outgrowth across CSPGs *in vitro* (Blake et al., 2022), restore sympathetic nerves in the infarct, and reduce arrhythmias *in vivo* (Sepe, 2022). To be sure, there is still much to learn about how sympathetic nerve regeneration in the heart reduces arrhythmias. Furthermore, there is a tremendous amount we still do not understand about how sulfation of CS-GAGs alters signaling in the regenerating neuron. If this dissertation is anything, it is a document in praise of scientific incrementalism, each discovery mentioned above has built on the next moving us closer towards our goal to improve health outcomes for those who have suffered an MI. To this end, this dissertation provides evidence for several new promising therapeutic targets and it is my hope that these would one day be translated to humans.

Chapter 7

Detailed methods

Animals: C57BL/6J mice obtained from Jackson Laboratories West (Sacramento, CA) were used for all experiments. All mice were kept on a 12h:12h light-dark cycle with *ad libitum* access to food and water. Age and gender-matched male and female mice 12-18 weeks old were used for myocardial-ischemia reperfusion surgeries, described below. For studies described in Chapter 2, animals were treated with 100μg of siRNA (scramble non-targeting control or Chst15-targeting) administered via tail vein days 3, 5 and 7 post-MI, detailed description below. For studies described in Chapter 3, animals were treated daily for 7 days with vehicle (5% DMSO/saline) or ISP (10µM) via IP injection beginning 3 days post-MI. Pregnant Sprague Dawley rats were purchased from Charles River Laboratories (Wilmington, MA) for experiments with sympathetic neurons. Superior cervical ganglia from male and female neonatal rats (P0-P2) were used to generate primary sympathetic neuron cultures and for microfluidic explant cultures. All rats were kept on a 12h:12h light-dark cycle with *ad libitum* access to food and water. All procedures were approved by the OHSU Institutional Animal Care and Use Committee and comply with the Guide for the Care and Use of Laboratory Animals published by the National Academies Press (8th edition).

Myocardial Ischemia Reperfusion procedure: Anesthesia was induced with 4% isoflurane and maintained with 2% isoflurane. Myocardial infarction (MI) induced when left anterior descending coronary artery (LAD) was reversibly ligated for 40 minutes and then

reperfused by release of the ligature. Occlusion was confirmed by sustained S-T wave elevation and regional cyanosis. Reperfusion was confirmed by the return of color to the ventricle distal to the ligation and reperfusion arrhythmia. Core body temperature was monitored by a rectal probe and maintained at 37°C, and a two-lead electrocardiogram was monitored.

Left ventricle tissue collection/processing: At the indicated time point left ventricle tissue was collected and processed for downstream analysis. Either MI animals or unoperated wild type (WT) control animals were euthanized and the heart was excised and rinsed in saline solution to remove as much blood as possible. With the heart tissue cleaned, the heart was placed into a brain slicer and sectioned into 1mM sections. Scar tissue was dissected from left ventricle (LV) of post-MI hearts, tissue from a similar region was dissected from unoperated control hearts. Tissue was processed for immunohistochemistry (IHC), western blot, or norepinephrine content. For western blot and norepinephrine (NE) content, tissue was snap frozen in liquid nitrogen and stored at -80°C for batch processing. For IHC, hearts were excised and fixed for 1 hour in 4% paraformaldehyde, rinsed in PBS, cryoprotected in 30% sucrose overnight at 4°C and frozen in OCT mounting media for sectioning.

Cell line culturing: In chapter 4 and Appendix A, HEK-293t cells were maintained in high-glucose Dulbecco's Minimum Essential Medium (HG-DMEM) supplemented with 10% Fetal Bovine Serum (FBS, Gibco) and 1% Anti-Anti (Gibco). For signaling experiments cells were split and plated on poly-d-lysine (Gibco) coated plates prior to transfection described in detail later in this methods section. In chapter 5, PC12 cells were used to

model some aspects of sympathetic nerve signaling. PC12 cells were maintained in RPMI-medium (ATCC) supplemented with 10% horse serum (HS, Hyclone), 5% FBS and 1% Anti-Anti. For experiments, PC12 cells were differentiated for 5-7 days in RPMI fortified with 2%FBS and 50ng/mL NGF (Alomone Labs), prior to transfection (described later) cells were serum starved in RPMI + 2ng/mL NGF for 4 hours. In chapter 3 differentiated C2C12 myoblasts were used to screen siRNA knockdown efficiency (described later). C2C12 myoblasts were maintained in HG-DMEM supplemented with 10% FBS, 1% Penicillin/streptomycin (Gibco). For differentiation, C2C12 cells were culture in HG-DMEM (no sodium pyruvate) supplemented with 2% HS, 1% Glutamine (Gibco), and 1% Penicillin/streptomycin for 4 days. All cells were grown at 37°C and 5% CO_2.

Primary Neuron cell culture: Primary Sympathetic neurons were derived from P0-P2 neonatal Sprague Dawley rats (Blake et al., 2022). Superior Cervical Ganglia (SCG) were isolated and enzymatically dissociated for 30 minutes in 1mg/mL Collagenase and 10mg/mL Dispase, this was followed by mechanical dissociation using a reduced bore size fire-polished borosilicate glass pipette. Once a homogenous solution was achieved, the enzymatic reaction was quenched using HG-DMEM fortified with 10% FBS, Cells were pelleted at 2000 RPM for 5 min, resuspended in growth medium and plated for 30 minutes on a 10cm plate at 37°C, 5% CO_2 to remove glial cells by sequential plating. The resulting growth medium was collected and the plate gently rinsed with growth medium to remove neurons that may have settled during plating, cells were pelleted and resuspended in C2 Media. C2 medium is a 50/50 mixture of F12 medium (Gibco) and

low-glucose DMEM, fortified with 0.5mg/mL BSA, 30nM Selenium, 10 µg/mL Transferrin, and 10 µg/mL Insulin (Gibco). For long term culturing SCG neurons were plated onto poly-d-lysine and Laminin (2µg/mL, R&D Systems) coated plates in C2 medium fortified with 10ng/mL NGF, 1% Penicllin/Streptomycin (Gibco) and 20μM Fluorodeoxyuridine to kill dividing cells.

Incucyte sympathetic outgrowth assay: Cultures of dissociated sympathetic neurons were prepared from superior cervical ganglia (SCG) of neonatal rats as described above. Cells were pre-plated for 30 minutes to remove non-neuronal cells, and then 5,000 neurons/well were plated onto a 96 well plate (TPP) coated with (poly-L-lysine PLL, 0.01%, Sigma-Aldrich) and either laminin (2µg/mL, R&D Systems), laminin and CSPGs (1-2µg/mL; Millipore). In Chapter 2, plates were also coated with laminin and CSPGs pre-treated with ARSB (0.3 or 0.6μg/mL; R&D systems) for 6-8hrs. In Chapter 4 and appendix A, neurons plated on laminin and CSPGs were treated with compounds to promote neurite outgrowth including; vehicle (5% DMSO), HJ-01, HJ-02, HJ-03, HJ-04, ISP or Illudalic acid at various concentrations as described in the chapter. In chapter 5, neurons plated on laminin alone or laminin and CSPGs were treated with vehicle (5% DMSO), cAMP, KT5720, PMA, or BIM at various concentrations as described in the chapter. Neurons were cultured in serum free C2 medium (Pellegrino et al., 2011) supplemented with 10 ng/mL NGF (Alomone Labs), 100 U/mL penicillin G, and 100 µg/mL streptomycin sulfate (Invitrogen). Live cell imaging was carried out using an Incucyte Zoom microscope (Essen BioScience), with 20x phase images acquired every 2 hours over a 40-hour

period. Neurite length was measured using Cell Player Neurotrack software (Essen BioScience) and was used to calculate the neurite length.

Compartmentalized cultures: Micro-fluidic chambers were generated by adding SYLGARD 184 silicone elastomer (Dow Corning) into a pre-cast mold, and heating at 50-60°C for 2 hours. Cleaned chambers were placed in 10cm culture dishes (Corning) pre-coated with 0.01% Poly-L-Lysine. The axonal compartment was then coated with 10µg/mL collagen or collagen + 1µg/mL CSPGs. Explant superior cervical ganglia were placed in reduced growth factor Matrigel (BD Bioscience) within the cell body compartment. C2 media supplemented with 10 ng/mL NGF was added to both compartments and cultures were maintained at 37°C in a humidified 5%CO_2 incubator. After 24 hours, or when axons were first visible in the axonal compartment, images were acquired (t=0) and vehicle (5% DMSO), 100nM HJ-01, 100nM HJ-02, or 4μU/mL chondroitinase ABC were added to the axonal compartment. Additional images were obtained 3 hours later (t=3), and a growth rate was calculated based on the distance extended during that 3-hour period.

Explant Co-culture Assay: Explants were generated as previously described (Gardner & Habecker, 2013). Neonatal mouse (P0-P2) superior cervical ganglia were explanted and placed into culture 1mm from left ventricle tissue – either cardiac scar tissue (10-14 days post-MI) or unoperated control tissue. Cardiac tissue from a single animal was split in half and cultured with the left or right ganglia from a single animal, this enabled tissue from the same mouse to be treated with either vehicle (5% DMSO) or ARSB to remove 4-sulfated CS-GAGs. The ganglia and the cardiac tissue were co-cultured inside a 30μL

Matrigel bubble which was set for 40 minutes at 37°C before addition of C2 media supplemented with 2ng/mL NGF. ARSB was added directly to the media (0.6 μg/mL) at the time of plating and again 24 hours later. After 48 hours, the explants were imaged by phase microscopy with a Keyence BZ-X microscope. Axon length from the edge of the ganglia to the most distal tip of visible neurites was measured using ImageJ.

Western blotting: Cardiac scar tissue from the left ventricle was dissected at 24 hours, 3 days, 7 days, 14 days and 40 days following MI (depending on the chapter of this dissertation), and from control left ventricle tissue from unoperated animals. Heart tissue was pulverized in a glass douncer in NP40 lysis buffer [50mM Tris (pH 8.0), 150mM NaCl, 2mM EDTA, 10mM NaF, 10% glycerol, and 1% NP-40] containing complete protease inhibitor cocktail (Roche), phosphatase inhibitor cocktails 2 and 3 (Sigma). Lysates sat on ice for 30 minutes with intermittent vortexing. Lysates were centrifuged (13,000 rpm, 10 minutes, 4°C) and resolved on 4-12% Bis-Tris gradient gel (3-8% Tris-Acetate gel for Chapter 2 sulfation studies) by SDS/PAGE, transferred to nitrocellulose membrane (GE Life Sciences), blocked in 5% nonfat milk, probed with either CHST11 (1:500; Invitrogen: PA5-68129), CHST15 (1:1000; Proteintech: 14298-1-AP), ARSB (1:500; Proteintech: 13227-1AP), NG2/CSPG4 (1:1000; Millipore: AB5320), Tyrosine Hydroxylase (1:1000; Millipore: AB1542), or Galectin-3 (1:500; Abcam: AB2785) then probed with goat anti-rabbit (or mouse) HRP-conjugated secondary antibody (1:10,000; ThermoFisher), and detected by chemiluminescence (Thermo Scientific). For chondroitin-sulfate proteoglycan detection, lysates were treated according to the detailed deglycosylation protocol from Mariano Viapiano Ph.D. lab website(Massey et al., 2008). 50-100μg of protein lysate

(depending on how much was available) was treated for 6-8hrs with chondroitinase ABC (100 μU/mL; R&D systems) before being subjected to traditional western blotting described above, probed with anti-chondroitin-4-sulfate (1:1000; Millipore: MAB2030) or anti-chondroitin-6-sulfate (1:1000; Millipore: MAB2035). Protein expression was quantified with ImageJ densitometry and normalized to total protein as measured by ponceau staining.

ERK signaling Western blotting: TrkB-HEK-293t cells (a kind gift from Dr. Moses Chao, NYU) were used to examine the effects of HJ-01 and HJ-02 on TrkB stimulated ERK phosphorylation. Cells were plated on 6-well plates in HG-DMEM (Gibco) with 10% FBS (Hyclone), 1% Penicillin/streptomycin (Gibco) and Geniticin (400 µg/mL; Life Technologies). At the appropriate density, cells were rinsed twice with 1x PBS and media was replaced with Opti-MEM (Gibco) containing 2% FBS. Cells were transfected with Lipofectamine 2000 (7μL per well), with either 2.5μg full-length PTPσ plasmid or 1μg GFP control plasmid per well. After 6 hours cells were rinsed once with 1x PBS and replaced with regular growth media and grown for 12 hours. Cells were then serum starved for 2 hours in HG-DMEM + B27. Following serum starving, cells were incubated with either HJ-01 or HJ-02 at 10nM, 100nM, or 1µM for 1 hour and then stimulated with 5ng/mL human BDNF (Alomone Labs) for 5 minutes. Cells were then rinsed with ice-cold PBS and lysed on ice with intermittent agitation for 30 minutes in NP40 lysis buffer [50mM Tris (pH 8.0), 150mM NaCl, 2mM EDTA, 10mM NaF, 10% glycerol, and 1% NP-40] containing complete protease inhibitor cocktail (Roche), phosphatase inhibitor cocktails 2 and 3 (Sigma), and 5mM iodoacetamide. Lysates sat on ice for 30min and were then treated

with 10mM dithiothreitol to inactive any remaining iodoacetamide. Protein lysate was cleared by centrifugation at 13,000 rcf for 10 minutes. The soluble fraction was retrieved and diluted with 4x XT sample buffer and 20x XT reducing reagent (Biorad) for western blot analysis as described above. Blots were probed with phospho-Erk1/2 (1:1000 Phospho-p44/42MAPK, Cell Signaling #9101) and Total-Erk1/2 (1:1000 p44/42MAPK, Cell Signaling #9102) antibodies.

TrkA immunoprecipitation assay: To test the hypothesis that small molecules HJ-01 and HJ-02 disrupt the binding of TrkA and PTPσ, HEK-293t cells were transfected with full length PTPσ or p75NTR (Addgene plasmid # 24091) and TrkA-RFP plasmid (Addgene plasmid #24093), and pulled down using RFP-trap nanobody conjugated to magnetic agarose (Chromotek). HEK-293t cells were plated onto 6-well plates coated with 0.01% poly-L-lysine (Sigma) and grown in HG-DMEM (Gibco) supplemented with 10% FBS (Hyclone) and 1% Anti-Anti (Gibco). 12 hours later cells were rinsed with 1x PBS and media was replaced with Opti-MEM (Gibco) containing 2% FBS. Cells were transfected using Lipofectamine 3000 (Thermo Scientific). For transfection, 1μg of TrkA-RFP and 1μg of PTPσ plasmid, 6μL of P3000 reagent, and 5μL of lipofectamine reagent were added to each well of the 6-well plate. 12-16 hours later cells were rinsed twice with 1x PBS and media was replaced with DMEM and B27 supplement (Gibco) and serum starved for 4 hours. Cells were then treated with small molecules (HJ-01, HJ-02, or HJ-03) or with vehicle (5% DMSO) for 1 hour and stimulated for an additional hour with 50ng/mL NGF (Alomone Labs, #N-100) and 2μg/mL CSPGs (EMD-Millipore, CC117). Cells were rinsed twice with ice-cold 1x PBS and lysed with IP lysis buffer [150mM NaCl, 50mM Hepes,

1.5mM $MgCl_2$, 1mM EGTA, 1% Triton-X, 10% glycerol, Roche complete protease inhibitor cocktail, and Sigma phosphatase inhibitor cocktails 2 and 3]. Two wells of each 6-well plate were pooled per condition, and cells were lysed for 30 minutes on ice with intermittent vortexing. Lysate was centrifuged at 13,000 rcf for 10 minutes leaving the soluble fraction. 10% of this lysate was set aside as the input fraction. TrkA immunoprecipitation was accomplished using 15μL of RFP-trap magnetic agarose added to the remaining lysate and incubated overnight at 4°C on a rotator. The protein bound to the RFP-trap agarose was then separated using a magnet and rinsed 3 x 10 minutes with IP lysis buffer. To remove the protein from the beads, 4x XT-sample buffer (Biorad) was diluted to 2x using the IP lysis buffer and XT reducing reagent was added, the sample was then incubated at 95°C for 10 minutes and separated from the beads using a magnet. Samples were subjected to the standard western blotting protocol and probed for TrkA (1:1000; Millipore Sigma #06-574) and PTPσ (1:500; Proteintech #13008-1-AP) or, p75NTR (1:1000; Cell Signaling, D4B3 XP #8238S). To quantify pulldown of PTPσ (or p75NTR) by TrkA-RFP the levels of each protein in the pulldown were quantified by pixel density, normalized to the respective input levels and then the ratio of PTPσ (or p75NTR) to TrkA was calculated and compared across samples.

siRNA pool knockdown efficiency screen: A pool of 4 siRNAs targeting the *Chst15* gene were purchased from Horizon Discovery (formerly GE Dharmacon) and were tested for their efficacy in reducing gene expression in C2C12 myoblasts. C2C12 myoblasts were plated on 12-well plates coated with collagen and were transfected with the various targeting and control siRNAs using the Dharmafect transfection reagent (3μL of

Dharmafect reagent per well with 120nM siRNA). The next day wells were split using Versene (Gibco), 1/3 of the cells were collected for a 24-hour time point and the other 2/3 were split into 2-wells for 48-hour and 72-hour knockdown timepoints. Cells were processed using an RNA Mini-kit (Qiagen) to purify RNA. 1μg of RNA was loaded into the cDNA reaction with the iScript cDNA synthesis kit. Gene expression was examined with multiplexed Taqman probes targeting *Chst15* and *Gapdh* using 2μL of cDNA template and Taqman reagents and measured with an ABI7500 Thermocycler. The delta delta ct method was used to calculate knockdown efficiency. Once an effective siRNA against *Chst15* was identified, knockdown efficiency was measured at the protein level with C2C12 myoblasts, 48 hours post-knockdown. CHST15 protein expression was assessed via western blot with a CHST15 antibody (1:1000; Proteintech: 14298-1-AP) normalized to GAPDH (1:1000; Thermo Scientific: MA1-16757); siRNA *Chst15-2* was selected for larger scale production and used for in vivo studies.

In vivo siRNA treatment: After MI surgery mice were treated with 100μg of siRNA targeting *Chst15* or a non-targeting control. siRNA was delivered systemically via tail-vein injection on days 3, 5 and 7 following MI. Arrhythmia assessment was done at day 10 post-MI before tissue collection. Tissue was collected at day 10 post-MI for either; western blot analysis of CSPG sulfation and the sympathetic neuron marker TH in the infarct, were processed to asses norepinephrine (NE) content in the infarct, or were fixed and mounted in OCT for immunohistochemistry. siRNA used for this experiment was custom synthesized by Horizon Discovery; siAccell *in vivo* formulation.

Norepinephrine content analysis by High-Performance Liquid Chromatography: Norepinephrine (NE) levels in heart tissue were measured by HPLC with electrochemical detection (Li, Knowlton et al. 2004). Frozen, pulverized tissue was weighed and homogenized in 300μL of 0.1 M perchloric acid (PCA) containing 0.5μM dihydroxxybenzylamine (DHBA, internal standard). The homogenate was centrifuged at 14,000 rpm for 4 minutes and NE in 100μL of the supernatant was adsorbed onto 15mg alumina, followed by 15 minutes of tumbling. The alumina was washed twice with ddH_2O and the catechols desorbed with 150μL of 0.1M PCA. The catechols were separated by reversed-phase HPLC on a C18 column (Agilent Microsorb, 150x4.6 mm, 5µm) and measured by an electrochemical detector (Coulochem III; ESA, Bedford, MA) with the electrode potential set at +180 mV as described previously (Parish et al. 2010). The mobile phase used consisted of 75 mM sodium phosphate (pH 3.0), 1.7 mM sodium octane sulfonate, 3.0% acetonitrile. NE standards (0.5μM) were processed in parallel with the tissue samples.

Immunohistochemistry: Tyrosine hydroxylase (TH; sympathetic nerve fibers) and Fibrinogen (Fib; infarct/scar) staining was carried out as described previously (Gardner et al., 2015) 10 days (Chapter 2) or 40 days (Chapter 3) after MI. Tissue was collected 10 or 40 days after surgery, fixed in 4% paraformaldehyde, frozen and 12μm sections generated. To reduce autofluorescence, sections were rinse 3 x 10 minutes in 10mg/mL Sodium Borohydride and rinsed for 3 x 10 minutes in 1x PBS. Slides were placed in 2% BSA, 0.3% Triton X-100 in 1x PBS for 1 hour and then incubated with rabbit anti-TH (1:1000; Millipore: AB1542) and sheep anti-fibrinogen (1:300; BioRad: 4400-8004)

overnight. The following day the slides were incubated with Alexa-Fluor IgG-specific antibodies (Molecular Probes, 1:1000) for 1.5 hours and rinsed 3 x 10 minutes in 1x PBS. Background autofluorescence was reduced further with a 30-minute incubation in 10mM $CuSO_4$ (diluted in 50mM Ammonium Acetate). Following this, slides were rinsed 3 x 10 minutes in 1x PBS before mounting in 1:1 glycerol:PBS and visualized by fluorescence microscopy. Threshold image analysis of TH staining was done as described previously (Gardner et al., 2015), the threshold function in ImageJ was used to generate black and white images discriminating TH+ nerves for 6 sections spanning 200μm of the infarct or peri-infarct region from each heart. Percent area TH+ fiber density (20x field of view) was quantified within the infarct and the area immediately adjacent to the infarct (peri-infarct). Images were acquired with a Keyence BZ-X 800 microscope.

Quantification of Cardiac Scar (infarct) size: Infarct size was determined 10 days (Chapter 2) or 40 days (Chapter 3) after MI and tissue was prepared for immunohistochemistry as previous mentioned, omitting the steps to reduce autofluorescence. Autofluorescence in the GFP channel was used to image the infarct size. Scar tissue is notably lacking autofluorescence enabling easy identification of the infarct. Images were acquired with a Keyence BZ-X 800 microscope at 2x magnification and analyzed using Image J freehand selection tool. Left ventricle (LV) and infarct was outlined, measured and the percent area of infarct was determined by (infarct area/ LV area) x 100. The infarct was imaged in 6 sections across 200μm of the infarct as done previously(Gardner et al., 2015).

Arrhythmia Assessment: Anesthesia was induced with 4% isoflurane and maintained with 2% isoflurane in animals 10 days (Chapter 2) or 40 days (Chapter 3) after MI. ECG leads

were connected to monitor arrhythmias and animals were maintained at 37°C throughout the analysis. All parameters were monitored with Powerlab LabChart software (AD Instruments). A 30-minute baseline was used to assess spontaneous arrhythmia susceptibility prior to administration of β-agonist Isoproterenol (50μg) and caffeine (3mg) as described previously(L. Wang et al., 2014). Arrhythmias were measured for 30 minutes following drug administration and scored according to the modified Lambeth conventions (Curtis et al., 2013) on a scale of 0-4. Individual animals received a single score based on the most severe arrhythmia observed. 0 indicates no arrhythmia. 1 indicates 1-2 premature ventricular contractions (PVCs) followed by normal sinus rhythm of at least 2 beats. 2 indicates bigeminy (1 PVC followed by one normal sinus beat, repeating for 4 or more continuous cycles) or salvo (3-5 PVCs in a row). 3 indicates non-sustained ventricular tachycardia (nsVT) defined as 6 or more PVCs in a row lasting less than 30 seconds. 4 indicates sustained VT (>30 seconds) or Torsades de Pointes.

Echocardiography: Cardiac function was assessed 40 days after MI (Chapter 3) using echocardiography. High-frequency fundamental imaging (Vevo 2100) was performed between 25 and 40 MHz. Mice were sedated with inhaled isoflurane (1.0%–1.5%). Cardiac function was analyzed under basal conditions and in response to the β-adrenergic agonist isoproterenol (10 µg or ~0.5 mg/kg). Images were obtained in the parasternal long-axis plane and parasternal short-axis planes at the midpapillary level. Left-ventricular (LV) function was assessed by measurement of LV end-diastolic, end-systolic area (short axis) and end-diastolic, end-systolic length (long axis). Stroke

volume was determined using the left ventricular outflow tract area and time-velocity integral on pulsed-wave Doppler.

PTPσ D1 D2 protein purification: D1D2 plasmid was a gift from (Brad Lang and Jerry Silver, Case Western Reserve University). Rosetta 2(DE3) competent cells (Novagen) were transformed with 1μL of D1D2 DNA and grown overnight at 37°C on LB agar plates supplemented with kanamycin and chloramphenicol. A ¼ swath of the bacteria from the LB agar plate was spiked into 50mL of LB media (with 50μg/mL kanamycin and 34μg/mL chloramphenicol) and grown at 37°C overnight with 225 rpm shaking. The next day the 50mL starter culture was pitched into 1L of terrific broth (TB) media (12 g bacto tryptone, 24 g yeast extract, 0.4% glycerol, 17mM KH2PO4, 72mM K2HPO4, 1% glucose, 50 µg/ml Kanamycin, 34 µg/ml chloramphenicol) and grown at 37°C, 225 rpm until reaching an OD600 reading of 0.6. At this point the TB media was placed on ice and the protein expression of D1D2 was induced with 0.4mM Isopropyl-β-thiogalactoside (IPTG, Sigma-Aldrich) and grown at 37°C overnight, 225 rpm. Cells were harvested by centrifugation at 4000 rpm 4°C for 15 minutes. The cell pellet was resuspended in 50mL of lysis buffer [20 mM HEPES, pH 7.5, 1 mM β-mercaptoethanol, 1 mM benzamidine, 0.2% NP-40, 0.2% Tween-20, 500 mM NaCl, 1 mM phenylmethylsulfonyl fluoride, 8.3 mg/L DNAse I] with a glass douncer and sonicated, on ice, 6 times for 30 seconds each time with 2 minutes rest between each cycle (Branson sonifier 450). The resulting lysate was cleared by centrifugation at 12,000 rcf, 4°C, for 30 minutes. Purification of the D1D2 protein was achieved using the attached his-tag by Ni-NTA affinity chromatography (Ni-NTA resin,

Qiagen). The resulting purified protein was verified by size using 10% SDS-PAGE before use in enzymatic activity assays.

PTPσ D1 D2 catalytic activity assessment: The catalytic activity of purified PTPσ D1D2 catalytic domain was assessed using p-nitrophenyl phosphate (p-NPP, Sigma-aldrich), a commonly used indicator of phosphatase activity. D1D2 is capable of using p-NPP as a substrate and catalysis of the phosphate group results in a colorimetric reaction that can be monitored by 405nm absorbance. The assay was conducted in ice cold 50mM MES buffer with either 2mM or 10mM p-NPP. To this reaction mixture 30nM of D1D2 protein were added with either vehicle (5% DMSO), 1μM HJ-02, or 12.5mM of sodium-orthovanadate (Sigma-Aldrich) as a control tyrosine phosphatase inhibitor. The reaction mixture was added to clear flat-bottom 96-well plates and kept on ice until the plate reading. A Spectra Max i3 (Molecular Devices) multi-well plate reader was used to measure 405nm absorbance. The reaction was induced by incubation at 30°C and measured continuously for 3 minutes.

Phosphatase Inhibition Assays: The ability of compounds HJ-01 and HJ-02 to inhibit a small panel of tyrosine phosphatase enzymes was investigated. The enzymes PTPσ, PTPRδ (protein tyrosine phosphatase receptor delta), LAR (leukocyte antigen-related tyrosine phosphatase), CD45 (cluster of differentiation antigen 45; also known as protein tyrosine phosphatase receptor C), SHP2 (Src homology 2 domain–containing phosphatase 2), and PTP1B (protein tyrosine phosphatase 1B) were incubated with 10 mM DTT for 30 min on ice in an assay buffer [50 mM HEPES pH 7.5, 100 mM NaCl, 1 mM EDTA, and 0.02% tween]. The activity assays were performed in black 96-well plates

in a total volume of 50 μL and 10% DMSO. The final concentration of enzyme in each reaction was 180pM for PTPσ, 9.7nM for PTPRδ, 4.2nM for LAR, 5nM for CD45, 5nM for SHP2, and 5nM for PTP1B. Each enzyme was incubated with HJ-01 or HJ-02 for 30 min at 37°C, after which time the reaction was initiated by addition of the fluorogenic substrate DiFMUP to a final concentration of 30μM. Enzyme activity was measured relative to an inhibitor-free control by monitoring the increase in fluorescence as DiFMUP was hydrolyzed to DiFMU. The fluorescence (λex = 350 nm, λem= 455 nm) was measured every 30 seconds for 30 minutes at 37°C. Each concentration was tested in triplicate.

Click chemistry with HJ analogs: Compound HJ-04 is an HJ-01 and HJ-02 analog with a terminal alkyne that was used to identify binding targets of HJ-01 and HJ-02 following a copper catalyzed click chemical reaction and pulldown. HEK-293t cells were serum starved for 4 hours in HG-DMEM fortified with B27(Gibco) before the assay. Cells were then treated with either vehicle (5% DMSO), 1μM HJ-04 for 30 minutes or with increasing doses of HJ-02 (100nM and 1μM) for 30 minutes followed by 1μM HJ-04 for 30 minutes. All cells were then stimulated with 50ng/mL NGF and 2 μg/mL CSPGs for 1 hour. Cells were then rinsed twice with ice cold 1x PBS and then frozen at -80°C. Cells were thawed and lysed with “Cell Lysis Buffer” [1x PBS, 0.5% Triton-X, Roche complete protease inhibitor, and sigma phosphatase inhibitors 2 and 3], plates were scraped and lysis was allowed to proceed for 30 minutes on ice with intermittent agitation. Lysates were centrifuged at 2,000 rcf for 10 minutes at 4°C to clear cell debris. Supernatant was collected and used to isolate membrane and soluble fractions by ultracentrifugation; 40,000 RPM for 1 hour at 4°C. Supernatant was used for soluble fraction analysis and

pellets were resuspended in Cell Lysis Buffer using an insulin syringe to properly solubilize pellets. Protein concentration of each respective sample/fraction were quantified using the Rapid Gold BCA assay (ThermoFisher). Protein concentrations were normalized across each sample to 2mg/mL of protein. Click chemistry biotin labeling was accomplished by combining 30μL protein lysate with 15μL "3x Click buffer" (combine 300μM TBTA(dissolved in DMSO), 3mM $CuSO_4$(make fresh in H_2O), 0.15mM Biotin-N_3(dissolved in DMSO), 3mM TCEP(Make fresh in PBS) all combined in 1x PBS in the sequence listed). Protein + Click buffer was incubated at room-temperature with rotation for 1 hr. Following the reaction, 10% of the sample was set aside in 4x Sample buffer (http://cshprotocols.cshlp.org/content/2014/7/pdb.rec081125.full?text_only=true) diluted to 1x, for the input fraction. The remaining reaction mixture of biotinylated proteins were enriched by pulldown with streptavidin resin (Thermo Scientific) overnight at 4°C with rotation. Biotinylated protein-bound streptavidin resin was centrifuged for 2,000 rcf for 3 minutes and supernatant was discarded. Streptavidin resin was then rinsed 3 times for 10 minutes with 4M Urea (dissolved in 1x PBS); with 2,000 rcf, 3-minute centrifugation between rinses. Streptavidin resin was rinsed one last time with 1x PBS and then centrifuged at 2,000 rcf for 3 minutes. Proteins were removed by addition of 45μL 2x Sample buffer (4x sample buffer diluted with PBS), boiled at 95°C for 5 minutes, and then centrifugated briefly to sediment the remain resin. The remaining protein-sample was removed leaving the resin in the tube and subjected to SDS-PAGE, ponceau staining, western blotting and probed with either anti-streptavidin-HRP (1:4000; Thermo Scientific)

or anti-Src (1:1000; Cell Signaling: 36D10) and visualized by chemiluminescent imaging as described in the western blotting section.

FRET biosensor transfections: To transfect PC12 cells we used the Neon electroporation system (10μL kit, Invitrogen). Cells were trypsinized, resuspended, pelleted, rinsed with PBS and resuspended in the neon transfection buffer. The cell density used in each 10uL reaction was $1X10^7$ cells/mL combined in solution with 0.75ug of biosensor DNA per reaction. Manufacturer recommended electroporation settings were used for PC12 cells: pulse voltage (1500 V), pulse width (10ms), and pulse number (3). Parameters used for primary SCG neurons have been described previously (Pellegrino & Habecker, 2013) but briefly: voltage (1500 V), pulse width (20ms), and pulse number (1).

FRET Biosensor screening and quantification: Initial FRET biosensor screening was accomplished using PC12 cells differentiated using the aforementioned protocol. Four identical transfections were completed as described above, and cells were pooled in a single well of a 12-well plate before being split into 12-wells of a 96-well glass bottom plate (Cellvis, 1.5H-N) coated with PDL and laminin. Cells were plated in an optimized media consisting of Fluorobrite media (Gibco) supplemented with 0.5mg/mL BSA, 3mM L-glutamine and 2ng/mL NGF. Fluorobrite media was used to reduce background autofluorescence during imaging. 12-16 hours after transfection, cells were imaged using an Olympus spinning disc confocal microscope housed in an environmental chamber held at 37C 5%CO2. Cells were excited with a 440nm LED (SpectraX), spectra passed through a bandpass filter, 425-452nm for CFP excitation. CFP fluorescence was then passed through an emission cube (483/32 (483 peak, 32 range)) for CFP image capture.

YFP fluorescence was passed through an emission cube (542/27 (542peak, 27range)) for YFP image capture. The ratio of YFP/CFP was calculated to determine the FRET emission ratio. Cells were scanned every 5 minutes for 30 minutes to establish a baseline measurement before addition of stimulus. Various stimuli were added; vehicle (Fluorobrite media), 50ng/mL NGF (diluted in Fluorobrite media), or 2ug/mL purified CSPGs (diluted in Fluorobrite media). These stimuli were added in various combinations as indicated in the figure legends then imaged for approximately 2hr. PC12 cell FRET ratios were calculated using several algorithms developed by the Carsten Schultz Lab. The first ImageJ macro combined all CFP and YFP images across the time course(Schindelin et al., 2012). The second ImageJ macro, FluoQ, analyzes FRET ratios and has been described in detail previously(Kuchenov et al., 2016; Stein et al., 2013). Briefly, combined CFP-YFP images are thresholded with the Triangle method, smoothed, and segmented with the binary mask generated using the Huang fuzzy method. Segmented-image FRET ratios are calculated and low-expressing cells and cells with erroneous FRET ratios are discarded. FRET/CFP ratios across the 30-minute baseline period are averaged and used to normalize FRET/CFP ratios after stimulus. FRET/CFP ratios for each cell measured are averaged at each time point and plotted in Figure 1 (chapter 5). Automated FRET analysis was not possible when analyzing primary sympathetic neurons given the high motility and polarized nature of these neurons. To analyze primary neurons, we generated 16-bit tiff images of each respective channel (CFP and YFP-FRET) across the time course. The ImageJ “Math” tool was used to divide the FRET image by the CFP image generating a new image that corresponds to the FRET/CFP ratio. The ImageJ manual

selection tool was then used to draw a region of interest (ROI) around a given cell body. Plotting the z-projection of this given ROI displays the FRET/CFP ratio over the time course which could be exported and used for analysis. The average FRET ratio across the 30-minute baseline was used to normalize the FRET ratios after cell stimulus. FRET ratios were averaged across each ROI (cell) for a given stimulus and plotted in Figures 2 and 3 (Chapter 5). Statistical analysis was done at the time point where the greatest difference was observed between stimuli.

FRET biosensors used:

Target	Sensor name	Domains	Name used	Reference
ERK	EKAR2G1	WW (phosphopeptide binding domain)-Substrate domain (PDVPRTPVDKAKLSFQFP)	ERK	(Komatsu et al., 2011)
RhoA	RhoA2G	RhoA-binding domain (RBD) of rhotekin– RhoA	RhoA	(Fritz et al., 2013)
FAK	FAK biosensor	SH2(c-Srk) -substrate	FAK	(Seong et al., 2011)
Src	Src biosensor	CFP-SH2 (Src)- Substrate (synthetic)	Src	(Ouyang et al., 2008)
PKA	AKAR3EV	FHA1 domain - PKA substrate (LRRATLVD) - NES	PKA	(Komatsu et al., 2011)
PKC	Eevee-PKC	PKCβ C1 domain - FHA1 domain (phosphopeptide binding) - Substrate domain (KKKKKRFTFKDSFKL) NES	PKC	(Komatsu et al., 2011)

Statistics: Sample size is indicated in each figure legend. Broadly speaking, animal experiments (arrhythmia assessment, immunohistochemistry, cardiac tissue western blotting, etc.) n-value corresponds to animal number used in experiment, other experiments utilizing cells (neurite outgrowth, western blotting, etc.) n-value corresponds

to number of individual experiments, for FRET-ratio quantification n-value corresponds to cell number quantified. Student's t-test was used for comparisons of just two samples. Data with more than two groups were analyzed by one-way ANOVA using the Tukey's post-hoc test to compare all conditions, in scenarios where samples are compared to a single control group (where appropriate) Dunnett's post-test was used. For experiments comparing multiple variables (e.g., drug treatment, surgical group) two-way ANOVA was used. Statistical significance of FRET ratio data (Chapter 5) was analyzed at a given time point where the largest difference was observed (indicated in each respective figure). One-way ANOVA and Dunnett's post-hoc test was used to compare all conditions to no stimulus controls. All statistical analyses were carried out using Prism 9.

Chapter 8

Appendix

HJ-04, Analog of HJ-01 and HJ-02 used for target identification:

Novel small molecules generated by Michael S. Cohen Ph.D were discussed at length in Chapter 4 of this dissertation. Here we attempt a method intended to identify the protein target of these small molecules. HJ-04 is an analog of HJ-01 and HJ-02 with an attached alkyne handle that can undergo a bio-orthogonal click chemistry reaction to label the small molecule bound to protein target(s) in a lysate. We first tested the efficacy of this analog in promoting sympathetic neurite outgrowth to ensure that the small molecule's biological activity was unaltered by addition of the alkyne chemical group. HJ-04 restored neurite outgrowth across CSPGs similarly to HJ-01 and HJ-02(Figure 8.1A,B).

We then treated HEK-293T cells with 1μM HJ-04 alone or HJ-02 at increasing doses 100nM and 1μM for 30 minutes followed by 1μM HJ-04 for 30 minutes. Cell lysates were then prepared and soluble and membrane enriched protein fractions were subjected to copper catalyzed click-chemistry biotinylation. Biotinylated proteins were enriched with streptavidin beads followed by stringent washing with 4M Urea. Protein lysates were placed in sample buffer and boiled for 5 minutes to remove proteins from streptavidin beads. Protein samples were subjected to SDS-PAGE and western blotting followed by streptavidin-HRP probe chemiluminescent imaging. We found a band at approximately

60kDa enriched in HJ-04 treated samples that was competed away with increasing doses of HJ-02 in the membrane but not soluble fractions of protein lysate (Figure 8.1C). Based on a single previous observation from a heavy-isotope labeling click-chemistry labeling mass spectrometry experiment with the Cravatt Lab (Scripps) we suspected that the protein might be Src kinase (59 kDa) when we probed with a Src antibody however we found that Src was non-specifically pulled down in all conditions (Figure 8.1C) including negative control conditions (vehicle, 5% DMSO). We used this same approach, only at larger scale, to prepare samples for an unbiased mass-spectrometry approach to identify the target but were (much to our frustration) unable to identify a putative target for the novel small molecules HJ-01 and HJ-02.

Brief discussion:

This result is one of our most promising from hundreds of different iterations of this experiment. In other variations, we modulated cell-type, serum starving time, lysis buffer recipe, reducing reagent presence, click-chemistry reaction constituents, labeling technique, protein enrichment methods but were unable to identify the target. The 60kDa protein target was pulled down and labeled on a number of occasions (Figure 8.1C) but was never consistently enriched, suggesting that we do not understand some aspect of how this small molecule interacts with its target. A few problems might explain this, one is that the target seems to be lowly abundant and enriched in the membrane. We only recently began membrane enrichment experiments which may explain why we have failed to see this band in previous western blots. Another issue is that it is difficult, bordering on impossible, to get enough protein material from cultured sympathetic neurons for a

western blot experiment let alone mass-spectrometry target identification experiments. Not using the cells in which the small molecule displays biologically activity may mean that we have been looking at protein lysates without the target protein expressed. In future experiments, using cortical neurons might help alleviate this problem since these neurons are easier to culture and could supply sufficient protein for mass-spectrometry approaches. The last and most critical issue that may explain our failure to identify a target is the matter of reversibility in our covalent inhibitor. HJ-01, HJ-02 and HJ-04 were designed to form a covalent adduct between the acrylamide of the small molecules and a cysteine in the enzymatic pocket of PTPσ via a Michael addition reaction. Recently, we became aware of a mechanism by which acrylamides may form adducts on amines in a structure that is reversible under certain conditions. It is possible that HJ-01, HJ-02 and HJ-04 bind to an amine on a protein target and that this adduct falls apart during our procedure for western blotting. Given these observations we think an experiment that utilizes lysate from neuronal cells treated with or without HJ-01 HJ-02 at increasing doses and utilization of a different approach like Cellular Thermal Shift Assay coupled to Mass-spectrometry may identify of putative target. If click-chemistry based methods are to be utilized it may be beneficial to generate a photo-reactive crosslinking analog of HJ-01 and HJ-02 that could be utilized in a similar set of experiments to the one used in this appendix but would be ensured to form a stable adduct that could be used to identify the target. For a detailed explanation of the methods used in this appendix including a description of the click-chemistry protein preparation please see Chapter 7 – “Detailed Methods” section of the dissertation.

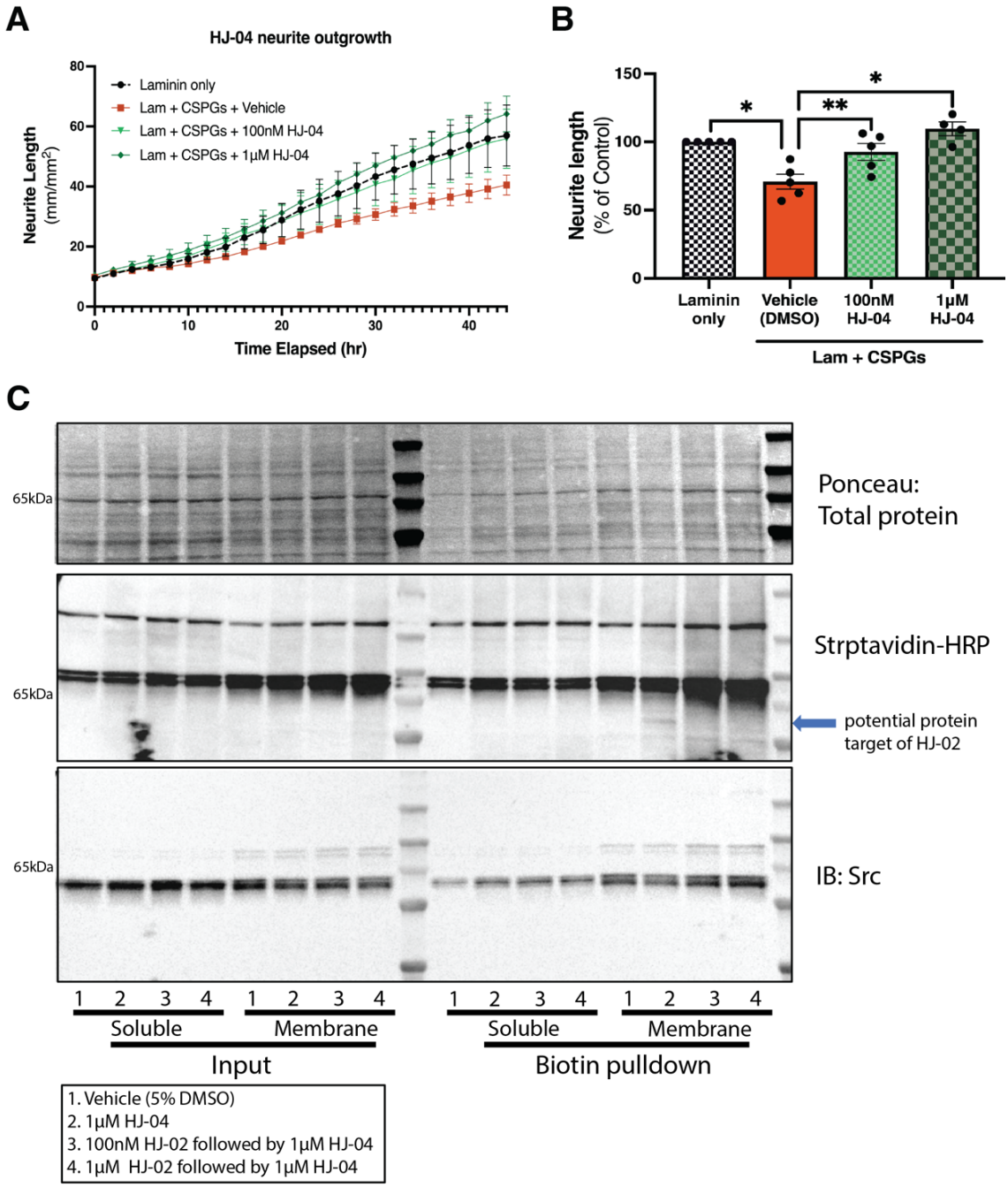

Figure 8.1: HJ-04, small molecules analog of HJ-01 and HJ-02. **(A)** HJ-04 promotes neurite outgrowth across CSPGs. Mean neurite length expressed as a percent of laminin only controls. Statistics one-way ANOVA Tukey's post test, select comparisons shown; * $p<0.05$, ** $p<0.01$. N=5 independent experiments except at 1μM HJ-04 which was only n=4. **(C)** Western blot experiment attempting to identify protein target of HJ-02 using competition labeling with alkyne analog HJ-04 + biotinylation using click-chemistry. Western blot shows first, total protein loading into each lane with ponceau. Second, streptavidin-HRP labeling of biotinylated proteins, blue arrow indicates the putative protein band that is labeled by HJ-04 and competed away by HJ-02. Third, Src immunoblot shows that Src is not selectively enriched and competed in small molecules treated lysates but rather is non-specifically pulled down in all samples.

Chapter 9

References

Al-Shawi, R., Hafner, A., Olsen, J., Chun, S., Raza, S., Thrasivoulou, C., . . . Cowen, T. (2008). Neurotoxic and neurotrophic roles of proNGF and the receptor sortilin in the adult and ageing nervous system. *Eur J Neurosci, 27*(8), 2103-2114. doi:10.1111/j.1460-9568.2008.06152.x

Anderson, M. A., Burda, J. E., Ren, Y., Ao, Y., O'Shea, T. M., Kawaguchi, R., . . . Sofroniew, M. V. (2016). Astrocyte scar formation aids central nervous system axon regeneration. *Nature, 532*(7598), 195-200. doi:10.1038/nature17623

Andoh, T., Sakamoto, A., & Kuraishi, Y. (2013). Effects of xaliproden, a 5-HT(1)A agonist, on mechanical allodynia caused by chemotherapeutic agents in mice. *Eur J Pharmacol, 721*(1-3), 231-236. doi:10.1016/j.ejphar.2013.09.030

Andreassi, C., Zimmermann, C., Mitter, R., Fusco, S., De Vita, S., Saiardi, A., & Riccio, A. (2010). An NGF-responsive element targets myo-inositol monophosphatase-1 mRNA to sympathetic neuron axons. *Nat Neurosci, 13*(3), 291-301. doi:10.1038/nn.2486

Aricescu, A. R., McKinnell, I. W., Halfter, W., & Stoker, A. W. (2002). Heparan sulfate proteoglycans are ligands for receptor protein tyrosine phosphatase sigma. *Mol Cell Biol, 22*(6), 1881-1892. doi:10.1128/MCB.22.6.1881-1892.2002

Aurora, A. B., Porrello, E. R., Tan, W., Mahmoud, A. I., Hill, J. A., Bassel-Duby, R., . . . Olson, E. N. (2014). Macrophages are required for neonatal heart regeneration. *J Clin Invest, 124*(3), 1382-1392. doi:10.1172/JCI72181

Bamji, S. X., Majdan, M., Pozniak, C. D., Belliveau, D. J., Aloyz, R., Kohn, J., . . . Miller, F. D. (1998). The p75 neurotrophin receptor mediates neuronal apoptosis and is essential for naturally occurring sympathetic neuron death. *J Cell Biol, 140*(4), 911-923. doi:10.1083/jcb.140.4.911

Bandtlow, C. E., & Zimmermann, D. R. (2000). Proteoglycans in the developing brain: new conceptual insights for old proteins. *Physiol Rev, 80*(4), 1267-1290. doi:10.1152/physrev.2000.80.4.1267

Barber, M. J., Mueller, T. M., Henry, D. P., Felten, S. Y., & Zipes, D. P. (1983). Transmural myocardial infarction in the dog produces sympathectomy in noninfarcted myocardium. *Circulation, 67*(4), 787-796. doi:10.1161/01.cir.67.4.787

Barde, Y. A., Edgar, D., & Thoenen, H. (1982). Purification of a new neurotrophic factor from mammalian brain. *EMBO J, 1*(5), 549-553. Retrieved from https://www.ncbi.nlm.nih.gov/pubmed/7188352

Barwad, P., Sinkar, K., Bachani, N., Shah, R., Shah, V., Kumar, B., . . . Lokhandwala, Y. (2021). Long-term clinical outcomes of cardiac sympathetic denervation in patients with refractory ventricular arrhythmias. *J Cardiovasc Electrophysiol, 32*(4), 1065-1074. doi:10.1111/jce.14947

Berkemeier, L. R., Winslow, J. W., Kaplan, D. R., Nikolics, K., Goeddel, D. V., & Rosenthal, A. (1991). Neurotrophin-5: a novel neurotrophic factor that activates trk and trkB. *Neuron, 7*(5), 857-866. doi:10.1016/0896-6273(91)90287-a

Bhattacharyya, S., Feferman, L., Han, X., Xia, K., Zhang, F., Linhardt, R. J., & Tobacman, J. K. (2020). Increased CHST15 follows decline in arylsulfatase B (ARSB) and disinhibition of non-canonical WNT signaling: potential impact on epithelial and mesenchymal identity. *Oncotarget, 11*(24), 2327-2344. doi:10.18632/oncotarget.27634

Bhattacharyya, S., Feferman, L., Terai, K., Dudek, A. Z., & Tobacman, J. K. (2017). Decline in arylsulfatase B leads to increased invasiveness of melanoma cells. *Oncotarget, 8*(3), 4169-4180. doi:10.18632/oncotarget.13751

Bhattacharyya, S., Feferman, L., & Tobacman, J. K. (2014). Arylsulfatase B regulates versican expression by galectin-3 and AP-1 mediated transcriptional effects. *Oncogene, 33*(47), 5467-5476. doi:10.1038/onc.2013.483

Bhattacharyya, S., Zhang, X., Feferman, L., Johnson, D., Tortella, F. C., Guizzetti, M., & Tobacman, J. K. (2015). Decline in arylsulfatase B and Increase in chondroitin 4-sulfotransferase combine to increase chondroitin 4-sulfate in traumatic brain injury. *J Neurochem, 134*(4), 728-739. doi:10.1111/jnc.13156

Blake, M. R., Gardner, R. T., Jin, H., Staffenson, M. A., Rueb, N. J., Barrios, A. M., . . . Habecker, B. A. (2022). Small Molecules Targeting PTPsigma-Trk Interactions Promote Sympathetic Nerve Regeneration. *ACS Chem Neurosci, 13*(5), 688-699. doi:10.1021/acschemneuro.1c00854

Boogers, M. J., Borleffs, C. J., Henneman, M. M., van Bommel, R. J., van Ramshorst, J., Boersma, E., . . . Bax, J. J. (2010). Cardiac sympathetic denervation assessed with 123-iodine metaiodobenzylguanidine imaging predicts ventricular arrhythmias in implantable cardioverter-defibrillator patients. *J Am Coll Cardiol, 55*(24), 2769-2777. doi:10.1016/j.jacc.2009.12.066

Bot, I., van Berkel, T. J., & Biessen, E. A. (2008). Mast cells: pivotal players in cardiovascular diseases. *Curr Cardiol Rev, 4*(3), 170-178. doi:10.2174/157340308785160624

Bothwell, M. (1991). Keeping track of neurotrophin receptors. *Cell, 65*(6), 915-918. doi:10.1016/0092-8674(91)90540-f

Bothwell, M. A., & Shooter, E. M. (1977). Dissociation equilibrium constant of beta nerve growth factor. *J Biol Chem, 252*(23), 8532-8536. Retrieved from https://www.ncbi.nlm.nih.gov/pubmed/925010

Boutselis, I. G., Yu, X., Zhang, Z. Y., & Borch, R. F. (2007). Synthesis and cell-based activity of a potent and selective protein tyrosine phosphatase 1B inhibitor prodrug. *J Med Chem, 50*(4), 856-864. doi:10.1021/jm061146x

Bradbury, E. J., & Burnside, E. R. (2019). Moving beyond the glial scar for spinal cord repair. *Nat Commun, 10*(1), 3879. doi:10.1038/s41467-019-11707-7

Bradbury, E. J., Moon, L. D., Popat, R. J., King, V. R., Bennett, G. S., Patel, P. N., . . . McMahon, S. B. (2002). Chondroitinase ABC promotes functional recovery after spinal cord injury. *Nature, 416*(6881), 636-640. doi:10.1038/416636a

Brittis, P. A., Canning, D. R., & Silver, J. (1992). Chondroitin sulfate as a regulator of neuronal patterning in the retina. *Science, 255*(5045), 733-736. doi:10.1126/science.1738848

Brown, J. M., Xia, J., Zhuang, B., Cho, K. S., Rogers, C. J., Gama, C. I., . . . Hsieh-Wilson, L. C. (2012). A sulfated carbohydrate epitope inhibits axon regeneration after injury. *Proc Natl Acad Sci U S A, 109*(13), 4768-4773. doi:10.1073/pnas.1121318109

Busch, S. A., & Silver, J. (2007). The role of extracellular matrix in CNS regeneration. *Curr Opin Neurobiol, 17*(1), 120-127. doi:10.1016/j.conb.2006.09.004

Chen, Z. Y., Ieraci, A., Tanowitz, M., & Lee, F. S. (2005). A novel endocytic recycling signal distinguishes biological responses of Trk neurotrophin receptors. *Mol Biol Cell, 16*(12), 5761-5772. doi:10.1091/mbc.e05-07-0651

Cheung, S. T., Miller, M. S., Pacoma, R., Roland, J., Liu, J., Schumacher, A. M., & Hsieh-Wilson, L. C. (2017). Discovery of a Small-Molecule Modulator of Glycosaminoglycan Sulfation. *ACS Chem Biol, 12*(12), 3126-3133. doi:10.1021/acschembio.7b00885

Chuang, H. H., Prescott, E. D., Kong, H., Shields, S., Jordt, S. E., Basbaum, A. I., . . . Julius, D. (2001). Bradykinin and nerve growth factor release the capsaicin receptor from PtdIns(4,5)P2-mediated inhibition. *Nature, 411*(6840), 957-962. doi:10.1038/35082088

Claing, A., Laporte, S. A., Caron, M. G., & Lefkowitz, R. J. (2002). Endocytosis of G protein-coupled receptors: roles of G protein-coupled receptor kinases and beta-arrestin proteins. *Prog Neurobiol, 66*(2), 61-79. doi:10.1016/s0301-0082(01)00023-5

Clary, D. O., & Reichardt, L. F. (1994). An alternatively spliced form of the nerve growth factor receptor TrkA confers an enhanced response to neurotrophin 3. *Proc Natl Acad Sci U S A, 91*(23), 11133-11137. doi:10.1073/pnas.91.23.11133

Cohen, S. (1960). Purification of a Nerve-Growth Promoting Protein from the Mouse Salivary Gland and Its Neuro-Cytotoxic Antiserum. *Proc Natl Acad Sci U S A, 46*(3), 302-311. doi:10.1073/pnas.46.3.302

Cohen, S., & Levi-Montalcini, R. (1956). A Nerve Growth-Stimulating Factor Isolated from Snake Venom. *Proc Natl Acad Sci U S A, 42*(9), 571-574. doi:10.1073/pnas.42.9.571

Coles, C. H., Shen, Y., Tenney, A. P., Siebold, C., Sutton, G. C., Lu, W., . . . Aricescu, A. R. (2011). Proteoglycan-specific molecular switch for RPTPsigma clustering and neuronal extension. *Science, 332*(6028), 484-488. doi:10.1126/science.1200840

Cristofaro, B., Stone, O. A., Caporali, A., Dawbarn, D., Ieronimakis, N., Reyes, M., . . . Emanueli, C. (2010). Neurotrophin-3 is a novel angiogenic factor capable of therapeutic neovascularization in a mouse model of limb ischemia. *Arterioscler Thromb Vasc Biol, 30*(6), 1143-1150. doi:10.1161/ATVBAHA.109.205468

Curtis, M. J., Hancox, J. C., Farkas, A., Wainwright, C. L., Stables, C. L., Saint, D. A., . . . Walker, M. J. (2013). The Lambeth Conventions (II): guidelines for the study of animal and human ventricular and supraventricular arrhythmias. *Pharmacol Ther, 139*(2), 213-248. doi:10.1016/j.pharmthera.2013.04.008

Cutler, M. J., Jeyaraj, D., & Rosenbaum, D. S. (2011). Cardiac electrical remodeling in health and disease. *Trends Pharmacol Sci, 32*(3), 174-180. doi:10.1016/j.tips.2010.12.001

Dae, M. W., O'Connell, J. W., Botvinick, E. H., & Chin, M. C. (1995). Acute and chronic effects of transient myocardial ischemia on sympathetic nerve activity, density, and norepinephrine content. *Cardiovasc Res, 30*(2), 270-280. Retrieved from https://www.ncbi.nlm.nih.gov/pubmed/7585815

Deepa, S. S., Carulli, D., Galtrey, C., Rhodes, K., Fukuda, J., Mikami, T., . . . Fawcett, J. W. (2006). Composition of perineuronal net extracellular matrix in rat brain: a different disaccharide composition for the net-associated proteoglycans. *J Biol Chem, 281*(26), 17789-17800. doi:10.1074/jbc.M600544200

Deppmann, C. D., Mihalas, S., Sharma, N., Lonze, B. E., Niebur, E., & Ginty, D. D. (2008). A model for neuronal competition during development. *Science, 320*(5874), 369-373. doi:10.1126/science.1152677

Dick, G., Tan, C. L., Alves, J. N., Ehlert, E. M. E., Miller, G. M., Hsieh-Wilson, L. C., . . . Kwok, J. C. F. (2013). Semaphorin 3A binds to the perineuronal nets via chondroitin

sulfate type E motifs in rodent brains. *J Biol Chem, 288*(38), 27384-27395. doi:10.1074/jbc.M111.310029

Dickendesher, T. L., Baldwin, K. T., Mironova, Y. A., Koriyama, Y., Raiker, S. J., Askew, K. L., . . . Giger, R. J. (2012). NgR1 and NgR3 are receptors for chondroitin sulfate proteoglycans. *Nat Neurosci, 15*(5), 703-712. doi:10.1038/nn.3070

Donovan, M. J., Hahn, R., Tessarollo, L., & Hempstead, B. L. (1996). Identification of an essential nonneuronal function of neurotrophin 3 in mammalian cardiac development. *Nat Genet, 14*(2), 210-213. doi:10.1038/ng1096-210

Donovan, M. J., Lin, M. I., Wiegn, P., Ringstedt, T., Kraemer, R., Hahn, R., . . . Hempstead, B. L. (2000). Brain derived neurotrophic factor is an endothelial cell survival factor required for intramyocardial vessel stabilization. *Development, 127*(21), 4531-4540. doi:10.1242/dev.127.21.4531

Dou, C. L., & Levine, J. M. (1994). Inhibition of neurite growth by the NG2 chondroitin sulfate proteoglycan. *J Neurosci, 14*(12), 7616-7628. Retrieved from https://www.ncbi.nlm.nih.gov/pubmed/7996200

Douillet, P., & Orgogozo, J. M. (2009). What we have learned from the Xaliproden Sanofi-aventis trials. *J Nutr Health Aging, 13*(4), 365-366. doi:10.1007/s12603-009-0045-6

Dziennis, S., & Habecker, B. A. (2003). Cytokine suppression of dopamine-beta-hydroxylase by extracellular signal-regulated kinase-dependent and -independent pathways. *J Biol Chem, 278*(18), 15897-15904. doi:10.1074/jbc.M212480200

Emanueli, C., Salis, M. B., Pinna, A., Graiani, G., Manni, L., & Madeddu, P. (2002). Nerve growth factor promotes angiogenesis and arteriogenesis in ischemic hindlimbs. *Circulation, 106*(17), 2257-2262. doi:10.1161/01.cir.0000033971.56802.c5

Fallavollita, J. A., Heavey, B. M., Luisi, A. J., Jr., Michalek, S. M., Baldwa, S., Mashtare, T. L., Jr., . . . Canty, J. M., Jr. (2014). Regional myocardial sympathetic denervation predicts the risk of sudden cardiac arrest in ischemic cardiomyopathy. *J Am Coll Cardiol, 63*(2), 141-149. doi:10.1016/j.jacc.2013.07.096

Faux, C., Hawadle, M., Nixon, J., Wallace, A., Lee, S., Murray, S., & Stoker, A. (2007). PTPsigma binds and dephosphorylates neurotrophin receptors and can suppress NGF-dependent neurite outgrowth from sensory neurons. *Biochim Biophys Acta, 1773*(11), 1689-1700. doi:10.1016/j.bbamcr.2007.06.008

Feyerabend, T. B., Weiser, A., Tietz, A., Stassen, M., Harris, N., Kopf, M., . . . Rodewald, H. R. (2011). Cre-mediated cell ablation contests mast cell contribution in models of antibody- and T cell-mediated autoimmunity. *Immunity, 35*(5), 832-844. doi:10.1016/j.immuni.2011.09.015

Finkbeiner, S., Tavazoie, S. F., Maloratsky, A., Jacobs, K. M., Harris, K. M., & Greenberg, M. E. (1997). CREB: a major mediator of neuronal neurotrophin responses. *Neuron, 19*(5), 1031-1047. doi:10.1016/s0896-6273(00)80395-5

Fisher, D., Xing, B., Dill, J., Li, H., Hoang, H. H., Zhao, Z., . . . Li, S. (2011). Leukocyte common antigen-related phosphatase is a functional receptor for chondroitin sulfate proteoglycan axon growth inhibitors. *J Neurosci, 31*(40), 14051-14066. doi:10.1523/JNEUROSCI.1737-11.2011

Florea, V. G., & Cohn, J. N. (2014). The autonomic nervous system and heart failure. *Circ Res, 114*(11), 1815-1826. doi:10.1161/CIRCRESAHA.114.302589

Fomovsky, G. M., & Holmes, J. W. (2010). Evolution of scar structure, mechanics, and ventricular function after myocardial infarction in the rat. *Am J Physiol Heart Circ Physiol, 298*(1), H221-228. doi:10.1152/ajpheart.00495.2009

Fomovsky, G. M., Thomopoulos, S., & Holmes, J. W. (2010). Contribution of extracellular matrix to the mechanical properties of the heart. *J Mol Cell Cardiol, 48*(3), 490-496. doi:10.1016/j.yjmcc.2009.08.003

Freedman, N. J., & Lefkowitz, R. J. (2004). Anti-beta(1)-adrenergic receptor antibodies and heart failure: causation, not just correlation. *J Clin Invest, 113*(10), 1379-1382. doi:10.1172/JCI21748

Freemantle, N., Cleland, J., Young, P., Mason, J., & Harrison, J. (1999). beta Blockade after myocardial infarction: systematic review and meta regression analysis. *BMJ, 318*(7200), 1730-1737. doi:10.1136/bmj.318.7200.1730

Fritz, R. D., Letzelter, M., Reimann, A., Martin, K., Fusco, L., Ritsma, L., . . . Pertz, O. (2013). A versatile toolkit to produce sensitive FRET biosensors to visualize signaling in time and space. *Sci Signal, 6*(285), rs12. doi:10.1126/scisignal.2004135

Fry, E. J., Chagnon, M. J., Lopez-Vales, R., Tremblay, M. L., & David, S. (2010). Corticospinal tract regeneration after spinal cord injury in receptor protein tyrosine phosphatase sigma deficient mice. *Glia., 58*(4), 423-433.

Fulo, H. F., Rueb, N. J., Gaston, R., Jr., Batsomboon, P., Ahmed, K. T., Barrios, A. M., & Dudley, G. B. (2021). Synthesis of illudalic acid and analogous phosphatase inhibitors. *Org Biomol Chem, 19*(48), 10596-10600. doi:10.1039/d1ob02106k

Gama, C. I., Tully, S. E., Sotogaku, N., Clark, P. M., Rawat, M., Vaidehi, N., . . . Hsieh-Wilson, L. C. (2006). Sulfation patterns of glycosaminoglycans encode molecular recognition and activity. *Nat Chem Biol, 2*(9), 467-473. doi:10.1038/nchembio810

Gardner, R. T., & Habecker, B. A. (2013). Infarct-derived chondroitin sulfate proteoglycans prevent sympathetic reinnervation after cardiac ischemia-reperfusion injury. *J Neurosci, 33*(17), 7175-7183. doi:10.1523/JNEUROSCI.5866-12.2013

Gardner, R. T., Ripplinger, C. M., Myles, R. C., & Habecker, B. A. (2016). Molecular Mechanisms of Sympathetic Remodeling and Arrhythmias. *Circ Arrhythm Electrophysiol, 9*(2), e001359. doi:10.1161/CIRCEP.115.001359

Gardner, R. T., Wang, L., Lang, B. T., Cregg, J. M., Dunbar, C. L., Woodward, W. R., . . . Habecker, B. A. (2015). Targeting protein tyrosine phosphatase sigma after myocardial infarction restores cardiac sympathetic innervation and prevents arrhythmias. *Nat Commun, 6*, 6235. doi:10.1038/ncomms7235

Gates, M. A., Thomas, L. B., Howard, E. M., Laywell, E. D., Sajin, B., Faissner, A., . . . Steindler, D. A. (1995). Cell and molecular analysis of the developing and adult mouse subventricular zone of the cerebral hemispheres. *J Comp Neurol, 361*(2), 249-266. doi:10.1002/cne.903610205

Gentek, R., & Hoeffel, G. (2017). The Innate Immune Response in Myocardial Infarction, Repair, and Regeneration. *Adv Exp Med Biol, 1003*, 251-272. doi:10.1007/978-3-319-57613-8_12

Georgieva, M. V., de Pablo, Y., Sanchis, D., Comella, J. X., & Llovera, M. (2011). Ubiquitination of TrkA by Nedd4-2 regulates receptor lysosomal targeting and mediates receptor signaling. *J Neurochem, 117*(3), 479-493. doi:10.1111/j.1471-4159.2011.07218.x

Gilbert, R. J., McKeon, R. J., Darr, A., Calabro, A., Hascall, V. C., & Bellamkonda, R. V. (2005). CS-4,6 is differentially upregulated in glial scar and is a potent inhibitor of neurite extension. *Mol Cell Neurosci, 29*(4), 545-558. doi:10.1016/j.mcn.2005.04.006

Glebova, N. O., & Ginty, D. D. (2004). Heterogeneous requirement of NGF for sympathetic target innervation in vivo. *J Neurosci, 24*(3), 743-751. doi:10.1523/JNEUROSCI.4523-03.2004

Glebova, N. O., & Ginty, D. D. (2005). Growth and survival signals controlling sympathetic nervous system development. *Annu Rev Neurosci, 28*, 191-222. doi:10.1146/annurev.neuro.28.061604.135659

Gopalakrishnan, S. M., Teusch, N., Imhof, C., Bakker, M. H., Schurdak, M., Burns, D. J., & Warrior, U. (2008). Role of Rho kinase pathway in chondroitin sulfate proteoglycan-mediated inhibition of neurite outgrowth in PC12 cells. *J Neurosci Res, 86*(10), 2214-2226. doi:10.1002/jnr.21671

Greene, L. A. (1978). Nerve growth factor prevents the death and stimulates the neuronal differentiation of clonal PC12 pheochromocytoma cells in serum-free medium. *J Cell Biol, 78*(3), 747-755. doi:10.1083/jcb.78.3.747

Greenwald, E. C., Mehta, S., & Zhang, J. (2018). Genetically Encoded Fluorescent Biosensors Illuminate the Spatiotemporal Regulation of Signaling Networks. *Chem Rev, 118*(24), 11707-11794. doi:10.1021/acs.chemrev.8b00333

Grimes, M. L., Zhou, J., Beattie, E. C., Yuen, E. C., Hall, D. E., Valletta, J. S., . . . Mobley, W. C. (1996). Endocytosis of activated TrkA: evidence that nerve growth factor induces formation of signaling endosomes. *J Neurosci, 16*(24), 7950-7964. Retrieved from https://www.ncbi.nlm.nih.gov/pubmed/8987823

Habecker, B. A., Bilimoria, P., Linick, C., Gritman, K., Lorentz, C. U., Woodward, W., & Birren, S. J. (2008). Regulation of cardiac innervation and function via the p75 neurotrophin receptor. *Auton Neurosci, 140*(1-2), 40-48. doi:10.1016/j.autneu.2008.03.002

Haglund, K., Shimokawa, N., Szymkiewicz, I., & Dikic, I. (2002). Cbl-directed monoubiquitination of CIN85 is involved in regulation of ligand-induced degradation of EGF receptors. *Proc Natl Acad Sci U S A, 99*(19), 12191-12196. doi:10.1073/pnas.192462299

Hamburger, V. (1934). The effects of wing bud extirpation on the development of the central nervous system in chick embryos. *J Exp Zool, 68*, 449-494.

Hamburger, V. (1939). Motor and sensory hyperplasia following limb-bud transplantations in chick embryos. *Physiol Zool, 12*, 268-284.

Hamburger, V., & Levi-Montalcini, R. (1949). Proliferation, differentiation and degeneration in the spinal ganglia of the chick embryo under normal and experimental conditions. *J Exp Zool, 111*(3), 457-501. doi:10.1002/jez.1401110308

Harmatz, P., Ketteridge, D., Giugliani, R., Guffon, N., Teles, E. L., Miranda, M. C., . . . Group, M. V. S. (2005). Direct comparison of measures of endurance, mobility, and joint function during enzyme-replacement therapy of mucopolysaccharidosis VI (Maroteaux-Lamy syndrome): results after 48 weeks in a phase 2 open-label clinical study of recombinant human N-acetylgalactosamine 4-sulfatase. *Pediatrics, 115*(6), e681-689. doi:10.1542/peds.2004-1023

Harmatz, P., Whitley, C. B., Waber, L., Pais, R., Steiner, R., Plecko, B., . . . Hopwood, J. J. (2004). Enzyme replacement therapy in mucopolysaccharidosis VI (Maroteaux-Lamy syndrome). *J Pediatr, 144*(5), 574-580. doi:10.1016/j.jpeds.2004.03.018

Harmatz, P. R., Garcia, P., Guffon, N., Randolph, L. M., Shediac, R., Braunlin, E., . . . Decker, C. (2014). Galsulfase (Naglazyme(R)) therapy in infants with

mucopolysaccharidosis VI. *J Inherit Metab Dis, 37*(2), 277-287. doi:10.1007/s10545-013-9654-7

Harrington, A. W., Leiner, B., Blechschmitt, C., Arevalo, J. C., Lee, R., Morl, K., . . . Giehl, K. M. (2004). Secreted proNGF is a pathophysiological death-inducing ligand after adult CNS injury. *Proc Natl Acad Sci U S A, 101*(16), 6226-6230. doi:10.1073/pnas.0305755101

Harrington, A. W., St Hillaire, C., Zweifel, L. S., Glebova, N. O., Philippidou, P., Halegoua, S., & Ginty, D. D. (2011). Recruitment of actin modifiers to TrkA endosomes governs retrograde NGF signaling and survival. *Cell, 146*(3), 421-434. doi:10.1016/j.cell.2011.07.008

Hartikainen, J., Kuikka, J., Mantysaari, M., Lansimies, E., & Pyorala, K. (1996). Sympathetic reinnervation after acute myocardial infarction. *Am J Cardiol, 77*(1), 5-9. doi:10.1016/s0002-9149(97)89125-4

Hasan, W., Jama, A., Donohue, T., Wernli, G., Onyszchuk, G., Al-Hafez, B., . . . Smith, P. G. (2006). Sympathetic hyperinnervation and inflammatory cell NGF synthesis following myocardial infarction in rats. *Brain Res, 1124*(1), 142-154. doi:10.1016/j.brainres.2006.09.054

Heerssen, H. M., Pazyra, M. F., & Segal, R. A. (2004). Dynein motors transport activated Trks to promote survival of target-dependent neurons. *Nat Neurosci, 7*(6), 596-604. doi:10.1038/nn1242

Hempstead, B. L., Martin-Zanca, D., Kaplan, D. R., Parada, L. F., & Chao, M. V. (1991). High-affinity NGF binding requires coexpression of the trk proto-oncogene and the low-affinity NGF receptor. *Nature, 350*(6320), 678-683. doi:10.1038/350678a0

Hendry, I. A., Stockel, K., Thoenen, H., & Iversen, L. L. (1974). The retrograde axonal transport of nerve growth factor. *Brain Res, 68*(1), 103-121. doi:10.1016/0006-8993(74)90536-8

Herring, N., Kalla, M., & Paterson, D. J. (2019). The autonomic nervous system and cardiac arrhythmias: current concepts and emerging therapies. *Nat Rev Cardiol, 16*(12), 707-726. doi:10.1038/s41569-019-0221-2

Hiltunen, J. O., Arumae, U., Moshnyakov, M., & Saarma, M. (1996). Expression of mRNAs for neurotrophins and their receptors in developing rat heart. *Circ Res, 79*(5), 930-939. doi:10.1161/01.res.79.5.930

Hiltunen, J. O., Laurikainen, A., Vakeva, A., Meri, S., & Saarma, M. (2001). Nerve growth factor and brain-derived neurotrophic factor mRNAs are regulated in distinct cell populations of rat heart after ischaemia and reperfusion. *J Pathol, 194*(2), 247-253. doi:10.1002/path.878

Hirokawa, N., Noda, Y., Tanaka, Y., & Niwa, S. (2009). Kinesin superfamily motor proteins and intracellular transport. *Nat Rev Mol Cell Biol, 10*(10), 682-696. doi:10.1038/nrm2774

Hohn, A., Leibrock, J., Bailey, K., & Barde, Y. A. (1990). Identification and characterization of a novel member of the nerve growth factor/brain-derived neurotrophic factor family. *Nature, 344*(6264), 339-341. doi:10.1038/344339a0

Horton, A. C., & Ehlers, M. D. (2003). Neuronal polarity and trafficking. *Neuron, 40*(2), 277-295. doi:10.1016/s0896-6273(03)00629-9

Howe, C. L., & Mobley, W. C. (2004). Signaling endosome hypothesis: A cellular mechanism for long distance communication. *J Neurobiol, 58*(2), 207-216. doi:10.1002/neu.10323

Howe, C. L., Valletta, J. S., Rusnak, A. S., & Mobley, W. C. (2001). NGF signaling from clathrin-coated vesicles: evidence that signaling endosomes serve as a platform for the Ras-MAPK pathway. *Neuron, 32*(5), 801-814. doi:10.1016/s0896-6273(01)00526-8

Hsu, J. Y., Stein, S. A., & Xu, X. M. (2005). Temporal and spatial distribution of growth-associated molecules and astroglial cells in the rat corticospinal tract during development. *J Neurosci Res, 80*(3), 330-340. doi:10.1002/jnr.20472

Huang, E. J., & Reichardt, L. F. (2001). Neurotrophins: roles in neuronal development and function. *Annu Rev Neurosci, 24*, 677-736. doi:10.1146/annurev.neuro.24.1.677

Huang, E. J., & Reichardt, L. F. (2003). Trk receptors: roles in neuronal signal transduction. *Annu Rev Biochem, 72*, 609-642. doi:10.1146/annurev.biochem.72.121801.161629

Humeres, C., & Frangogiannis, N. G. (2019). Fibroblasts in the Infarcted, Remodeling, and Failing Heart. *JACC Basic Transl Sci, 4*(3), 449-467. doi:10.1016/j.jacbts.2019.02.006

Ibanez, C. F. (2007). Message in a bottle: long-range retrograde signaling in the nervous system. *Trends Cell Biol, 17*(11), 519-528. doi:10.1016/j.tcb.2007.09.003

Ip, N. Y., Ibanez, C. F., Nye, S. H., McClain, J., Jones, P. F., Gies, D. R., . . . et al. (1992). Mammalian neurotrophin-4: structure, chromosomal localization, tissue distribution, and receptor specificity. *Proc Natl Acad Sci U S A, 89*(7), 3060-3064. doi:10.1073/pnas.89.7.3060

Ivey, M. J., & Tallquist, M. D. (2016). Defining the Cardiac Fibroblast. *Circ J, 80*(11), 2269-2276. doi:10.1253/circj.CJ-16-1003

Jackson, K. (2007). The evolution of venom-conducting fangs: insights from developmental biology. *Toxicon, 49*(7), 975-981. doi:10.1016/j.toxicon.2007.01.007

Janicki, J. S., Brower, G. L., & Levick, S. P. (2015). The emerging prominence of the cardiac mast cell as a potent mediator of adverse myocardial remodeling. *Methods Mol Biol, 1220*, 121-139. doi:10.1007/978-1-4939-1568-2_8

Jones, K. R., & Reichardt, L. F. (1990). Molecular cloning of a human gene that is a member of the nerve growth factor family. *Proc Natl Acad Sci U S A, 87*(20), 8060-8064. doi:10.1073/pnas.87.20.8060

Jones, L. L., Margolis, R. U., & Tuszynski, M. H. (2003). The chondroitin sulfate proteoglycans neurocan, brevican, phosphacan, and versican are differentially regulated following spinal cord injury. *Exp Neurol, 182*(2), 399-411. doi:10.1016/s0014-4886(03)00087-6

Kandel, E. R. (2013). *Principles of neural science* (5th ed.). New York: McGraw-Hill.

Kanisicak, O., Khalil, H., Ivey, M. J., Karch, J., Maliken, B. D., Correll, R. N., . . . Molkentin, J. D. (2016). Genetic lineage tracing defines myofibroblast origin and function in the injured heart. *Nat Commun, 7*, 12260. doi:10.1038/ncomms12260

Kantor, D. B., Chivatakarn, O., Peer, K. L., Oster, S. F., Inatani, M., Hansen, M. J., . . . Kolodkin, A. L. (2004). Semaphorin 5A is a bifunctional axon guidance cue regulated by heparan and chondroitin sulfate proteoglycans. *Neuron, 44*(6), 961-975. doi:10.1016/j.neuron.2004.12.002

Kardon, J. R., & Vale, R. D. (2009). Regulators of the cytoplasmic dynein motor. *Nat Rev Mol Cell Biol, 10*(12), 854-865. doi:10.1038/nrm2804

Kermani, P., Rafii, D., Jin, D. K., Whitlock, P., Schaffer, W., Chiang, A., . . . Hempstead, B. L. (2005). Neurotrophins promote revascularization by local recruitment of TrkB+ endothelial cells and systemic mobilization of hematopoietic progenitors. *J Clin Invest, 115*(3), 653-663. doi:10.1172/JCI22655

Kimura, K., Ieda, M., Kanazawa, H., Yagi, T., Tsunoda, M., Ninomiya, S., . . . Fukuda, K. (2007). Cardiac sympathetic rejuvenation: a link between nerve function and cardiac hypertrophy. *Circ Res, 100*(12), 1755-1764. doi:10.1161/01.RES.0000269828.62250.ab

Komatsu, N., Aoki, K., Yamada, M., Yukinaga, H., Fujita, Y., Kamioka, Y., & Matsuda, M. (2011). Development of an optimized backbone of FRET biosensors for kinases and GTPases. *Mol Biol Cell, 22*(23), 4647-4656. doi:10.1091/mbc.E11-01-0072

Kuchenov, D., Laketa, V., Stein, F., Salopiata, F., Klingmuller, U., & Schultz, C. (2016). High-Content Imaging Platform for Profiling Intracellular Signaling Network Activity in Living Cells. *Cell Chem Biol, 23*(12), 1550-1559. doi:10.1016/j.chembiol.2016.11.008

Kuruvilla, R., Zweifel, L. S., Glebova, N. O., Lonze, B. E., Valdez, G., Ye, H., & Ginty, D. D. (2004). A neurotrophin signaling cascade coordinates sympathetic neuron development through differential control of TrkA trafficking and retrograde signaling. *Cell, 118*(2), 243-255. doi:10.1016/j.cell.2004.06.021

La Rovere, M. T., Bigger, J. T., Jr., Marcus, F. I., Mortara, A., & Schwartz, P. J. (1998). Baroreflex sensitivity and heart-rate variability in prediction of total cardiac mortality after myocardial infarction. ATRAMI (Autonomic Tone and Reflexes After Myocardial Infarction) Investigators. *Lancet, 351*(9101), 478-484. doi:10.1016/s0140-6736(97)11144-8

Lang, B. T., Cregg, J. M., DePaul, M. A., Tran, A. P., Xu, K., Dyck, S. M., . . . Silver, J. (2015). Modulation of the proteoglycan receptor PTPsigma promotes recovery after spinal cord injury. *Nature, 518*(7539), 404-408. doi:10.1038/nature13974

Lee, F. S., Rajagopal, R., & Chao, M. V. (2002). Distinctive features of Trk neurotrophin receptor transactivation by G protein-coupled receptors. *Cytokine Growth Factor Rev, 13*(1), 11-17. doi:10.1016/s1359-6101(01)00024-7

Lee, R., Kermani, P., Teng, K. K., & Hempstead, B. L. (2001). Regulation of cell survival by secreted proneurotrophins. *Science, 294*(5548), 1945-1948. doi:10.1126/science.1065057

Lein, P., Johnson, M., Guo, X., Rueger, D., & Higgins, D. (1995). Osteogenic protein-1 induces dendritic growth in rat sympathetic neurons. *Neuron, 15*(3), 597-605.

Levi-Montalcini, R., & Angeletti, P. U. (1968). Nerve growth factor. *Physiol Rev, 48*(3), 534-569. doi:10.1152/physrev.1968.48.3.534

Levi-Montalcini, R., & Hamburger, V. (1953). A diffusible agent of mouse sarcoma producing hyperplasia of sympathetic ganglia and hyperneurotization of viscera in the chick embyro. *J Exp Zool, 123*, 233-287.

Lewin, G. R., & Carter, B. D. (2014). Neurotrophic factors. Preface. *Handb Exp Pharmacol, 220*, v-vi. Retrieved from https://www.ncbi.nlm.nih.gov/pubmed/24941498

Lewin, G. R., & Mendell, L. M. (1993). Nerve growth factor and nociception. *Trends Neurosci, 16*(9), 353-359. doi:10.1016/0166-2236(93)90092-z

Li, W., Knowlton, D., Van Winkle, D. M., & Habecker, B. A. (2004). Infarction alters both the distribution and noradrenergic properties of cardiac sympathetic neurons. *Am J Physiol Heart Circ Physiol, 286*(6), H2229-2236. doi:10.1152/ajpheart.00768.2003

Lin, R., Rosahl, T. W., Whiting, P. J., Fawcett, J. W., & Kwok, J. C. (2011). 6-Sulphated chondroitins have a positive influence on axonal regeneration. *PLoS One, 6*(7), e21499. doi:10.1371/journal.pone.0021499

Ling, Q., Huang, Y., Zhou, Y., Cai, Z., Xiong, B., Zhang, Y., . . . Shen, J. (2008). Illudalic acid as a potential LAR inhibitor: Synthesis, SAR, and preliminary studies on the mechanism of action. *Bioorganic & Medicinal Chemistry, 16*(15), 7399-7409. doi:https://doi.org/10.1016/j.bmc.2008.06.014

Lopez-Sendon, J., Swedberg, K., McMurray, J., Tamargo, J., Maggioni, A. P., Dargie, H., . . . Task ForceOn Beta-Blockers of the European Society of, C. (2004). Expert consensus document on beta-adrenergic receptor blockers. *Eur Heart J, 25*(15), 1341-1362. doi:10.1016/j.ehj.2004.06.002

Lorentz, C. U., Alston, E. N., Belcik, T., Lindner, J. R., Giraud, G. D., & Habecker, B. A. (2010). Heterogeneous ventricular sympathetic innervation, altered beta-adrenergic receptor expression, and rhythm instability in mice lacking the p75 neurotrophin receptor. *Am J Physiol Heart Circ Physiol, 298*(6), H1652-1660. doi:10.1152/ajpheart.01128.2009

Luo, F., Tran, A. P., Xin, L., Sanapala, C., Lang, B. T., Silver, J., & Yang, Y. (2018). Modulation of proteoglycan receptor PTPsigma enhances MMP-2 activity to promote recovery from multiple sclerosis. *Nat Commun, 9*(1), 4126. doi:10.1038/s41467-018-06505-6

Maisonpierre, P. C., Belluscio, L., Squinto, S., Ip, N. Y., Furth, M. E., Lindsay, R. M., & Yancopoulos, G. D. (1990). Neurotrophin-3: a neurotrophic factor related to NGF and BDNF. *Science, 247*(4949 Pt 1), 1446-1451. doi:10.1126/science.247.4949.1446

Majeti, R., Bilwes, A. M., Noel, J. P., Hunter, T., & Weiss, A. (1998). Dimerization-induced inhibition of receptor protein tyrosine phosphatase function through an inhibitory wedge. *Science, 279*(5347), 88-91. doi:10.1126/science.279.5347.88

Marmor, M. D., & Yarden, Y. (2004). Role of protein ubiquitylation in regulating endocytosis of receptor tyrosine kinases. *Oncogene, 23*(11), 2057-2070. doi:10.1038/sj.onc.1207390

Martin, J. H. (2021). *Neuroanatomy : text and atlas* (Fifth edition. ed.). New York: McGraw Hill.

Massey, J. M., Amps, J., Viapiano, M. S., Matthews, R. T., Wagoner, M. R., Whitaker, C. M., . . . Onifer, S. M. (2008). Increased chondroitin sulfate proteoglycan expression in denervated brainstem targets following spinal cord injury creates a barrier to axonal regeneration overcome by chondroitinase ABC and neurotrophin-3. *Exp Neurol, 209*(2), 426-445. doi:10.1016/j.expneurol.2007.03.029

McCullough, B. S., Batsomboon, P., Hutchinson, K. B., Dudley, G. B., & Barrios, A. M. (2019). Synthesis and PTP Inhibitory Activity of Illudalic Acid and Its Methyl Ether, with Insights into Selectivity for LAR PTP over Other Tyrosine Phosphatases under

Physiologically Relevant Conditions. *J Nat Prod, 82*(12), 3386-3393. doi:10.1021/acs.jnatprod.9b00663

McKeon, R. J., Jurynec, M. J., & Buck, C. R. (1999). The chondroitin sulfate proteoglycans neurocan and phosphacan are expressed by reactive astrocytes in the chronic CNS glial scar. *J Neurosci, 19*(24), 10778-10788. Retrieved from https://www.ncbi.nlm.nih.gov/pubmed/10594061

McKeon, R. J., Schreiber, R. C., Rudge, J. S., & Silver, J. (1991). Reduction of neurite outgrowth in a model of glial scarring following CNS injury is correlated with the expression of inhibitory molecules on reactive astrocytes. *J Neurosci, 11*(11), 3398-3411. Retrieved from https://www.ncbi.nlm.nih.gov/pubmed/1719160

Meloni, M., Caporali, A., Graiani, G., Lagrasta, C., Katare, R., Van Linthout, S., . . . Emanueli, C. (2010). Nerve growth factor promotes cardiac repair following myocardial infarction. *Circ Res, 106*(7), 1275-1284. doi:10.1161/CIRCRESAHA.109.210088

Mencio, C. P., Hussein, R. K., Yu, P., & Geller, H. M. (2021). The Role of Chondroitin Sulfate Proteoglycans in Nervous System Development. *J Histochem Cytochem, 69*(1), 61-80. doi:10.1369/0022155420959147

Meredith, I. T., Broughton, A., Jennings, G. L., & Esler, M. D. (1991). Evidence of a selective increase in cardiac sympathetic activity in patients with sustained ventricular arrhythmias. *N Engl J Med, 325*(9), 618-624. doi:10.1056/NEJM199108293250905

Miller, G. M., & Hsieh-Wilson, L. C. (2015). Sugar-dependent modulation of neuronal development, regeneration, and plasticity by chondroitin sulfate proteoglycans. *Exp Neurol, 274*(Pt B), 115-125. doi:10.1016/j.expneurol.2015.08.015

Mohrman, D. E., & Heller, L. J. (1997). *Cardiovascular physiology* (4th ed.). New York: McGraw-Hill, Health Professions Division.

Munoz-Rojas, M. V., Horovitz, D. D., Jardim, L. B., Raymundo, M., Llerena, J. C., Jr., de Magalhaes Tde, S., . . . Giugliani, R. (2010). Intrathecal administration of recombinant human N-acetylgalactosamine 4-sulfatase to a MPS VI patient with pachymeningitis cervicalis. *Mol Genet Metab, 99*(4), 346-350. doi:10.1016/j.ymgme.2009.11.008

Myles, R. C., Wang, L., Kang, C., Bers, D. M., & Ripplinger, C. M. (2012). Local beta-adrenergic stimulation overcomes source-sink mismatch to generate focal arrhythmia. *Circ Res, 110*(11), 1454-1464. doi:10.1161/CIRCRESAHA.111.262345

Naumann, T., Casademunt, E., Hollerbach, E., Hofmann, J., Dechant, G., Frotscher, M., & Barde, Y. A. (2002). Complete deletion of the neurotrophin receptor p75NTR leads to long-lasting increases in the number of basal forebrain cholinergic neurons. *J Neurosci, 22*(7), 2409-2418. doi:20026171

Ngkelo, A., Richart, A., Kirk, J. A., Bonnin, P., Vilar, J., Lemitre, M., . . . Silvestre, J. S. (2016). Mast cells regulate myofilament calcium sensitization and heart function after myocardial infarction. *J Exp Med, 213*(7), 1353-1374. doi:10.1084/jem.20160081

Niknam, P., Raoufy, M. R., Fathollahi, Y., & Javan, M. (2019). Modulating proteoglycan receptor PTPsigma using intracellular sigma peptide improves remyelination and functional recovery in mice with demyelinated optic chiasm. *Mol Cell Neurosci, 99*, 103391. doi:10.1016/j.mcn.2019.103391

Nishisato, K., Hashimoto, A., Nakata, T., Doi, T., Yamamoto, H., Nagahara, D., . . . Shimamoto, K. (2010). Impaired cardiac sympathetic innervation and myocardial perfusion are related to lethal arrhythmia: quantification of cardiac tracers in patients with ICDs. *J Nucl Med, 51*(8), 1241-1249. doi:10.2967/jnumed.110.074971

Nunes, A. R., Sample, V., Xiang, Y. K., Monteiro, E. C., Gauda, E., & Zhang, J. (2012). Effect of oxygen on phosphodiesterases (PDE) 3 and 4 isoforms and PKA activity in the superior cervical ganglia. *Adv Exp Med Biol, 758*, 287-294. doi:10.1007/978-94-007-4584-1_39

Obara, Y., Labudda, K., Dillon, T. J., & Stork, P. J. (2004). PKA phosphorylation of Src mediates Rap1 activation in NGF and cAMP signaling in PC12 cells. *J Cell Sci, 117*(Pt 25), 6085-6094. doi:10.1242/jcs.01527

Ohtake, Y., & Li, S. (2015). Molecular mechanisms of scar-sourced axon growth inhibitors. *Brain Res, 1619*, 22-35. doi:10.1016/j.brainres.2014.08.064

Ohtake, Y., Saito, A., & Li, S. (2018). Diverse functions of protein tyrosine phosphatase σ in the nervous and immune systems. *Exp Neurol, 302*, 196-204. doi:10.1016/j.expneurol.2018.01.014

Ohtake, Y., Wong, D., Abdul-Muneer, P. M., Selzer, M. E., & Li, S. (2016). Two PTP receptors mediate CSPG inhibition by convergent and divergent signaling pathways in neurons. *Sci Rep, 6*, 37152. doi:10.1038/srep37152

Orecchioni, M., Ghosheh, Y., Pramod, A. B., & Ley, K. (2019). Macrophage Polarization: Different Gene Signatures in M1(LPS+) vs. Classically and M2(LPS-) vs. Alternatively Activated Macrophages. *Front Immunol, 10*, 1084. doi:10.3389/fimmu.2019.01084

Ouyang, M., Sun, J., Chien, S., & Wang, Y. (2008). Determination of hierarchical relationship of Src and Rac at subcellular locations with FRET biosensors. *Proc Natl Acad Sci U S A, 105*(38), 14353-14358. doi:10.1073/pnas.0807537105

Parrish, D. C., Alston, E. N., Rohrer, H., Hermes, S. M., Aicher, S. A., Nkadi, P., . . . Habecker, B. A. (2009). Absence of gp130 in dopamine beta-hydroxylase-expressing

neurons leads to autonomic imbalance and increased reperfusion arrhythmias. *Am J Physiol Heart Circ Physiol, 297*(3), H960-967. doi:10.1152/ajpheart.00409.2009

Parrish, D. C., Alston, E. N., Rohrer, H., Nkadi, P., Woodward, W. R., Schutz, G., & Habecker, B. A. (2010). Infarction-induced cytokines cause local depletion of tyrosine hydroxylase in cardiac sympathetic nerves. *Exp Physiol, 95*(2), 304-314. doi:10.1113/expphysiol.2009.049965

Pavoine, C., & Defer, N. (2005). The cardiac beta2-adrenergic signalling a new role for the cPLA2. *Cell Signal, 17*(2), 141-152. doi:10.1016/j.cellsig.2004.09.001

Pearson, C. S., Mencio, C. P., Barber, A. C., Martin, K. R., & Geller, H. M. (2018). Identification of a critical sulfation in chondroitin that inhibits axonal regeneration. *Elife, 7*. doi:10.7554/eLife.37139

Pellegrino, M. J., & Habecker, B. A. (2013). STAT3 integrates cytokine and neurotrophin signals to promote sympathetic axon regeneration. *Mol Cell Neurosci, 56*, 272-282. doi:10.1016/j.mcn.2013.06.005

Pellegrino, M. J., Parrish, D. C., Zigmond, R. E., & Habecker, B. A. (2011). Cytokines inhibit norepinephrine transporter expression by decreasing Hand2. *Mol Cell Neurosci, 46*(3), 671-680. doi:10.1016/j.mcn.2011.01.008

Petty, B. G., Cornblath, D. R., Adornato, B. T., Chaudhry, V., Flexner, C., Wachsman, M., . . . Peroutka, S. J. (1994). The effect of systemically administered recombinant human nerve growth factor in healthy human subjects. *Ann Neurol, 36*(2), 244-246. doi:10.1002/ana.410360221

Pires-Neto, M. A., Braga-De-Souza, S., & Lent, R. (1998). Molecular tunnels and boundaries for growing axons in the anterior commissure of hamster embryos. *J Comp Neurol, 399*(2), 176-188. doi:10.1002/(sici)1096-9861(19980921)399:2<176::aid-cne3>3.0.co;2-y

Poelzing, S., & Rosenbaum, D. S. (2004). Altered connexin43 expression produces arrhythmia substrate in heart failure. *Am J Physiol Heart Circ Physiol, 287*(4), H1762-1770. doi:10.1152/ajpheart.00346.2004

Pogwizd, S. M., & Bers, D. M. (2004). Cellular basis of triggered arrhythmias in heart failure. *Trends Cardiovasc Med, 14*(2), 61-66. doi:10.1016/j.tcm.2003.12.002

Pogwizd, S. M., Qi, M., Yuan, W., Samarel, A. M., & Bers, D. M. (1999). Upregulation of Na(+)/Ca(2+) exchanger expression and function in an arrhythmogenic rabbit model of heart failure. *Circ Res, 85*(11), 1009-1019. doi:10.1161/01.res.85.11.1009

Pogwizd, S. M., Schlotthauer, K., Li, L., Yuan, W., & Bers, D. M. (2001). Arrhythmogenesis and contractile dysfunction in heart failure: Roles of sodium-calcium

exchange, inward rectifier potassium current, and residual beta-adrenergic responsiveness. *Circ Res, 88*(11), 1159-1167. doi:10.1161/hh1101.091193

Popovich, P. G., Guan, Z., Wei, P., Huitinga, I., van Rooijen, N., & Stokes, B. T. (1999). Depletion of hematogenous macrophages promotes partial hindlimb recovery and neuroanatomical repair after experimental spinal cord injury. *Exp Neurol, 158*(2), 351-365. doi:10.1006/exnr.1999.7118

Pouleur, A. C., Barkoudah, E., Uno, H., Skali, H., Finn, P. V., Zelenkofske, S. L., . . . Investigators, V. (2010). Pathogenesis of sudden unexpected death in a clinical trial of patients with myocardial infarction and left ventricular dysfunction, heart failure, or both. *Circulation, 122*(6), 597-602. doi:10.1161/CIRCULATIONAHA.110.940619

Prabhu, N., Dai, L., & Nordlund, P. (2020). CETSA in integrated proteomics studies of cellular processes. *Curr Opin Chem Biol, 54*, 54-62. doi:10.1016/j.cbpa.2019.11.004

Prabhu, S. D., & Frangogiannis, N. G. (2016). The Biological Basis for Cardiac Repair After Myocardial Infarction: From Inflammation to Fibrosis. *Circ Res, 119*(1), 91-112. doi:10.1161/CIRCRESAHA.116.303577

Price, R. D., Milne, S. A., Sharkey, J., & Matsuoka, N. (2007). Advances in small molecules promoting neurotrophic function. *Pharmacol Ther, 115*(2), 292-306. doi:10.1016/j.pharmthera.2007.03.005

Pu, A., Stephenson, E. L., & Yong, V. W. (2018). The extracellular matrix: Focus on oligodendrocyte biology and targeting CSPGs for remyelination therapies. *Glia, 66*(9), 1809-1825. doi:10.1002/glia.23333

Raake, P. W., Zhang, X., Vinge, L. E., Brinks, H., Gao, E., Jaleel, N., . . . Koch, W. J. (2012). Cardiac G-protein-coupled receptor kinase 2 ablation induces a novel Ca2+ handling phenotype resistant to adverse alterations and remodeling after myocardial infarction. *Circulation, 125*(17), 2108-2118. doi:10.1161/CIRCULATIONAHA.111.044255

Regot, S., Hughey, J. J., Bajar, B. T., Carrasco, S., & Covert, M. W. (2014). High-sensitivity measurements of multiple kinase activities in live single cells. *Cell, 157*(7), 1724-1734. doi:10.1016/j.cell.2014.04.039

Reynoso, M. A., Juntawong, P., Lancia, M., Blanco, F. A., Bailey-Serres, J., & Zanetti, M. E. (2015). Translating Ribosome Affinity Purification (TRAP) followed by RNA sequencing technology (TRAP-SEQ) for quantitative assessment of plant translatomes. *Methods Mol Biol, 1284*, 185-207. doi:10.1007/978-1-4939-2444-8_9

Ripplinger, C. M., Noujaim, S. F., & Linz, D. (2016). The nervous heart. *Prog Biophys Mol Biol, 120*(1-3), 199-209. doi:10.1016/j.pbiomolbio.2015.12.015

Rog-Zielinska, E. A., Norris, R. A., Kohl, P., & Markwald, R. (2016). The Living Scar--Cardiac Fibroblasts and the Injured Heart. *Trends Mol Med, 22*(2), 99-114. doi:10.1016/j.molmed.2015.12.006

Roger, V. L., Go, A. S., Lloyd-Jones, D. M., Benjamin, E. J., Berry, J. D., Borden, W. B., . . . Stroke Statistics, S. (2012). Heart disease and stroke statistics--2012 update: a report from the American Heart Association. *Circulation, 125*(1), e2-e220. doi:10.1161/CIR.0b013e31823ac046

Rosenthal, A., Goeddel, D. V., Nguyen, T., Lewis, M., Shih, A., Laramee, G. R., . . . Winslow, J. W. (1990). Primary structure and biological activity of a novel human neurotrophic factor. *Neuron, 4*(5), 767-773. doi:10.1016/0896-6273(90)90203-r

Roth, G. A., Mensah, G. A., Johnson, C. O., Addolorato, G., Ammirati, E., Baddour, L. M., . . . Group, G.-N.-J. G. B. o. C. D. W. (2020). Global Burden of Cardiovascular Diseases and Risk Factors, 1990-2019: Update From the GBD 2019 Study. *J Am Coll Cardiol, 76*(25), 2982-3021. doi:10.1016/j.jacc.2020.11.010

Rubart, M., & Zipes, D. P. (2005). Mechanisms of sudden cardiac death. *J Clin Invest, 115*(9), 2305-2315. doi:10.1172/JCI26381

Sapieha, P. S., Duplan, L., Uetani, N., Joly, S., Tremblay, M. L., Kennedy, T. E., & Di Polo, A. (2005). Receptor protein tyrosine phosphatase sigma inhibits axon regrowth in the adult injured CNS. *Molecular and Cellular Neuroscience, 28*(4), 625-635. Retrieved from http://www.sciencedirect.com/science/article/B6WNB-4FG8983-1/2/3962e91902947ab11fceb2706eca6c78

Saucerman, J. J., Zhang, J., Martin, J. C., Peng, L. X., Stenbit, A. E., Tsien, R. Y., & McCulloch, A. D. (2006). Systems analysis of PKA-mediated phosphorylation gradients in live cardiac myocytes. *Proc Natl Acad Sci U S A, 103*(34), 12923-12928. doi:10.1073/pnas.0600137103

Saxena, S., Howe, C. L., Cosgaya, J. M., Steiner, P., Hirling, H., Chan, J. R., . . . Kruttgen, A. (2005). Differential endocytic sorting of p75NTR and TrkA in response to NGF: a role for late endosomes in TrkA trafficking. *Mol Cell Neurosci, 28*(3), 571-587. doi:10.1016/j.mcn.2004.11.011

Schindelin, J., Arganda-Carreras, I., Frise, E., Kaynig, V., Longair, M., Pietzsch, T., . . . Cardona, A. (2012). Fiji: an open-source platform for biological-image analysis. *Nat Methods, 9*(7), 676-682. doi:10.1038/nmeth.2019

Scott-Solomon, E., & Kuruvilla, R. (2020). Prenylation of Axonally Translated Rac1 Controls NGF-Dependent Axon Growth. *Dev Cell, 53*(6), 691-705 e697. doi:10.1016/j.devcel.2020.05.020

Seidah, N. G., Benjannet, S., Pareek, S., Chretien, M., & Murphy, R. A. (1996). Cellular processing of the neurotrophin precursors of NT3 and BDNF by the mammalian proprotein convertases. *FEBS Lett, 379*(3), 247-250. doi:10.1016/0014-5793(95)01520-5

Seong, J., Ouyang, M., Kim, T., Sun, J., Wen, P. C., Lu, S., . . . Wang, Y. (2011). Detection of focal adhesion kinase activation at membrane microdomains by fluorescence resonance energy transfer. *Nat Commun, 2*, 406. doi:10.1038/ncomms1414

Sepe, J. J.; Gardner, R. T.; Blake, M. R.; Brooks, D. M.; Staffenson, M. A.; Betts, C. B.; Sivagnanam, S.; Larson, W.; Kumar, S.; Bayles, R. G.; Jin, H.; Cohen, M. S.; Coussens, L. M.; Habecker, B. A. (2022). Therapeutics that Promote Sympathetic Reinnervation Modulate the Inflammatory Response after Myocardial Infarction. *JACC: Basic to Translational Science, In press*.

Sharma, K., Selzer, M. E., & Li, S. (2012). Scar-mediated inhibition and CSPG receptors in the CNS. *Exp Neurol, 237*(2), 370-378. doi:10.1016/j.expneurol.2012.07.009

Shen, Y., Tenney, A. P., Busch, S. A., Horn, K. P., Cuascut, F. X., Liu, K., . . . Flanagan, J. G. (2009b). PTPsigma is a receptor for chondroitin sulfate proteoglycan, an inhibitor of neural regeneration. *Science, 326*(5952), 592-596. doi:10.1126/science.1178310

Sherman, L. S., & Back, S. A. (2008). A 'GAG' reflex prevents repair of the damaged CNS. *Trends Neurosci., 31*(1), 44-52. doi:10.1016/j.tins.2007.11.001

Shi, X., & Habecker, B. A. (2012). gp130 cytokines stimulate proteasomal degradation of tyrosine hydroxylase via extracellular signal regulated kinases 1 and 2. *J Neurochem, 120*(2), 239-247. doi:10.1111/j.1471-4159.2011.07539.x

Siao, C. J., Lorentz, C. U., Kermani, P., Marinic, T., Carter, J., McGrath, K., . . . Hempstead, B. L. (2012). ProNGF, a cytokine induced after myocardial infarction in humans, targets pericytes to promote microvascular damage and activation. *J Exp Med, 209*(12), 2291-2305. doi:10.1084/jem.20111749

Simula, S., Lakka, T., Kuikka, J., Laitinen, T., Remes, J., Kettunen, R., & Hartikainen, J. (2000). Cardiac adrenergic innervation within the first 3 months after acute myocardial infarction. *Clin Physiol, 20*(5), 366-373. doi:10.1046/j.1365-2281.2000.00278.x

Sivasankaran, R., Pei, J., Wang, K. C., Zhang, Y. P., Shields, C. B., Xu, X. M., & He, Z. (2004). PKC mediates inhibitory effects of myelin and chondroitin sulfate proteoglycans on axonal regeneration. *Nat Neurosci, 7*(3), 261-268. doi:10.1038/nn1193

Smith, C. C., Mauricio, R., Nobre, L., Marsh, B., Wust, R. C., Rossiter, H. B., & Ichiyama, R. M. (2015). Differential regulation of perineuronal nets in the brain and

spinal cord with exercise training. *Brain Res Bull, 111*, 20-26. doi:10.1016/j.brainresbull.2014.12.005

Snow, D. M., Lemmon, V., Carrino, D. A., Caplan, A. I., & Silver, J. (1990). Sulfated proteoglycans in astroglial barriers inhibit neurite outgrowth in vitro. *Exp Neurol, 109*(1), 111-130. doi:10.1016/s0014-4886(05)80013-5

Solomon, S. D., Zelenkofske, S., McMurray, J. J., Finn, P. V., Velazquez, E., Ertl, G., . . . Valsartan in Acute Myocardial Infarction Trial, I. (2005). Sudden death in patients with myocardial infarction and left ventricular dysfunction, heart failure, or both. *N Engl J Med, 352*(25), 2581-2588. doi:10.1056/NEJMoa043938

Stanton, M. S., Tuli, M. M., Radtke, N. L., Heger, J. J., Miles, W. M., Mock, B. H., . . . Zipes, D. P. (1989). Regional sympathetic denervation after myocardial infarction in humans detected noninvasively using I-123-metaiodobenzylguanidine. *J Am Coll Cardiol, 14*(6), 1519-1526. doi:10.1016/0735-1097(89)90391-4

Stein, F., Kress, M., Reither, S., Piljic, A., & Schultz, C. (2013). FluoQ: a tool for rapid analysis of multiparameter fluorescence imaging data applied to oscillatory events. *ACS Chem Biol, 8*(9), 1862-1868. doi:10.1021/cb4003442

Suzuki, K., Arumugam, S., Yokoyama, J., Kawauchi, Y., Honda, Y., Sato, H., . . . Asakura, H. (2016). Pivotal Role of Carbohydrate Sulfotransferase 15 in Fibrosis and Mucosal Healing in Mouse Colitis. *PLoS One, 11*(7), e0158967. doi:10.1371/journal.pone.0158967

Suzuki, K., Yokoyama, J., Kawauchi, Y., Honda, Y., Sato, H., Aoyagi, Y., . . . Asakura, H. (2017). Phase 1 Clinical Study of siRNA Targeting Carbohydrate Sulphotransferase 15 in Crohn's Disease Patients with Active Mucosal Lesions. *J Crohns Colitis, 11*(2), 221-228. doi:10.1093/ecco-jcc/jjw143

Teng, H. K., Teng, K. K., Lee, R., Wright, S., Tevar, S., Almeida, R. D., . . . Hempstead, B. L. (2005). ProBDNF induces neuronal apoptosis via activation of a receptor complex of p75NTR and sortilin. *J Neurosci, 25*(22), 5455-5463. doi:10.1523/JNEUROSCI.5123-04.2005

Tessarollo, L., Tsoulfas, P., Donovan, M. J., Palko, M. E., Blair-Flynn, J., Hempstead, B. L., & Parada, L. F. (1997). Targeted deletion of all isoforms of the trkC gene suggests the use of alternate receptors by its ligand neurotrophin-3 in neuronal development and implicates trkC in normal cardiogenesis. *Proc Natl Acad Sci U S A, 94*(26), 14776-14781. doi:10.1073/pnas.94.26.14776

Tian, Y., Koganti, T., Yao, Z., Cannon, P., Shah, P., Pietrovito, L., . . . Lindsey, M. L. (2014). Cardiac extracellular proteome profiling and membrane topology analysis using glycoproteomics. *Proteomics Clin Appl, 8*(7-8), 595-602. doi:10.1002/prca.201400009

Tom, V. J., Kadakia, R., Santi, L., & Houle, J. D. (2009). Administration of chondroitinase ABC rostral or caudal to a spinal cord injury site promotes anatomical but not functional plasticity. *J.Neurotrauma., 26*(12), 2323-2333.

Tom, V. J., Sandrow-Feinberg, H. R., Miller, K., Domitrovich, C., Bouyer, J., Zhukareva, V., . . . Houle, J. D. (2013). Exogenous BDNF enhances the integration of chronically injured axons that regenerate through a peripheral nerve grafted into a chondroitinase-treated spinal cord injury site. *Exp.Neurol., 239:91-100. doi: 10.1016/j.expneurol.2012.09.011. Epub@2012 Sep 27.*, 91-100.

Tsuchiya, T., Fujisawa, T., Kato, M., Mizuide, M., Torisu, Y., Nishimura, M., . . . Yahagi, N. (2021). A phase I/IIa trial of the RNA oligonucleotide STNM01 by EUS-FNI to investigate the safety and efficacy in patients with first-line refractory, unresectable pancreatic cancer. *Journal of Clinical Oncology, 39*(15_suppl), 4120-4120. doi:10.1200/JCO.2021.39.15_suppl.4120

Udina, E., Ladak, A., Furey, M., Brushart, T., Tyreman, N., & Gordon, T. (2010). Rolipram-induced elevation of cAMP or chondroitinase ABC breakdown of inhibitory proteoglycans in the extracellular matrix promotes peripheral nerve regeneration. *Exp Neurol, 223*(1), 143-152. doi:10.1016/j.expneurol.2009.08.026

Ughrin, Y. M., Chen, Z. J., & Levine, J. M. (2003). Multiple regions of the NG2 proteoglycan inhibit neurite growth and induce growth cone collapse. *J Neurosci, 23*(1), 175-186. Retrieved from https://www.ncbi.nlm.nih.gov/pubmed/12514214

Uhlin-Hansen, L., Wik, T., Kjellen, L., Berg, E., Forsdahl, F., & Kolset, S. O. (1993). Proteoglycan metabolism in normal and inflammatory human macrophages. *Blood, 82*(9), 2880-2889. Retrieved from https://www.ncbi.nlm.nih.gov/pubmed/8219236

Vaseghi, M., Gima, J., Kanaan, C., Ajijola, O. A., Marmureanu, A., Mahajan, A., & Shivkumar, K. (2014). Cardiac sympathetic denervation in patients with refractory ventricular arrhythmias or electrical storm: intermediate and long-term follow-up. *Heart Rhythm, 11*(3), 360-366. doi:10.1016/j.hrthm.2013.11.028

Vaseghi, M., Lux, R. L., Mahajan, A., & Shivkumar, K. (2012). Sympathetic stimulation increases dispersion of repolarization in humans with myocardial infarction. *Am J Physiol Heart Circ Physiol, 302*(9), H1838-1846. doi:10.1152/ajpheart.01106.2011

Vassilatis, D. K., Hohmann, J. G., Zeng, H., Li, F., Ranchalis, J. E., Mortrud, M. T., . . . Gaitanaris, G. A. (2003). The G protein-coupled receptor repertoires of human and mouse. *Proc Natl Acad Sci U S A, 100*(8), 4903-4908. doi:10.1073/pnas.0230374100

von Schack, D., Casademunt, E., Schweigreiter, R., Meyer, M., Bibel, M., & Dechant, G. (2001). Complete ablation of the neurotrophin receptor p75NTR causes defects both in the nervous and the vascular system. *Nat Neurosci, 4*(10), 977-978. doi:10.1038/nn730

Wagner, N., Wagner, K. D., Theres, H., Englert, C., Schedl, A., & Scholz, H. (2005). Coronary vessel development requires activation of the TrkB neurotrophin receptor by the Wilms' tumor transcription factor Wt1. *Genes Dev, 19*(21), 2631-2642. doi:10.1101/gad.346405

Wang, H., Katagiri, Y., McCann, T. E., Unsworth, E., Goldsmith, P., Yu, Z. X., . . . Geller, H. M. (2008). Chondroitin-4-sulfation negatively regulates axonal guidance and growth. *J Cell Sci, 121*(Pt 18), 3083-3091. doi:10.1242/jcs.032649

Wang, L., Myles, R. C., De Jesus, N. M., Ohlendorf, A. K., Bers, D. M., & Ripplinger, C. M. (2014). Optical mapping of sarcoplasmic reticulum Ca2+ in the intact heart: ryanodine receptor refractoriness during alternans and fibrillation. *Circ Res, 114*(9), 1410-1421. doi:10.1161/CIRCRESAHA.114.302505

Watanabe, K., Arumugam, S., Sreedhar, R., Thandavarayan, R. A., Nakamura, T., Nakamura, M., . . . Suzuki, K. (2015). Small interfering RNA therapy against carbohydrate sulfotransferase 15 inhibits cardiac remodeling in rats with dilated cardiomyopathy. *Cell Signal, 27*(7), 1517-1524. doi:10.1016/j.cellsig.2015.03.004

Willis, D. E., van Niekerk, E. A., Sasaki, Y., Mesngon, M., Merianda, T. T., Williams, G. G., . . . Twiss, J. L. (2007). Extracellular stimuli specifically regulate localized levels of individual neuronal mRNAs. *J Cell Biol, 178*(6), 965-980. doi:10.1083/jcb.200703209

Wilson-Pauwels, L., Stewart, P. A., & Akesson, E. J. (1997). *Autonomic nerves : basic science, clinical aspects, case studies*. Hamilton Ont. Malden, MA, U.S.A.

Wu, C. L., Hardy, S., Aubry, I., Landry, M., Haggarty, A., Saragovi, H. U., & Tremblay, M. L. (2017). Identification of function-regulating antibodies targeting the receptor protein tyrosine phosphatase sigma ectodomain. *PLoS ONE, 12*(5), e0178489. doi:10.1371/journal.pone.0178489

Xie, Y., Massa, S. M., Ensslen-Craig, S. E., Major, D. L., Yang, T., Tisi, M. A., . . . Longo, F. M. (2006). Protein-tyrosine phosphatase (PTP) wedge domain peptides: a novel approach for inhibition of PTP function and augmentation of protein-tyrosine kinase function. *J Biol.Chem., 281*(24), 16482-16492.

Xie, Y., Sato, D., Garfinkel, A., Qu, Z., & Weiss, J. N. (2010). So little source, so much sink: requirements for afterdepolarizations to propagate in tissue. *Biophys J, 99*(5), 1408-1415. doi:10.1016/j.bpj.2010.06.042

Yi, J. H., Katagiri, Y., Susarla, B., Figge, D., Symes, A. J., & Geller, H. M. (2012). Alterations in sulfated chondroitin glycosaminoglycans following controlled cortical impact injury in mice. *J Comp Neurol, 520*(15), 3295-3313. doi:10.1002/cne.23156

York, R. D., Molliver, D. C., Grewal, S. S., Stenberg, P. E., McCleskey, E. W., & Stork, P. J. (2000). Role of phosphoinositide 3-kinase and endocytosis in nerve growth factor-

induced extracellular signal-regulated kinase activation via Ras and Rap1. *Mol Cell Biol, 20*(21), 8069-8083. doi:10.1128/MCB.20.21.8069-8083.2000

Zamora, R., Delgado, R. M., & Hidalgo, F. J. (2010). Model reactions of acrylamide with selected amino compounds. *J Agric Food Chem, 58*(3), 1708-1713. doi:10.1021/jf903378x

Zaro, B. W., Vinogradova, E. V., Lazar, D. C., Blewett, M. M., Suciu, R. M., Takaya, J., . . . Teijaro, J. R. (2019). Dimethyl Fumarate Disrupts Human Innate Immune Signaling by Targeting the IRAK4-MyD88 Complex. *J Immunol, 202*(9), 2737-2746. doi:10.4049/jimmunol.1801627

Zhang, B., Tian, X., Qu, Z., Liu, J., & Yang, L. (2021). Relative Efficacy and Safety of Tanezumab for Osteoarthritis: A Systematic Review and Meta-analysis of Randomized-Controlled Trials. *Clin J Pain, 37*(12), 914-924. doi:10.1097/AJP.0000000000000986

Zhang, Y., Conrad, A. H., Tasheva, E. S., An, K., Corpuz, L. M., Kariya, Y., . . . Conrad, G. W. (2005). Detection and quantification of sulfated disaccharides from keratan sulfate and chondroitin/dermatan sulfate during chick corneal development by ESI-MS/MS. *Invest Ophthalmol Vis Sci, 46*(5), 1604-1614. doi:10.1167/iovs.04-1453

Zhao, R. R., Muir, E. M., Alves, J. N., Rickman, H., Allan, A. Y., Kwok, J. C., . . . Rogers, J. H. (2011). Lentiviral vectors express chondroitinase ABC in cortical projections and promote sprouting of injured corticospinal axons. *J.Neurosci.Methods., 201*(1), 228-238.

Zhou, B., Cai, Q., Xie, Y., & Sheng, Z. H. (2012). Snapin recruits dynein to BDNF-TrkB signaling endosomes for retrograde axonal transport and is essential for dendrite growth of cortical neurons. *Cell Rep, 2*(1), 42-51. doi:10.1016/j.celrep.2012.06.010

Zhou, S., Chen, L. S., Miyauchi, Y., Miyauchi, M., Kar, S., Kangavari, S., . . . Chen, P. S. (2004). Mechanisms of cardiac nerve sprouting after myocardial infarction in dogs. *Circ Res, 95*(1), 76-83. doi:10.1161/01.RES.0000133678.22968.e3

Ziegler, K. A., Ahles, A., Wille, T., Kerler, J., Ramanujam, D., & Engelhardt, S. (2018). Local sympathetic denervation attenuates myocardial inflammation and improves cardiac function after myocardial infarction in mice. *Cardiovasc Res, 114*(2), 291-299. doi:10.1093/cvr/cvx227

Zipes, D. P., & Rubart, M. (2006). Neural modulation of cardiac arrhythmias and sudden cardiac death. *Heart Rhythm, 3*(1), 108-113. doi:10.1016/j.hrthm.2005.09.021